Department of Biosciences and Bioengineering
Indian Institute of Technology Guwahati
Assam, India

Therapeutic Insights of Entomopathogenic Mycotoxins in Breast Cancer Cells

A Thesis

submitted for the award of the degree of

DOCTOR OF PHILOSOPHY

Submitted by

Arupam Patra

(Roll No. 186106116)

Under the Supervision of

Prof. Gurvinder Kaur Saini
Professor

Prof. Siddhartha Sankar Ghosh
Professor

TH-3487_186106116

TH-3487_186106116

Dedicated To

My Beloved Parents And The Almighty

TH-3487_186106116

TH-3487_186106116

Department of Biosciences and Bioengineering (BSBE)
Indian Institute of Technology (IIT) Guwahati
Assam, India

Declaration Statement

I hereby declare that the research embodied in this thesis, entitled "**Therapeutic Insights of Entomopathogenic Mycotoxins in Breast Cancer Cells"** is the result of investigations conducted by me under the supervision of Prof. Gurvinder Kaur Saini and Prof. Siddhartha Sankar Ghosh, Department of Biosciences and Bioengineering, Indian Institute of Technology Guwahati, Assam, India, for the award of Degree of **Doctor of Philosophy**. This work has not been submitted elsewhere for any degree, diploma, etc. of any institute or university to the best of my knowledge and belief.

Date: 1st August, 2024

Place: Guwahati

Arupam Patra

Arupam Patra
(Roll No. – 186106116)

TH-3487_186106116

TH-3487_186106116

Department of Biosciences and Bioengineering (BSBE)
Indian Institute of Technology (IIT) Guwahati
Assam, India

Certificate

This is to certify that the thesis entitled "**Therapeutic Insights of Entomopathogenic Mycotoxins in Breast Cancer Cells**", submitted to the **Indian Institute of Technology Guwahati** by ***Arupam Patra*** (***Roll no. 186106116***) for the award of the degree of **Doctor of Philosophy** in **Biosciences and Bioengineering** is a bonafide record of research work conducted by him. The information and data reported are solely the results of his original findings. He has meticulously conducted the investigations and adhered to the guidelines of the laboratory. The contents of this thesis have not been submitted to any other university or institute for the award of any degree or diploma.

Date: 1st August, 2024

Place: Guwahati

Prof. Gurvinder Kaur Saini
(Thesis Supervisor)

Prof. Siddhartha Sankar Ghosh
(Thesis Supervisor)

TH-3487_186106116

TH-3487_186106116

A C K N O W L E D G E M E N T

"*If I have seen further, it is by standing on the shoulders of giants*"

- *Sir Isaac Newton*

The completion of my PhD thesis would not have been possible without the invaluable support, guidance, and encouragement from numerous individuals. I would like to take this opportunity to express my deepest gratitude to all those who have contributed to this journey.

First and foremost, I would like to extend my heartfelt sincere gratitude to my supervisors, ***Prof. Gurvinder Kaur Saini*** and ***Prof. Siddhartha Sankar Ghosh***, whose expertise, patience, and unwavering support have been instrumental in guiding me through this research. Their insightful feedback and constructive criticism have greatly enhanced the quality of my work, and their encouragement has been a constant source of motivation.

I am profoundly grateful to the members of my doctoral committee, *Prof. Biplab Bose* (Chairperson), *Prof. Aiyagiri Ramesh*, *Prof. Gopal Das* and *Prof. Senthilkumar Sivaprakasam*, for their valuable suggestions and guidance throughout the course of my research. Their diverse perspectives and critical insights have significantly contributed to the refinement of my thesis.

Special thanks go to the faculty members and staff of the Department of Biosciences and Bioengineering at the Indian Institute of Technology Guwahati. Their support, both academic and administrative, has been crucial in the successful completion of my PhD. I would also like to express my gratitude to the Centre for Nanotechnology and the Central Instruments Facility at IIT Guwahati. The access to state-of-the-art equipment and facilities, coupled with the technical support provided, has been invaluable to my research.

To my beloved parents, your unwavering love, patience, and belief in me have been my greatest source of strength. You have always encouraged me to pursue my dreams and have supported me in every possible way. I am forever indebted to you for your sacrifices and constant support.

TH-3487_186106116

My heartfelt thanks also go to my other family members, especially my brother Souvik, for their encouragement and understanding throughout this journey. Your support has been a pillar of strength during the challenging times of my research.

I would like to acknowledge the senior members of our lab, particularly *Dr. Balwant Singh*, *Dr. Dhanasingh M.*, *Dr. Neha Maurya*, *Dr. Anitha T Simon*, *Dr. Rajib Shome*, *Dr. Muktashree Saha*, *Dr. Debashree Debasmita* and *Dr. Plaboni Sen*, for their mentorship and guidance. Your experience and knowledge have been invaluable, and your willingness to help has made a significant difference in my research.

To my present lab members, Arman Mohanty, Dr. Konika Choudhury, Shilpi Sarkar, Hirakjyoti Roy, Sayantani Mukhopadhyay, K. Thirukumaran, Sawna Roy, Arisha Arora, Sujisha S., Sayantani Biswas, Basab Ghosh, Pijush K. Khanra and Hachina Begum, working alongside you has been a pleasure. Your camaraderie, support, and collaborative spirit have made the lab environment enjoyable and productive. I am grateful for the stimulating discussions and the moments of shared laughter.

I would also like to thank my friends, both within and outside IIT Guwahati, for their unwavering support and companionship. Special thanks to Susmita Dhar, Pratik Das Gupta, Subhashree Barik, Muktashree Saha and Barlina Konwar for always being there for me, offering a listening ear, and providing much-needed encouragement during difficult times. I am also grateful to Dr. Uday Pandey, Greeshma S., Dr. Suraj K. Panda, Dr. Alok Senapati and Alok K. Pandey for their immense support and constant motivation.

Lastly, I extend my gratitude to the Indian Institute of Technology Guwahati for providing an excellent academic environment and the necessary resources to conduct my research. The opportunities for learning and growth offered by this esteemed institution have been instrumental in shaping my academic career.

This thesis is a testament to the collective efforts and support of all these remarkable individuals. I am deeply grateful to each one of you for contributing to this significant milestone in my life.

Arupam Patra

August, 2024

TH-3487_186106116

CONTENTS

TH-3487_186106116

TH-3487_186106116

TH-3487_186106116

TH-3487_186106116

TH-3487_186106116

TH-3487_186106116

A B S T R A C T

Cancer continues to be a significant global health concern due to its constant rise in the number of new cases and cancer-related deaths each year. Breast cancer being the second most prevalent cancer type after Lung cancer, accounts for a major portion of all cancer cases globally. Several therapeutic strategies have been employed to counter breast cancer related mortality, focusing on overcoming the challenges in its treatment, such as chemotherapeutic resistance, EMT, metastasis etc. Among them, Natural sources like plants and microorganisms, are extensively studied for their potential to produce cancer specific inhibitors, contributing to over 60% of contemporary anticancer drugs. Among these microorganisms, entomopathogenic fungi serves as a vital source of various naturally occurring protein-based toxins and secondary metabolites with potential bioactivities, enabling them to thrive within their specific insect hosts. These mycotoxins are often cytotoxic in nature and possess unique mechanisms of action against other organisms. The unique functions of these mycotoxins can be redirected against cancer cells in order to overcome the existing challenges in breast cancer treatment.

While researches often prioritize screening potential anticancer agents based on their cytotoxicity, other dimensions of their therapeutic impacts remain largely unexplored. In addition to their cytotoxic effects on cancer cells, it is imperative to elucidate their specific mechanism of action by investigating their intracellular molecular targets, the signaling pathways they interfere and their potential to reverse drug resistance. Additionally, their ability to reverse epithelial-to-mesenchymal transition (EMT), inhibit cellular migration, invasion, angiogenesis and other cellular events involved in cancer progression should be thoroughly examined.

Hence, the present thesis emphasizes various therapeutic aspects of Anisoplin, a fungal ribotoxin produced by entomopathogenic fungi *Metarhizium anisopliae* and Beauvericin, a secondary metabolite of *Beauveria bassiana* on both 2D and 3D models of breast cancer cells, *in vitro*. By investigating their impact across various experimental

TH-3487_186106116

procedures, this research showcases the potential of the mycotoxins in advancing breast cancer treatment strategies.

The present thesis is structured into four distinct chapters. **Chapter 1** entitled as '**Introduction and Review of Literature**' provides a comprehensive overview of breast cancer, with a particular emphasis on triple negative subtype. It mainly addresses the challenges involved in treatment and explores its intricate relationship with certain cancer associated cellular events and signaling pathways. Additionally, this chapter discusses the available therapeutic options and natural sources of anticancer drugs, with a particular focus on microbial sources like bacteria and fungi. It also provides a detailed review on the anticancer properties of both protein-based and non-protein-based toxins produced by entomopathogenic fungi, emphasizing their mechanisms of action and potential therapeutic applications against different types of cancer. Finally, the chapter delineated the scope of research and specific objectives of the thesis.

Chapter 2 entitled as '**Materials and Methods**", meticulously outlines the materials essential for the experiments and provides a comprehensive account of the exact methodologies employed. It elaborates on the formulas utilized for specific calculations and the software applied in data analysis associated with flowcytometry, quantitative real time PCR (qRT-PCR), Immunoblotting etc. Furthermore, this chapter delves into the methodologies involved in some prerequisites of certain experiments, like cell line maintenance, EMT induction, Spheroid formation etc. Ultimately, it encompasses detailed procedures for all statistical analyses, ensuring a thorough understanding of the experimental framework.

Chapter 3 entitled as '**Results and Discussions**' delineates the detailed outcomes of the following objectives and their correlation with existing researches.

In the context of the first objective, the fungal recombinant ribotoxin anisoplin was produced in bacterial expression system. Following overexpression, the recombinant anisoplin (rAnp) was purified by the chromatographic techniques and characterized using a

TH-3487_186106116

range of biophysical and functional characterization techniques. The therapeutic potential of the functionally active rAnp was further evaluated on MCF-7 breast cancer cells. The cytotoxic effects of rAnp on MCF-7 cells was examined by MTT based cell viability assay. Additionally, induction of oxidative stress mediated apoptotic cell death was assessed by determining the reactive oxygen species (ROS) level and mitochondrial transmembrane potential. Finally, the molecular events of ribotoxic stress response was evaluated by analyzing SAPK/JNK activation and NFκB expression level. The findings demonstrated an approximately 8.9-fold upregulation in the active variant of SAPK/JNK (P-SAPK/JNK) and 2-fold reduction in the expression of NFκB.

The subsequent objective concentrated on the identification of molecular targets of beauvericin using an *in silico* approach. Molecular docking and molecular dynamics (MD) simulation methodologies were employed to screen potential molecular targets of beauvericin in triple negative breast cancer (TNBC) cells. *In vitro* therapeutic effects of beauvericin was evaluated on MDA-MB-231 and MDA-MB-468 TNBC cells. This evaluation included assessing cell viability, induction of oxidative stress by elevating ROS and reducing mitochondrial transmembrane potential and subsequent triggering of apoptotic cell death. Additionally, beauvericin's ability to restrict cell cycle progression and reduction of clonal expansion and regeneration capability of TNBC cells were investigated. The findings demonstrated cell cycle arrest at G1 phase and approximately 2.2 and 2.3-fold reduction in the colony formation abilities of MDA-MB-468 and MDA-MB-231 cells, respectively. Finally, its impact on the spheroids of TNBC cells was examined through assessment of spheroid viability, spheroid formation ability and live-dead staining assays, which showed detrimental effects of beauvericin on TNBC spheroids with approximately 1.2 and 1.3-fold reduction in the spheroid size (in diameter) of MDA-MB-231 and MDA-MB-468 cells, respectively.

In the final objective, the effect of beauvericin was investigated in EMT-induced TNBC cells, which exhibit enhanced metastatic traits compared to the uninduced cells, making them a suitable model for studying anti-metastatic agents. The detrimental impact of beauvericin was studied on the viability of EMT-induced monolayers and spheroids of TNBC cells. Additionally, its ability to induce oxidative stress in EMT-induced TNBC cells was established by determining the ROS level and mitochondrial transmembrane potential.

TH-3487_186106116

Furthermore, beauvericin was shown to significantly inhibit the cellular migration by reversing EMT. Following beauvericin treatment, changes in the expression of EMT markers were analyzed using qRT-PCR and western blotting. The findings demonstrated 1.7-fold upregulation in the epithelial marker E-cadherin and 1.7-fold downregulation in both mesenchymal markers N-cadherin and vimentin in MDA-MB-231 cells. In contrast, E-cadherin was upregulated by 2.2-fold, while N-cadherin and vimentin were downregulated by 2.2 and 2.6-fold, respectively, in MDA-MB-468 cells. The underlying mechanism of EMT reversal has been further investigated by exploring the notch signaling inhibitory effects and autophagy inducing capability of beauvericin in TNBC cells through detailed gene and protein expression analyses. Beauvericin significantly downregulated Notch-1, Notch-3, HES-1 and CyclinD3 expression by approximately 2.1, 1.9, 3.2 and 2.2-fold, while upregulated the autophagy markers LC-3 and Beclin-1 by 1.7 and 1.2-fold in MDA-MB-231 cells. In contrast, the expression of Notch-1, Notch-3, HES-1 and CyclinD3 was reduced by approximately 2.9, 1.3, 2.1 and 1.7-fold, while upregulating LC-3 and Beclin-1 by 2.7 and 4.9-fold in MDA-MB-468 cells.

Chapter 4 entitled as '**Conclusion and Future Prospects**' elucidates the key findings of this thesis and their implications in the improvement of breast cancer treatment. This chapter documents the potential therapeutic properties of entomopathogenic mycotoxins, proposing a sustainable approach to breast cancer therapy. Beyond summarizing the main discoveries, it discusses potential future initiatives aimed at transforming these threats (mycotoxins) into viable therapeutic agents. These insights and proposed future prospects emphasize the promise of mycotoxins in developing innovative and effective breast cancer therapy.

TH-3487_186106116

ABBREVIATIONS

μL	Microliter
μM	Micromolar
ABCC1	ATP Binding Cassette Subfamily C Member 1
AKT	Ak Strain Transforming
ALDH1	Aldehyde Dehydrogenase
Anp	Anisoplin
APS	Ammonium Persulfate
ATCC	American Type Culture Collection
ATG	Autophagy Protein
ATP	Adenosine Triphosphate
BCA	Bicinchoninic Acid
BCN1	Beclin 1
BCS	Breast Conserving Surgery
BL	Basal-like
BSA	Bovine Serum Albumin
c-MYC	Cellular Myc
CAR-T	Chimeric Antigen Receptor T-cell
CD	Circular Dichroism
CD22	Cluster of Differentiation 22

TH-3487_186106116

CDC25C	Cell Division Cycle 25 C
CDK2	Cyclin Dependent Kinase 2
cDNA	Complementary DNA
CEA	Carcinoembryonic Antigen
CHEK1	Checkpoint Kinase 1
CPTAC	Clinical Proteomic Tumor Analysis Consortium
CSCs	Cancer Stem Cells
CSLC	Cancer Stem Like Cells
Da	Dalton
dATP	Deoxyadenosine Triphosphate
DCFDA	2',7'-dichlorodihydrofluorescein diacetate
DEDD	Death Effector Domain Containing DNA Binding protein
DMEM	Dulbecco's Modified Eagle Medium
DMSO	Dimethyl Sulfoxide
DNA	Deoxyribonucleic acid
dNTPs	Deoxyribonucleotides
DTT	Dithiothreitol
EDTA	Ethylenediaminetetraacetic Acid
EF	Elongation Factor
EGF	Epidermal Growth Factor
EMT	Epithelial To Mesenchymal Transition
ER	Estrogen Receptor

TH-3487_186106116

ERK	Extracellular Signal Regulated Kinase
EtBr	Ethidium Bromide
FBS	Fetal Bovine Serum
FDA	Food and Drug Administration
FGFR	Fibroblast Growth Factor Receptor
GPA33	Glycoprotein A33
GRAVY	Grand Average of Hydropathy
GTP	Guanosine Triphosphate
h	Hour
HDAC	Histone Deacetylase
HDI	Human Development Index
HEK	Human Embryonic Kidney
hENT	Human Equllibrative Nucleoside Transporter
HER-2	Human Epidermal Growth Factor Receptor 2
HES1	Hairy and Enhancer of Split 1
HEY1	Hairy/enhancer-of-split related with YRPW motif protein 1
hMSCs	Human Mesenchymal Stem Cells
HR	Hormone Receptors
HRP	Horse Radish Peroxidase
HtA	Hirsutellin A
IC_{50}	Inhibitory Concentration of 50% population
IM	Immunomodulatory

TH-3487_186106116

IPTG	Isopropyl β- d-1-thiogalactopyranoside
JAG1	Jagged canonical notch ligand
JC-1	Tetraethyl-benzimidazolylcarbocyanine Iodide
kDa	Kilodalton
KEAP1	Kelch-like ECH-associated Protein 1
LAR	Luminal Androgen Receptor
LB	Luria-Bertani
LC3	Microtubule-associated protein 1A/1B-light chain 3
LCK	Lymphocyte Cell Specific Protein Tyrosine Kinase
LRR	Locoregional Recurrence
LSM	Laser Scanning Microscope
MALDI-TOF-MS	Matrix Assisted Laser Desorption Ionization – Mass Spectrometry
MAML	Mastermind-like
MAPK	Mitogen-Activated Protein Kinase
MBP	Maltose Binding Protein
MCF	Michigan Cancer Foundation
MD	Molecular Dynamics
MDA MB	M. D. Anderson Metastatic Breast cancer
MDR	Multi Drug Resistance
MET	Mesenchymal to Epithelial Transition
min	Minute
miRNA	Micro Ribonucleic Acid

TH-3487_186106116

ML	Mesenchymal Like
mL	Mililiter
mM	Milimolar
MMC	Mitomycin C
MMP	Matrix Metalloprotease
MMPBSA	Molecular Mechanics Poisson-Boltzmann Surface Area
mRNA	Messenger Ribonucleic Acid
MRP1	Multidrug Resistance Protein 1
MSL	Mesenchymal Stem Like
MTCC	Microbial Type Culture Collection
mTOR	Mammalian target of rapamycin
MTT	3-(4,5-Dimethylthiazol-2-yl)-2,5-diphenyltetrazolium bromide
NCCS	National Centre for Cell Science
NFκB	Nuclear factor kappa B
NICD	Notch Intracellular Domain
NRF2	Nuclear Factor Erythroid 2 related Factor 2
ns	Nanosecond
OD	Optical Density
PBS	Phosphate Buffer Saline
PCR	Polymerase Chain Reaction
PD	Paired Distance
PDB	Protein Database

TH-3487_186106116

PI	Propidium Iodide
PI3K	Phosphoinositide 3-Kinase
pmols	Picomoles
PMSF	Phenylmethanesulfonyl fluoride
PR	Progesterone Receptor
PVDF	Polyvinylidene Difluoride
qRT-PCR	Quantitative Real Time Polymerase Chain Reaction
rAnp	Recombinant anisoplin
RDF	Radial Distribution Function
Rg	Radius of Gyration
RIPA	Radioimmunoprecipitation Assay Buffer
RMSD	Root Mean Square Deviation
RMSF	Root Mean Square Fluctuation
RNase	Ribonuclease
ROS	Reactive Oxygen Species
rpm	Revolutions Per Minute
rRNA	Ribosomal Ribonucleic Acid
RT	Radiotherapy
RTK	Receptor Tyrosine Kinase
SAPK/JNK	Stress Activated Protein Kinase / c-Jun N-terminal Kinase
SASA	Solvent Accessible Surface Area
scFv	Single Chain Variable Fragment

TH-3487_186106116

SDS	Sodium Dodecyl Sulphate
SDS PAGE	Sodium Dodecyl Sulphate Polyacrylamide Gel Electrophoresis
SQSTM	Sequestosome
SRL	Sarcin Ricin Loop
SYK	Spleen Tyrosine Kinase
TAE	Tris Acetate EDTA
TBS	Tris Buffered Saline
TBST	Tris Buffered Saline with 0.1% Tween
TCGA	The Cancer Genome Atlas
TEMED	Tetramethylethylenediamine
TFA	Trifluoracetic Acid
TLR	Toll-Like Receptor
T_m	Melting Temperature
TNBC	Triple Negative Breast Cancer
TNFα	Tumour Necrosis Factor-alpha
TNM	Tumour Node Metastasis
TRAIL	Tumor Necrosis Factor Related Apoptosis Inducing Ligand
Tris	Trizma Base
tRNA	Transfer Ribonucleic Acid
TWIST	Twist Family BHLH Transcription Factor
WNT	Wingless/Integrated
ZEB1	Zinc finger E-box-binding homeobox 1

TH-3487_186106116

LIST OF SCHEMES

TH-3487_186106116

TH-3487_186106116

LIST OF FIGURES

TH-3487_186106116

TH-3487_186106116

and SRL substrate. **(C)** Agarose gel electrophoresis image of rabbit reticulocyte lysate treated with 0.01 µM (lane 2), 0.1 µM (lane 3), 1 µM (lane 4) and 10 µM (lane 5) rAnp (lane 1 – untreated sample).

Figure 3.1.8

Cytotoxicity and induction of oxidative stress in MCF-7 cells upon rAnp treatment. (A) Antiproliferative effect of rAnp against MCF-7 breast cancer cells and **(B)** non-cancerous HEK-293 cells. **(C)** Confocal microscopic images showing live (Green) and dead (red) populations of MCF-7 cells. **(D)** Generation of intracellular reactive oxygen species (ROS) in MCF-7 cells upon treatment with increasing concentration of rAnp. **(E)** Fold change in ROS content of MCF-7 cells in respective rAnp concentrations.

Figure 3.1.9

Mitochondrial depolarization, activation of apoptosis and reduction in clonal expansion of MCF-7 cells upon rAnp treatment. (A) Flow cytometric analysis of mitochondrial membrane depolarization of MCF-7 cells upon treatment with increasing concentrations of rAnp. **(B)** Flow cytometric analysis of the apoptotic population of MCF-7 cells upon treatment with increasing concentrations of rAnp. **(C)** Assessment of colony formation ability of single cells of MCF-7 upon treatment with increasing concentrations of rAnp. **(D)** Fold change in the colony formation of MCF-7 cells upon treatment with increasing concentrations of rAnp.

Figure 3.1.10

SAPK/JNK activation and downregulation of NFκB upon rAnp treatment. **(A)** Western blot images showing changes in P-SAPK/JNK expression in MCF-7 cells upon treatment with increasing concentrations of rAnp. **(B)** Fold change in P-SAPK/JNK expression. **(C)** Changes in NFκB expression in

TH-3487_186106116

TH-3487_186106116

TH-3487_186106116

TH-3487_186106116

Figure 3.3.4

Expression analysis of EMT markers and Notch receptors by qRT-PCR. Expression profile of **A)** E-cadherin, **B)** N-cadherin and **C)** Vimentin in MDA-MB-468 cells and **D)** E-cadherin, **E)** N-cadherin and **F)** Vimentin in MDA-MB-231 cells. Expression profile of **G)** Notch1 and **H)** Notch3 receptors in MDA-MB-468 cells and **I)** Notch1 and **J)** Notch3 receptors in MDA-MB-231 cells.

Figure 3.3.5

Protein expression analysis of EMT markers in TNBC cells. Immunoblots depicting alterations in **A)** E-Cadherin, N-Cadherin, Vimentin, Slug, Snail and **H)** β-catenin expression levels in MDA-MB-468 cells, following beauvericin treatment, while corresponding quantitative assessment of expression in terms of fold changes are illustrated in panels **B)**, **C)**, **D)**, **E)**, **F)** and **G)** respectively. Likewise, **L)** and **M)** depicting the immunoblots of Snail, Slug and β-catenin in MDA-MB-231 cells with **I)**, **J)** and **K)** illustrating their quantitative expression level in terms of fold change.

Figure 3.3.6

Expression analysis of Notch signaling and autophagy related proteins in EMT induced TNBC cells. Immunoblots depicting alterations in **A)** Hes-1and CyclinD3 and **B)** LC3 and **C)** Beclin-1 expression levels in MDA-MB-468 cells, due to beauvericin treatment, while corresponding quantitative assessment of expression in terms of fold changes are illustrated in panels **F)**, **G)**, **H)**, and **I)** respectively. Likewise, **D)** and **E)** depicting the immunoblots of Hes-1, CyclinD3, Beclin-1 and LC3 in MDA-MB-231 cells with **J)**, **K)**, **L)** and **M)** illustrating their quantitative expression level in terms of fold change.

TH-3487_186106116

LIST OF TABLES

TH-3487_186106116

TH-3487_186106116

Chapter 1

Introduction and Review of Literatures

TH-3487_186106116

TH-3487_186106116

1.1. The cancer paradox

Cancer paradox highlights the complex and often contradictory aspects of cancer, illustrating its dual role as both, a consequence of life's essential processes and it's manifestation as a lethal disease. Fundamentally, cancer emerges from the essential mechanisms that sustain life; including cell division, genetic mutations and cellular adaptation, which are essential for growth, healing, and evolutionary processes. These mechanisms enable cells to divide and regenerate, promote genetic diversity through mutations and enables organisms to thrive in changing environments. However, when these processes malfunction or become dysregulated, they can result in the uncontrolled cell proliferation leading to cancer. (Weinberg, 1996)

Mutations play a pivotal role in the cancer paradox. While they serve as the building blocks for evolutionary adaptation, enabling species to thrive and endure, mutations can also disturb normal cellular processes and trigger cancer. Tumour cells frequently amass multiple mutations, some of which conferring survival benefits such as resistance to programmed cell death (apoptosis), increased proliferation, and the capacity to invade surrounding tissues (Loeb et al., 2003). Furthermore, the body's immune responses against cancer can paradoxically aid its progression. Inflammation, a natural reaction to injury or infection, can foster an environment conducive to tumour growth and spread. The immune system, typically a safeguard against diseases, plays a dual role in cancer. Tumours may evade detection by immune cells or exploit them to facilitate their own growth and metastasis. (Keibel et al., 2009)

Another facet of the cancer paradox lies in the complexities of treatment. While advances in medical research have resulted in targeted therapies, immunotherapies, and personalized medicine that have markedly enhanced patient outcomes, the diverse nature of cancer variations both between different types of cancer and within individual tumours poses a formidable challenge. Cancer cells possess the ability to develop resistance to treatments, diminishing their effectiveness over time. This adaptability mirrors evolutionary processes crucial for species survival, yet in the context of cancer, it often translates into treatment resistance and disease advancement. Moreover, although intensive treatments such as chemotherapy and radiation therapy are capable of effectively eliminating cancer cells, they

TH-3487_186106116

can also inflict considerable damage on healthy cells and tissues, resulting in severe side effects that significantly affect patients' quality of life. This highlights the delicate balance required between eradicating cancer and maintaining the overall health and well-being of the patient.

Cancer paradox embodies the complex and sometimes conflicting interplay between the life-sustaining processes that can lead to cancer and the ongoing challenge of treating and conquering this multifaceted disease. It emphasizes the necessity for a profound grasp of cancer biology and the continual advancement of inventive and refined treatment strategies. Resolving this paradox demands not just scientific and medical progress, but also a holistic approach that prioritizes the patient's overall well-being and quality of life.

1.2. Current global breast cancer scenario

The global cancer situation remains alarming, with nearly 20 million new cases and 9.7 million deaths reported in 2022. This number is projected to rise to 35 million new cases by 2050, signaling a potential major global health crisis. Breast cancer is particularly concerning, with around 2.3 million new cases in 2022, making it the second most common cancer worldwide and the fourth leading cause of cancer-related deaths, with approximately 666,000 fatalities. It is the most frequently diagnosed cancer among women and the leading cause of cancer death in women, representing nearly one in four cancer cases and one in six cancer deaths globally. (Bray et al., 2024)

The impact of cancer varies widely between countries with different Human Development Index (HDI) levels. Developed regions show higher incidence rates, while less developed regions experience disproportionately higher mortality rates due to disparities in healthcare access, early detection, and treatment. Although cancer incidence is increasing globally, especially in developing areas, some high-income countries have seen a decrease in mortality rates due to advancements in treatment and early detection. The WHO's Global Breast Cancer Initiative aims to reduce mortality by enhancing breast health and early detection, addressing these global disparities and improving outcomes for breast cancer patients. Given the challenges, there is a critical need to develop innovative treatments to improve patient survival and treatment effectiveness. (Bray et al., 2024)

TH-3487_186106116

1.3. Molecular subtypes of breast cancer

Breast cancer, characterized by its heterogenicity, can be categorized into four different molecular subtypes based on the differential expression of various hormonal receptors on the cell surface. These subtypes play a crucial role in predicting prognosis, guiding treatment choices, and influencing patient outcomes.

- **Luminal A (ER+ and/or PR+, HER2-):** Luminal A tumours, accounting for about 50% of breast cancers, express hormone receptors like estrogen receptor (ER) and/or progesterone receptor (PR). These tumours generally have slow growth rates and are linked to a positive prognosis. The main treatment approach for Luminal A breast cancer involves endocrine therapy, which aims to block hormone receptors and prevent tumour progression. (Perou et al., 2000)

- **Luminal B (ER+ and/or PR+, HER2-/+):** Luminal B tumours exhibit similarities to Luminal A but are distinguished by increased proliferation rates and frequent overexpression of the human epidermal growth factor receptor 2 (HER2). This subtype is associated with a less favourable prognosis compared to Luminal A. Treatment for Luminal B cancers typically involves a combination of endocrine therapy and HER2-targeted agents for those with HER2 overexpression. This combined treatment strategy aims to address both hormone receptor-positive and HER2-driven pathways. (Feeley et al., 2014)

- **HER2-positive (HR-/HER2+):** Around 20% of breast cancers are HER2-positive, marked by excessive HER2 protein expression that stimulates aggressive tumour growth. Targeted treatments like trastuzumab (Herceptin) and pertuzumab (Perjeta) have notably enhanced outcomes for HER2 positive breast cancer patients. These therapies specifically block the HER2 protein, thereby restraining tumour growth and enhancing survival rates. (Figueroa-Magalhães et al., 2014)

- **Triple-negative (HR-/HER2-):** Comprising approximately 15-20% of breast cancer instances, triple-negative breast cancers (TNBC) do not express hormone

TH-3487_186106116

receptors (HR) or HER2. TNBC is characterized by its aggressive behaviour and elevated recurrence rates. Treatment options are restricted due to the absence of targetable receptors, with chemotherapy serving as the principal therapeutic method. Current research efforts are concentrated on discovering more efficacious treatments for this particularly challenging subtype. (Dent et al., 2007)

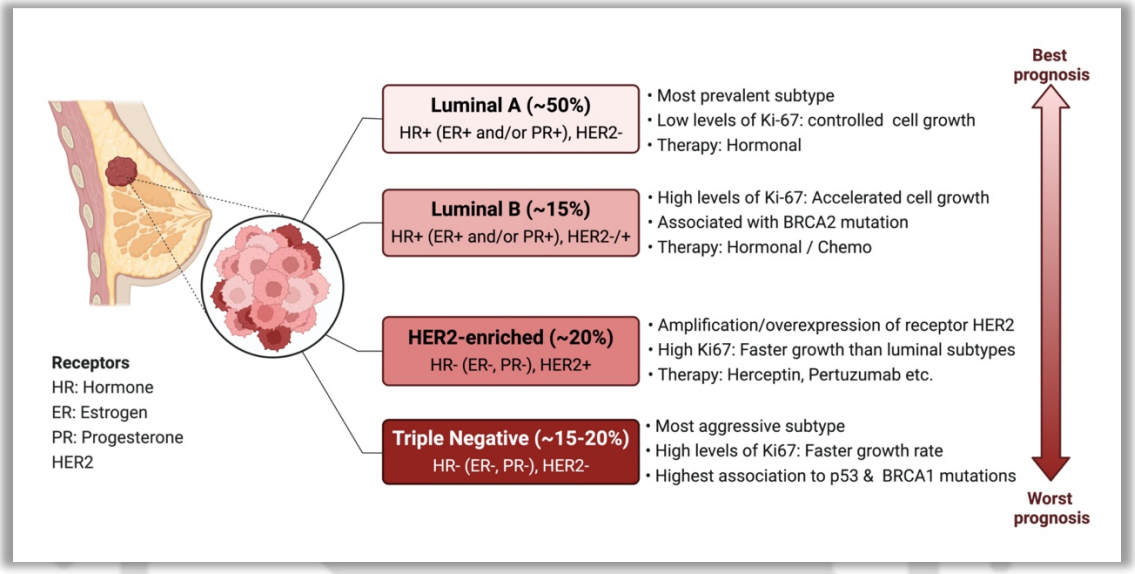

Scheme 1.1. Schematic depiction of various molecular subtypes of breast cancer along with their distinct characteristics. [*Conceptualised and illustrated based on* (Feeley et al., 2014; Mayrovitz, 2022) *using BioRender*]

Comprehending these molecular subtypes is essential for crafting personalized treatment strategies. By customizing therapies to align with the distinct characteristics of each subtype, healthcare providers can enhance patient outcomes and mitigate the side effects associated with broader treatment methods. This personalized approach emphasizes the significance of targeted therapies and individualized care in the management of breast cancer.

In summary, the molecular variability of breast cancer requires customized treatment strategies that integrate surgery, chemotherapy, endocrine therapy and targeted medications. Early detection and interdisciplinary cooperation remain pivotal in combating this widespread malignancy. As research progresses, there is optimism that further

TH-3487_186106116

refinement of subtype understanding will contribute to increasingly effective and personalized treatment approaches for breast cancer patients.

1.4. Triple-negative breast cancer and associated challenges in treatment

Triple-negative breast cancer represents one of the most lethal forms of cancer, comprising 15-20% of all breast cancer cases globally (Zagami and Carey, 2022). This specific subtype is distinguished by cells lacking human epidermal growth factor receptor 2 (HER2), progesterone receptor (PR) and estrogen receptor (ER) on their surface (Anders et al., 2008). TNBC poses significant clinical challenges due to the scarcity of treatment alternatives, frequently resulting in unfavorable prognoses (Griffiths and Olin, 2012). At molecular level, TNBC exhibits significant heterogenicity, encompassing minimum of six molecular subtypes (Lehmann et al., 2011). The majority of TNBC cases fall within the basal-like subtypes, such as Basal-Like-1 (BL1) and Basal-Like-2 (BL2) as well as the mesenchymal subtypes including Mesenchymal-Like (ML) and Mesenchymal/Stem-Like (MSL) categories (Wang et al., 2019). Additionally, two other subtypes exist: immunomodulatory (IM) and luminal androgen receptor (LAR) enriched tumors (Lehmann et al., 2011). Among these subtypes, ML and MSL are linked to poor survival outcomes, drug resistance and epithelial-to-mesenchymal transition (EMT) (Fedele et al., 2017).

TNBC is associated with a more aggressive phenotype, higher rates of metastasis, and poorer prognosis as compared to other subtypes of breast cancer (Griffiths and Olin, 2012). Treatment options for TNBC primarily rely on surgery, chemotherapy, and radiotherapy, which are linked to a variety of side effects (Cleator et al., 2007). In contrast, targeted therapy of TNBC has become increasingly popular in recent years, aiming to specifically target the molecular features of TNBC and improve treatment outcomes (Hwang et al., 2019). However, TNBC poses significant challenges due to several factors. Firstly, treatment options are limited for this subtype due to the absence of hormone-specific cell surface receptors. Currently, there are no approved targeted therapy to counter TNBC (Diana et al., 2020). Secondly, TNBC has a high risk of recurrence and metastasis, leading to poor long-term outcomes for patients (Chang-Qing et al., 2020). Thirdly, the heterogeneous nature of TNBC makes it difficult to predict treatment responses and tailor personalized therapies (Chang-Qing et al., 2020). Furthermore, TNBC is often associated

TH-3487_186106116

with a higher tumour burden, larger tumour size and a higher grade, which further contributes to the challenges in its treatment (Medina et al., 2020).

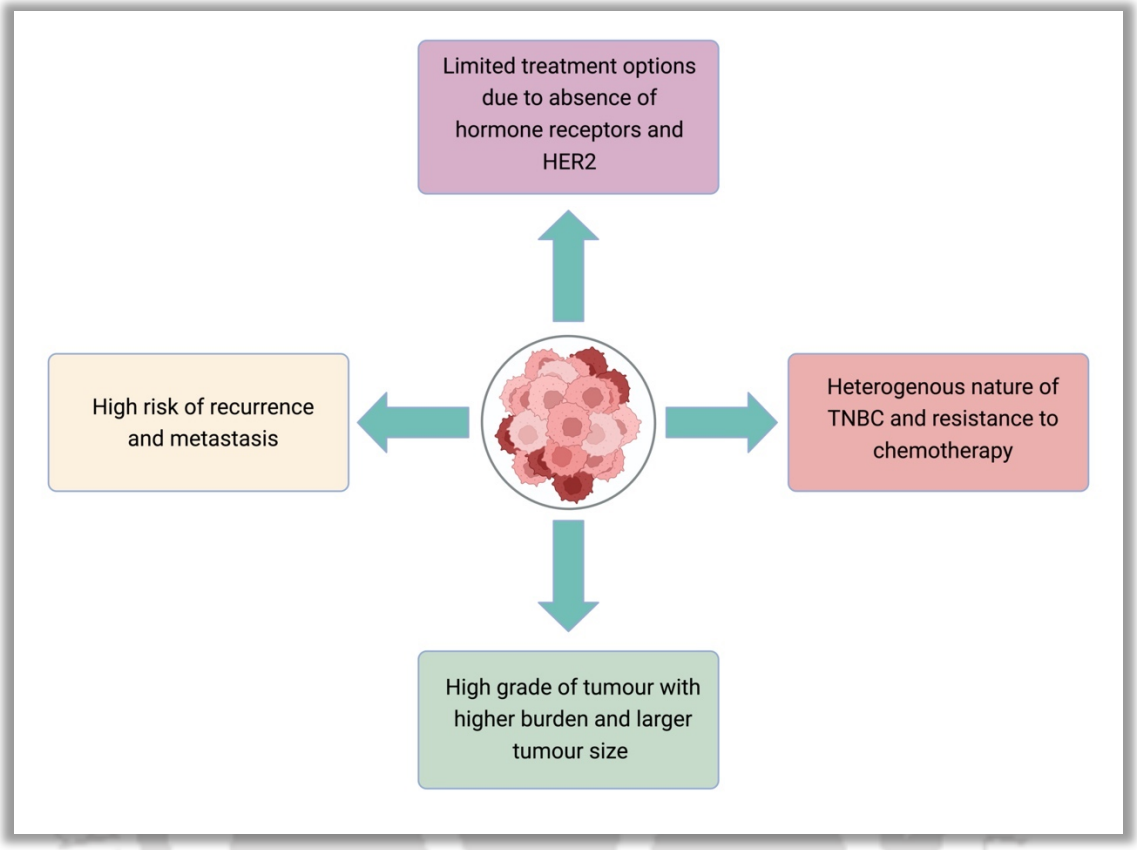

Scheme 1.2. Schematic depiction of the challenges involved in the treatment of triple-negative breast cancer (TNBC). [*Conceptualised and illustrated based on* (Chang-Qing et al., 2020; Diana et al., 2020; Medina et al., 2020; Telli and Ford, 2010) *using BioRender*]

Heterogeneity in breast cancer, particularly in triple-negative breast cancer (TNBC), significantly affects treatment responses and outcomes due to variations at the genomic, transcriptomic, and proteomic levels. TNBC includes distinct subtypes such as basal-like immune-activated (BLIA), which responds well to immunotherapy, and basal-like immune-suppressed (BLIS), which shows resistance. Proteomic studies further reveal subtype-specific vulnerabilities, such as DNA repair pathway alterations in mesenchymal TNBC, leading to chemotherapy resistance. This complexity underscores the need for multi-omic profiling to guide personalized treatment strategies and improve clinical trial

TH-3487_186106116

designs, allowing for more effective, targeted therapies (Asleh et al., 2022; Guo et al., 2023).

Despite the challenges, there have been some advancements in therapy. Researchers have identified several biomarkers that may act as therapeutic targets for TNBC, including DNA repair proteins, immune checkpoint molecules and growth factor receptors (Lu et al., 2023). Researches have demonstrated that targeting Wnt signaling in TNBC via specific inhibition of fizzled receptor (a known receptor of Wnt) ultimately leads to the inhibition of cell proliferation and induction of apoptotic cell death (Bilir et al., 2013; Uttarkar et al., 2023), projecting targeted therapy as an emerging treatment option against TNBC. Clinical trials are currently under evaluation to determine the efficacy of targeted therapies in TNBC (Chang-Qing et al., 2020). Additionally, immunotherapy has also shown promise in the treatment of TNBC, with studies demonstrating positive responses in some patients (Sivaganesh et al., 2021). Overall, the severity of TNBC and the challenges in its treatment are evident. Additionally, developing resistance to conventional chemotherapy is another significant obstacle in TNBC treatment (Telli and Ford, 2010). Further research and clinical trials are required to develop more effective therapeutic strategies to counter TNBC and improve patient outcomes. The lack of specific targeted therapies, the high risk of recurrence and metastasis, the heterogeneity of the disease and the larger tumour burden all contribute to the severity of TNBC and the challenges in its treatment are driven by the need for more effective and personalized therapeutic strategies.

1.5. Epithelial to mesenchymal transition (EMT) in TNBC pathogenesis

Several studies have suggested that the existence of EMT is correlated to heightened tumor aggressiveness and metastatic capability in TNBC (Fedele et al., 2017). EMT refers to a cellular mechanism where epithelial cells adopt traits typical of mesenchymal cells, resulting in enhanced capabilities of invasion and migration (Bae et al., 2015). In the investigation conducted by Jang M. et. al., the expression of EMT associated markers were assessed in TNBC along with corresponding transcription factors. The findings have revealed increased expression of mesenchymal markers like vimentin, osteonectin, smooth muscle actin, and ZEB1 and reduced expression of epithelial marker E-cadherin, suggesting the occurrence of EMT in TNBC (Jang et al., 2015).

TH-3487_186106116

The EMT phenomenon proposes that with reduced expression of epithelial markers, TNBC cells adopt mesenchymal characteristics, enabling them to invade tissues, enter the blood stream and survive during transit to establish secondary tumors in distant locations (Greenburg and Hay, 1982; Hay, 1995), a phenomenon known as metastasis. Despite significant progress in diagnosis and treatment, metastasis continues to be the primary cause of deaths related to breast cancer (Siegel et al., 2021). The role of EMT in TNBC is crucial because it allows cancer cells to spread from the primary tumour site to other parts of the body, forming new, secondary tumours that are often more difficult to treat and are associated with poorer patient outcomes.

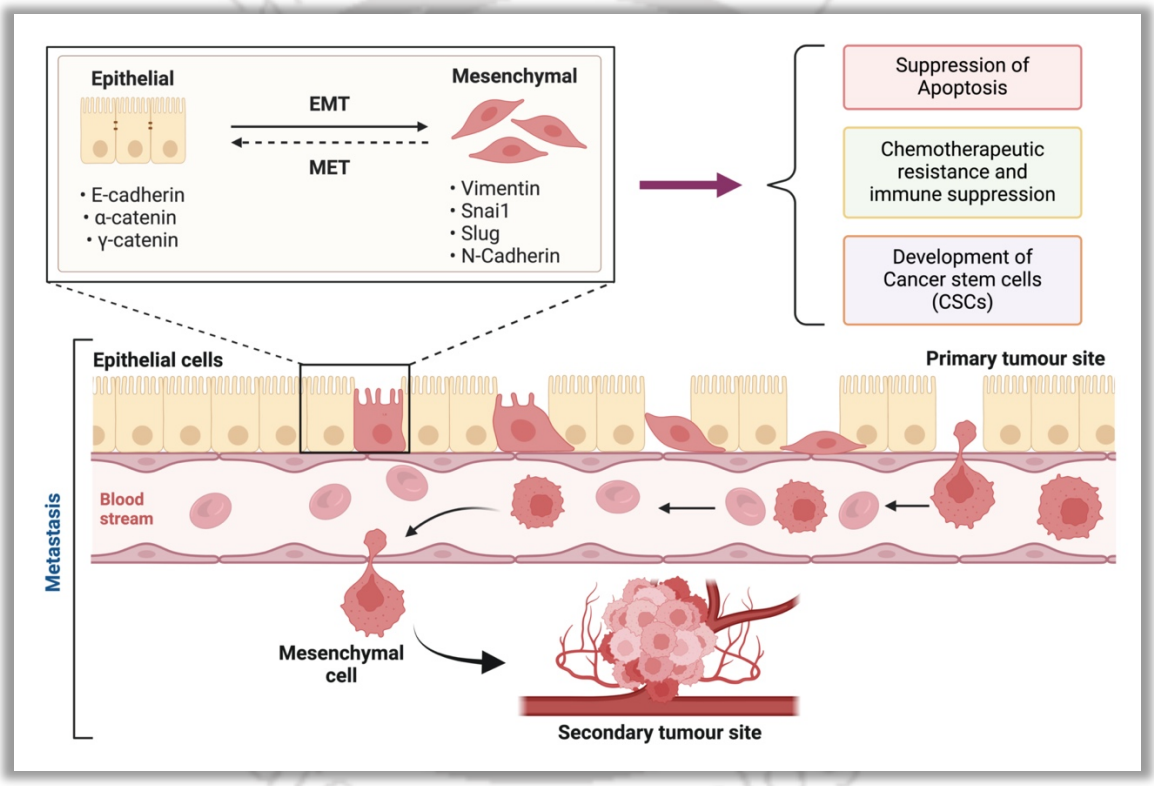

Scheme 1.3. Schematic representation of the role of EMT in cancer pathogenesis, highlighting its involvement in metastasis and other cellular events. [*Conceptualised and illustrated based on* (Bae et al., 2015; Lu and Kang, 2019; Song et al., 2018) *using BioRender*]

The role of EMT is not only limited to promoting cancer invasiveness and metastasis but also involved in suppression of apoptosis, which is the programmed cell death that normally

TH-3487_186106116

helps to regulate cell growth and eliminate damaged cells. This suppression occurs through the modulation of p53 pathway, a key regulator of cell cycle and apoptosis, or by suppressing proapoptotic genes, like BCL2L11/BIM (Hill et al., 2013; Song et al., 2018). By evading apoptosis, TNBC cells can survive longer and resist treatments that would typically induce cell death, contributing to the cancer's aggressiveness and resistance to therapy.

Furthermore, a hallmark of EMT is the weakened transition from G1 phase to S phase of the cell cycle. This weakened transition makes cancer cells less responsive to genotoxic stresses and therapies aimed at inhibiting proliferation (Marcucci et al., 2016). Genotoxic therapies, which damage the genetic material of cancer cells to prevent their replication, are less effective against cells that have undergone EMT because these cells have adapted mechanisms to bypass such damage and continue to proliferate.

Considering the detrimental characteristics associated with epithelial-mesenchymal transition (EMT), directing therapeutic efforts towards its inhibition or reversal may be beneficial in managing TNBC. Targeting EMT has the potential to reduce the invasiveness and metastatic capabilities of TNBC cells, thereby increasing their susceptibility to conventional therapies and improving overall patient outcomes. Various therapeutic strategies are under investigation, including the use of small molecule inhibitors, monoclonal antibodies and other agents that can disrupt the signaling pathways involved in EMT. A deeper understanding of the mechanisms underlying EMT and the development of targeted therapies to inhibit this process could significantly influence the management and prognosis of TNBC. This approach could lead to the creation of more effective treatments that specifically address the aggressive and resistant nature of TNBC, ultimately enhancing survival rates and quality of life for patients afflicted by this challenging form of breast cancer. The ongoing research in this area shows promise for the future of TNBC treatment, offering hope for more targeted and effective therapeutic options.

1.6. Notch signaling in TNBC pathogenesis

The involvement of notch signaling in TNBC has been explored extensively by several researches. The Notch signaling pathway, known for its high conservation, serves a vital

TH-3487_186106116

function in numerous cellular activities such as development and maintaining tissue homeostasis (Gozlan and Sprinzak, 2023), cancer stem cell renewal, proliferation, angiogenesis and EMT (Miele et al., 2006). Dysregulation of Notch signaling has been detected in several cancer forms, including breast cancer (Bai et al., 2020). TNBC, in particular, displays aberrantly heightened Notch signaling activity. Elevated expression of the Notch receptors is strongly associated with the aggressive invasive behavior, drug resistance and metastasis in TNBC (Giuli et al., 2019; Zhong et al., 2016).

Numerous studies have linked Notch-1 signaling to TNBC (Speiser et al., 2012), with specific emphasis on the BL1 and MSL subtypes that exhibit elevated expression of the Notch1 receptor (C. W. Lee et al., 2008; Zhang et al., 2015), which is closely associated with unfavorable tumor outcomes. Furthermore, a correlation has been established between the presence of Notch1 receptor and prognostic factors associated with metastatic breast cancer. The detection of Notch1 in tumour tissue has shown significant associations with the TNBC subtype, increased metastatic potential, tumour-node-metastasis (TNM) stages and the presence of ALDH1, a recognized cancer stem cell marker (CSCs) (Zhong et al., 2016). *In vitro* researches have provided evidences supporting the oncogenic function of Notch2 signaling, as demonstrated by the inhibition of cell migration and reduced viability of cancer stem cells, upon Notch2 knockdown (Chao et al., 2014; Kim et al., 2012).

Interestingly, earlier findings indicated that altered expression of Notch3 triggers cancer progressing events across various subtypes of TNBC. Specifically targeting Notch3 impedes tumour growth, whereas its activation is associated with malignant phenotypes, enhanced proliferation and the upregulation of the c-myc oncogene, defining a Notch signature (Choy et al., 2017). Moreover, Xue et. al. has demonstrated that Jagged1 and Notch3 are notably more abundant in TNBC than in other subtypes of breast cancer. Their expression correlates with more aggressive clinicopathological features as well as worse prognosis (Xue et al., 2017), consistent with earlier research findings (Cohen et al., 2010). Researchers have also noted a correlation between Notch4 and metastasis in TNBC. They observed elevated expression of Notch4 in metastatic cells through an analysis of the transcriptomic profile of patient derived TNBC xenografts (Lawson et al., 2015). Consistent with these discoveries, Notch4 expression was associated with an overall

TH-3487_186106116

unfavourable prognosis. Experimental evidence suggests that Notch4 promotes tumour invasion and metastasis by maintaining EMT in primary tumours (Castro et al., 2015).

Conclusively, the collective findings emphasize the critical importance of Notch signaling in the progression of TNBC. Notch receptors, notably Notch1, Notch2, Notch3, and Notch4, play significant roles in various aspects of TNBC, including cell proliferation, invasion, metastasis, and resistance to therapy. The correlation between elevated Notch receptor expression and poor clinical outcomes suggests that Notch signaling is a key driver of the aggressive behaviour observed in TNBC. This emphasizes the therapeutic potential of targeting Notch signaling pathways in TNBC. By inhibiting Notch signaling, it would be possible to reduce the migratory and invasive properties of TNBC cells, thereby improving patient outcomes. The ongoing research in this field is promising, offering hope for more effective and targeted therapeutic strategies against this challenging form of breast cancer.

1.7. The intricate relationship between Notch signaling and EMT

Notch signaling is frequently implicated in the enhancement of invasiveness and metastatic tendencies in breast cancer cells through the process of epithelial to mesenchymal transition (EMT). Activation of Notch signaling in non-metastatic breast cancer cells stimulates migration and invasiveness, while its suppression in metastatic cells results in reduction of these potential (Bolós et al., 2013; Lai et al., 2017; Leontovich et al., 2018). Suppression of Notch signaling also induces the typical cobblestone-to-spindle cell morphology transition linked to EMT, along with a switch in associated markers (Shao et al., 2015; J. Zhang et al., 2016). Furthermore, Notch signaling is associated with *in vivo* metastasis (Kontomanolis et al., 2014) through upregulation of Notch3, Notch4 and JAG1 in the metastatic cells compared to the primary tumour cells based xenografts (Lawson et al., 2015).

On the mechanistic level, Notch triggers EMT by activating Snail and Slug, the transcriptional regulators responsible for downregulating E-cadherin (Leong et al., 2007; Martin et al., 2005; Shao et al., 2015). Additionally, *in vivo* suppression of Notch4 leads to the reduced size of metastatic MDA-MB-231 xenograft, coinciding with the reinstatement

TH-3487_186106116

of E-cadherin expression, deactivation of β-catenin and reduction in Slug expression (Leong et al., 2007). Researches have indicated that Notch1 is intricately associated with EMT in TNBC, as a result of targeted inhibition by miRNA-3178 (a downregulated inhibitory miRNA in TNBC) and is also involved in EMT by Snail regulation (Kong et al., 2018).

Notch signaling is additionally involved in a reciprocal interaction with the mesenchymal marker ZEB1. Silencing ZEB1 supresses Notch activity, leading to reduced expression of HEY1, MAML2/3 and JAG1 expression, achieved through the derepression of miRNA-200. Elevated ZEB1 expression is frequently associated with increased JAG1 expression and heightened Notch activity in invasive regions of primary TNBC tumours (Brabletz et al., 2011). These interactions emphasize the complexity and interdependence of Notch signaling pathway and EMT in driving TNBC progression.

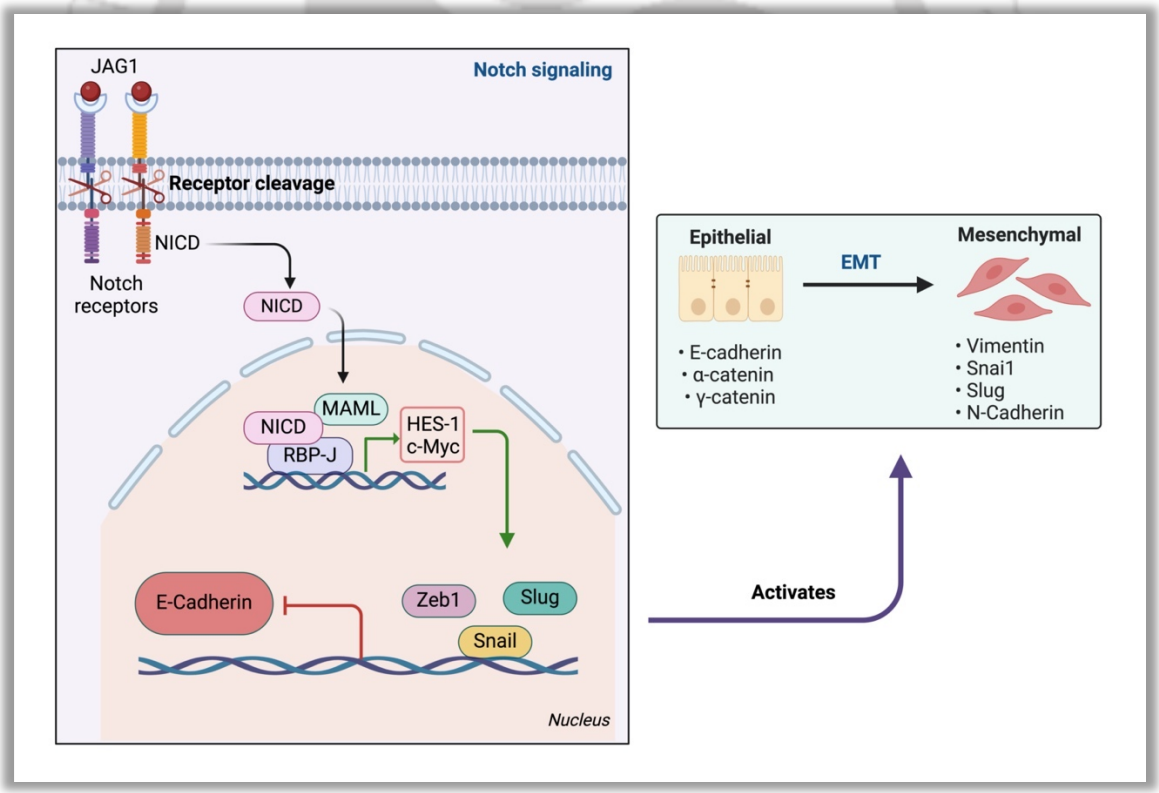

Scheme 1.4. Schematic illustration of Notch signaling mediated activation of EMT through activation of mesenchymal markers (Zeb1, Snail & Slug). [*Conceptualised and illustrated based on* (Leong et al., 2007; Shao et al., 2015; Zhou et al., 2022) *using BioRender*]

TH-3487_186106116

Therapeutic targeting of Notch signaling holds significant potential to yield substantial benefits by reversing epithelial-mesenchymal transition (EMT) in TNBC cells, thereby reducing their migratory and invasive characteristics. Inhibiting Notch signaling has the capacity to transform the aggressive phenotype of TNBC cells, rendering them less invasive and more responsive to conventional therapies. This strategic approach offers promise in improving patient outcomes by diminishing metastasis and augmenting the effectiveness of current treatments. Ongoing research endeavours actively explore diverse strategies to inhibit Notch signaling, encompassing the use of small molecule inhibitors, monoclonal antibodies, and other agents that disrupt the EMT-related signaling pathways.

Furthermore, gaining a comprehensive understanding of the intricate mechanisms underlying Notch signaling and its pivotal role in EMT provides a promising avenue for developing targeted therapies against TNBC. These initiatives are squarely aimed at addressing the inherently aggressive and treatment-resistant nature of TNBC, with the ultimate objective of enhancing survival rates and elevating the quality of life for patients grappling with this formidable type of breast cancer. As research continues to progress, the prospect of advancing more effective and personalized therapeutic options against TNBC grows increasingly feasible, offering renewed optimism for the improved management and treatment outcomes of this challenging disease.

1.8. Autophagy and its intricate relationship with EMT and Notch signaling

Autophagy, a highly conserved cellular process, involves the degradation and recycling of damaged organelles and proteins to maintain cellular homeostasis and function. It serves as a "double-edged sword" in tumours, either facilitating or inhibiting tumour development depending on various factors such as cell type, tissue context, and stage of the tumour. In some contexts, autophagy can provide the necessary nutrients and energy for rapidly growing tumour cells, thereby promoting tumour progression. However, in other contexts, autophagy can inhibit tumour growth by degrading damaged organelles and proteins that could otherwise contribute to cancer progression.

TH-3487_186106116

Studies have shown that activating autophagy through the regulation of the PI3K/AKT/mTOR signaling pathway can inhibit EMT in human ovarian and breast cancer cells (Zhou et al., 2015; Zi et al., 2015). Conversely, impairing autophagy can have the opposite effect. Studies have shown that silencing ATG5, ATG7, or BCN1 can increase cell motility and invasiveness in glioblastoma cells. This indicates that autophagy impairment can promote EMT and enhance the invasive potential of cancer cells (Catalano et al., 2015).

Autophagy plays a complex, dual role in cancer, acting as both a tumour suppressor and promoter depending on the stage of tumour development. In early tumorigenesis, autophagy suppresses tumour formation by removing damaged organelles and proteins, thereby maintaining cellular homeostasis and preventing genomic instability. Conversely, in established tumours, autophagy supports tumour survival by enabling cancer cells to endure stress conditions, such as nutrient deprivation and hypoxia, through recycling cellular components to maintain metabolism and energy production. This context-dependent role makes autophagy a key therapeutic target. Inhibition of autophagy may be effective in advanced cancers where it promotes tumour growth and therapy resistance, while enhancing autophagy could prevent tumour initiation. Developing targeted therapies to modulate autophagy based on tumour stage and context is critical for improving cancer treatment strategies (Amaravadi et al., 2019; Li et al., 2020).

Further insights into the mechanisms of autophagy reveal that the death effector domain-containing DNA-binding protein (DEDD) directly interacts with the autophagy-regulating complex PI3K/BCN1. This interaction induces the autophagy-mediated lysosomal degradation of SNAIL and TWIST and consequently reverses the EMT phenotype in breast cancer cells, shifting them back to a less invasive, epithelial state (Lv et al., 2012). Similarly, the activation of autophagy leads to the downregulation of EMT inducing transcription factors SNAIL and SLUG in glioblastoma cells. This alteration in the transcriptional program leads to the re-expression of epithelial markers and the reversal of the EMT phenotype (Catalano et al., 2015). Additionally, silencing CDH6 also reverses the EMT phenotype by decreasing the proliferation and migration of thyroid cancer cells. This effect is associated with the induction of autophagy and changes in mitochondrial

TH-3487_186106116

dynamics, further illustrating the complex interplay between autophagy and EMT (Gugnoni et al., 2017).

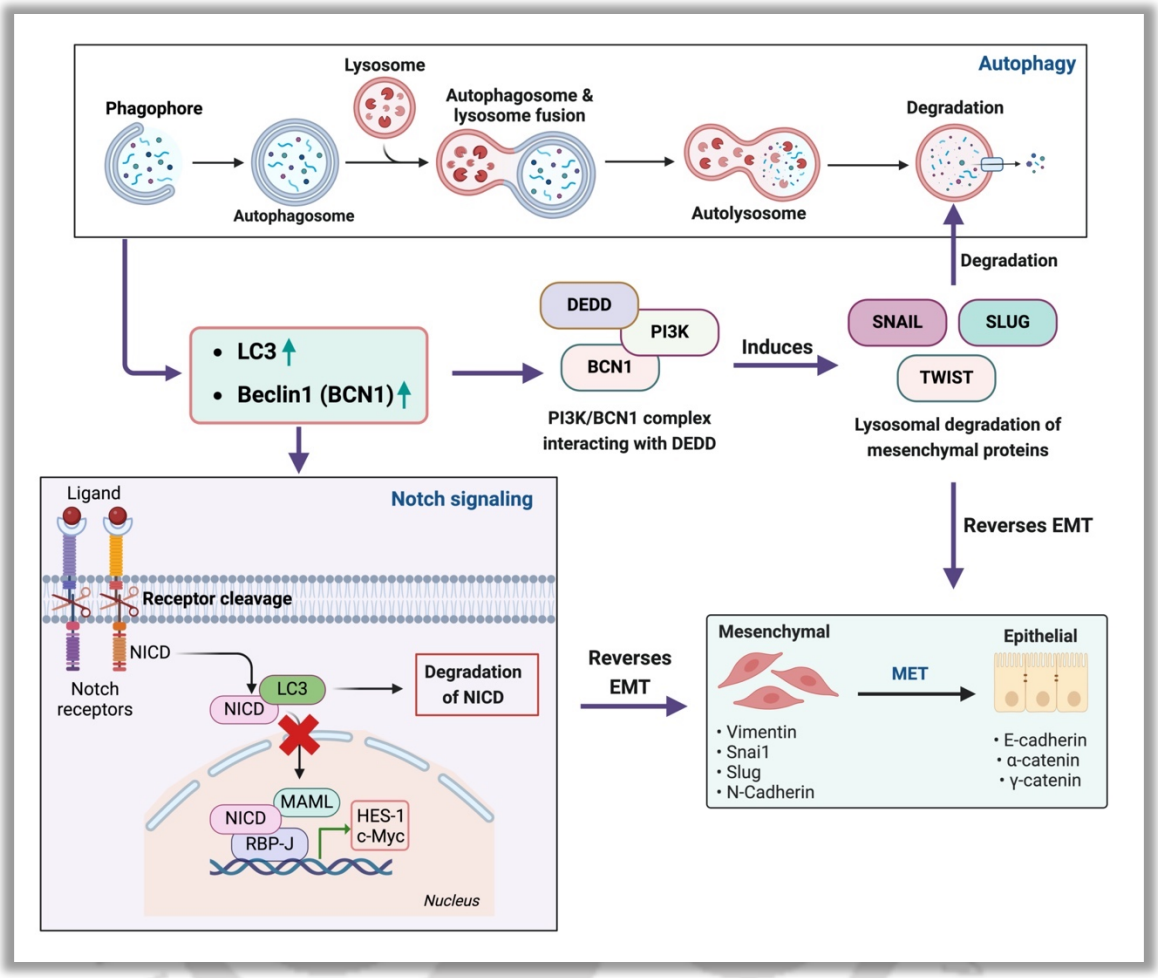

Scheme 1.5. Schematic depiction illustrating the intricate relationship between Autophagy, Notch signaling and EMT. [*Conceptualised and illustrated based on* (Catalano et al., 2015; Lv et al., 2012; Zada et al., 2022) *using BioRender*]

Research has shown that the activation of autophagy is crucial for the degradation of the Notch intracellular domain (NICD), a vital component of Notch-1 signaling. Notch-1 signaling is a key regulator of epithelial-mesenchymal transition (EMT) (Zada et al., 2022). Specifically, autophagy activation leads to the breakdown of NICD, disrupting the signaling pathway that facilitates EMT and subsequent metastasis. Additionally, the study demonstrated that LC3, an important autophagy protein, forms a complex with NICD,

TH-3487_186106116

SNAI1, and SQSTM1. This complex inhibits the nuclear translocation of NICD, reducing the transcriptional activity of Notch-1 target genes. Consequently, this suppression of Notch-1 signaling results in decreased cancer cell migration and invasion, suggesting a potential therapeutic target for mitigating metastasis (Zada et al., 2022).

Moreover, another study identified a significant correlation between the expression of Beclin-1, another key autophagy-related protein, and E-cadherin, a protein essential for maintaining epithelial cell integrity. Increased Beclin-1 expression is associated with higher levels of E-cadherin, indicating its role in preserving epithelial characteristics and inhibiting EMT (Qin et al., 2015). Conversely, decreased Beclin-1 expression is linked to poorer patient prognosis and shorter overall survival, highlighting its potential as a prognostic marker in cancer (Geng et al., 2012). These findings emphasize the complex interplay between autophagy and Notch signaling in cancer progression and suggest promising directions for therapeutic intervention.

The interplay between autophagy and EMT highlights the potential of regulating autophagy pathways as a therapeutic strategy in cancer treatment. By manipulating the autophagy process, it may be possible to inhibit EMT, thereby reducing the migratory and invasive properties of cancer cells. This approach offers a promising avenue for improving patient outcomes, particularly in aggressive cancers like TNBC that are resistant to conventional therapies. Understanding the mechanisms through which autophagy influences EMT provides valuable insights for developing targeted treatments. These treatments could not only inhibit the progression of EMT but also enhance the effectiveness of existing therapies by making cancer cells more susceptible to treatment.

Ongoing research in this area continues to explore various methods to modulate autophagy, including the use of small molecule inhibitors, genetic manipulation, and other agents that can influence the signaling pathways involved. The potential to reverse EMT through autophagy modulation represents a significant step forward in the fight against TNBC. This strategy holds promise for developing more effective and targeted therapeutic options, ultimately aiming to improve survival rates and the quality of life for patients facing this challenging form of breast cancer. As research advances, the intricate relationship between

TH-3487_186106116

autophagy and EMT will likely reveal new therapeutic targets and strategies. By focusing on these cellular processes, there is always a hope to create treatments that can better manage the aggressive behaviour of TNBC, reduce metastasis, and improve the overall prognosis for patients. The continued exploration of autophagy's role in cancer biology is critical for unlocking new avenues of treatment and enhancing the arsenal of tools available to combat this difficult-to-treat disease.

1.9. Current therapeutic landscape of breast cancer

The therapeutic landscape for breast cancer is multifaceted, comprising surgical procedures, chemotherapy, radiotherapy, endocrine therapy, targeted therapy, and immunotherapy. Effective management frequently requires a multidisciplinary approach, as surgical intervention is essential for non-metastatic breast cancer (Cardoso et al., 2019), while systemic treatments are generally the preferred option for metastatic cases (Senkus and Łacko, 2017).

- **Surgery:** For early invasive breast cancer, surgical options generally include breast-conserving surgery (BCS) and mastectomy, with the possibility of immediate reconstruction. Advances in systemic therapies have markedly decreased locoregional recurrence (LRR) and distant metastasis rates (Zumsteg et al., 2013), establishing BCS followed by radiotherapy as a standard treatment due to its favourable cosmetic results and its positive impact on life satisfaction (Cipora et al., 2018).

- **Chemotherapy:** Chemotherapy, administered both preoperatively and postoperatively, is designed to reduce tumour size to facilitate breast conservation and to lessen the necessity for extensive lymph node dissection (Mano and Awada, 2004). This approach is especially vital in managing triple-negative breast cancer (TNBC) and HER-2 positive breast cancer, where the aggressive nature of these diseases demands strong systemic control (Moo et al., 2018).

TH-3487_186106116

- **Radiotherapy:** Radiotherapy (RT) is crucial in decreasing locoregional recurrence (LRR) following breast-conserving surgery (BCS) (EBCTCG (Early Breast Cancer Trialists' Collaborative Group), 2014). Emerging techniques like hypofractionated RT and accelerated partial breast irradiation present shorter treatment durations while maintaining effectiveness (Haviland et al., 2013; Strnad et al., 2016). Research, such as the UK IMPORT LOW trial, has shown that these approaches yield results comparable to traditional whole-breast irradiation (Coles et al., 2017).

- **Endocrine therapy:** Endocrine therapy is essential for hormone receptor-positive breast cancer and is frequently combined with other treatments to reduce the risk of recurrence (Du et al., 2021). The administration of agents such as tamoxifen and aromatase inhibitors has significantly improved outcomes, especially in postmenopausal women (Early Breast Cancer Trialists' Collaborative Group (EBCTCG), 2011).

- **Targeted therapy:** Targeted therapies have transformed the treatment landscape for HER-2 positive breast cancers (Tolaney et al., 2017). Medications like trastuzumab and pertuzumab have demonstrated significant effectiveness in lowering recurrence rates and enhancing survival (Gianni et al., 2012). The continuous development of new agents is further broadening the range of therapeutic options aimed at the specific molecular targets.

- **Immunotherapy:** Immunotherapy is increasingly recognized as a promising treatment approach, particularly for triple-negative breast cancer (TNBC). Immune checkpoint inhibitors such as pembrolizumab have exhibited promising outcomes in clinical trials, offering a new outlook for patients with this aggressive breast cancer subtype (Nanda et al., 2016). Furthermore, ongoing research into innovative treatments like gene therapy, vaccines, and adoptive cell therapies such as CAR-T is showing encouraging results (NCT04430595). These strategies aim to leverage the body's immune response and genetic manipulation for more targeted and effective cancer treatment.

TH-3487_186106116

The ongoing advancement of breast cancer treatment highlights the critical role of multidisciplinary and personalized approaches in optimizing patient outcomes. Future research and clinical trials are anticipated to further refine these strategies, ultimately improving survival rates and enhancing the quality of life for individuals affected by breast cancer.

1.10. Natural products as anticancer agents

Natural medicine, sourced from plants, insects, animals, aquatic organisms, and microorganisms, is essential in drug development due to its pharmacological properties. Historically, natural products have been used to treat diseases and remain highly valuable in contemporary drug discovery. Between January 1981 and September 2019, 32% of approved small-molecule drugs were derived from natural products or their derivatives (Newman and Cragg, 2020). Furthermore, from 1981 to 2014, 51% of the 1211 newly approved small molecule drugs globally originated from natural products (Newman and Cragg, 2016). The FDA approved 547 natural products for medications from 1827 to 2013, predominantly for treating cancer, bacterial infections, and hypertension (Patridge et al., 2016).

Natural products offer significant potential as adjuncts to conventional therapies, particularly in aggressive cancers like triple-negative breast cancer (TNBC), by enhancing therapeutic efficacy, modulating the tumour microenvironment, and reducing adverse effects. These bioactive compounds, including polyphenols, flavonoids, and alkaloids, can synergize with chemotherapy and immunotherapy by improving immune responses, targeting multiple oncogenic pathways, and overcoming drug resistance. Their immunomodulatory effects help counteract tumour-induced immunosuppression, while their ability to mitigate side effects like cardiotoxicity makes them valuable in personalized medicine. Integrating natural products into cancer treatment strategies holds promise for more effective, tailored therapies that account for individual patient profiles (Ghosh et al., 2024; Kan et al., 2023).

TH-3487_186106116

Plants, with over 350,000 species, represent a significant source of biologically active compounds such as terpenes, alkaloids, and flavonoids. These compounds have been instrumental in treating various diseases and are particularly valued for their structural diversity and complexity, which provide unique scaffolds for drug development (Cadoná et al., 2022; Priya and Satheeshkumar, 2020). Phytochemicals, like berberine, are extensively researched for their anticancer properties. Berberine, commonly found in the roots, rhizomes, and stem barks of Chinese herbs and plants of the Berberis genus, has demonstrated beneficial biological activities against a variety of human diseases, including inflammation, metabolic dysfunction, depression, cardiovascular diseases, neurodegenerative diseases, and different types of cancers (Šudomová et al., 2021). Compared to synthetic molecules, natural products offer a broader range of scaffolds and greater structural complexity, advantageous for drug discovery (Atanasov et al., 2021). They are particularly important for oral drugs that surpass Lipinski's rule of five. Taxol, derived from the Pacific yew tree (*Taxus brevifolia*), and vincristine, sourced from the Madagascar periwinkle (*Catharanthus roseus*), are prominent examples of plant-based drugs that have made significant contributions to cancer therapy (Dey et al., 2020). Natural products aid in chemoprevention and chemotherapy by inhibiting cell proliferation and disrupting tumorigenic pathways. They effectively suppress cell proliferation, regulate the cell cycle, and interfere with several tumorigenic signaling pathways, such as phosphoinositide 3-kinase (PI3K), matrix metalloprotease (MMP), MAPK/ERK, toll-like receptor (TLR), and AKT pathways. Additionally, natural products may stimulate DNA repair mechanisms through the action of gene products like p21, p27, p51, and p53, leading to the synthesis of protective enzymes such as caspases and the modulation of antioxidant enzymes (Găman et al., 2020).

The traditional utilization of natural products offers valuable insights into their efficacy and safety. Their extensive range of bioactive compounds encompasses a broader chemical space than conventional synthetic small molecule libraries. Natural products play a crucial role in drug development, presenting unique and complex molecular structures that are challenging to replicate synthetically. Ongoing exploration and application of these natural compounds hold significant promise for future drug discovery and development, especially in treating cancer and other severe diseases.

TH-3487_186106116

1.11. Microbial metabolites as anticancer agents

For more than a century, microorganisms have played a crucial role in drug discovery. The discovery of penicillin from various *Penicillium sp.* in the 20th century spurred the screening of numerous bacterial and fungal strains, leading to a significant increase in life expectancy. The vast diversity of microbial species has resulted in the identification of approximately 22,500 bioactive compounds, facilitating advancements in therapeutics beyond antibiotics (Bérdy, 2005). Microbial metabolites, categorized as primary or secondary, possess extensive therapeutic applications. Primary metabolites are vital for essential cellular processes (Horak et al., 2019), while secondary metabolites offer ecological advantages and serve as a rich source for antibiotics, antivirals, analgesics, and novel anticancer therapies, inspiring the development of many synthetic therapeutics (Mohan et al., 2022).

1.11.1. Bacterial metabolites

By 1990, biologically active natural products formed a substantial part of the pharmaceutical landscape, including numerous bacterial metabolites with antineoplastic properties. Recognized for their potent cytotoxic effects, these compounds have become indispensable in modern cancer treatment. This section provides a comprehensive review of the mechanisms of action and toxicities associated with several critical anticancer agents of bacterial origin: DNA intercalators (actinomycin D, inotuzumab ozogamicin), topoisomerase II inhibitors (doxorubicin), DNA crosslinkers (mitomycin C), proteasome inhibitors (carfilzomib), nucleoside analogs (pentostatin), and DNA free radical inducers (bleomycins).

- **DNA intercalators:** DNA intercalating agents are pivotal in cancer therapy as they disrupt essential cellular processes. Actinomycin D, derived from *Streptomyces parvulus*, functions as an antineoplastic antibiotic used to treat cancers such as Wilms' tumour and testicular cancer (Koba and Konopa, 2005). Its mechanism involves intercalation into DNA, which inhibits RNA polymerase activity and subsequently impedes RNA synthesis, particularly affecting cancer cells characterized by heightened transcription rates (Hollstein, 1974). Despite its effectiveness, its clinical utility is hindered by severe side effects such as

TH-3487_186106116

myelosuppression and gastrointestinal ulceration (COOPER and BRAVERMAN, 1977). Conversely, Inotuzumab ozogamicin, an antibody-drug conjugate targeting B-cell malignancies via CD22 binding, delivers the cytotoxic antibiotic ozogamicin. This induces DNA double-strand breaks that trigger apoptosis in cancer cells. However, its use carries risks such as liver toxicity, notably hepatic veno-occlusive disease (George et al., 2016; Shor et al., 2015).

- **Topoisomerase-II inhibitors:** Topoisomerase II inhibitors are pivotal in cancer treatment. Doxorubicin, an anthracycline antibiotic derived from *Streptomyces peucetius*, serving as a prominent example. It is widely used across various cancers such as breast, lung, gastric, ovarian, thyroid, lymphoma, myeloma, sarcoma, and pediatric cancers (Thorn et al., 2011). Upon forming a complex with the proteasome in the cytoplasm, doxorubicin enters the nucleus where it intercalates into DNA and stabilizes Topoisomerase II-DNA complexes, effectively hindering DNA repair mechanisms (van der Zanden et al., 2021). Furthermore, the quinone structure of doxorubicin induces apoptosis by generating reactive oxygen species (ROS), leading to lipid peroxidation and DNA damage (van der Zanden et al., 2021). Despite its efficacy, doxorubicin's clinical application is hampered by significant dose-related toxicities, including cardiomyocyte apoptosis, acute cardiotoxicity, myelosuppression, neutropenic enterocolitis, and alopecia (Zhao and Zhang, 2017).

- **DNA crosslinkers:** DNA crosslinkers are pivotal in cancer treatment, as demonstrated by Mitomycin C (MMC), derived from *Streptomyces caespitosis* (Tomasz, 1995). MMC functions as a potent antibiotic in bacteria by inducing cell death through crosslinking DNA strands (Tomasz, 1995). In cancer cells, MMC undergoes reductive activation in the cytosol, facilitated by NRF2 in KEAP1-KO cancer cells (Baird and Yamamoto, 2021). It forms covalent bonds with DNA at positions C1 and C10, primarily crosslinking adenine and guanine residues (Baird and Yamamoto, 2021). This impedes DNA synthesis, resulting in cell cycle arrest and apoptosis (Tomasz, 1995; Verweij and Pinedo, 1990). MMC also suppresses

TH-3487_186106116

RNA synthesis and protein translation at higher concentrations (Snodgrass et al., 2010). Its ability to be activated under hypoxic conditions allows selective toxicity against tumours while sparing oxygenated noncancerous tissues (Tomasz, 1995). MMC is particularly effective in treating bladder, breast, anal, and gastrointestinal cancers (Sinawe and Casadesus, 2024).

- **Proteasome inhibitors:** Proteasome inhibitors are pivotal in cancer treatment, demonstrated by carfilzomib, a tetrapeptide epoxyketone analogue of epoxomicin sourced from Actinomyces strain No. Q996-17 (HANADA et al., 1992). Specifically indicated for relapsed or refractory multiple myeloma, carfilzomib binds irreversibly to the 20 S proteasome through its peptide-binding domain and epoxyketone pharmacophore, inhibiting the catalytic threonine on the β5 subunit (Jayaweera et al., 2021). This inhibition induces cell death by promoting the accumulation of typically degraded proteins, activating apoptotic pathways involving Bak, Bax, stabilizing p53 and arresting the cell cycle through cyclin inhibitors like p21 and p27 (Jayaweera et al., 2021; Khan and Badros, 2012). Clinical usage is associated with side effects including hypertension, dyspnea, neuropathy, cardiac complications, and renal issues in specific treatment protocols (Jayaweera et al., 2021).

- **Nucleoside analogues:** Nucleoside analogues play a crucial role in cancer treatment, demonstrated by pentostatin, sourced from *Streptomyces antibioticus* (Johnston, 2011). Pentostatin structurally resembles adenosine but includes modifications such as a 7-membered purine ring and a hydroxyl group in place of an amino group (Johnston, 2011). It enters cells via nucleoside transporters hENT1 and hENT2 (Pastor-Anglada and PÃ©rez-Torras, 2015), where it inhibits adenosine deaminase (ADA), an enzyme pivotal in adenosine metabolism (Johnston, 2011). This inhibition increases intracellular levels of adenosine and deoxyadenosine, leading to the conversion of deoxyadenosine to deoxyadenosine triphosphate (dATP) (Johnston, 2011). Elevated dATP levels inhibit ribonucleotide reductase, disrupting nucleotide synthesis and arresting DNA and RNA

TH-3487_186106116

production, ultimately inducing cell death (Johnston, 2011). Pentostatin's selective action in the S-phase of the cell cycle is crucial for treating hairy cell leukemia (Johnston, 2011). Moreover, it synergizes effectively with cyclophosphamide and rituximab in chronic lymphocytic leukemia, enhancing treatment efficacy with minimal adverse effects (Lamanna et al., 2006).

- **DNA free radical inducers:** DNA free radical inducers are pivotal in cancer treatment, as seen in bleomycins derived from *Streptomyces verticullis* (Mohan et al., 2022). These glycopeptide antibiotics possess functional domains such as metal-binding, DNA-binding and carbohydrate domains. Combinations like bleomycin A2 and B2 are clinically effective against ovarian cancer, head and neck squamous cell carcinomas, testicular cancer, Hodgkin's and non-Hodgkin's lymphoma (Priyanka Vegesana, 2023). Administered intravenously, bleomycins bind Cu+ in serum to form a bleomycin-Cu(II) complex, aiding cellular uptake, although the specific transporter remains unidentified (Dorr, 1992). Inside the nucleus, bleomycin exchanges Cu(II) for Fe(II), forming an activated bleomycin-Fe(II) complex that induces DNA breakage by abstracting C4' hydrogen atoms from pyrimidine nucleotide deoxyribose, thereby inhibiting DNA synthesis (Dorr, 1992). Despite their efficacy, pulmonary toxicity limits bleomycins' use, affecting approximately 10% of patients with manifestations ranging from pneumonitis to pulmonary fibrosis (Priyanka Vegesana, 2023).

1.11.2. Fungal metabolites

Fungi are prolific producers of secondary metabolites characterized by diverse structures and biological activities, including anticancer properties. These metabolites arise from various biosynthetic pathways and are classified into different compound families such as amino acids, polyketides, alkaloids, anthraquinones, terpenes, non-ribosomal peptides and others. Numerous fungal metabolites hold significant potential for applications in agriculture, food chemistry, cosmetics, pharmacology, and medicine.

Fungi can be majorly categorized into toxigenic and endophytic microorganisms. Toxigenic fungi are known to produce toxins that cause severe diseases in humans, plants,

TH-3487_186106116

and other organisms, whereas endophytic fungi do not produce toxins. The subsequent section is dedicated to discuss anticancer metabolites synthesized by terrestrial toxigenic fungi, with a particular emphasis on those produced by plant pathogens.

- **Anticancer metabolites by toxigenic fungi:** Anticancer metabolites produced by toxigenic fungi present significant potential for the development of novel cancer therapies. Among these, notable compounds include fischerindoline and its analogs from *Neosartorya pseudofischeri*, which have demonstrated substantial growth inhibition when tested against six cancer cell lines (Masi et al., 2013). Eurochevalierine from *Eurotium chevalieri* has exhibited cytostatic activity and the capacity to inhibit sirtuins, impacting cancer cell proliferation without affecting healthy cells (Kanokmedhakul et al., 2011). Similarly, Higginsianins A and B, synthesized by *Colletotrichum higginsianum*, show strong antiproliferative activity against various cancer cell lines, with additional derivatives also exhibiting significant cytotoxicity (Cimmino et al., 2016). Chlorogenic acid from *Sclerotium rolfsii* has been proven effective in reversing multidrug resistance and inhibiting lymphoma cell proliferation (Ahmad et al., 2017). Cyclodepsipeptides, including beauvericins and enniatins from *Fusarium sp.* and other fungi, demonstrate promise for antimicrobial and anticancer applications (Urbaniak et al., 2020). Furthermore, radicinin from *Cochlobolus australiensis*, tested against three human cancer cell lines, has shown promising toxicity, with synthetic derivatives confirming its essential structural features for anticancer activity (Mathieu et al., 2022). Massarilactones D and H from *Kalmusia variispora*, associated with grapevine trunk diseases, have demonstrated both phytotoxicity and cytotoxicity, with massarilactone H showing notable anticancer activity (Teponno et al., 2017). These findings highlight the potential of these fungal metabolites for developing new anticancer therapies, despite challenges such as low natural yields.

- **Anticancer metabolites by endophytic fungi:** Anticancer metabolites derived from endophytic fungi show significant potential for advancing cancer treatment. For instance, pestheic acid, a chlorinated diphenylic ether produced by

TH-3487_186106116

Pestalotiopsis guepinii found in *Virola michelii*, exhibited cytotoxic, cytostatic, and genotoxic effects against gastric adenocarcinoma cells, albeit with moderate potency (Sousa et al., 2013). Helicascolide F and talaromydine from *Talaromyces assiutensis* demonstrated moderate inhibition of various cancer cell lines (Li et al., 2022). *Epicoccum sorghinum* yielded episorin A and other compounds with notable antifungal and cytotoxic properties (against cancer cells) (Wang et al., 2022). Metabolites from *Aspergillus terreus* displayed potent inhibition of acetylcholinesterase and cytotoxicity against cancer cells (Deng et al., 2013). Chrysotriazoles A and B derived from *Penicillium chrysogenum*, along with Conioazasterol and S-dehydroazasirosterol from *Coniothyrium cereale*, exhibited moderate cytotoxic effects against cancer cells (An et al., 2013; Elsebai et al., 2016). *Eurotium chevalieri*-derived metabolites suppressed neuroblastoma cell migration, particularly dihydroauroglaucin (Kanokmedhakul et al., 2011). Chrysin, a versatile flavonoid compound, demonstrated anticancer effects by inducing apoptosis in various human cells and rat models (Salari et al., 2022). These findings underscore the diverse therapeutic potential of fungal metabolites, despite challenges such as low yields.

1.12. Entomopathogenic fungi as a potential source of anticancer agents

Entomopathogenic fungi, recognized for their capability to infect and thrive on insect hosts, have attracted considerable scientific interest for their potential as a source of bioactive agents. These fungi synthesize a wide variety of bioactive proteins and secondary metabolic compounds with significant medicinal properties. Notably, their anticancer effects are of particular interest, as these compounds have been shown to induce apoptosis, inhibit cell proliferation, and disrupt the cell cycle in cancer cells. This distinctive ability positions entomopathogenic fungi as a promising resource for the development of novel anticancer therapies.

1.12.1. Bioactive proteins from entomopathogenic fungi

Entomopathogenic fungi produce a diverse range of extracellular enzymes, such as chitinase, protease, and lipase, which enable them to degrade the structural components of their insect hosts and thrive (Hasan et al., 2013). These lytic enzymes break down

TH-3487_186106116

the insect's exoskeleton and thereby, facilitates nutrient absorption (Hasan et al., 2013). In addition to these enzymes, these fungi also synthesize protein-based toxins, including fungal ribotoxins, which serve to incapacitate their hosts and defend against competing microorganisms. These toxins disrupt vital cellular processes in the insect, ensuring their survival and proliferation in a competitive environment.

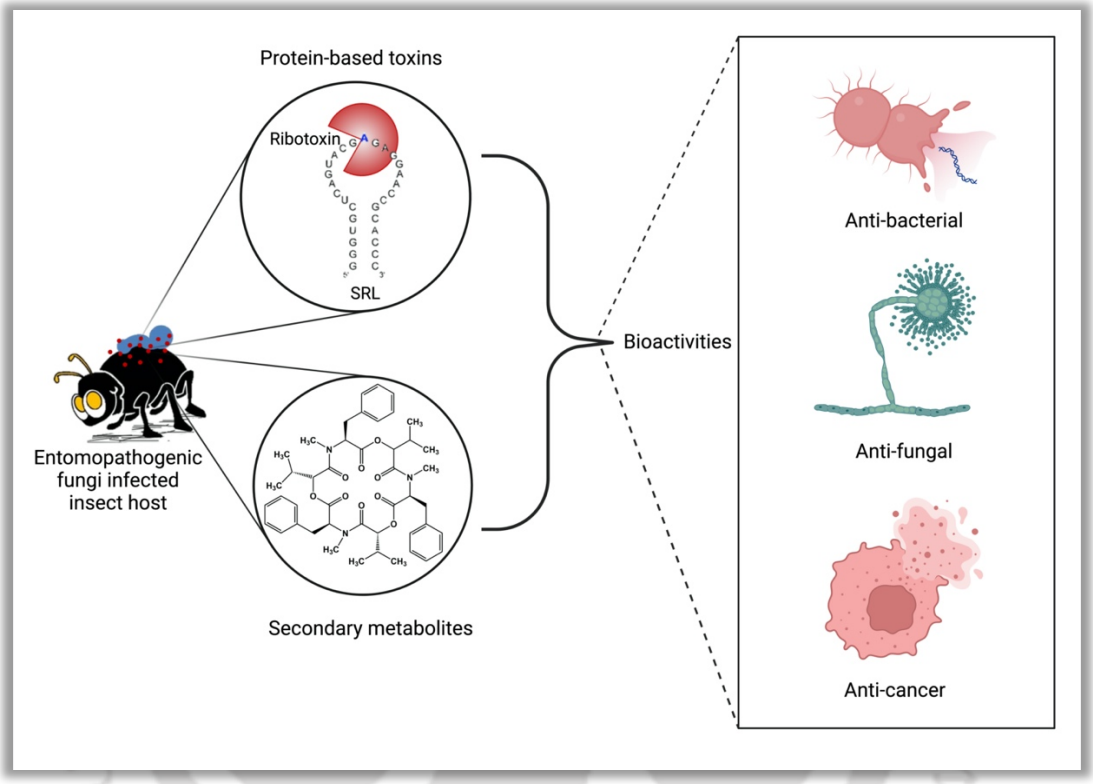

Schematic 1.6. Schematic depiction illustrating entomopathogenic fungi producing both protein-based and non-protein-based toxins offering several bioactivities. [*Conceptualised and illustrated based on* (Litwin et al., 2020) *using BioRender*]

1.12.1.1. Fungal ribotoxins

Fungal ribotoxins are extracellular ribonucleases synthesized by a wide variety of endophytic fungi, including entomopathogenic species (Brandhorst and Kenealy, 1992; Liu et al., 1995; Olombrada et al., 2017; Turnay et al., 1993; Yuan et al., 2020). Unlike other non-specific ribonucleases, these ribonucleases can specifically recognize and cleave the universally conserved sarcin-ricin loop (SRL) present in the 28S and 23S rRNA of the large ribosomal subunits in both eukaryotic and prokaryotic ribosomes.

TH-3487_186106116

This is accomplished by cleaving a single phosphodiester bond between the G4325 and A4326 residues in 28S rRNA and between the G2661 and A2662 residues in 23S rRNA (Endo and Wool, 1982; Hausner et al., 1987), although higher concentrations are necessary to inactivate the prokaryotic ribosomal subunit (Sanz and Amils, 1984).

1.12.1.1.1. Mechanism of action of fungal ribotoxins

Ribotoxins facilitate RNA cleavage through a precise two-step mechanism involving transphosphorylation and hydrolysis. In the initial transphosphorylation step, ribotoxins create a break in the RNA strand, resulting in the formation of a 2',3'-cyclic phosphate intermediate. This intermediate is crucial for the subsequent hydrolysis step, wherein ribotoxins remove the 2' phosphate linkage. This process culminates in the formation of a 3'-phosphate at the cleavage site, effectively severing the phosphodiester bond within the RNA (Lacadena et al., 1998). The targeted cleavage of the sarcin-ricin loop (SRL) by ribotoxins produces a 300-400 nucleotides long RNA fragment, known as the α-fragment (Schindler and Davies, 1977). The ability to generate this α-fragment is a definitive indicator of a protein's capacity to inhibit protein synthesis, as the cleavage of the SRL disrupts critical ribosomal functions, thereby hindering the translation process and leading to cellular death (Lacadena et al., 2007).

1.12.1.1.2. Fungal ribotoxins induced cytotoxicity

The ribotoxin cleavage site in the sarcin-ricin loop (SRL) of 23S rRNA in prokaryotic ribosomes includes binding sites for the elongation factors EF-G and EF-Tu. Cleavage at this site disrupts the binding of these factors, decreasing GTP hydrolysis by EF-G and thereby inhibiting the translocation of aminoacyl tRNA (García-Ortega et al., 2010). Similarly, the disruption of EF-Tu binding prevents the attachment of aminoacyl tRNA to the A site of the prokaryotic ribosome (García-Ortega et al., 2010).

Similarly, in eukaryotic cells, the cleavage of the SRL in 28S rRNA obstructs EF1-dependent binding of aminoacyl tRNA and EF2-mediated GTP hydrolysis, which hinders the translocation of aminoacyl tRNA. Consequently, SRL cleavage results

TH-3487_186106116

in the inactivation of functional ribosomes and the inhibition of protein synthesis in both prokaryotic and eukaryotic cells.

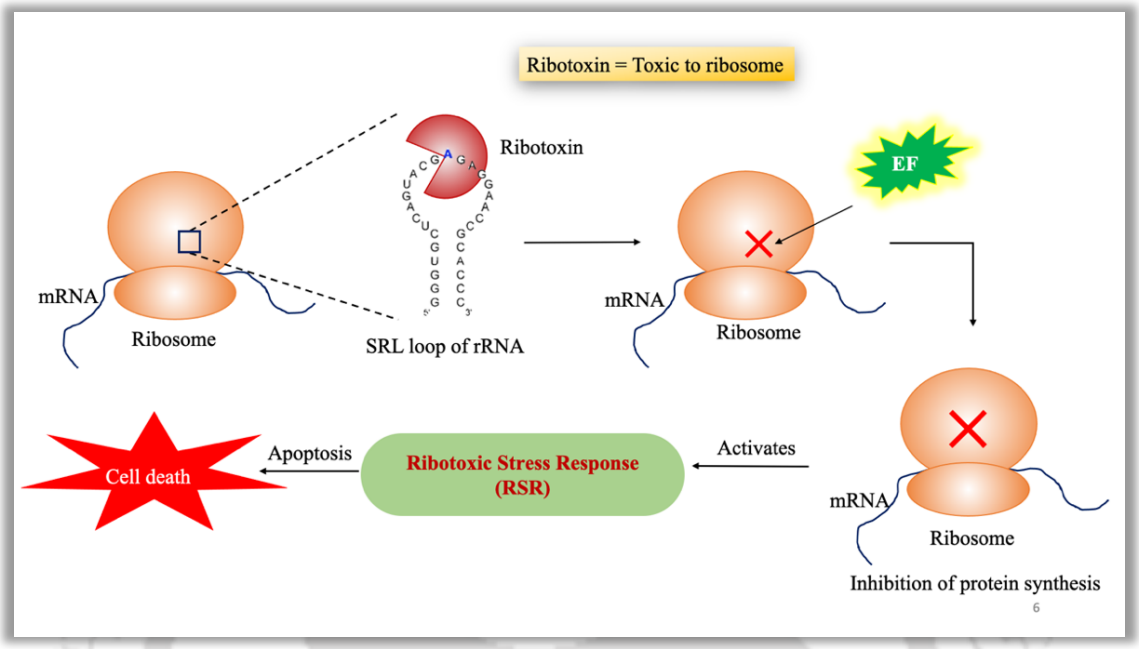

Scheme 1.7. Schematic representation of the mechanism of action underlying the cytotoxic potential of ribotoxins through inhibition of protein synthesis. [*Conceptualised and illustrated based on* (García-Ortega et al., 2010; M. et al., 2010; Olmo et al., 2001; Schindler and Davies, 1977) *using BioRender*]

Pioneering research by Ramakrishnan et al. highlighted the essential role of the sarcin-ricin loop (SRL) in GTPase activation, which is crucial for the GTP hydrolysis of elongation factors necessary for the translation process (M. et al., 2010). Furthermore, the SRL is more critical for EF-G binding to the ribosome than the ternary complex EF-Tu-GTP-tRNA, emphasizing its vital role in maintaining proper ribosomal function (García-Ortega et al., 2010). Consequently, the cleavage of the SRL by ribotoxins disrupts the binding and activation of elongation factors, leading to the inhibition of protein biosynthesis and ultimately causing cellular death through the activation of downstream apoptotic signaling pathways (Olmo et al., 2001).

TH-3487_186106116

1.12.1.1.3. Therapeutic application of fungal ribotoxins in cancer

Ribotoxins, originally noted for their undefined role in natural habitat, have been repurposed for therapeutic applications, particularly through the development of immunotoxins. α-sarcin, initially identified as an antitumor agent, demonstrated nonspecific cytotoxicity towards non-cancerous cells upon further investigation (Olson and Goerner, 1965). Subsequent advances in immunotoxin technology renewed interest in ribotoxin research. Immunotoxins are composite molecules comprising of a toxin component and a target-specific antibody or its variable fragment (Kreitman, 2001; Reiter and Pastan, 1998). In anticancer immunotoxins, the antibody fragment confers specificity for cancer cells, while the toxin induces detrimental effects (Kreitman, 2001; Reiter and Pastan, 1998).

For instance, the α-sarcin-based immunotoxin (scFvA33asarcin) for colon cancer, which includes the single-chain variable fragment (scFv) of the monoclonal antibody against glycoprotein A33 (GPA33), demonstrated highly selective cytotoxicity against GPA33-positive colon cancer cells, while sparing GPA33-negative cells (Carreras-Sangrà et al., 2012). Another immunotoxin (IMTXA33HtA3DW), utilizing hirsutellin A and targeting the same antigen, exhibited superior efficacy with an IC_{50} of 0.5 mM compared to 1.00 mM for scFvA33asarcin (Carreras-Sangrà et al., 2012; Tomé-Amat et al., 2015a). Notably, IMTXA33HtA3DW employed a triple mutant variant of hirsutellin A (HtA3DW) lacking cell internalization ability, whereas the toxin in α-sarcin-GPA33 was wild-type (Carreras-Sangrà et al., 2012; Tomé-Amat et al., 2015a). However, despite these advancements, a significant obstacle in the application of therapeutic immunotoxins persists as the development of strong immune responses against them, resulting in their elimination from the body (Becker and Benhar, 2012). To address this issue, researchers developed a deimmunized version of α-sarcin (D9T/Q142T), which demonstrated no capability to activate T-cells *in vitro*. This makes it a promisingly safer choice for immunotoxin applications aimed at targeting Her2-positive breast cancer cells (Jones et al., 2016).

Furthermore, researchers fused α-sarcin with the single-chain variable fragment (scFv) of the anti-carcinoembryonic antigen (CEA) antibody MFE23, developing

TH-3487_186106116

both monomeric and novel trimeric formats that exhibited targeted antitumor activity against human colorectal cancer xenografts, with the trimeric form demonstrating enhanced efficacy in terms of size, biodistribution, and functional potency compared to the monomeric counterpart (Lázaro-Gorines et al., 2019). Additional efforts focused on developing immunotoxins targeting the transferrin receptor using α-sarcin and restrictocin, which demonstrated selective cytotoxicity against cancer cells overexpressing transferrin receptors *in vitro* (Goyal and Batra, 2000; Rathore et al., 1997).

Beyond immunotoxin development, type-1 ribotoxin curcin has been rendered target-specific by conjugating it with a nano-formulation comprising pegylated gold nanoparticles linked with transferrin and folate receptor antibodies, resulting in a dual-targeted nano delivery system for treating glioma cells *in vitro*. The observed antiproliferative effects in glioma cells stemmed from the combined actions of curcin and the photothermal therapeutic capabilities of gold nanoparticles (Mohamed et al., 2014).

1.12.2. Secondary metabolites from entomopathogenic fungi with anticancer potential

Entomopathogenic fungi generate a diverse array of secondary metabolic compounds with notable anticancer properties. These compounds, such as non-ribosomal peptides, polyketides, terpenoids etc., possess unique mechanisms of action against cancer cells. The evolutionary adaptations of these fungi, shaped by their symbiotic relationships with insect hosts, enhance the potency and specificity of these bioactive substances. Investigating these metabolites presents promising opportunities for developing new cancer therapies, potentially addressing current treatment challenges like drug resistance, epithelial-mesenchymal transition (EMT) and metastasis. This underscores the significant value of entomopathogenic fungi in oncology drug discovery. Notably, among all secondary metabolic compounds from entomopathogenic fungi, cytochalasins, destruxins, and beauvericin stand out for their potent therapeutic effects against various cancer types.

TH-3487_186106116

1.12.2.1. Cytochalasins

Cytochalasins, a diverse group of over 60 fungal metabolites, are classified into subgroups based on the size of their macrocyclic ring and substitutions at the C-3 position (Trendowski, 2015). This chemical diversity substantially influences their biological properties. These compounds inhibit actin polymerization and disrupt microfilament assembly, leading to changes in cell morphology and division (Brown and Spudich, 1981; Spudich and Lin, 1972). Cytochalasins B and Cytochalasins D are particularly notable for their extensive use in research due to their reversible effects on cell morphology (Trendowski, 2015; Yahara et al., 1982). Cytochalasins B, produced by *Helminthosporium dematioideum*, inhibits actin polymerization, interferes with cytokinesis, and can inhibit glucose uptake and endocytosis (Flanagan and Lin, 1980; MacLean-Fletcher, 1980). Cytochalasins D, an isomer of Cytochalasins B derived from *Metarrhizium anisopliae* and *Zygosporium mansonii*, possesses a unique chemical structure that enhances its potency in preventing actin polymerization and enables it to activate the tumour suppressor protein p53, leading to cell cycle arrest (Goddette and Frieden, 1986). Cytochalasins D is also considered as a promising chemotherapeutic agent because it blocks cytokinesis in cancer cells without affecting DNA synthesis (Trendowski, 2015). Additionally, cytochalasins influence differentiation processes, particularly in human mesenchymal stem cells (hMSCs) and stem cells from other species (Pampanella et al., 2024).

1.12.2.2. Destruxins

Destruxins (Dtx), primarily sourced from the entomopathogenic fungus *Metarhizium anisopliae*, have attracted considerable attention due to their potential as anticancer agents (Pedras et al., 2002). These cyclic hexadepsipeptides, exemplified by variants such as Destruxin A, Destruxin B and Destruxin E, exhibit a range of biological activities extending beyond their original insecticidal role (Dumas et al., 1994; Pal et al., 2007; Pedras et al., 2000). Extensive research into their anticancer properties has unveiled compelling mechanisms, positioning them as promising candidates for therapeutic advancement.

TH-3487_186106116

In various cancer cell models, Destruxins have demonstrated significant antiproliferative effects. For example, Destruxin B has been observed to induce apoptosis in human lung cancer cells (A549 and H1299) by activating caspases -2, -3, and -9, key enzymes involved in apoptotic pathways (C.-C. Wu et al., 2013). This apoptotic process involves the upregulation of the proapoptotic protein PUMA and concurrent downregulation of the antiapoptotic protein Mcl-1(C.-C. Wu et al., 2013). Importantly, even in cells lacking functional p53, Destruxin B induces mitochondrial dysfunction by facilitating the translocation of Bax to the mitochondrial membrane, thereby initiating apoptotic cell death independently of p53 signaling (C.-C. Wu et al., 2013).

Furthermore, Destruxin A, Destruxin B and Destruxin E demonstrate extensive antiproliferative effects across diverse cancer types, including colorectal cancer cell lines such as HCT116 and CaCo-2 (Dornetshuber-Fleiss et al., 2013). These compounds disrupt normal cell cycle progression and suppress the PI3K/Akt signaling pathway, which is essential for cancer cell survival and proliferation (Dornetshuber-Fleiss et al., 2013). Particularly noteworthy is Destruxin E, which shows additional potential by altering intracellular redox balance and inhibiting angiogenesis, critical processes involved in tumour progression and metastasis (Dornetshuber-Fleiss et al., 2013).

These findings emphasize the diverse potential of Destruxins as therapeutic candidates for cancer treatment. Further exploration of their intricate molecular mechanisms and rigorous preclinical investigations will be crucial for advancing Destruxins toward clinical use, particularly in the context of colorectal cancer therapy, where their effectiveness has demonstrated notable promise.

1.12.2.3. Beauvericin

Numerous investigations have explored the anticancer properties of beauvericin, a naturally occurring fungal secondary metabolite, primarily produced by the entomopathogenic fungi *Beauveria bassiana*, has gained considerable attention in recent years (Wu et al., 2019a). Its mode of action involves activation of antioxidant response elements by triggering the expression of cytoprotective enzymes (glutathione

TH-3487_186106116

reductase, superoxide dismutase, glutathione-s-transferase, catalase, glutathione-peroxidase etc.) (Mallebrera et al., 2016, 2014). It has also suppressed the viability of various cancer cell lines *in vitro* (Dornetshuber et al., 2009; H.-S. Lee et al., 2008; LIN et al., 2005; Nilanonta et al., 2002; Prosperini et al., 2013; Zhan et al., 2007) by its ionophoric activity that ultimately results in cellular death (Theuerkauf and Kepler, 2022). Additionally, beauvericin has been found to exert anti-inflammatory characteristics, hindering the generation of proinflammatory enzymes and cytokines (Sun and Andersson, n.d.) by inhibiting TNFα mediated activation of NFκB (Wätjen et al., 2014). Interestingly, beauvericin has been found to inhibit angiogenesis, a key process responsible for the formation of new blood vessels that tumours rely on for growth and metastasis (Zhan et al., 2007). Furthermore, beauvericin has demonstrated the ability to induce apoptosis (Jow et al., 2004; Wätjen et al., 2014) and inhibit cell migration (Zhan et al., 2007) by modulating Epithelial to Mesenchymal Transition (EMT) specific biomarkers' expression in pancreatic cancer cells (Yahagi et al., 2020) which reflects its potential to restrict cancer metastasis. Additionally, beauvericin has shown synergistic effects when combined with other active molecules, suggesting that it can be used as part of combination therapies to enhance their effectiveness (Albonico et al., 2017; Ficheux et al., 2012; M.-J. Ruiz et al., 2011; M. J. Ruiz et al., 2011; Zouaoui et al., 2016). Although the mechanism behind beauvericin's anticancer effects is not completely understood, it is believed to disrupt the key signaling pathways responsible for cancer cell survival and proliferation (Kim et al., 2023; Lu et al., 2016; X.-F. Wu et al., 2013; Yoo et al., 2017).

Despite these promising findings, the precise molecular mechanisms underlying the anticancer properties of beauvericin is still unknown. Therefore, further research is necessary to specifically identify the molecular target proteins of beauvericin to provide clarity in its molecular mechanism of action. Identification of these targets will eventually reveal the cellular events they are associated with. Consequently, it will become more convenient to identify the unfavourable cellular events (such as drug resistance, EMT, uncontrolled proliferation etc.), where beauvericin could be very effective. Furthermore, understanding beauvericin's molecular mechanism of action offers significant benefits for targeted therapy, including the development of effective

TH-3487_186106116

combination therapies, optimization of drug efficacy, anticipation of potential resistance, and the exploration of additional therapeutic applications.

However, several challenges need to be addressed before these fungal compounds can be widely used in clinical settings. Ensuring bioavailability and minimizing toxicity are significant hurdles that researchers must overcome. Moreover, extensive clinical trials are necessary to establish the safety and efficacy of these compounds in humans. Despite these challenges, the ongoing efforts in drug development aim to synthesize and modify fungal compounds to enhance their anticancer properties and pharmacological profiles.

In summary, entomopathogenic fungi represent a promising and relatively untapped source of anticancer agents. With their unique mechanisms of action and potential for synergy with existing treatments, these fungi could contribute significantly to the development of new cancer therapies. Continued research and development are essential to realize their full potential and bring these innovative treatments from the laboratory to the clinic.

1.13. Key features and scope of research

The current global landscape of breast cancer, characterized by its rising incidence and increasing mortality rates, underscores the severity of the disease and the critical need for continuous research into various therapeutic approaches to develop effective treatment strategies. Challenges in treating breast cancer include multidrug resistance, epithelial-mesenchymal transition (EMT), and metastasis. This global health crisis necessitates the exploration of novel therapeutic molecules from diverse natural sources to address these challenges. Developing targeted therapies to counteract cancer progression-related cellular events (such as multidrug resistance, EMT, and increased cellular migration and invasiveness) and associated signaling pathways (such as MAPK, PI3K/Akt, and Notch signaling) presents new therapeutic opportunities. Entomopathogenic fungi, as a natural source, hold significant potential to produce bioactive toxins that target specific cellular events and associated signaling pathways, which may be beneficial in reducing breast cancer-related mortality and improving patient outcomes. This thesis investigates different

TH-3487_186106116

therapeutic aspects of the entomopathogenic ribotoxin Anisoplin and the secondary metabolic compound Beauvericin on breast cancer cells, emphasizing the following scopes of research -

- Heterologous production of the entomopathogenic ribotoxin Anisoplin in bacterial expression system though molecular cloning approach and its subsequent purification employing chromatographic techniques.

- Characterization of the recombinant Anisoplin by *in silico* approach, along with experimental evaluation of its biophysical and functional properties.

- Understanding the therapeutic potential of recombinant Anisoplin on breast cancer cells and elucidating the underlying mechanism of action.

- Identification of possible molecular targets of beauvericin in triple-negative breast cancer cells for better understanding of its potential in targeted therapy.

- *In vitro* therapeutic evaluation of beauvericin to elucidate its potential in countering triple-negative breast cancer cells in monolayers as well as spheroids.

- Understanding the role of Beauvericin in combating EMT and other metastasis associated cellular events such as cellular migration in triple-negative breast cancer cells.

- Exploring the regulatory effect of beauvericin on EMT associated Notch signaling and autophagic events.

TH-3487_186106116

1.14. Objectives of the thesis

- Heterologous production, purification and characterization of Anisoplin from *Metarhizium anisopliae* and its therapeutic effects on breast cancer cells.

- Evaluation of intracellular therapeutic targets and *in vitro* therapeutic effects of beauvericin on triple-negative breast cancer (TNBC) cells.

- Evaluation of beauvericin's therapeutic effects on the metastatic attributes of triple-negative breast cancer (TNBC) cells.

TH-3487_186106116

TH-3487_186106116

Chapter 2

Materials and Methods

TH-3487_186106116

TH-3487_186106116

2.1. Materials

2.1.1. Chemicals and Reagents

Following chemicals were procured to conduct the experiments –

Sigma Aldrich - Agarose, Dulbecco's Modified Eagle's Medium (DMEM) supplemented with L-glutamine and sodium pyruvate, Sodium bicarbonate, Formamide, Trifluoracetic acid (TFA), Sinapinic acid, 3-(4,5-dimethylthiazol-2-yl)-2,5-diphenyltetrazolium bromide (MTT), Acridine orange, 2',7'-dichlorofluorescin diacetate (DCFDA), Epidermal growth factor (EGF), Beauvericin, Ponceau S, Propidium Iodide (PI), RIPA cell lysis Buffer, Tetramethylethylenediamine (TEMED), Ammonium persulphate (APS), Dimethylsulphoxide (DMSO), Phosphate-buffered saline (PBS) for cell culture, RNAse A, PVDF membrane.

HiMedia Laboratories: Luria-Bertani (LB) media, Agar powder, Potato dextrose media, triton-X-100, Tris base, Tween-20, Diluent for DNA extraction (100% ethanol), Glycerol, Glacial acetic acid, Ethylenediamine tetraacetic acid (EDTA), Sodium dodecyl sulphate (SDS), Bromophenol blue, Xylene cyanol FF, ethidium bromide (EtBr), Calcium chloride ($CaCl_2$), Magnesium chloride ($MgCl_2$), Ampicillin, Diethyl pyrocarbonate (DEPC), Isopropyl β- d-1-thiogalactopyranoside (IPTG), Tris-HCL, Sodium hydroxide (NaOH), Potassium acetate, Glycine, Dithiothreitol (DTT), Sodium chloride (NaCl), Maltose, disodium hydrogen phosphate (Na_2HPO_4), Potassium dihydrogen phosphate (KH_2PO_4), Bovine serum albumin (BSA).

New England Biolabs (NEB): pMAL-p5X plasmid, BamHI-HF and NdeI restriction enzymes, Factor-Xa protease, Phusion high-fidelity DNA polymerase, *Escherichia coli* DH5α and *Escherichia coli* BL21(DE3) bacterial strains, Gibson assembly master-mix, Amylose resin.

BioRad Laboratories: Prestained protein molecular weight marker, iScript cDNA synthesis kit, SYBR green master mix, ECl western blotting substrate.

TakaraBio: RNAIso Plus, Prime-script cDNA synthesis kit.

Merck: Chloroform, phenol-chloroform-isoamyl alcohol mixture, isopropanol.

TH-3487_186106116

ThermoFisher Scientific: Taq-DNA polymerase, deoxyribonucleotides (dNTPs), nuclease free water, Acetonitrile, Alamar blue, JC-1 assay kit, Annexin-V-Alexa flour 488- Propidium Iodide apoptosis kit, Calcein-AM, bicinchoninic acid (BCA) reagent, Protein molecular weight marker, DNA molecular weight marker.

Gibco: Fetal bovine serum (FBS), antibiotic solution (100 units/mL penicillin + 0.1 mg/mL streptomycin + 0.025 mg/mL amphotericin B).

Promega: RNase free DNase – I, Rabbit reticulocyte lysate.

Integrated DNA Technologies (IDT):

Table 2.1.1.1. The list of primers used to amplify anisoplin gene and study the expression profile of the other enlisted genes by qRT-PCR.

Name	Forward primer	Reverse primer
Anisoplin	5'-CTCGGGATCGAGGGAAGGATTTCACATATGGGCCCTGTCACCCGGGCTGA-3'	5'-TATTTAATTACCTGCAGGGAATTCGGATCCTTATCAGGTGCACTTCAGGAAGA-3'
E-cadherin	5'-TGGGTGAATTCGGGCTTGTT-3'	5'-TGAAGGTGACAGAGCCTCTGGAT-3'
N-cadherin	5'-GCAGATCGGACCGGATACTG-3'	5'-CCATCAAGCCTGTGGGAATC-3'

TH-3487_186106116

Vimentin	5'-CATTTCACGCATCTGGCGTTC-3'	5'-AGTCCACTGAGTACCGGAGAC-3'
Notch-1	5'-TGGGCAGTGGCAGAT-3'	5'-CTGGTCAGGGAAATCGT-3'
Notch-3	5'-GAGCCAATGCCAACTGAAGAG-3'	5′-GGCAGATCAGGTCGGAGATG-3'
β-actin	5'-AAGGGACTTCCTGTAACAATGCA-3'	5'-CTGGAACGGTGAAGGTGACA-3'

Cell Signaling Technology (CST):

Table 2.1.1.2. The list of antibodies used to study the expression profile of the enlisted genes.

Antibodies	Product code
P-SAPK/JNK	8206
SAPK/JNK	8206
NF-kB p65-Alexa fluor 647	8801
E-cadherin	9782T
N-cadherin	9782T
Vimentin	9782T
Snail	9782T
Slug	9782T
β-catenin	9782T

TH-3487_186106116

Hes-1	68309T
CyclinD3	68309T
LC3	4445T
Beclin-1	4445T
HRP linked Anti-rabbit antibody	7074
HRP linked Anti-mouse antibody	7076
β-actin	8457S

2.1.2. Glassware and Plasticwares

Following glassware and plasticwares were used to conduct the experiments –

Borosil: Test tubes, conical flasks, beakers etc.

Tarsons Products Pvt. Ltd: Petri-dishes, microtips, spreaders, microcentrifuge tubes, centrifuge tubes, cryo-chill vials, PCR tubes etc.

ThermoFisher Scientific: Cell culture dishes, cell culture T-flasks, 96-well plates, 6-well plates etc.

Merck: Centrifugal concentrators

2.2. Bacterial culture conditions and maintenance

Escherichia coli DH5α and *Escherichia coli* BL21(DE3) bacterial strains were procured from New England Biolabs (NEB). The strains were cultured on Luria-Bertani (LB) broth at 37°C temperature in a humidified incubator for 18-24 h. The bacterial cultures were stored as glycerol stocks at -80°C storage. The stocks were revived and restored in an interval of 1-2 months.

2.3. Fungal culture conditions and maintenance

Metarhizium anisopliae (MTCC 892 equivalent to ATCC 26852) was procured from microbial type culture collection (MTCC), Chandigarh, India. A series of five replicates of the strain is cultured on potato dextrose agar at 25°C temperature in a humidified

TH-3487_186106116

incubator for 5-7 days or until spores were generated. The fungal spores were collected using 0.01% (v/v) Triton X-100 (A non-ionic detergent). These spores were stored at 4°C and revived frequently in an interval of 3-4 weeks.

2.4. Cell Lines, culture conditions and maintenance

MCF-7 breast cancer cell line, MDA-MB-231 and MDA-MB-468 triple-negative breast cancer cell lines and non-cancerous HEK-293 human embryonic kidney cell lines were procured from the National Centre for Cell Sciences (NCCS) cell repository, Pune, India. The cell lines were cultured in high glucose Dulbecco's Modified Eagle Medium (DMEM) supplemented with L-glutamine, sodium pyruvate, 10% fetal bovine serum (FBS), sodium bicarbonate and 1% (v/v) antibiotic solution (100 units/mL penicillin + 0.1 mg/mL streptomycin + 0.025 mg/mL amphotericin B) and maintained in a humidified incubator at 37°C and 5% CO_2. The growth media was replaced with fresh media every 2 to 3 days. Cell culture plates with above 80% confluent cells were used for all the experiments.

2.5. Culture conditions and generation of 3D spheroids

To generate 3D spheroids using the force flotation method (Ivascu and Kubbies, 2006), MDA-MB231 and MDA-MB-468 triple-negative breast cancer cells were seeded at a density of 10,000 cells per well into an agarose-coated 96-well plate. The agarose coating prevents cell attachment to the well surface, promoting spheroid formation. The plate was then centrifuged at 700 × g for 10 minutes to aggregate the cells at the bottom of each well. Following centrifugation, the plate was incubated under standard conditions (37°C, 5% CO_2) in a serum-supplemented growth medium for 96 h. This incubation period allowed the cells to proliferate and self-assemble into 3D spheroids, closely mimicking the in vivo tissue microenvironment for subsequent experimental applications.

2.6. Experimental Methodologies

2.6.1. Fungal RNA isolation

Briefly, fungal mycelia were harvested from 48h old broth culture of *M. anisopliae* by centrifuged at 5000 rpm for 10 minutes and washed thrice with sterile distilled water. The mycelia was further homogenised by grinding in mortar and pestle in presence of 1mL RNAiso plus reagent and incubated in room temperature for 5 minutes followed

TH-3487_186106116

by centrifuged at 12,000 × g for 5 minutes. The supernatant was collected and vigorously mixed with 0.2 volume of chloroform-isoamyl alcohol (24:1). After incubating the solution at RT for 5 minutes it was subjected to centrifugation at 12,000 × g for 15 minutes at 4°C. The upper layer was carefully transferred to a new vial and mixed with equal volume of ice-cold isopropanol. After incubating for 10 minutes in RT, the solution was centrifuged at 12,000 × g for 10 minutes at 4°C. the translucent pellet obtained was further washed with equal volume of 70% ethanol and air dried. Finally the RNA pellet was dissolved in desired amount of molecular grade nuclease free water. Adequate amount of RNA was subjected to agarose gel electrophoresis, quantification and purity evaluation ($A_{260/280}$) and stored in -20°C for further application.

2.6.2. DNase treatment and cDNA synthesis

The isolated fungal RNA sample was further treated with DNase-I to eliminate any DNA sample present and further used to synthesize cDNA using Prime-script cDNA synthesis kit as per the manufacturer's protocol. Briefly, 5 µg of DNA free total RNA was mixed with 1 µL of 50 µM oligo dT primers, 1 µL of 10 mM dNTPs mix and diluted with nuclease free water up to 10 µL. This solution was heated at 65°C for 5 minutes and immediately cooled on ice. Furthermore, 10 µL of the prepared solution was mixed with 4 µL of 5X prime-script buffer, 20 units RNase inhibitor, 100 units of prime-script reverse transcriptase and volume was finally made up to 20 µL. The final reaction mix was incubated at 50°C for an hour followed by heated at 70°C for 15 minutes and immediately cooled on ice.

2.6.3. Amplification of anisoplin gene

The synthesized cDNA was used as template to amplify anisoplin gene using gene specific primers. The primers used to amplify the anisoplin gene are designed to have extra 20 bp overhang complementary to the vector of interest for downstream application. Briefly, 20 µL cocktail of the amplification reaction was prepared by mixing 2 µL 10X reaction buffer, 1.6 µL 2.5mM dNTPs, 0.4 µL of each primers (10 µM), 1µL of cDNA, 0.2 µL Phusion high fidelity DNA polymerase and required amount of nuclease free water. The amplification cocktail was subjected to PCR amplification

TH-3487_186106116

as per the following condition – Initial denaturation at 95˚C for 3 minutes, denaturation at 95˚C for 20 seconds, primers annealing at 53˚C for 45 seconds, extension at 72˚C for 1 minutes, final extension at 72˚C for 10 minutes, storage at 4˚C until the sample was collected. The amplification was carried out for 30 cycles. The amplified gene was subjected to quantification using nanodrop spectrophotometer and the quality was also assessed using agarose gel electrophoresis.

2.6.4. Double digestion of pMAL-p5X vector

pMAL-p5X expression vector was digested using BamHI-HF and NdeI restriction enzyme as per the manufacturer's protocol. Briefly, 5 µL 10X cut smart buffer was mixed with 1 µg vector plasmid DNA, 1 µL of each restriction enzymes and adequate nuclease free water to make a 50 µL reaction cocktail. The reaction was performed at 37˚C for 4 hours followed by the enzymes were heat inactivated at 65˚C for 15 minutes.

2.6.5. Ligation (Gibson assembly method)

Double digested vector was ligated to the gene of interest using Gibson assembly reaction. Briefly, 10 µL of Gibson assembly mix was mixed with 0.5 pmols of insert DNA with the double digested vector DNA (pMALp5X) at a molar ratio of 3:1 and the final volume was adjusted to 20 µL with nuclease free water. The reaction was performed at 50˚C for an hour.

2.6.6. Preparation of competent cells

An overnight grown liquid culture of E. coli DH5α was inoculated into 200 mL LB broth (0.1% inoculation) and the bacterial culture was grown for approximately 3 hours until the culture OD reaches up to 0.3 – 0.4. The culture was incubated in ice for at least 30 minutes and the bacterial cells were collected by centrifuging it at 10000 rpm for 10 minutes. The obtained pellet was washed with 85 mM $MgCl_2$ solution. Furthermore, the bacterial pellet was resuspended with 5 mL of 100 mM $CaCl_2$ solution and incubated in ice for 30 minutes. Bacterial pellet was collected by centrifuging it at 10000 rpm for 10 minutes. Finally, the pellet was resuspended in 1.5 mL of 200 mM $CaCl_2$ containing

TH-3487_186106116

30% glycerol. The competent cell suspension was aliquoted in microcentrifuge tubes each containing 100 µL and stored at -80˚C freezer.

2.6.7. Bacterial transformation

The ligation mixture was further transformed into chemically competent *E. coli* DH5α strain using heat shock method. Briefly, the whole ligation mixture was mixed with 100 µL of chemically competent *E. coli* DH5α strain. The mixture was incubated in ice for 30 minutes followed by incubation at 42˚C for 90 seconds and immediately transferred into ice and further incubated at least 5 minutes. 1 mL of LB broth was added to the mixture and incubated at 37˚C for an hour. The bacterial culture was centrifuged at 5000 rpm for 5 minutes. The supernatant was discarded leaving behind 50 – 100 µL. the pellet was redissolved in the remaining medium and spread over LB agar medium plate supplemented with 100 µg/mL of ampicillin. The LB agar plate was incubated at 37˚C for 12 hours and observed for the colony formation.

2.6.8. Screening of positive clones by colony PCR

4 colonies from the transformation plate was selected and subjected to colony PCR to amplify the anisoplin gene. Briefly, Each of the selected colonies were grown separately in 200 µL of ampicillin supplemented LB broth and grown for 2 hours at 37˚C. To prepare the reaction mixture, 2 µL of each colony culture was separately mixed with 2 µL of 10X standard Taq buffer, 1.6 µL of 2.5 mM dNTPs, 0.4 µL of each 10 mM primers, 0.3 µL of Taq DNA polymerase enzyme and the reaction volume was made up to 20 µL with nuclease free water. A similar reaction was prepared as positive control using the anisoplin gene as template instead of bacterial culture. The reaction cocktails were subjected to amplification as per the PCR conditions stated in 2.6.3. Amplification of the anisoplin gene was confirmed by agarose gel electrophoresis.

2.6.9. Plasmid DNA isolation

Plasmids from the positively screened clones were isolated as per the following method. 5 mL of each overnight grown clone samples were centrifuged to obtain the pellet. Each pellet was resuspended in 200 µL resuspension buffer. To this 200 µL of lysis buffer

TH-3487_186106116

was added, mixed gently by inverting the tubes and incubated in ice for 2 and half minutes and immediately mixed with 350 µL of neutralization buffer. The mixture was centrifuged at 12,000 x g for 5 minutes at 4°C. The supernatant was collected in a fresh vial and mixed 5 µL of RNase-A (10 mg/mL) and incubated at 37°C for an hour. To this 200 µL of phenol-chloroform-isoamyl alcohol mixture was added and mixed vigorously. The mixture was centrifuged at 12,000 x g for 5 minutes. Upper layer of the solution was gently transferred to a fresh tube and vigorously mixed with 0.8 volume of ice cold isopropanol. the mixture was centrifuged at 12,000 x g for 10 minutes and the supernatant was discarded. The pellet was washed with ice cold 70% ethanol and air dried. Finally the air dried pellet was resuspended in 20 µL nuclease free water for further application.

2.6.10. Clone confirmation by double restriction digestion

The plasmids were double digested with BamHI-HF and NdeI restriction enzymes. Briefly, 5 µL 10X cut smart buffer was mixed with 1 µg recombinant plasmid DNA, 1 µL of each restriction enzymes and adequate nuclease free water to make a 50 µL reaction cocktail. The reaction was performed at 37°C for 4 hours followed by the enzymes were heat inactivated at 65°C for 15 minutes. The digested samples were subjected to agarose gel electrophoresis for further confirmation of successful clones.

2.6.11. Clone confirmation by Sequencing

Anisoplin gene was amplified using gene specific primers from the positively screened recombinant plasmids, column purified and subjected to sanger sequencing (Agrigenomes pvt. Ltd.) to confirm that the anisoplin gene has been successfully cloned into pMAL-p5X vector.

2.6.12. Overexpression of MBP-Anisoplin (MBP-Anp) fusion protein

The positively cloned plasmid was transformed into *E. coli* BL21(DE3) competent cells. Single colony was isolated and sub-cultured. Overnight grown culture was inoculated as 1% (v/v) inoculation into 10 mL LB broth and incubated at 37°C for 2 to 3 hours until the bacterial growth reaches log phase. After the culture OD reaches 0.5-0.6, the culture

TH-3487_186106116

medium was induced with 0.3 mM IPTG and incubated at 37°C for further 6 hours. 1 mL of bacterial culture was collected in 1 h interval after induction and centrifuged to collect the bacterial pellet. Samples of different time intervals were further lysed with lysis buffer followed by sonication with probe sonicator and further subjected to SDS-PAGE to confirm overexpression of MBP-Anp fusion protein.

2.6.13. Solubility optimization of MBP-Anp fusion protein

Anisoplin was overexpressed as per the protocol mentioned in the previous subsection (2.6.12.) along with that another two sets of the same experiment were carried out in two different temperature 25°C and 16°C for 12 and 16 hours respectively after induction with 0.3 mM IPTG. The periplasmic fraction from each sample was isolated and all samples were analysed by SDS-PAGE.

2.6.14. Production and purification of MBP-Anp fusion protein by affinity chromatography

Anisoplin was overexpressed in large volume and the periplasmic fraction containing anisoplin was subjected to affinity chromatography. Briefly, the amylose column was washed properly with filtered deionized water, regenerated with 0.1% SDS as per manufacturer's protocol then equilibrated with 1X column buffer (20mM Tris-Hcl, 200 mM NaCl, 1mM EDTA). The crude protein sample was passed through the column multiple times followed by the column was washed twice with the column buffer. Finally the recombinant anisoplin was eluted using required volume of elution buffer (column buffer containing 10mM maltose) in fractionated volume. The eluted fractions were further analysed by SDS-PAGE to evaluate the purity. The eluted fractions were pulled up and concentrated using centrifugal concentrators (MWCO 30 KDa) followed by buffer exchanged with 1X phosphate buffered saline (PBS).

2.6.15. Separation of MBP-Anp fusion protein

Recombinant MBP-Anp fusion protein was digested with Factor-Xa protease as per the manufacturer's protocol. Digestion of the MBP tag was optimised with various concentrations of enzyme ranging from 0.01% to 1% (w/w). shortly, the required volume of purified protein was mixed with required volume of Factor-Xa protease

TH-3487_186106116

followed by incubated at 4°C overnight. The digestion was confirmed by analyzing the sample with SDS-PAGE.

2.6.16. Purification of Anisoplin (Anp) by size exclusion chromatography

Factor-Xa digested MBP-Anp sample was urified using Superdex 200pg gel filtration column (GE healthcare). Briefly the column was washed with two column volumes of filtered 0.5M NaOH solution followed by washed with 3 column volume of filtered deionized water. Furthermore, the column was equilibrated with 2 column volume of 1X PBS followed by injected with 1 mL of digested MBP-Anp sample. Fraction of anisoplin was collected and concentrated to obtain pure anisoplin.

2.6.17. Secondary structural element (SSE) composition and thermal stability evaluation by circular dichroism spectroscopy

The circular dichroism spectra of recombinant anisoplin were recorded using Jasco J-1500 circular dichroism (CD) spectrometer. The thermostability of the recombinant protein was determined by recording the CD spectra at varying temperatures starting from 20°C to 100°C. The thermal denaturation profile was obtained from the ellipticity values at 203 nm, and melting temperature (T_m) was calculated as the corresponding temperature to the midpoint of the curve as per the earlier report by Olombrada et al., 2017 (Olombrada et al., 2017). Furthermore, all the recorded circular dichroism (CD) spectra were analyzed using the BeStSel (Micsonai et al., 2018) webserver to calculate the amount of secondary structural elements (SSE) present.

2.6.18. MALDI-TOF mass spectrometry

The molecular weight of the recombinant anisoplin was characterized using Bruker autoflex speed MALDI-TOF mass spectrometer. Briefly, 0.01% of trifluoroacetic acid (TFA) was mixed with acetonitrile in 7:3 ratio. Sinapinic acid solution was prepared in the mixed solvent at 16 mg/mL concentration. Different concentrations of the recombinant anisoplin were mixed with the matrix solution at 1:2 ratio and then analyzed with the MALDI-TOF mass spectrometer using an autosampler. A peptide mass calibration standard kit was used to ensure accurate mass measurement and verify the mass accuracy.

TH-3487_186106116

2.6.19. *In silico* characterization of anisoplin

Physicochemical properties of the anisoplin protein were predicted using the ProtParam tool of Expasy (Gasteiger et al., 2005). The conserved domain of anisoplin was predicted and analyzed using the CDD search tool of NCBI (Lu et al., 2020). The homologous protein was identified by a homology search based on local alignment using the protein BLAST (p-BLAST) tool (Altschul et al., 1990). A sequence-based phylogenetic tree was constructed based on the CLUSTALW algorithm using the maximum likelihood method in MEGA-11 software (Tamura et al., 2021).

2.6.20. *In silico* prediction and validation of 3D tertiary structure of anisoplin

The three-dimensional tertiary structure was predicted using four different webservers: the Swiss model (Waterhouse et al., 2018), AlphaFold2 (Jumper et al., 2021), Phyre2 (Kelley et al., 2015) and I-TASSER (Roy et al., 2010). The predicted structures were refined using GalaxyRefine (Heo et al., 2013) webserver. The refined structures were further analyzed using the ProCheck tool of SAVES (Laskowski et al., 1993) webserver to generate Ramachandran plots for each refined structure. All the predicted structures were validated based on the Ramachandran plot statistics, and the Z-scores were calculated using the PROSA webserver (Wiederstein and Sippl, 2007). The best structure was selected based on Ramachandran plot statistics and Z-score.

2.6.21. *In silico* prediction of SRL binding pocket and its validation through molecular dynamics (MD) simulation

Active site residues of anisoplin were mapped by sequence alignment of both hirsutellin A and anisoplin based on the CLUSTRALW algorithm of the BioEdit tool (Hall et al., 2011). The structural integrity of the predicted three-dimensional model of anisoplin was further analyzed in the dynamic environment using the molecular dynamics (MD) simulation method. In this study, dynamic simulation of anisoplin and anisoplin – SRL (sarcin-ricin-loop of 28s rRNA) complex was performed in a water-rich environment using GROMACS 2019.6 and CHARMM27 force field (Shelke Roscoe, J. A., Morrow, G. R., Colman, L. K., Banerjee, T. K., & Kirshner, J. J., 2008). The MD simulation of

TH-3487_186106116

protein and protein-RNA complex was carried out by following Justin's gromacs tutorial (Lemkul, 2019). The protein and protein-RNA complex were covered with dodecahedron box with 1.0 nanometer distance from the box edge. Then, the system was solvated by the TIP3P water model and neutralized with Na^+ ions and Cl^- ions (buffered with 0.15 M NaCl to mimic physiological concentrations). Energy minimization of the system was performed using the steepest descent algorithm up to 10 kJ/mol where the energy threshold is for the maximum force. Followed by NVT (canonical ensemble), and NPT (Isobaric- isothermal ensemble) equilibration of the system was performed by velocity-rescale thermostat with the reference temperature of 300K and Berendsen pressure coupling with a reference 1 atm reference pressure over 100 picoseconds. The final molecular dynamics (MD) simulation of the anisoplin and anisoplin-SRL complex was performed for 100 nanoseconds.

2.6.22. Ribonucleolytic activity assay

The ability of recombinant anisoplin to cleave 28s rRNA of the eukaryotic ribosome was characterized by the formation of 400 nucleotide RNA fragment after treating cell-free rabbit reticulocyte lysate procured from Promega as per the protocol described by Stephen P. et al. (Miller and Bodley, 1988). Briefly, the rabbit reticulocyte lysate was diluted 3 fold with 40 mM Tris-Hcl, pH 7.5, containing 40 mM potassium chloride (KCl) and 10 mM ethylenediaminetetraacetic acid (EDTA). 0.05 mL of the diluted lysate was then incubated with increasing concentrations of recombinant anisoplin for 15 minutes at 25°C. The reaction was stopped by adding 0.25 mL stop solution containing 50 mM Tris-Hcl (pH 7.4) and 0.5% (w/v) SDS, followed by vigorous mixing. The RNA was then isolated by phenol-chloroform-isoamyl alcohol extraction and ice-cold isopropanol precipitation. Finally, the RNA pellets were washed with 70% (v/v) ice-cold ethanol and air-dried. The RNA pellets were then resuspended in 0.01 mL of molecular grade nuclease-free water and subjected to electrophoresis in 2% denaturing agarose gel to visualize the RNA bands.

2.6.23. Cell viability assessment upon recombinant anisoplin (rAnp) treatment

To evaluate the viability of MCF-7 and HEK-293 cells, $5x10^3$ cells were seeded per well in a 96 well-plate for 24 hours in an incubator maintained at 37°C and 5% CO_2 for

TH-3487_186106116

attachment. Subsequently, the cells were treated with increasing concentrations of recombinant anisoplin for further 48 hours, followed by incubation with 0.5 mg/mL concentration of 3-(4,5-dimethylthiazol-2-yl)-2,5-diphenyltetrazolium bromide (MTT) at 37°C and 5% CO_2 under humidified condition for another 90 minutes. The assay media was discarded, and the formazan crystals were dissolved in 0.07 mL dimethyl sulfoxide (DMSO) and the absorbance of each well was recorded at 570 nm with reference to 630 nm in Thermo Fisher Scientific Multiskan SkyHigh spectroscopic plate reader. Cell viability percentages were determined from the absorbance values based on the equation:

$$\text{Cell viability (\%)} = \frac{\text{Average absorbance of treated wells}}{\text{Average absorbance of untreated wells}} \times 100$$

2.6.24. Live - dead cells imaging of MCF-7 cells on monolayer

Live–dead cell imaging of anisoplin treated MCF-7 cells was performed by acridine orange/Propidium Iodide dual staining. Briefly, following treatment with IC_{50} concentrations of recombinant anisoplin, MCF-7 cells were incubated with 0.002 mM acridine orange and 0.004 mM Propidium Iodide for 30 minutes at 37°C in a humidified incubator containing 5% CO_2. After incubation, cells were washed with PBS and visualized using a Zeiss LSM 880 confocal microscope.

2.6.25. Immuno-flowcytometry

The expression of NF-kB upon treatment with recombinant anisoplin was determined by immunoflowcytometric method using NF-kB p65 rabbit monoclonal antibody conjugated with Alexa fluor 647 (Cell signaling technology). Following treatment, MCF-7 cells were processed as per the manufacturer's protocol and analyzed using CytoFLEX flow cytometer (Beckman coulter).

2.6.26. *In silico* prediction and shortlisting of potential molecular targets of beauvericin

The possible molecular targets of beauvericin were predicted using two different approaches. DrugBank (Wishart et al., 2018) and BindingDB (Gilson et al., 2016) databases were used to shortlist drugs or small molecules with greater than or equal to

TH-3487_186106116

50% structural similarity with beauvericin. Protein targets of the shortlisted molecules were considered to be possible targets for beauvericin as they share structural similarities. On the other hand, SwissTargetPrediction (Gfeller et al., 2014) and SuperPred target prediction (Gallo et al., 2022) tools were used to predict possible molecular targets of beauvericin. Furthermore, the Enrichr tool was used to refine all the targets (Kuleshov et al., 2016) and the targets that have a role in cancer and cancer-related pathways were shortlisted based on KEGG pathway analysis. Among the cancer-related proteins, the targets upregulated both at transcriptomic and proteomic levels were refined based on multi-omics data analysis of The Cancer Genome Atlas – Invasive Breast Carcinoma (TCGA-BRCA) and The National Cancer Institute's Clinical Proteomic Tumor Analysis Consortium (CPTAC) databases using UALCAN web server (Chandrashekar et al., 2022).

2.6.27. Protein, ligand preparation and molecular docking studies

The 3D coordinates of the target proteins were obtained in pdb format from the Protein Data Bank (https://www.rcsb.org). Subsequently, ions, small molecules and water molecules were excluded using PyMol 2.3 (Schrodinger, LLC. 2010. The PyMOL Molecular Graphics System. Version 2.3). Hydrogen atoms and kollman charges were introduced to the corresponding PDB structures, and the type of atoms was converted to AD4 type using the MGL Tools 1.5.7 of AutoDock4. The resulting protein and ligand structures were saved in the pdbqt format for subsequent docking studies. AutoDock Vina 1.2.0 (Eberhardt et al., 2021) was employed to forecast the binding affinity of beauvericin with the shortlisted target proteins. For blind docking, grid boxes were configured to fully encompass the respective proteins. The visual representations of the interactions between beauvericin and the target proteins were created, and corresponding images were generated using Discovery Studio Visualizer and PyMol 2.3, respectively. Standard inhibitors of the molecular target proteins of beauvericin were employed as a positive control to validate their inhibition by beauvericin.

2.6.28. Molecular dynamics (MD) simulation studies

For more than a decade, various molecular dynamics (MD) simulation methods have effectively investigated the dynamic behaviours of biomolecules like lipids, proteins,

TH-3487_186106116

and nucleic acids within a condition mimicking their microenvironment. This study specifically delves into the dynamic simulation of complexes involving the beauvericin ligand and selected target proteins within a water-rich environment. Additionally, the dynamic behaviour of the MRP1/ABCC1 (transmembrane protein) – beauvericin complex has been explored within an environment containing both a membrane and water.

2.6.28.1. MD simulation of beauvericin bound cytosolic proteins

The study utilized GROMACS 2021 to examine dynamic behavioural changes in the shortlisted target proteins upon binding with beauvericin. Protein structures in PDB format were transformed into gmx format using the CHARMM36 force field (Jo et al., 2008) (Lee et al., 2016). The topology of protein-beauvericin complexes was established following Justin's GROMACS tutorial (Lemkul, 2019). These complexes were confined in a dodecahedron box, maintaining a 1nm distance from the box edge. The TIP3P water model solvated the complex system. Na+ and Cl- ions were added based on net charge using the "genion" model of GROMACS. System energy minimization employed the steepest descent algorithm until the maximum force attended was below 10 KJ/mol. The LINCS algorithm was employed to constrain bonds involving hydrogen. Electrostatic interactions were determined using particle-mesh Ewald (PME), Van der Waals interactions were obtained with neighbour searching with short range Van der Waals cut-off of 1.2 nm, using the Verlet algorithm. Confirmation of equal ion and solvent distribution around protein-beauvericin complexes occurred through canonical ensembles (NVT equilibration) with a velocity rescale-thermostat and isobaric-isothermal (NPT) ensemble (NPT equilibration) with Brendsen pressure coupling for 100 picoseconds. Reference temperature and pressure were set at 310K and 1 atm for NVT and NPT ensembles, respectively. The final MD run of the equilibrated system spanned 100 ns with a two fs time step. Post-MD simulation analyses such as root mean square deviation (RMSD), root mean square fluctuation (RMSF), and radius of gyration (Rg) of protein-beauvericin complexes were analyzed using standard GROMACS functions. Further analysis such as the binding distance between beauvericin and respective target proteins (paired distance), the number of hydrogen

TH-3487_186106116

bonds formed and the radial distribution function analysis were conducted using the gmx_pairdist, gmx_hbond and gmx_rdf functions, respectively.

2.6.28.2. MD simulation of beauvericin bound transmembrane proteins

The simulation of proteins in the membrane was conducted using GROMACS 2021 and the CHARMM36 force field (Lee et al., 2016). Input files for GROMACS were generated through the CHARMM-GUI server (https://www.charmm-gui.org/). The simulated membrane composition included 72 molecules of cholesterol, 74 molecules of POPE (1-palmitoyl-2-oleoyl-sn-glycero-3-phosphoethanolamine), and 67 molecules of PSM (palmitoylsphingomyelin) in the upper leaflet, while the lower leaflet comprised 73 molecules of cholesterol, 75 molecules of POPE, and 68 molecules of PSM, mimicking the mammalian cell membrane (Sen et al., 2023). The membrane molecules were constructed around the MRP1 protein-ligand complex with the assistance of the CHARMM-GUI membrane builder (Jo et al., 2007; Wu et al., 2014)Click or tap here to enter text.. The system was supplemented with water molecules and neutralized using K+ and Cl− ions. Input files in GROMACS format were downloaded from CHARMM-GUI. Subsequent procedures, including energy minimization, equilibration, and MD runs, followed the protocol mentioned in the MD simulation in water. The final MD run was extended up to 100 ns with 2 femtosecond time steps.

2.6.29. Estimation of binding free energy of the stable beauvericin-target interactions

The Molecular Mechanics Poisson Boltzmann Surface Area (MMPBSA) represents a widely accepted approach for the binding free energy calculation of target-inhibitor complexes by analyzing molecular dynamics (MD) trajectories. During simulation, the binding free energy was evaluated using the g_mmpbsa feature of GROMACS, employing a time interval of 1 ns over a complete MD trajectory spanning 100 ns (Kumari et al., 2014). The dielectric constants used for the solute and the solvent were 2 and 80, respectively. The binding free energy (ΔGbind) of beauvericin with stable targets was computed utilizing the subsequent equation and the time interval considered for the calculation was 5 ns:

$$\Delta G_B = \Delta E_{MM} + \Delta G_{SA} - T\Delta S_{MM}$$

TH-3487_186106116

In this context,

ΔG_B = mean binding free energy of the target-inhibitor complex.

ΔE_{MM} = average molecular mechanics energy.

ΔG_{SA} = solvation free energy.

$T\Delta S_{MM}$ = solute configuration entropy (Kollman et al., 2000).

2.6.30. Viability assessment of TNBC cells on monolayer

Cell viability assays using Alamar blue were conducted on monolayer of TNBC cells MDA-MB-231 and MDA-MB-468. Briefly, 5×10^3 cells were cultured per wells of a 96-well plate as per the growth condition mentioned in the above section for 24 h. Following this, cells were treated with escalating dosage of beauvericin and incubated for another 48 h. Following treatment, cells were incubated with 1X Alamar blue for 90 min. The optical absorbance of the plate was subsequently recorded at 570 nm with reference to 600 nm. Cell viability percentages were determined from the absorbance values based on the equation:

$$\text{Cell viability (\%)} = \frac{\text{Average absorbance of treated wells}}{\text{Average absorbance of untreated wells}} \times 100$$

2.6.31. Detection of intracellular reactive oxygen species (ROS)

The alterations in intracellular reactive oxygen species (ROS) generation in MCF-7 cells post-anisoplin treatment and TNBC cells post-beauvericin treatment were assessed using 2',7'-dichlorofluorescin diacetate (DCFDA) (Eruslanov and Kusmartsev, 2010). In brief, 1×10^5 cells were initially cultured in growth media for 24 h. The attached MCF-7 cells were subjected to treatment with increasing concentrations of recombinant anisoplin for 4 h, while the MDA-MB-231 and MDA-MB-468 cells were exposed to respective IC_{50} concentrations of beauvericin for 6 h. The treated cells were further incubated with 10 µM DCFDA for an additional 30 min, then trypsinized, washed with 1X PBS (phosphate buffered saline), and subjected to data acquisition of 10,000 cells per sample using the CytoFLEX flow cytometer by Beckman Coulter and analyzed by Flow-Jo software by normalizing ROS generation against control cells.

TH-3487_186106116

2.6.32. Detection of depolarized mitochondrial membrane

The mitochondrial membrane potential changes in MCF-7 cells treated with recombinant anisoplin, as well as in MDA-MB-231 and MDA-MB-468 cells treated with beauvericin at their IC_{50} concentrations, were evaluated using JC-1 staining to assess mitochondrial health (Sivandzade et al., 2019). Following treatment, MCF-7, MDA-MB-231 and MDA-MB-468 cells were stained with 10 µM JC-1 dye for 30 min at 37°C. Subsequently, the cells were thoroughly washed with 1X PBS to remove excess dye and analyzed using CytoFLEX flow cytometer (Beckman Coulter).

2.6.33. Detection of apoptotic population

Following the treatment of MCF-7 cells with escalating concentrations of recombinant anisoplin and MDA-MB-231 and MDA-MB-468 cells with beauvericin at their IC_{50} concentrations, the apoptotic cell population was assessed using an Annexin-V based apoptosis kit, adhering to the procedure provided by the manufacturer. Post treatment, MCF-7, MDA-MB-231 and MDA-MB-468 cells underwent trypsinization. Following that cells were incubated with both annexin-V-Alexa-Fluor-488 and Propidium Iodide fluorochromes in 1X binding buffer for another 30 min. Subsequently, CytoFLEX, Beckman Coulter flow cytometer and Flow-Jo software were used to analyze the samples and data, respectively. The gating strategy was employed based on the positive and negative control samples and the early and late apoptotic population were distinguished based on gating.

2.6.34. Assessment of cell cycle progression

The impact of beauvericin on cell cycle progression of TNBC cells was investigated using flow cytometry based analysis. Initially, A 6-well plate was seeded with 2×10^5 cells for 24 h. Following attachment, cells underwent serum starvation in growth media containing 0.5% serum for synchronization for another 12h. subsequently, cells were treated with beauvericin at IC_{50} concentration for 48 h. Following trypsinization, the cells were fixed in 75% ice-cold ethanol at -20°C for minimum 12 h. Following that, the cells underwent thorough washing with ice cold PBS and RNase treatment for 1h at 37°C, and additional washing with PBS. Subsequently the cells were stained with Propidium Iodide (PI) for 30 min in dark. Then the sample analyses were performed

TH-3487_186106116

using a BD FACSMelody flow cytometer, and the obtained data were analyzed in FlowJo software.

2.6.35. Colony formation assay

The ability of clonal expansion and regeneration ability of rAnp treated MCF-7 cells and beauvericin treated TNBC cells were assessed by colony formation assay (Franken et al., 2006). Briefly, rAnp treated MCF-7 cells (with increasing concentrations) and beauvericin treated TNBC cells (at respective IC_{50} concentrations) were trypsinized and resuspended in a fresh DMEM medium. The cell counts were further estimated using haemocytometer. Then cells were cultured at a concentration of 400 cells/mL in a 6-well plate and for another 7 days with media exchange in every 3 alternate days. After fixing the colonies for 10 min in ice-cold methanol, they were stained for 30 min with 0.5% crystal violet. Finally the wells were washed with PBS. After drying, An inverted brightfield microscope was used to visualize and count the colonies.

2.6.36. Spheroid formation assay

To assess the ability of spheroid formation of beauvericin treated TNBC cells, Initially, monolayers of MDA-MB-231 and MDA-MB-468 cells were treated with beauvericin at respective IC_{50} concentrations for 48 hours. Following treatment, the respective cells were counted using a haemocytometer and 1×10^4 cells per well were used to form spheroids as per the protocol mentioned in section 2.5. After formation, spheroid images were captured under brightfield using an LSM 880 microscope and analyzed using ImageJ software.

2.6.37. Assessment of cellular viability of spheroids

To assess the viability of spheroids of TNBC cells upon beauvericin treatment, 3D spheroids were generated following the protocol mentioned in section 2.5. The spheroids were then incubated with escalating concentrations of beauvericin for another 72 h. Post treatment, the cells were incubated with 1X Alamar blue for the next 4 h, and each well's absorbance was recorded at 570 nm with reference to 600 nm.

TH-3487_186106116

2.6.38. Live – dead staining of 3D spheroids

In order to visualize the live and dead population in a 3D spheroid, the spheroids were first formed as detailed in the section 2.5 and subjected to treatment with the IC_{50} concentration of beauvericin, Subsequent to a 72 h treatment period, calcein-AM (2 µM) and Propidium Iodide (4 µM) were used to stain the spheroids for an additional 30 min in dark. Post-staining images were captured using an LSM 880 confocal microscope.

2.6.39. Cell viability assessment of EMT induced TNBC cells

The viability of EMT induced TNBC cells was assessed using Alamar Blue assay (Walzl et al., 2014). Briefly, 5×10^3 cells per well were seeded in a 96 well cell culture plate. The EMT induced cells were treated with increasing concentrations of beauvericin for another 48 h. Following treatment, cells were incubated with 1X Alamar Blue solution for further 2h. The absorbance of each well was measured at 570 nm with a reference of 600 nm using a microplate reader (MultiSkan microplate reader, ThermoFisher Scientific). The cell viability was calculated using the following equation –

$$\text{Cell viability (\%)} = \frac{\text{Average (A570}-\text{A600) of treated wells}}{\text{Average (A570}-\text{A600) of untreated wells}} \times 100$$

2.6.40. Wound closure assay

The changes in the migratory ability of TNBC cells were investigated by wound closure assay as per the established protocol (Wu et al., 2008). Briefly, cells were grown in 35-mm cell culture plates up to 90% confluency. Post confluency, cells were scrapped using a sterile micropipette tip to create wound. Following wound creation, the monolayer was gently washed with PBS to remove cell debris. Next, the cells were treated with beauvericin at IC_{50} concentration and incubated maintaining the cell growth conditions for a period of 18h. The images of wound prior to treatment and post treatment were recorded using ZOE™ cell imaging microscope (BioRad). The images were further analyzed and wound width was measured using ImageJ software. The migration rate of each sample was calculated according to the following formula

TH-3487_186106116

$$\text{Migration rate } (\mu m/h) = \frac{\text{Initial distance (0th h)} - \text{Final distance (18th h)}}{\text{Total time (h)}}$$

2.6.41. Quantitative real-time PCR

After treating EMT induced TNBC cells with beauvericin at respective IC_{50} concentrations, total RNA was extracted using Trizol reagent (RNAiso Plus) following the manufacturer's instruction. Following extraction, cDNA was synthesized using the iScript cDNA synthesis kit according to the manufacturer's protocol. Amplification of the gene of interest was performed templating the cDNA, using SYBR® Green master mix and Rotor-gene Q (Qiagen) real-time PCR cycler to quantitatively estimate the gene expression. The obtained data was normalized with β-actin expression and quantified using delta-delta CT method. Further data analysis was conducted using LinReg PCR software. The specific primer sequences used for gene amplification are enlisted in section 2.1.1.

2.6.42. Immunoblotting

TNBC cells induced with EMT were treated with beauvericin at IC_{50} concentrations for 48h. Following treatment, Cells were harvested and total protein was extracted using RIPA lysis buffer. The total protein content was estimated using bicinchoninic acid (BCA) reagent and equal amounts of protein from each sample were separated via SDS-PAGE. The separated protein bands were then transferred onto PVDF membranes, which were subsequently blocked using blocking buffer (4% BSA in TBST). Following blocking, the membranes were incubated with the respective primary antibodies overnight. The following day, membranes were thoroughly washed with TBST and incubated in HRP linked secondary antibody. The membranes were further washed with TBST and the signals were developed using ECL western blotting substrate. Images were captured using Bio-Rad ChemiDoc™ Imager and analyzed using ImageJ software. Details of the primary and secondary antibodies, along with their respective catalogue numbers, are enlisted in section 2.1.1.

TH-3487_186106116

2.6.43. Statistical analysis

All collected data were analyzed for statistical significance using GraphPad Prism (v9.0) software. The experimental results were expressed as mean ± standard error of mean (SEM). To evaluate possible correlations among experimental groups, One-way ANOVA was conducted for comparisons involving three or more groups, while unpaired t-test were employed for comparisons between two groups. A p-value exceeding 0.05 was deemed as statistically insignificant, whereas p-value < 0.05 was considered statistically significant, denoted as follows: * = $p < 0.05$, ** = $p < 0.01$, *** = $p < 0.001$, and **** = $p < 0.000$.

TH-3487_186106116

TH-3487_186106116

Chapter 3

Results and Discussions

TH-3487_186106116

TH-3487_186106116

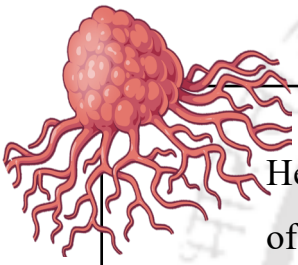

Heterologous production, purification and characterization of anisoplin from *Metarhizium anisopliae* and its therapeutic effects on breast cancer cells.

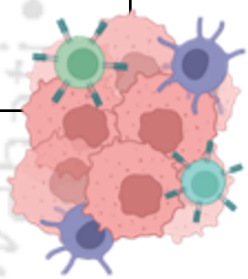

Toxicology in Vitro 94, 105737.

TH-3487_186106116

TH-3487_186106116

GRAPHICAL ABSTRACT

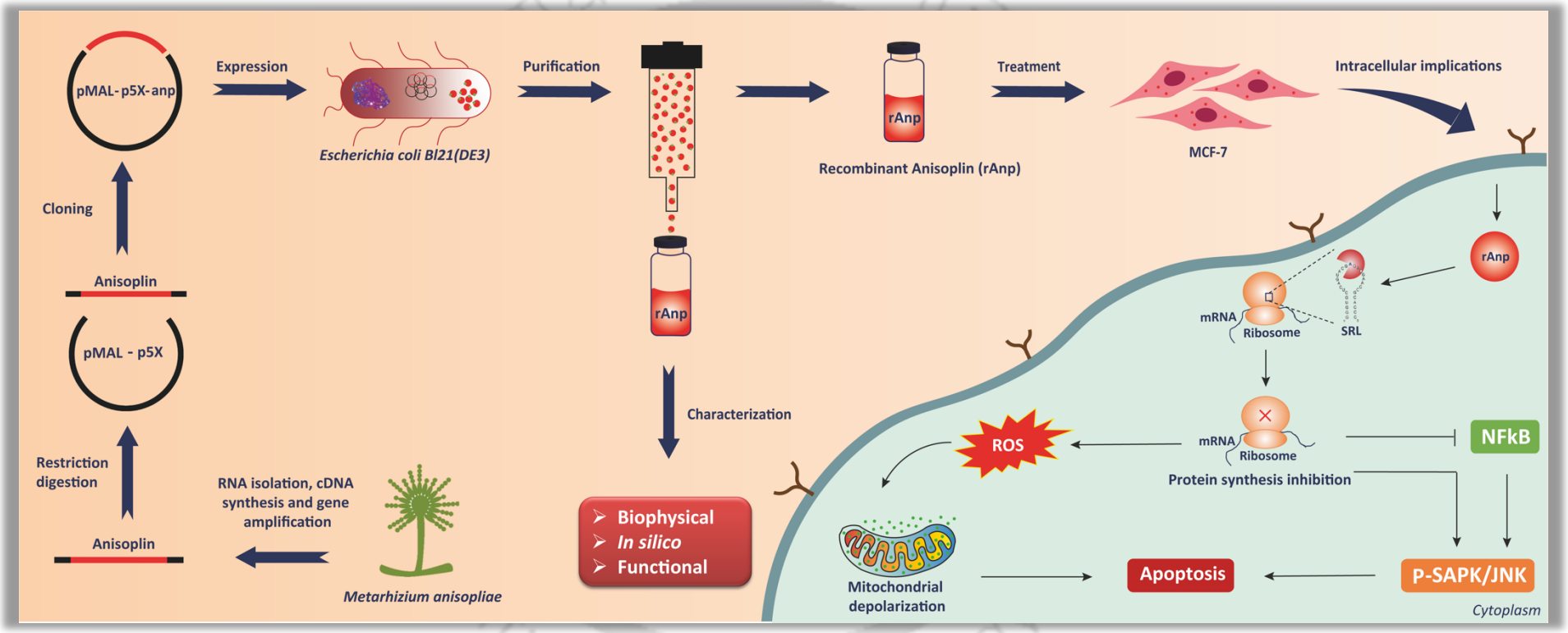

Scheme 3.1: Schematic representation of heterologous production of fungal ribotoxin Anisoplin, its characterization and *in vitro* anticancer effects on MCF-7 breast cancer cells.

TH-3487_186106116

TH-3487_186106116

A B S T R A C T

Emerging resistance to traditional chemotherapy poses a significant challenge in the treatment of breast cancer. Fungal ribotoxins possess promising therapeutic potential against cancer due to their ability to inhibit protein synthesis by targeting ribosomes. Despite previous characterization efforts, the therapeutic effectiveness of the entomopathogenic ribotoxin anisoplin against cancer cells remain unexplored. In this study, recombinant anisoplin has been successfully produced using the Escherichia coli BL21(DE3) expression system, followed by thorough purification and validation through in silico, biophysical, and functional analyses. The findings showed that recombinant anisoplin effectively reduced the viability of MCF-7 breast cancer cells in a dose-dependent manner, achieving an IC_{50} value of 4 μM. Treatment with anisoplin also led to a significant 3.5-fold increase in intracellular reactive oxygen species, indicating heightened oxidative stress within the cells. Additionally, anisoplin induced mitochondrial membrane depolarization and subsequent apoptosis, as evidenced by flow cytometric analyses. Moreover, MCF-7 cells treated with anisoplin exhibited a notable loss of their self-renewal capacity for clonal expansion and regeneration. Further mechanistic investigations revealed that anisoplin triggered a ribotoxic stress response, activating the JNK-dependent MAP kinase signaling pathway. Immunoblotting confirmed increased expression of phospho-SAPK/JNK, which correlated with changes in NFκB expression profiles and ultimately contributed to cell death. These results underscore the therapeutic potential of recombinant anisoplin in breast cancer treatment, demonstrating its ability to induce cytotoxic effects and disrupt key cellular pathways essential for cancer cell survival and proliferation.

TH-3487_186106116

TH-3487_186106116

3.1.1. RESULTS

3.1.1.1. Construction of pMAL-p5X-anp recombinant plasmid

In order to produce recombinant anisoplin, the pMAL-p5X expression vector was chosen to express the *anisoplin* gene in *Escherichia coli* BL21(DE3) expression system. The pMAL-p5X vector was explicitly designed to recombinantly produce the protein of choice along with a signal peptide for its periplasmic transport that provides an oxidative environment to the protein for the formation of possible disulphide bonds (di Guana et al., 1988). Apart from this, pMAL-p5X produces the protein of interest as a fusion protein with maltose binding protein (MBP) for its easy solubilization and purification based on affinity chromatography (Maina et al., 1988). To produce recombinant anisoplin, the *anisoplin* gene was amplified using gene specific primers, templating the cDNA synthesized from the total RNA isolated from *Metarhizium anisopliae* (MTCC 892 equivalent to ATCC 26852). By estimating its size against DNA markers of specific lengths, successful amplification was confirmed using agarose gel electrophoresis.

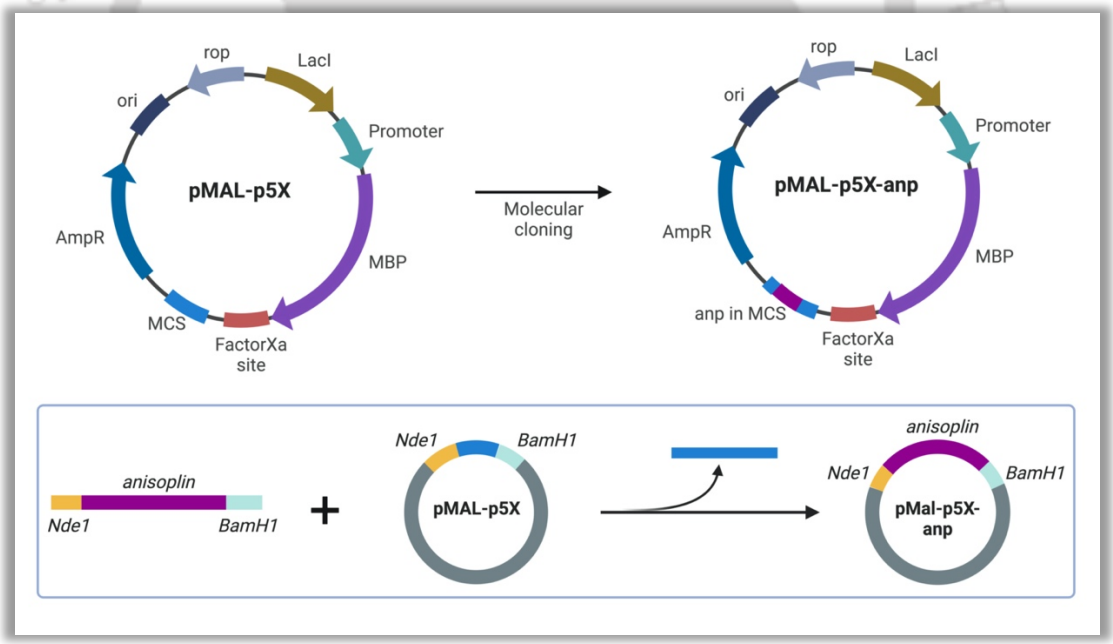

Scheme 3.1.1. Schematic depiction illustrating the cloning strategy of *anisoplin* gene in pMAL-p5X expression vector at MCS region between BamHI and NdeI restriction sites.

TH-3487_186106116

BamHI-HF and NdeI double digested pMAL-p5X vector was used to build the recombinant pMAL-p5X-anp plasmid by incorporating the amplified *anisoplin* gene in the desired location (**Scheme 3.1.1.**).

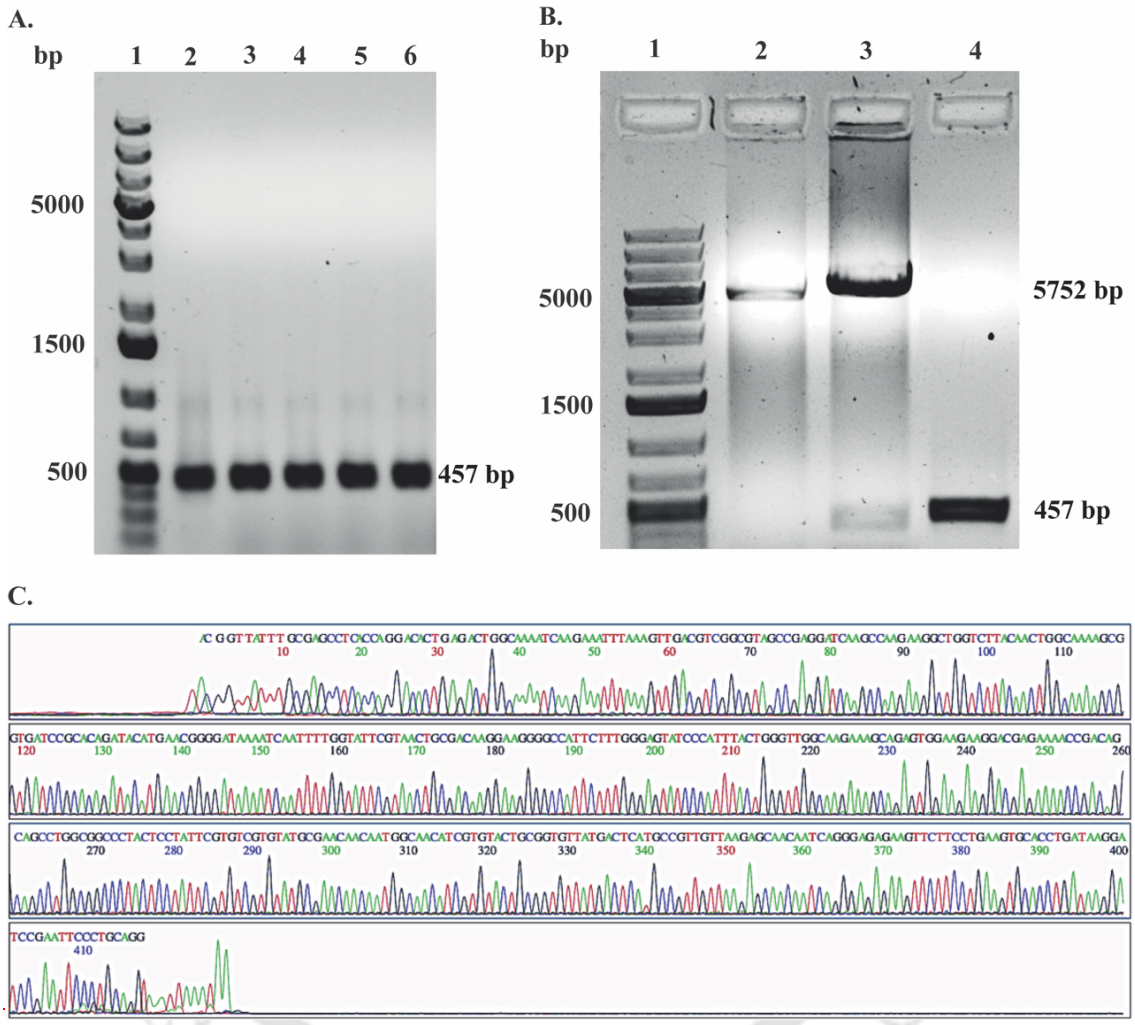

Figure 3.1.1. Confirmation of anisoplin clone (A) pMAL-p5X-anp clone confirmation by amplification of *anisoplin* gene through colony PCR. DNA ladder (lane 1), *anisoplin* gene as positive control (lane 2), amplified *anisoplin* gene from four different transformed colonies (lane 3-4). **(B)** Reconfirmation of *anisoplin* gene by BamHI-NdeI double restriction digestion of pMAL-p5X-anp recombinant plasmid. DNA molecular weight marker (lane 1), double digested pMAL-p5X vector (lane 2), double digested pMAL-p5X-anp recombinant plasmid (lane 3), *anisoplin* gene (lane 4). **(C)** Sequencing results showing the cloned sequence of the inserted gene of *anisoplin*.

TH-3487_186106116

The successful construction of pMAL-p5X-anp recombinant plasmid was preliminarily confirmed by amplification of the *anisoplin* gene of the same size as that of the previously amplified one (~ 457 bp), through colony PCR (**Figure 3.1.1A**). Following this, double restriction digestion of pMAL-p5X-anp recombinant plasmid was performed to obtain the insert of approximately 457 bp (**Figure 3.1.1B**). The clone was further validated by gene sequencing (**Figure 3.1.1C**).

3.1.1.2. Overexpression, solubility optimization and purification of recombinant anisoplin

The *anisoplin* gene was over-expressed in *Escherichia coli* BL21(DE3) expression system under the control of isopropyl-β-D-1-thiogalactopyranoside (IPTG) inducible lac promoter as MBP-Anp fusion protein. **Figure 3.1.2A** showed the increase in the MBP-Anp fusion protein of approximately 58 kDa upon induction with 0.3 mM IPTG with increasing time when subjected to SDS-PAGE.

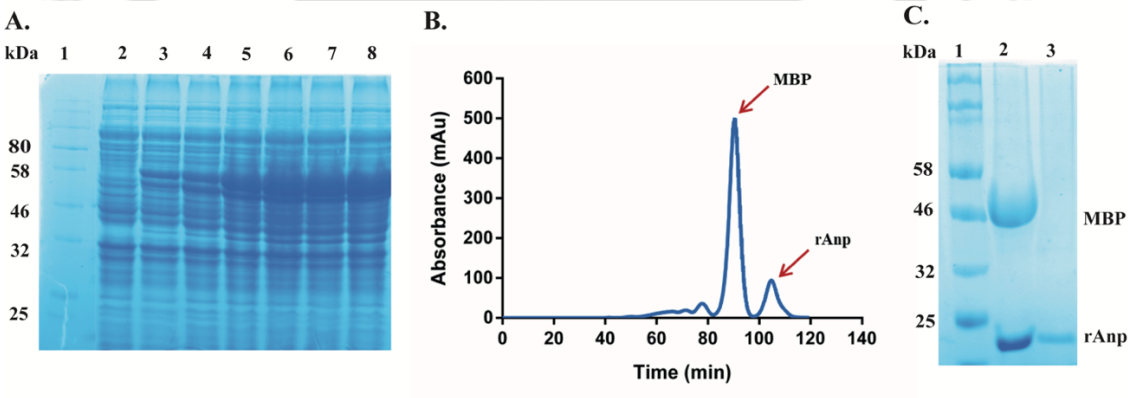

Figure 3.1.2. Overexpression and purification of rAnp. **(A)** SDS-PAGE showing overexpression of MBP-Anp fusion protein. Lane 1 – Protein molecular weight marker, Lane 2 – Uninduced bacterial lysate, Lane 3-8 – 0.3 mM IPTG induced lysate after 1, 2, 3, 4, 5 and 6 hours of induction, respectively. **(B)** Size exclusion chromatogram showing separation of maltose binding protein (MBP) and recombinant anisoplin (rAnp) from Factor-Xa protease digested MBP-Anp fusion protein. **(C)** SDS-PAGE showing Factor-Xa protease digested MBP and rAnp bands separately (lane 2) and rAnp band purified through size exclusion chromatography (lane 3), Lane 1 – protein molecular weight marker.

TH-3487_186106116

This observation confirmed overexpression of the fusion protein inside the bacterial expression system upon IPTG induction. Further, solubility of the fusion protein was optimized by expressing it under three different temperatures: 37˚C, 25˚C and 16˚C for 6 h, 12 h and 16 h, respectively. The SDS-PAGE analysis of the soluble and insoluble fractions showed that the MBP-Anp fusion protein was partially soluble in 37˚C and 25˚C. However, the protein was completely soluble in the aqueous phase at 16˚C (**Figure 3.1.3A** and **3.1.3B**).

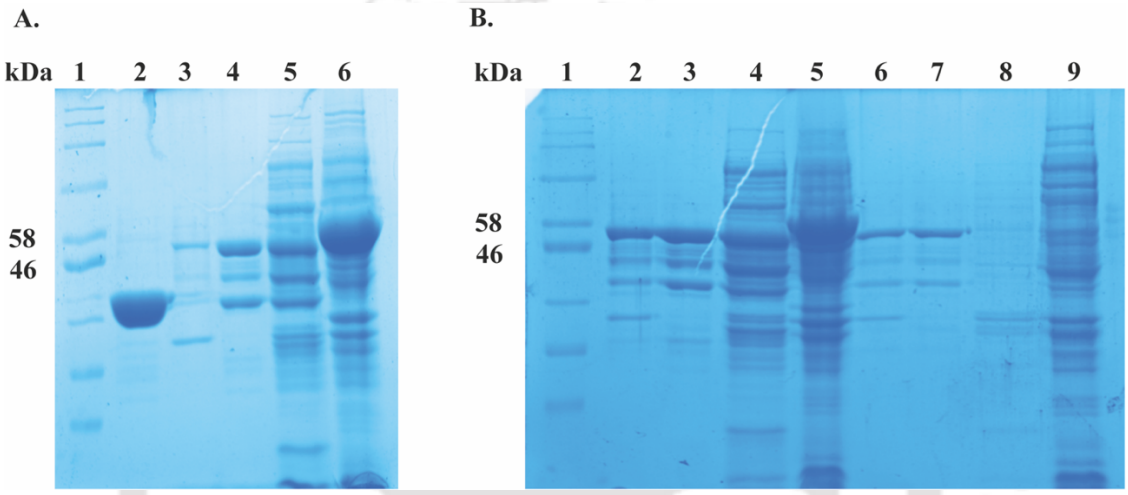

Figure 3.1.3. Solubility optimization of MBP-Anp fusion protein. (A) Solubility optimisation of rAnp protein expressed at 37˚C for 6 hours. Protein molecular weight marker (lane 1), periplasmic fraction (lane 2) and insoluble fraction (lane 3) of MBP (positive control) expressing bacterial lysate. Periplasmic fraction (lane 4), cytosolic fraction (lane 5) and insoluble fraction (lane 6) of MBP-Anp fusion protein expressing bacterial lysate. **(B)** Solubility optimisation of MBP-Anp fusion protein expressed at 25˚C and 16˚C for 12 hours and 16 hours respectively. protein molecular weight marker (lane 1), sucrose buffer fraction (lane 2), periplasmic fraction (lane 3), cytosolic fraction (lane 4) and insoluble fraction (lane 5) of MBP-Anp fusion protein expressing bacterial lysate at 25˚C. Sucrose buffer fraction (lane 6), periplasmic fraction (lane 7), cytosolic fraction (lane 8) and insoluble fraction (lane 9) of MBP-Anp fusion protein expressing bacterial lysate at 16˚C.

TH-3487_186106116

The proteins produced in the soluble fractions were initially purified using affinity chromatography based on the strong affinity of maltose binding protein (MBP) towards maltose. Following this, the eluted fusion protein was concentrated and analyzed by SDS-PAGE. The purified fusion protein was further subjected to digestion by Factor-Xa protease to cleave the MBP tag so that pure recombinant anisoplin (rAnp) could be obtained. Furthermore, purified rAnp was obtained by separating it from the cleaved MBP through size exclusion chromatography (**Figure 3.1.2B**) and analyzed by SDS-PAGE to confirm its purity. **Figure 3.1.2C** showed the successful cleavage of MBP-Anp fusion protein and the separation of pure rAnp protein.

3.1.1.3. *In silico* characterization of anisoplin

Although Olombrada et al., 2017 characterized the recombinant anisoplin in the earlier study (Olombrada et al., 2017), adequate information about this protein remained unexplored. Here, *in silico* approach has been undertaken to characterize the protein to reveal more information about it that would help for its further studies. Firstly, sequence-based physicochemical properties of anisoplin were determined using the ProtParam tool (**Table 3.1.1**). The analysis revealed that the protein was comprised of 138 amino acid residues with a molecular weight of approximately 15359.46 Da. The theoretical extinction coefficient was found to be 24200 $M^{-1}cm^{-1}$ in the presence of all possible disulphide bonds and 23950 $M^{-1}cm^{-1}$ in absence of them. The theoretical isoelectric point (pI) of anisoplin was found to be 9.0. Generally, proteins are positively charged at pH below their pI (Tokmakov et al., 2021). Hence, at physiological pH (~ 7.4), anisoplin should be positively charged, which may help its attachment to negatively charged cell membranes for better internalization. The protein was found to be composed of 22 positively charged amino acids (Arg + Lys) and 17 negatively charged amino acids (Asp +Glu).

TH-3487_186106116

Table 3.1.1. Predicted physicochemical properties of anisoplin.

PROPERTIES	VALUES	REMARKS
No. of amino acids	138	No remarks
Molecular weight	15359.46 Da	No remarks
Extinction coefficient ($M^{-1}cm^{-1}$), having all possible disulfide bonds	24200	No remarks
Extinction coefficient ($M^{-1}cm^{-1}$), with no possible disulfide bonds	23950	No remarks
Theoretical PI	9.00	positively charged at physiological pH
Total no. of positively charged residues (Arg + Lys)	22	No remarks
Total no. of negatively charged residues (Asp + Glu)	17	No remarks
Instability index (II)	11.04	Stable (Instability index < 40 = stable)
Aliphatic index	62.10	More or less thermostable
Grand average of hydropathicity (GRAVY)	-0.733	Hydrophilic

TH-3487_186106116

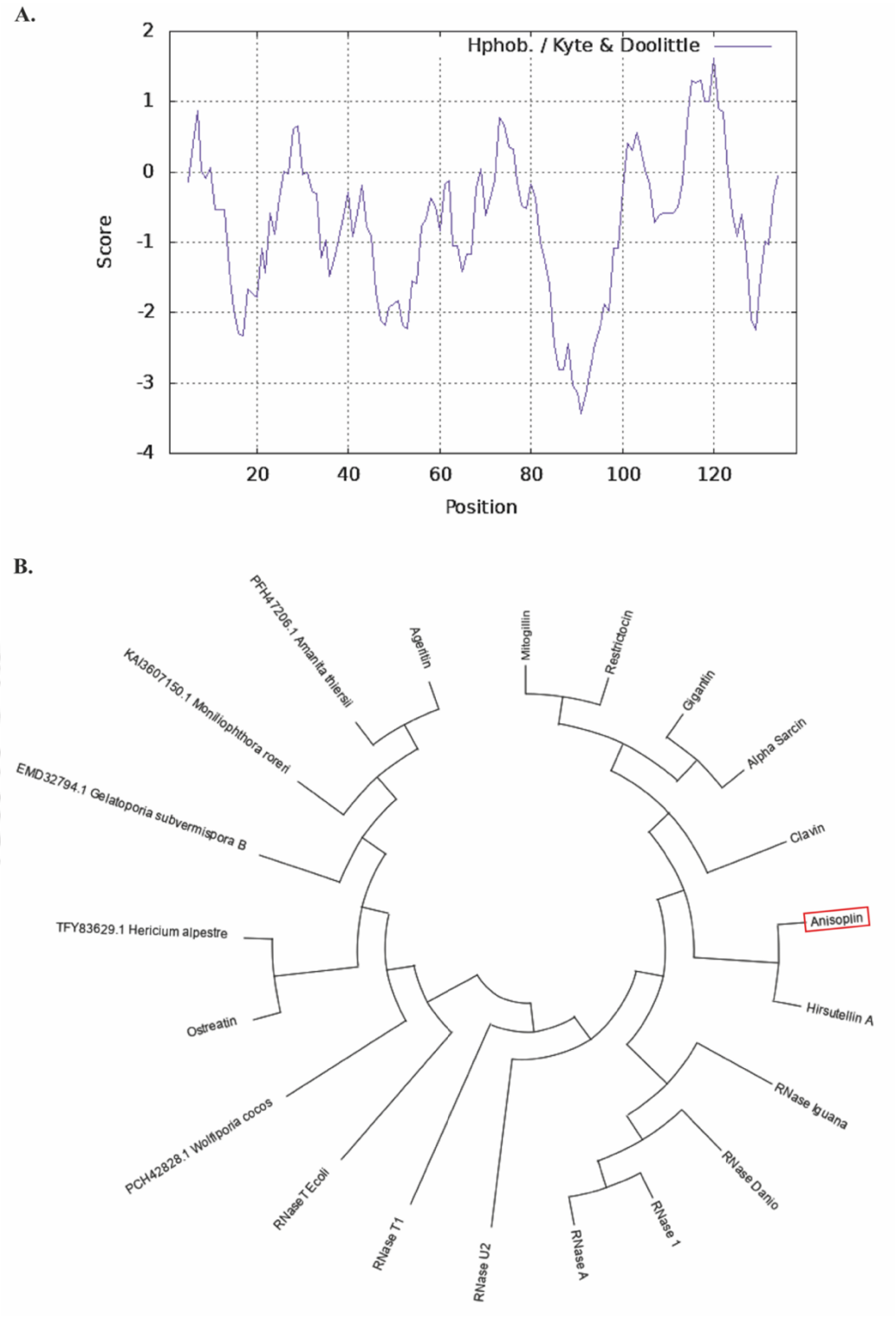

Figure 3.1.4. *In silico* analysis of Anisoplin (A) Kyte & Doolittle hydropathy plot of anisoplin. **(B)** Phylogenetic tree analysis of ribotoxin anisoplin.

TH-3487_186106116

A higher number of positively charged amino acid residues also indicated that the protein might be positively charged at neutral pH. The instability index was found to be 11.04, indicating that the protein is stable (instability index < 40 = stable) (Gasteiger et al., 2005). The aliphatic index of 62.10 indicated its thermostability and the negative grand average of hydropathy (GRAVY) value -0.733 stipulated the protein to be hydrophilic in nature (Gasteiger et al., 2005). The Kyte-Doolittle hydropathy plot also suggested the hydrophilicity of the protein by scoring more towards the negative scores (**Figure 3.1.4A**). The conserved domain prediction using NCBI's conserved domain database (CDD) suggested that anisoplin contains a conserved domain of fungal ribonuclease (cd00212/cd00606) matching 35th to 138th residues of the query sequence with an E-value of 2.06x10^{-04}. **Table 3.1.2** also suggested that the protein could be a guanyl-specific ribotoxin.

Table 3.1.2. Conserved domain prediction of Anisoplin.

PROPERTIES	DESCRIPTION
Domain name and CDD accession no.	Microbial RNases superfamily (Fungal RNase) (cd00212 / cd00606)
Domain interval matched	35th - 138th residues in the query sequence
E-value	2.06e^{-04}
Super family description	Microbial RNases. Ribonucleases (RNases) cleave phosphodiester bonds in RNA and

TH-3487_186106116

	are essential for both non-specific RNA degradation and for numerous forms of RNA processing. The alignment contains fungal RNases (U2, T1, F1, Th, Pb, N1, and Ms) and bacterial RNases (barnase, binase, RNase Sa) , the majority of which are guanyl specific and **fungal ribotoxins**.

The p-blast results of the anisoplin query sequence against the protein database (PDB) revealed its only known homologous protein hit Hirsutellin A with 95% query coverage and 66.67% identity, indicating it being a Hirsutellin A like fungal ribotoxin as also reported by Olombrada et al., 2017 (Olombrada et al., 2017). The evolutionary conservation with other ribotoxins and ribonucleases by phylogenetic analysis also supported the fact that it is closely related to only Hirsutellin A and distantly related to other ribotoxins (**Figure 3.1.4B**).

3.1.1.4. Biophysical characterization of recombinant anisoplin (rAnp)

The secondary structural components of purified recombinant anisoplin (rAnp) were experimentally determined by analyzing the circular dichroism (CD). The circular dichroism (CD) graph of rAnp (**Figure 3.1.5A**) showed that it is composed of 15.3% α-Helix, 8.7% of antiparallel β-sheet, 9.5% turns and 56.5% of other structural components as per the data analyzed by BeStSel server. rAnp possesses almost a similar amount of all secondary structural components as its homolog Hirsutellin A with a significant difference in β-sheets content (Viegas et al., 2009). The structural thermostability of the rAnp was studied in increasing temperatures, starting from 20°C to 100°C. **Figure 3.1.5B** showed that the circular dichroism (CD) curve pattern of rAnp remained almost similar up to 40°C; however, ellipticity (mdeg) was significantly changed in the following temperatures. This observation indicated the stability of rAnp up to 40°C, followed by its structural deformation as temperature increased.

TH-3487_186106116

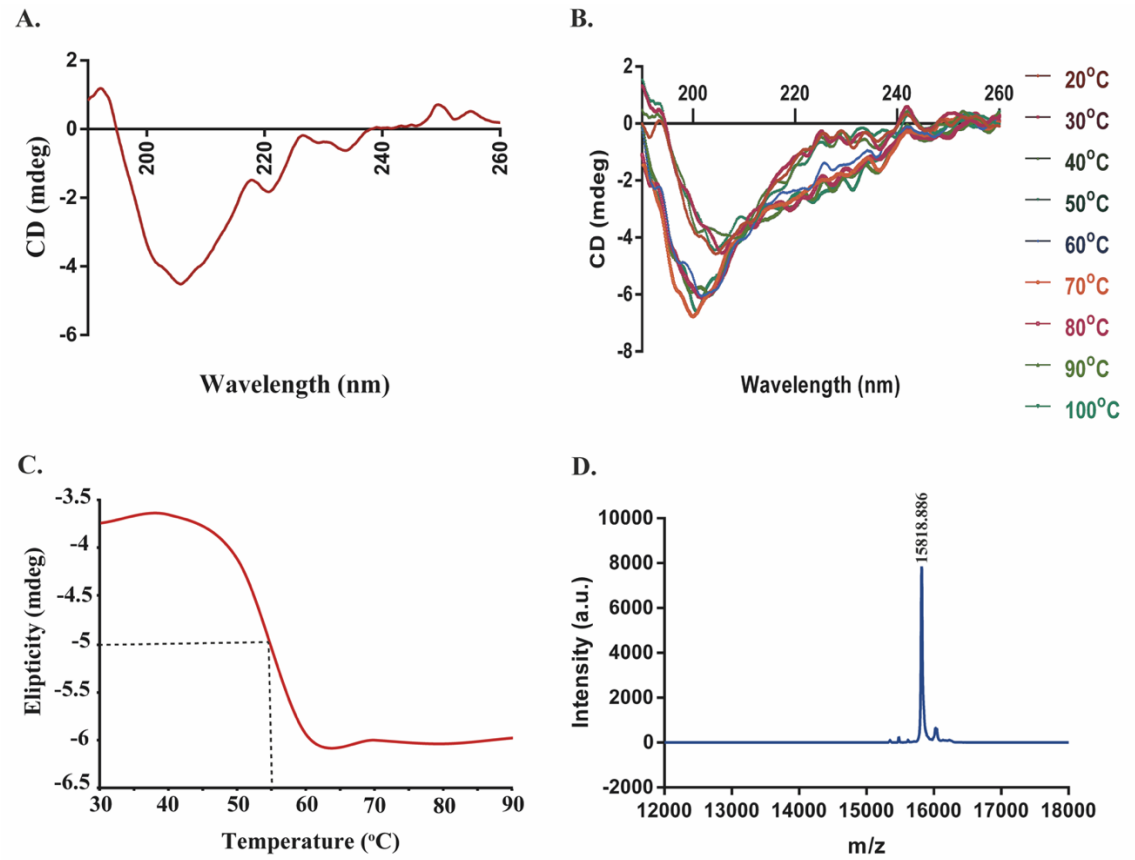

Figure 3.1.5. Biophysical characterization of rAnp. (A) Circular dichroism (CD) graph showing the pattern of secondary structural elements content in pure rAnp. **(B)** Circular dichroism (CD) graph of rAnp showing the changes in the graph pattern in increasing temperature (20˚C – 100˚C). **(C)** Thermal denaturation profile of recombinant anisoplin (rAnp) at 203 nm. **(D)** MALDI-TOF-MS plot of recombinant anisoplin (rAnp).

The thermal denaturation profile of rAnp was obtained by plotting the ellipticity (mdeg) at 203 nm against corresponding temperatures in increasing order. The curve showed a folded to unfolded transition of rAnp structure with a T_m value of 55˚C (**Figure 3.1.5C**), similar to the previously reported value (Olombrada et al., 2017). MALDI-TOF MS data analysis revealed the rAnp was 15818.88 Da in size (**Figure 3.1.5D**), approximately 500 Da more than the theoretically calculated molecular mass, which was primarily due to the incorporation of some extra amino acid residues in the process of its heterologous production.

TH-3487_186106116

3.1.1.5. In silico prediction and validation of 3D tertiary structure of anisoplin

The three-dimensional tertiary structure of anisoplin was predicted using four different webservers, such as the SWISS-MODEL prediction tool of ExPASy, AlphaFold 2, Phyre2 and I-TASSER web servers as shown in Fig. S4. All the predicted structures were refined using GalaxyRefine web server and Ramachandran plots of the refined structures were predicted using PROCHECK tool as shown in **Figure 3.1.6.**

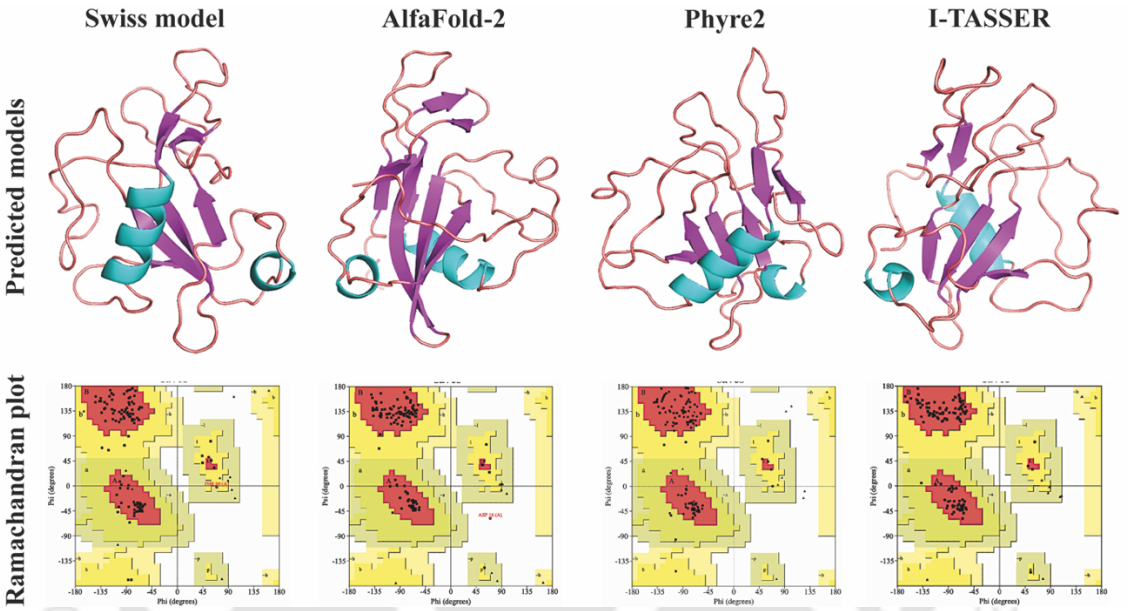

Figure 3.1.6. *In silico* 3D tertiary structure of anisoplin modelled using Swiss model, AlfaFold2, Phyre2 and I-TASSER web servers and their respective Ramachandran plots.

Based on the data obtained from Ramachandran plots the structure predicted by I-TASSER server was determined as the best fit model as it was predicted to have 98.3% amino acid residues in the most favoured region, 1.7% residues in the additional allowed region and no residues in generously allowed and disallowed regions compared to the predicted structures from other web servers as per **Table 3.1.3.**

TH-3487_186106116

Table 3.1.3. Ramachandran plot analysis of predicted anisoplin structures.

SERVER	RESIDUES IN MOST FAVORED REGIONS (%)	RESIDUES IN ADDITIONAL ALLOWED REGIONS (%)	RESIDUES IN GENEROUSLY ALLOWED REGIONS (%)	RESIDUES IN DISALLOWED REGIONS (%)
Swiss model	77.5	21.6	0.0	0.9
Alphafold2	95.7	3.5	0.0	0.9
Phyre2	91.3	8.7	0.0	0.0
I-TASSER	98.3	1.7	0.0	0.0

Table 3.1.4. Z-score table of predicted anisoplin structures.

SERVER	Z-SCORE
Hirsutellin A (PDB ID 2KAA)	-5.54
Swiss model	-6.36
Alphafold2	-6.44
Phyre2	-6.16
I-TASSER	-6.84

TH-3487_186106116

The modelled structures were also validated based on the Z-score obtained by the ProSA web server, as shown in **Table 3.1.4.** The Z-score value of the refined model obtained from the I-TASSER server was -6.84, within the acceptable range of -10 to 10. The Z-score value of the only homologous protein Hirsutellin A (PDB ID 2KAA) -5.54 suggests that the obtained model is reliable and close to the experimentally determined homologous protein structure. The Z-score depends on the protein's length, and negative Z-scores are very good for a reliable model. Z-score represents the overall quality and measures the deviation of the total energy of the protein structure (Wiederstein and Sippl, 2007). The best modelled structure predicted by the I-TASSER server was used for further analysis.

3.1.1.6. *In silico* prediction of SRL binding pocket and its validation through molecular dynamics (MD) simulation

In order to map the active site residues, the anisoplin sequence was aligned with its only homologous protein, Hirsutellin A (PDB ID 2KAA). The active site residues of Hirsutellin A, as reported previously (D40, H42, E66, R95, H113, F126) (Viegas et al., 2009) were highlighted with the corresponding residues of anisoplin (D48, H50, E74, R103, H121, F134) in **Figure 3.1.7A.** The residues in the vicinity of the highlighted anisoplin residues may also contribute in the interaction with SRL. The transphosphorylation reaction of SRL occurs at the active site of Hirsutellin A involving a catalytic pair of residues E66 and H113. They work as acidic and basic residues on each side of the hydrolyzed bond, stabilizing the nucleotides (Viegas et al., 2009). Other residues in the vicinity (D40, H42, R95 and F126) might be helpful in stabilizing electrostatic interaction with the SRL substrate. The interaction profile of anisoplin with the SRL loop was established in a dynamic environment using molecular dynamics (MD) simulation. The molecular dynamics (MD) simulation of the anisoplin-SRL complex was performed using GROMACS for 100 nanoseconds (ns).

TH-3487_186106116

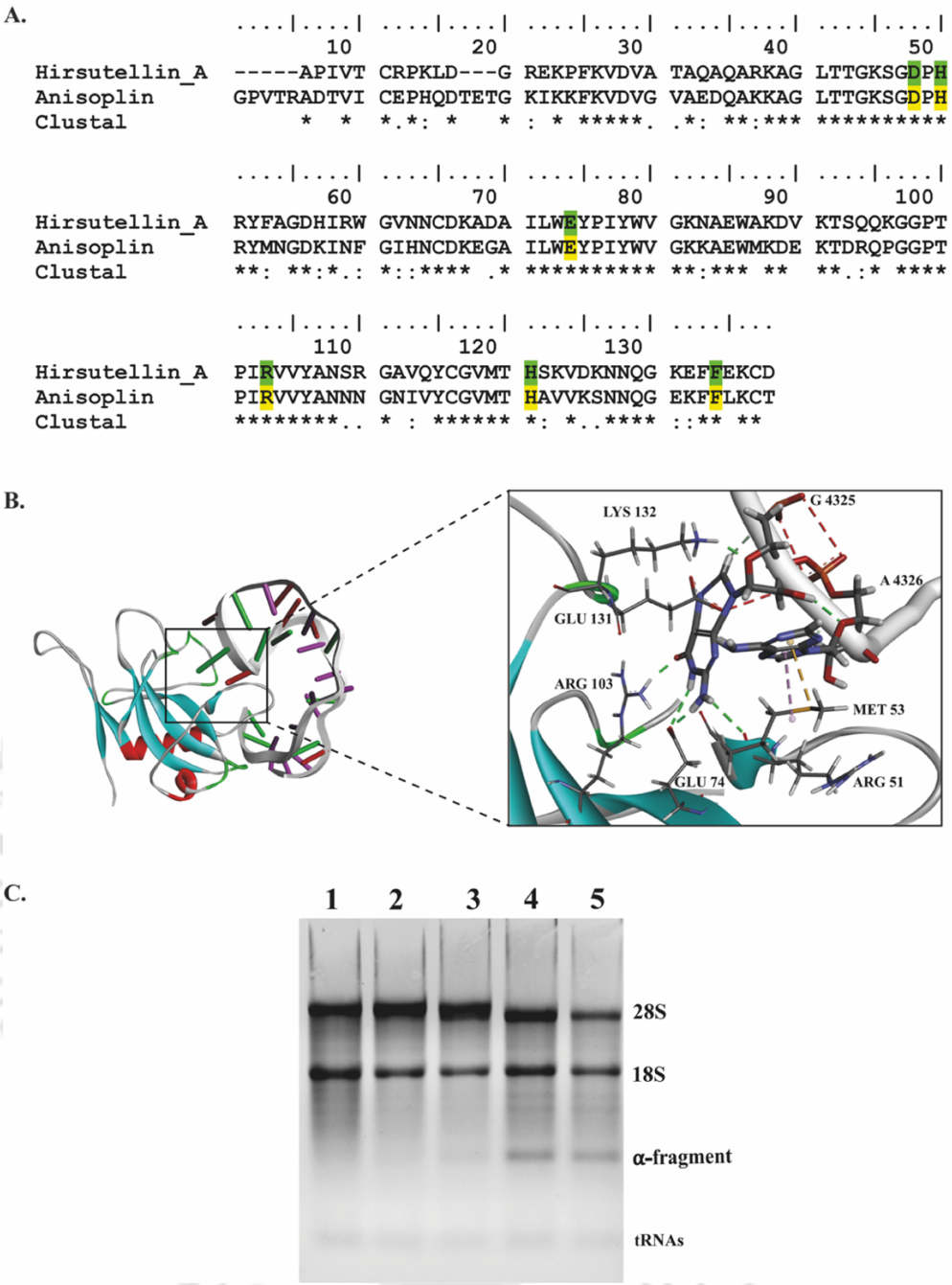

Figure 3.1.7. ***In silico*** **and functional characterization of rAnp. (A)** Sequence alignment of Hirsutellin A and anisoplin with highlighted possible active site residues. **(B)** Sarcin-ricin-loop (SRL) bound anisoplin structure (I-TASSER model) obtained through molecular dynamics (MD) simulation showing the possible interactions between the probable active site residues and SRL substrate. **(C)** Agarose gel electrophoresis image of rabbit reticulocyte lysate treated with 0.01 µM (lane 2), 0.1 µM (lane 3), 1 µM (lane 4) and 10 µM (lane 5) rAnp (lane 1 – untreated sample).

TH-3487_186106116

The interaction between the SRL and active site residues of anisoplin after 100 ns simulation was shown in **Figure 3.1.7B.** It was observed that the active site residues R51, M53, E74, R103, E131 and K132 of anisoplin interacted with G4325 and A4326 of GAGA region of universally conserved SRL. Based on the comparative analysis with the Hirsutellin A (Viegas et al., 2009), E74 (acidic) and K132 (basic) of anisoplin may be considered as the catalytic pair of residues required for the transphosphorylation reaction of SRL and other residues (R51, M53, R103, E131) may assist in the stabilization of electrostatic interaction with SRL.

3.1.1.7. Functional characterization of recombinant anisoplin (rAnp)

The substrate specific ribonucleolytic activity of rAnp was determined *in vitro* using rabbit reticulocyte lysate as substrate. Rabbit reticulocyte lysate contains active ribosomes that provide the ribotoxin with sarcin-ricin-loop (SRL) to act upon. The appearance of approximately 400 nucleotide α-fragment during gel electrophoresis when treated with increasing concentration of rAnp indicated the ability of the rAnp to specifically cleave the sarcin-ricin loop (SRL) of 28S rRNA present in 60S large subunit of the eukaryotic ribosome (**Figure 3.1.7C**). The result obtained was similar to the earlier report of Olombrada et al., 2017 confirming the ribotoxic activity of the rAnp. This event might significantly inhibit the process of intracellular protein biosynthesis in cancer cells and halt their further growth and development.

3.1.1.8. Effects of anisoplin on the viability and intracellular ROS levels in MCF-7 cells

Due to the specific cleavage of SRL, the protein biosynthesis inhibitory action of recombinant anisoplin (rAnp) ultimately contributes to cellular death (Olombrada et al., 2017). This characteristic of the rAnp was evaluated by employing the cell viability assay using MTT as the reagent to detect the viable cells when treated with increasing concentrations against cell types from cancerous and non-cancerous origins. In both cases, the treatment showed dose dependent cytotoxicity. However, in MCF-7 cells, the dosage was significantly lower than in the non-cancerous HEK-293 cells (**Figure 3.1.8A** and **3.1.8B**).

TH-3487_186106116

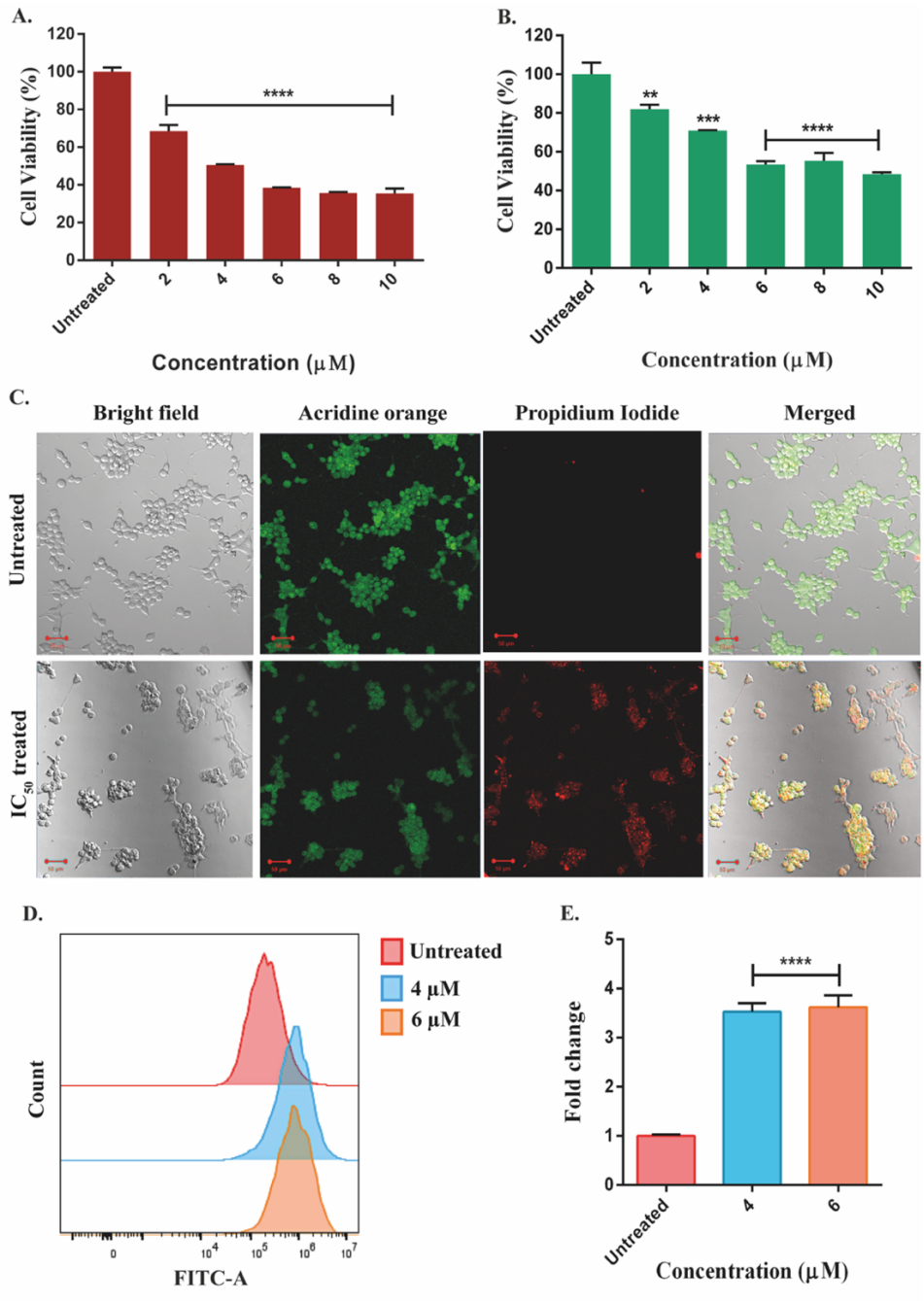

Figure 3.1.8. Cytotoxicity and induction of oxidative stress in MCF-7 cells upon rAnp treatment. (A) Antiproliferative effect of rAnp against MCF-7 breast cancer cells and **(B)** non-cancerous HEK-293 cells. **(C)** Confocal microscopic images showing live (Green) and dead (red) populations of MCF-7 cells. **(D)** Generation of intracellular reactive oxygen species (ROS) in MCF-7 cells upon treatment with increasing concentration of rAnp. **(E)** Fold change in ROS content of MCF-7 cells in respective rAnp concentrations.

TH-3487_186106116

The dosage required to inhibit the growth of 50% cell population (IC_{50}) was found to be 4 µM in the case of MCF-7 cells, whereas it was 7 µM in the case of HEK293 cells, making it a potential therapeutic candidate to be studied further on breast cancer cells. Furthermore, the MCF-7 cells treated with IC_{50} concentration of rAnp were stained with acridine orange and Propidium Iodide to visualize the live and dead populations, respectively. The confocal microscopic images of rAnp treated MCF-7 cells showed increased Propidium Iodide uptake in contrast with the untreated cells, confirming the cellular death of MCF-7 cells (**Figure 3.1.8C**). In order to investigate the mechanism underlying cellular death caused by rAnp in MCF-7 cells, its ability to elevate intracellular reactive oxygen species (ROS) was determined via DCFDA based flow cytometric analysis. The rAnp induced oxidative stress by enhancing intracellular ROS within 4 hours of treatment by approximately 3.5 and 3.6-fold when treated with 4 and 6 µM, respectively, in contrast to the untreated sample (**Figure 3.1.8D** and **Figure 3.1.8E**).

3.1.1.9. Depolarization of mitochondrial the membrane and subsequent induction of apoptosis

The detrimental effect of elevated intracellular ROS level on mitochondrial membrane integrity and transmembrane potential was further assessed by JC-1 based flow cytometry. In polarized mitochondria, the cyanine dye JC-1 forms J-aggregates exhibiting red fluorescence, whereas in depolarized mitochondria, it remains in its monomeric form, producing green fluorescence (Perelman et al., 2012). Following treatment with increasing concentrations of rAnp, the MCF-7 cells underwent mitochondrial depolarization. Healthy mitochondria of untreated cells showed prominent red fluorescence, whereas, approximately 9.72% and 16.14% of cells were observed to have depolarized mitochondrial membranes projecting more green fluorescence when treated with 4 and 6 µM of rAnp respectively, as shown in **Figure 3.1.9A.** The flipping of the plasma membrane in apoptotic cells exposes the phosphatidylserine residues to the outer leaflet, which can bind the Annexin-V-Alexa Flour 488, exhibiting green fluorescence. In contrast, the compromised plasma membrane of the necrotic cell population allows nucleic acid staining by Propidium Iodide, projecting red fluorescence.

TH-3487_186106116

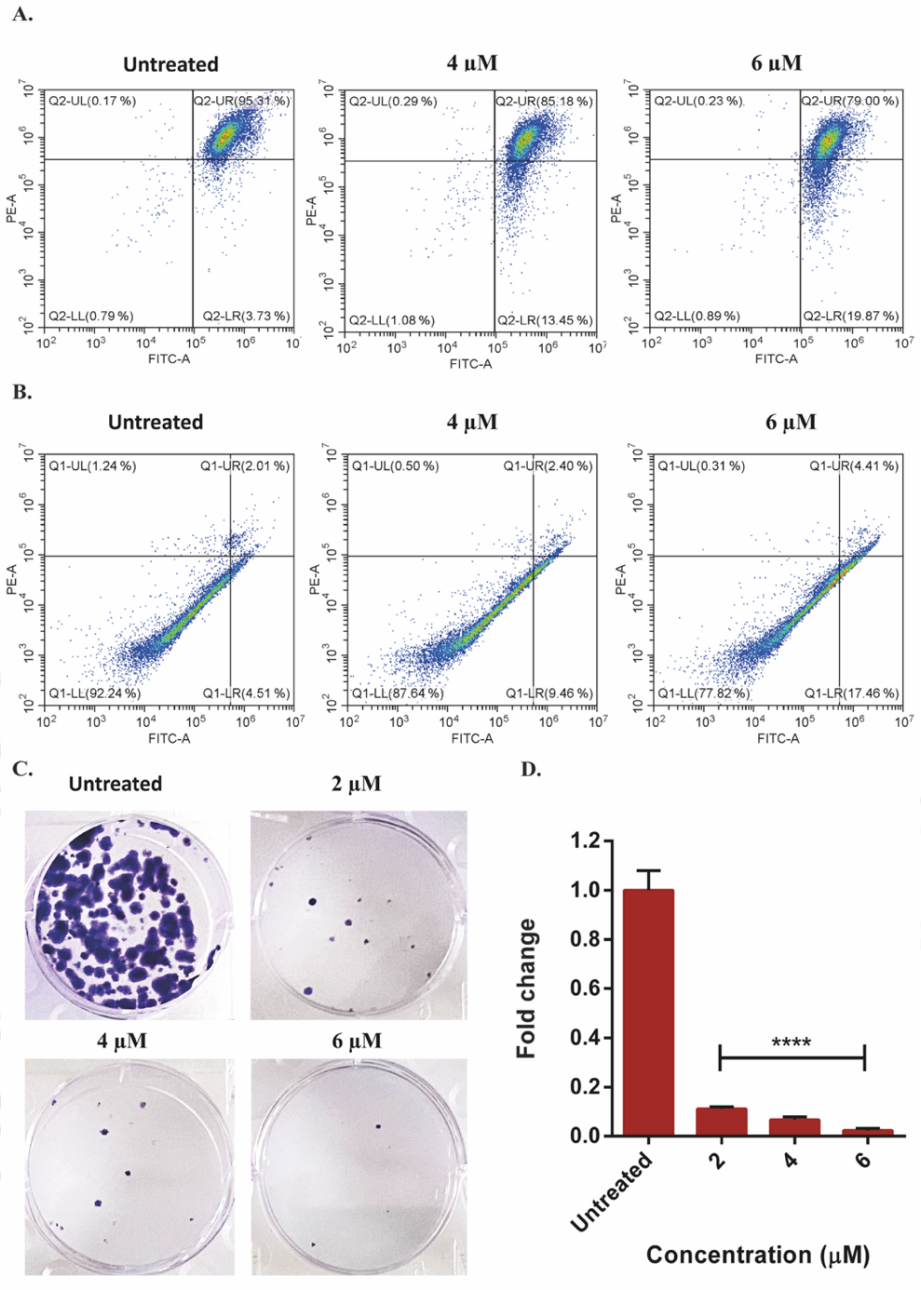

Figure 3.1.9. Mitochondrial depolarization, activation of apoptosis and reduction in clonal expansion of MCF-7 cells upon rAnp treatment. (A) Flow cytometric analysis of mitochondrial membrane depolarization of MCF-7 cells upon treatment with increasing concentrations of rAnp. **(B)** Flow cytometric analysis of the apoptotic population of MCF-7 cells upon treatment with increasing concentrations of rAnp. **(C)** Assessment of colony formation ability of single cells of MCF-7 upon treatment with increasing concentrations of rAnp. **(D)** Fold change in the colony formation of MCF-7 cells upon treatment with increasing concentrations of rAnp.

TH-3487_186106116

Hence, flow cytometric detection quantitatively estimates the apoptotic and necrotic cells in a given cell population (Crowley et al., 2016). The flow cytometric analysis showed 5.34% and 15.35% increase in the apoptotic population of MCF-7 cells following treatment with 4 and 6 μM rAnp, respectively (**Figure 3.1.9B**).

3.1.1.10. Reduction in clonal expansion ability of MCF-7 cells

The clonal expansion ability of cancerous cells is more rapid compared to those of non-cancerous origin. The self-renewal ability of a single cell to form colonies *in vitro* is generally measured by clonogenic assay. Following treatment with increasing concentration of rAnp, MCF-7 cells showed substantial decrease in the number of colonies formed in comparison with untreated cells, confirming loss of their self-renewal ability (**Figure 3.1.9C**). Further quantitative evaluation exhibited 9, 16.6 and 50-fold reduction in the colony formation ability of MCF-7 cells upon treatment with 2, 4 and 6 μM rAnp, respectively, in contrast to the untreated cells (**Figure 3.1.9D**).

3.1.1.11. Regulation of intracellular signaling pathways

Ribotoxin induced stress response activates some downstream intracellular signaling in response to stressed conditions. Mitogen activated protein kinase (MAP kinase) pathway is one of the most common signaling pathways activated in stress conditions (Kyriakis and Avruch, 2001). Among three groups of MAP kinases [extracellular signaling regulated kinases 1 and 2 (ERK1and 2), c-Jun N-terminal kinases (JNK1, 2 and 3), p38 (α, β, γ, δ)], JNKs and p38s are the stress activated protein kinases (SAPKs), which are triggered in response to various exogenous and endogenous stimuli (Vind et al., 2020). Phosphorylation of such kinases indicates their functional activation. Following treatment with increasing concentrations of rAnp (2, 4 and 6 μM), MCF-7 cells exhibited 7.3, 8.9, and 7.8-fold upregulation in the phosphorylated variant of JNK (P-SAPK/JNK) protein (**Figure 3.1.10A** and **3.1.10B**), as confirmed by Western blot analysis. Furthermore, immune-flowcytometric analysis showed downregulation of NFκB expression by approximately 2-fold upon treatment with both 4 and 6 μM of rAnp (**Figure 3.1.10C** and **3.1.10D**). Hence, the experimental results demonstrated that rAnp induced activation of SAPK/JNK signaling while significantly downregulating NFκB expression.

TH-3487_186106116

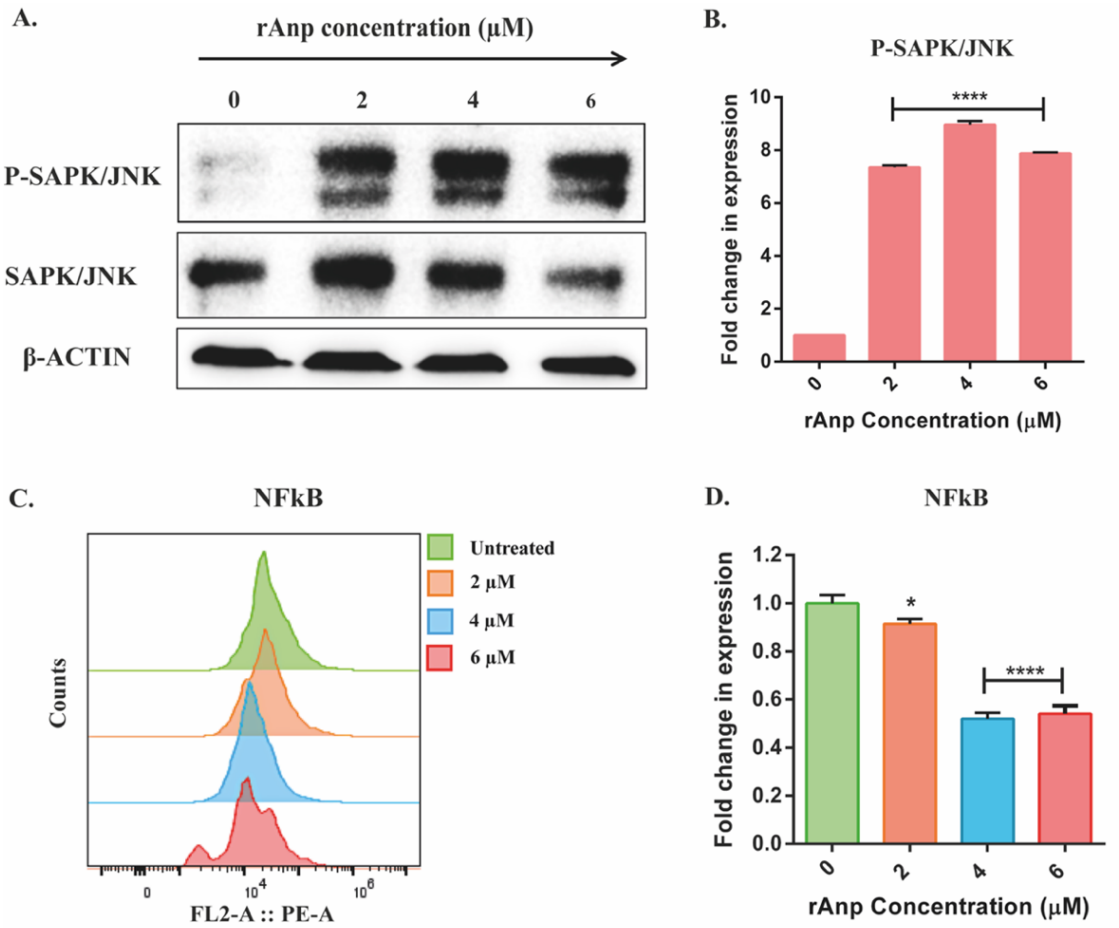

Figure 3.1.10. SAPK/JNK activation and downregulation of NFκB upon rAnp treatment. **(A)** Western blot images showing changes in P-SAPK/JNK expression in MCF-7 cells upon treatment with increasing concentrations of rAnp. **(B)** Fold change in P-SAPK/JNK expression. **(C)** Changes in NFκB expression in MCF-7 cells upon treatment with increasing rAnp concentration. **(D)** Fold changes in NFκB expression.

TH-3487_186106116

3.1.2. DISCUSSION

Owing to the ribosome inhibitory cytotoxic nature, fungal ribotoxins are suitable candidates for their therapeutic impact on different types of cancer. They are utilized either in the form of immunotoxins (Carreras-Sangrà et al., 2012; Goyal and Batra, 2000; Lázaro-Gorines et al., 2019; Rathore et al., 1997; Tomé-Amat et al., 2015b, 2015a) or nanoconjugate (Mohamed et al., 2014) to ensure their target specific action. They have also been evaluated for their therapeutic efficacy on *in vitro* as well as *in vivo* cancer models. Anisoplin, the smallest ribotoxin ever reported after Hirsutellin A (Olombrada et al., 2017), necessitates further investigation of its anticancer potential. In this study, heterologous production of recombinant anisoplin has been accomplished in the *Escherichia coli* BL21(DE3) expression system and further characterized to validate its successful production based on earlier report (Olombrada et al., 2017). *In silico* studies have revealed the most reliable three-dimensional tertiary structural model of anisoplin, which was used to predict the probable active site residues interacting with SRL substrate at the GAGA site. This prediction was further validated by molecular dynamics (MD) simulation.

The findings of the study have also revealed that rAnp is able to induce cellular death in MCF-7 breast cancer cells in a dose-dependent manner, mostly due to its ribosome inhibitory action by specific cleavage of SRL in the large subunit of the active eukaryotic ribosome. In order to investigate the intracellular implications of the cytotoxic nature of rAnp, a series of microscopic, flow cytometric and immunoblotting experiments have been performed. Approximately 3.5-fold elevation in the intracellular reactive oxygen species (ROS) generation suggested induction of intracellular oxidative stress as a consequence of protein synthesis inhibitory action of rAnp. The anticancer effect of most of the chemotherapeutic agents is due to their ability to induce ROS-mediated oxidative stress, contributing to cellular injury (Yang et al., 2018). Hence, the elevation of intracellular ROS level upon rAnp treatment implied the possible alteration in the redox homeostasis of MCF-7 cells, eventually triggering cellular death and contributing to the tumour suppression process. Ribotoxins are often reported to induce apoptosis mediated cellular death, where ROS generation is a part of the process (Redza-Dutordoir and Averill-Bates, 2016). Similar results obtained in the case of rAnp treatment indicated its potential anticancer effect through the induction of oxidative stress.

TH-3487_186106116

Mitochondrial depolarization and loss of electrochemical gradient across the mitochondrial inner membrane (Δψ) are mostly associated with cellular death via mitochondrial pathway mediated apoptosis (Matsuyama and Reed, 2000). Significant depolarization of mitochondrial membrane observed in rAnp treated MCF-7 cells also suggested a similar effect. The rapid intracellular response against imbalanced redox and mitochondrial membrane potential (Δψ) eventually activates downstream apoptotic signaling cascades, ultimately resulting in tumor necrosis factor related apoptosis inducing ligand (TRAIL) induced cellular death in cancer cells (Suzuki-Karasaki et al., 2014). A substantial increment in the apoptotic population of MCF-7 cells in a dose dependent manner also indicated the continuity of the intracellular response cascade due to rAnp induced anticancer effects. Similar to this observation, other ribotoxins α-sarcin and Ageritin reportedly induced apoptosis in human rhabdomyosarcoma and cervical carcinoma cells *in vitro* (Olmo et al., 2001) (Citores et al., 2019). This study demonstrated the rapid loss of the self-renewal capability of MCF-7 cells as a result of rAnp treatment. Significant reduction in the colony formation indicated their inability in further clonal expansion and regeneration. Due to the ribosome inhibitory action, rAnp induced ribotoxic stress in MCF-7 cells, eventually initiating intracellular ribotoxic stress response (RSR) by activating downstream signaling pathways. One such pathway is the activation of SAPK/JNK signaling. Significant elevation in the phosphorylated SAPK/JNK upon rAnp treatment implied its successful activation. As a consequence of SAPK/JNK activation, a series of downstream cascades get activated inside cells. This SAPK/JNK activation has two consequences, either saving the cells by further activation of survival signaling pathways by an unknown mechanism (Wu et al., 2019b) or tumor necrosis factor related apoptosis inducing ligand (TRAIL) mediated activation of downstream mitochondrial apoptotic pathway (Jin et al., 2013)·(Weston and Davis, 2007). Ribotoxic stress induced SAPK/JNK activation mostly follows the latter course of action leading to apoptotic cell death (Sauter et al., 2010)·(Jetzt et al., 2009). In correlation with these reports, an increase in the cell population of depolarized mitochondrial membrane and apoptotic population upon rAnp treatment indicated the occurrence of mitochondrial pathway mediated induction of apoptotic cell death in MCF-7 breast cancer cells. Activation of SAPK/JNK was also reported previously in the case of other ribotoxins like acrolein, anisomycin, α-sarcin and tricothecene induced ribotoxic

TH-3487_186106116

stress response (Huang et al., 2018; Iordanov et al., 1997; Shifrin and Anderson, 1999; Xia et al., 2007). Recent studies revealed that inhibition of the SAPK/JNK signaling pathway often promotes the growth and epithelial-to-mesenchymal transition (EMT) of cancer cells. Thus, activation of the SAPK/JNK signaling pathway upon rAnp treatment is an indication of its anticancer and EMT inhibitory properties (Xiao et al., 2023). Similarly, Chen et al. also found that activation of the JNK signaling pathway promotes inhibition of cell growth, migration and invasion and induces apoptosis and G2 phase cell cycle arrest in bladder cancer (Chen et al., 2022). These reports strongly support and validate the anticancer properties of rAnp and project it as a potential candidate for breast cancer therapy. Downregulation of NFκB is often a determinant of reduced aggressiveness of breast cancer stem like cells (CSLC) (Biswas et al., 2023). Similarly, a significant reduction in NFκB expression upon rAnp treatment indicated its therapeutic effects on cancer cells.

Crosstalk between JNK and NFκB signaling pathway play a crucial role in the cells' fate of survival or death. Activation of JNK is often negatively correlated with NFκB. Hence, downregulation of NFκB expression is always a determinant of prolonged JNK activation and subsequent apoptotic cell death (Tang et al., 2002). Along with the activation of SAPK/JNK, findings of this study showed significant downregulation in NFκB expression, supporting the phenomenon of SAPK/JNK mediated anticancer effects of rAnp.

Although rAnp showed potential therapeutic properties against breast cancer cells, it might cause cytotoxicity to non-cancerous healthy cells due to the lack of specificity. Hence, it can be considered as a promising candidate for its future anticancer application by making it target specific. A target specific immunoconjugate or a functionalized nano-formulation of rAnp may help in achieving increased therapeutic efficiency compared to its native form, which needs to be further validated by *in vivo* studies. Targeted delivery of the toxin may significantly reduce off-target effects, making it safer for future clinical applications.

TH-3487_186106116

3.1.3. CONCLUSION

In conclusion, this study emphasizes the significant therapeutic promise of recombinant anisoplin for breast cancer treatment. Employing rigorous procedures for production, purification, and validation, anisoplin effectively reduced the viability of MCF-7 breast cancer cells in a dose-dependent manner, achieving an IC_{50} of 4 μM. The treatment induced notable oxidative stress characterized by increased intracellular reactive oxygen species and resulted in mitochondrial membrane depolarization, initiating apoptosis as confirmed by flow cytometric analyses. Notably, anisoplin treatment also impeded the self-renewal capacity of MCF-7 cells, inhibiting their ability of clonal expansion and regeneration. Mechanistic investigations revealed that anisoplin exerts its cytotoxic effects by triggering a ribotoxic stress response, activating the JNK-dependent MAP kinase signaling pathway. Immunoblotting corroborated these findings by demonstrating elevated phospho-SAPK/JNK levels and correlating changes in NFκB expression profiles, collectively contributing to the death of MCF-7 breast cancer cells.

TH-3487_186106116

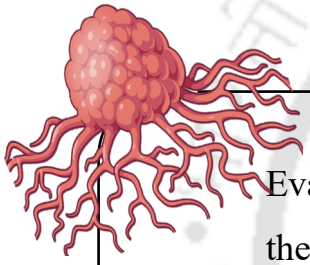

Evaluation of intracellular therapeutic targets and *in vitro* therapeutic effects of beauvericin on triple-negative breast cancer (TNBC) cells.

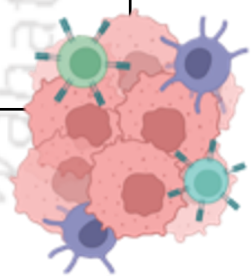

***Computational Biology and Chemistry*, *112*, p.108154.**

TH-3487_186106116

TH-3487_186106116

GRAPHICAL ABSTRACT

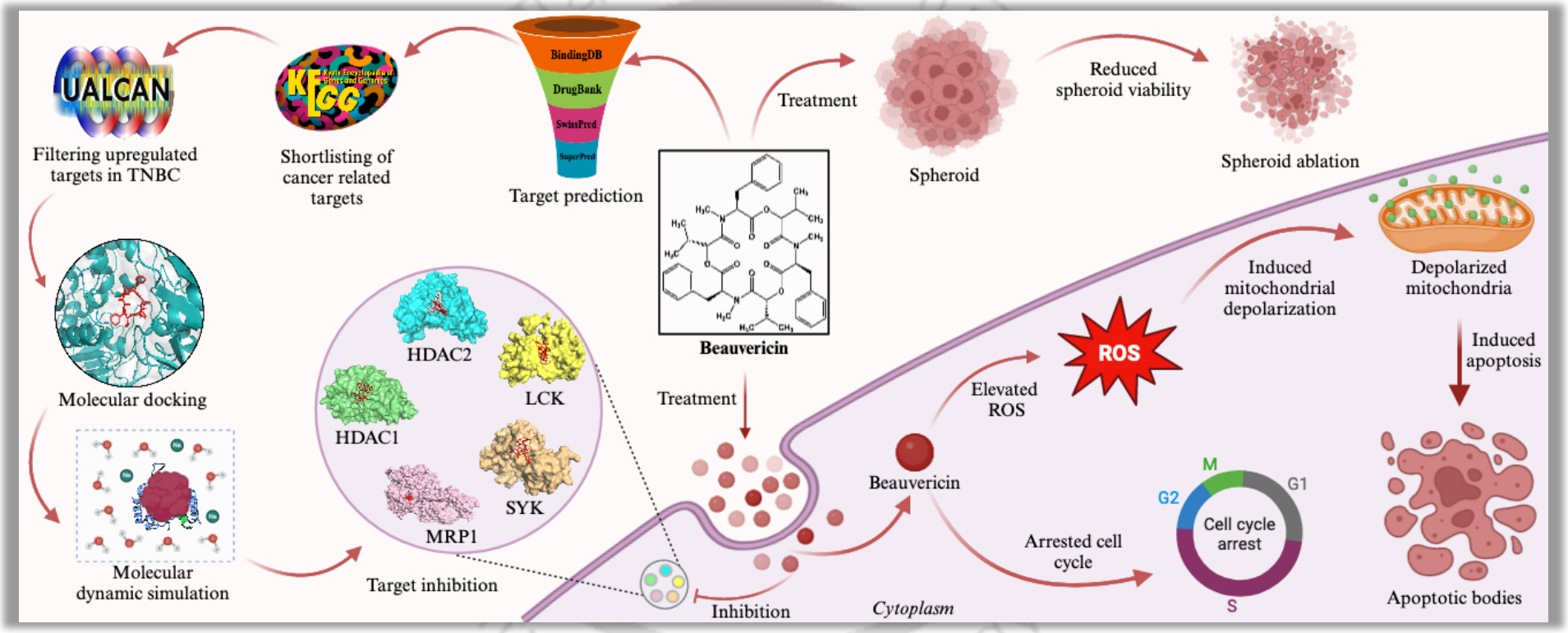

Scheme 3.2: Schematic depiction of identification of intracellular molecular targets of beauvericin through *in silico* approach and its *in vitro* anticancer effects on triple-negative breast cancer cells.

TH-3487_186106116

TH-3487_186106116

A B S T R A C T

Triple negative breast cancer (TNBC) presents a significant global health concern due to its aggressive nature, high mortality rate and limited treatment options, highlighting the urgent need for targeted therapies. Beauvericin, a bioactive fungal secondary metabolite, possess significant anticancer potential, although its molecular targets in cancer cells remain unexplored. This study has investigated possible molecular targets of beauvericin and its therapeutic insights in TNBC cells. *In silico* studies using molecular docking and MD simulation predicted the molecular targets of beauvericin. The identified targets included MRP-1 (ABCC1), HDAC-1, HDAC-2, LCK and SYK with average binding energy of -90.1, -44.3, -72.1, -105 and -60.8 KJ/mol, respectively, implying its multifaceted roles in reversing drug resistance, inhibiting epigenetic modulators and oncogenic tyrosine kinases. Beauvericin has significantly reduced the viability of MDA-MB-231 and MDA-MB-468 cells, with IC_{50} concentrations of 4.4 and 3.9 µM, while concurrently elevating the intracellular ROS by 9.0 and 7.9-fold, respectively. Subsequent reduction of mitochondrial transmembrane potential in TNBC cells, has confirmed the induction of oxidative stress, leading to apoptotic cell death, as observed by flow cytometric analyses. Beauvericin has also arrested cell cycle at G1-phase and impaired the spheroid formation and clonal expansion abilities of TNBC cells. The viability of spheroids was reduced upon beauvericin treatment, exhibiting IC_{50} concentrations of 10.3 and 6.2 µM in MDA-MB-468 and MDA-MB-231 cells, respectively. In conclusion, beauvericin has demonstrated promising therapeutic potential against TNBC cells through possible inhibition of MRP-1 (ABCC1), HDAC-1, HDAC-2, LCK and SYK.

TH-3487_186106116

TH-3487_186106116

3.2.1. RESULTS AND DISCUSSION

3.2.1.1. Prediction and screening of possible molecular targets of beauvericin in TNBC

Beauvericin is a naturally occurring bioactive cyclohexadepsipeptide derived from entomopathogenic fungi *Beauveria bassiana* (Hamill et al., 1969) and also produced by other endophytic fungi like members of *Fusarium sp.* (Logrieco et al., 1998), *Isaria sp.* (Luangsa-ard et al., 2009) and *Cordyceps sp.* (Luangsa-ard et al., 2009).

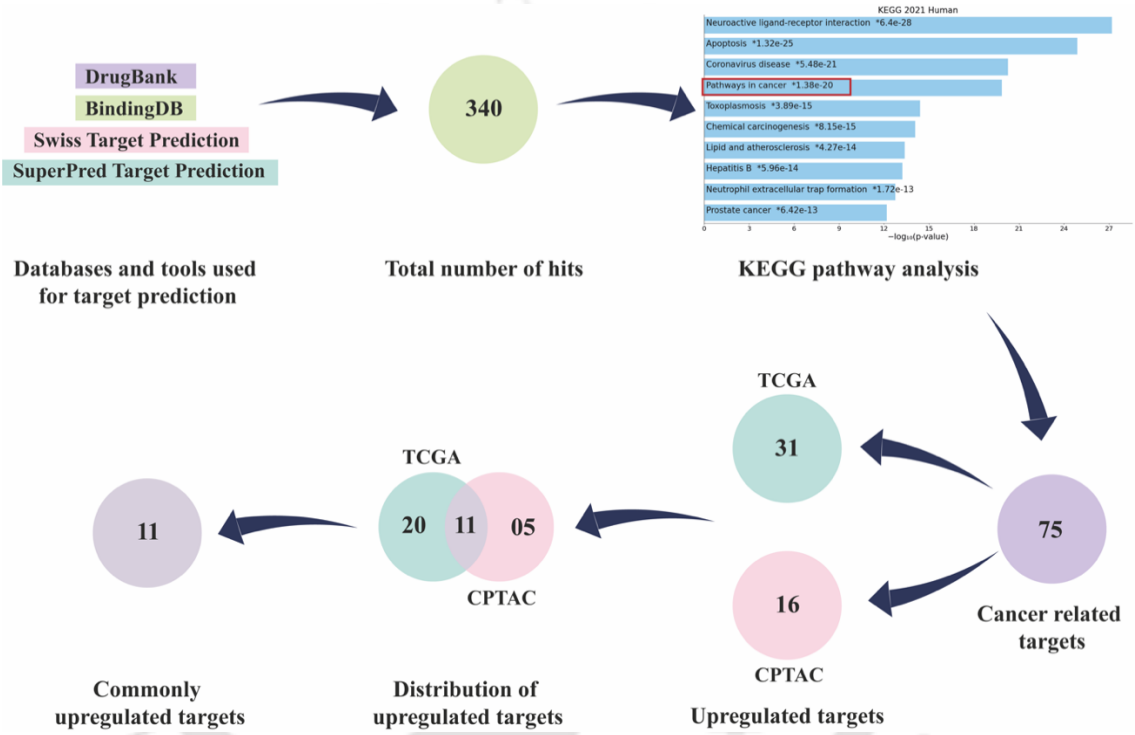

Figure 3.2.1. Prediction and shortlisting of possible molecular targets of beauvericin.

It is recognized for its various bioactivities, including antibacterial (Castlebury et al., 1999; Dzoyem et al., 2017; Meca et al., 2010; Sondergaard et al., 2016; Xu et al., 2010; H. Zhang et al., 2016), antifungal ("New Beauvericins, Potentiators of Antifungal Miconazole Activity, Produced by Beauveria sp. FKI-1366," n.d.; Shekhar-Guturja et al., 2016; Tong et al., 2016; Zhang et al., 2007), antiviral (Shin et al., 2009), nematocidal ("Nematicidal Activity of Beauvericin Produced by the Fungus Fusarium bulbicola," n.d.) insecticidal (Frederick GROVE and Pople, 1980), antimycobacterial

TH-3487_186106116

("Antimycobacterial and Antiplasmodial Cyclodepsipeptides from the Insect Pathogenic Fungus Paecilomyces tenuipes BCC 1614," n.d.) and also anticancer properties (Jow et al., 2004; LIN et al., 2005; Prosperini et al., 2013; Wu et al., 2019).

Despite the numerous known bioactivities, there have been no molecular-level investigations to identify the molecular targets of beauvericin in cancer cells. *In silico* studies have been conducted to explore the potential molecular targets of beauvericin in TNBC. Initially, BindingDB and DrugBank databases have been utilized to identify likely targets of beauvericin by assessing its structural homology (over 50% structural similarity) with known molecules and determining their targets. Additionally, SwissPred and SuperPred tools have been employed to forecast the potential targets of beauvericin computationally. Both the databases and prediction tools have yielded 340 potential intracellular and cell surface target proteins, of which 75 have been identified as cancer-related proteins based on the data analyzed by KEGG pathway analysis (**Figure 3.2.1**). Moreover, out of the 75 cancer-related targets, 31 have exhibited significant upregulation in mRNA expression level (according to the UALCAN webserver's analysis of TCGA-BRCA data), while 16 have shown upregulation in protein expression level (based on UALCAN webserver's analysis of CPTAC data) in TNBC patients (**Figure 3.2.1**). Notably, 11 of these targets have displayed upregulation at both mRNA (**Figure 3.2.2**) and protein (**Figure 3.2.3**) expression levels in TNBC. Significant upregulation of these 11 proteins have projected their role in the development and progression of TNBC. Subsequently, these 11 proteins have been selected for further validation as targets of beauvericin through molecular docking and molecular dynamics (MD) simulation studies.

TH-3487_186106116

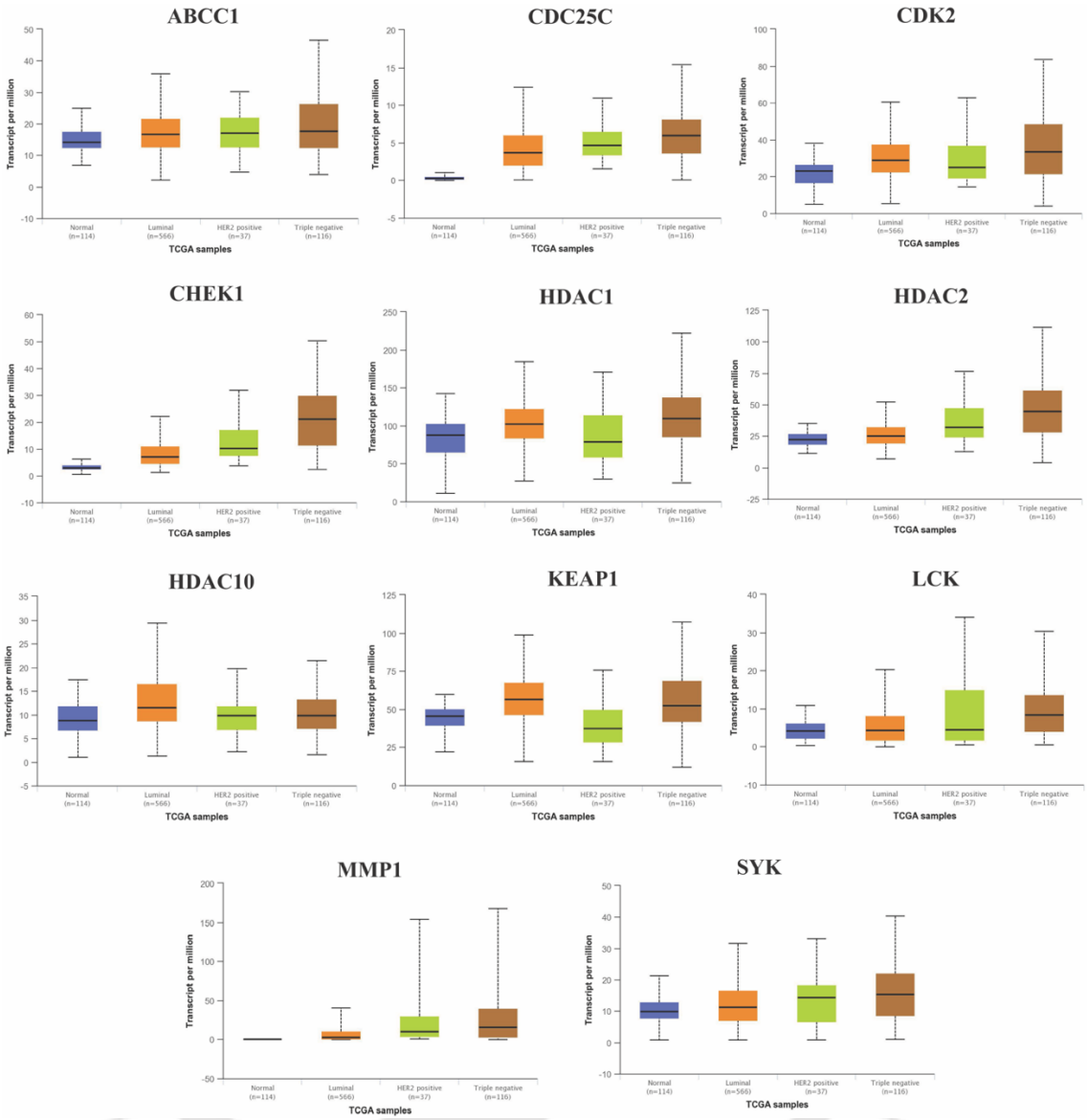

Figure 3.2.2. Box plots showing overexpression of commonly upregulated TNBC target proteins in TCGA database.

TH-3487_186106116

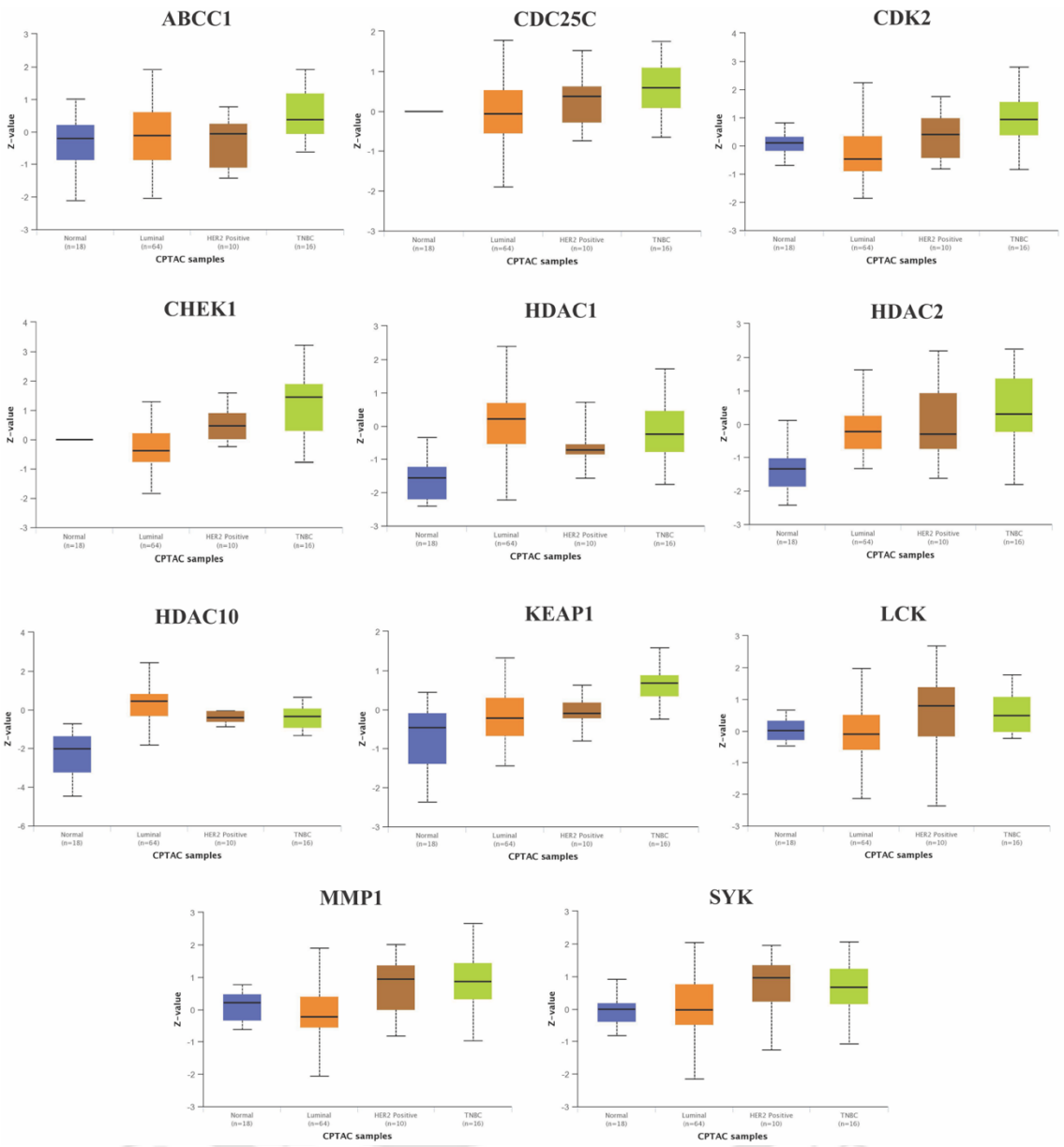

Figure 3.2.3. Box plots showing overexpression of commonly upregulated TNBC target proteins in CPTAC database.

3.2.1.2. Molecular docking of beauvericin with TNBC targets

The field of molecular docking plays a crucial role in the validation of drug targets in drug discovery and medicinal chemistry. Molecular docking is a computational technique that predicts the binding mode and affinity between a small molecule (ligand) and its target protein.

TH-3487_186106116

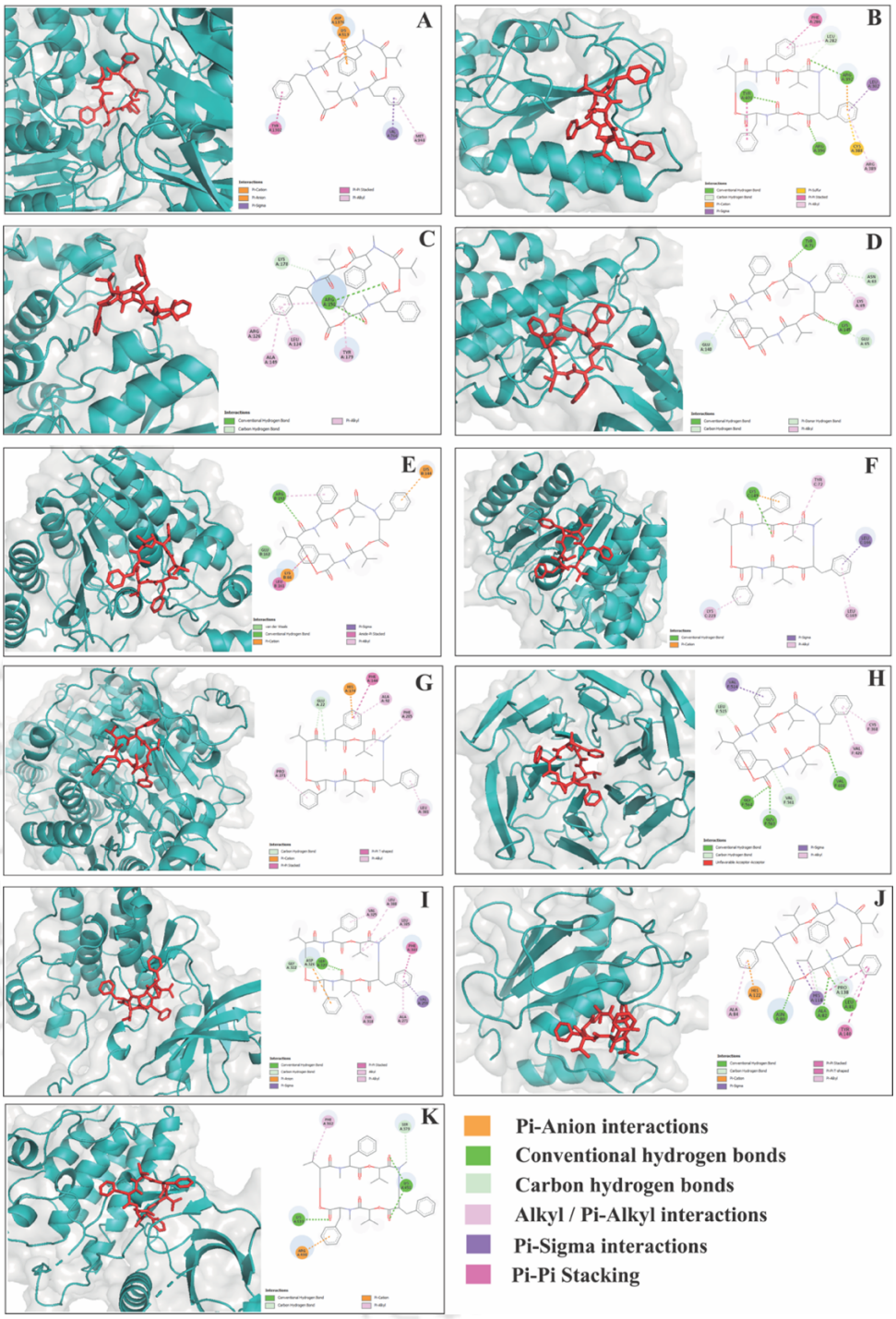

Figure 3.2.4. Molecular docking interactions between beauvericin and predicted TNBC target proteins. **A)** Beauvericin-ABCC1 complex, **B)** Beauvericin-CDC25C complex, **C)** Beauvericin-CDK2 complex, **D)** Beauvericin-CHEK1 complex, **E)** Beauvericin-HDAC1 complex, **F)** Beauvericin-HDAC2 complex, **G)** Beauvericin-HDAC10 complex, **H)** Beauvericin-KEAP1 complex, **I)** Beauvericin-LCK complex, **J)** Beauvericin-MMP1 complex, **K)** Beauvericin-SYK complex.

TH-3487_186106116

Using molecular docking, potential optimal binding orientation and conformation of a drug candidate can be determined within a target protein. This information helps in the rational design and optimization of drug compounds by providing insights into their binding interactions and potential efficacy (Pujadas et al., 2008). Several studies have employed docking to evaluate the inhibitors against respective target proteins. For example, molecular docking study has been employed to evaluate the pyrrolizidine alkaloids and flavonoid glycoside-based inhibitors of urease enzyme (Mukhtar et al., 2023) and pyrimidine-based inhibitors of CDK9 (Habib et al., 2024), respectively. Hence, the shortlisted TNBC target candidates have been further evaluated for their possible inhibition by beauvericin through molecular docking approach. The initial results have indicated strong affinity of beauvericin within the respective target proteins, revealing possible interactions between each protein-ligand complex (**Figure 3.2.4**). Each complex has resulted in significantly negative binding free energy of less than -7 Kcal/mol (**Table 3.2.1**), indicating a strong affinity of beauvericin with each target proteins. Furthermore, each complex has been analyzed for the interacting amino acid residues of respective target proteins and tabulated in **Table 3.2.1**, along with the number of hydrogen bonds present in each individual complex.

Table 3.2.1. Molecular docking results of beauvericin with predicted TNBC targets.

Predicted targets	**Binding free energy (Kcal/mol)**	**Interacting amino acid residues**	**Number of hydrogen bonds present**
ABCC1	-9.0	Asp (A:1376), Lys (A:513), Tyr (A:1302), Val (A:766), Met (A:948)	0
CDC25C	-8.6	Phe (A:286), Leu (A:282), Arg (A:392), Leu (A:302), Cys (A:388), Arg (A:389), Arg (A:396), Tyr (A:401)	3

TH-3487_186106116

CDK2	-7.2	Lys (A:178), Arg (A:150), Arg (A:126), Ala (A:149), Leu (A:124), Tyr (A:179)	2
CHEK1	-7.3	Tyr (A:71), Asn (A:63), Lys(A:69), Lys (A:145), Glu (A:65), Glu (A:140)	2
HDAC1	-7.9	Arg (B:192), Lys (B:144), Glu (B:162), Lys (B:66), Leu (B:161)	1
HDAC2	-7.8	Lys (C:149), Tyr (C:72), Leu (C:166), Leu (C:169), Lys (C:223)	1
HDAC10	-8.9	Glu (A:22), His (A:174), Phe (A:144), Ala (A:92), Phe (A:205), Leu (A:381), Pro (A:271)	0
KEAP1	-9.5	Val (F:514), Leu (F:515), Gly (F:564), Gln (F:563), Val (F:561), Val (F:608), Val (F:420), Cys (F:368)	3
LCK	-9.1	Val (A:325), Leu (A:388), Leu (A:385), Phe (A:383), Val (A:259), Ala (A:271), Tyr (A:318), Ser (A:323), Asp (A:326), Gly (A:322)	1
MMP1	-8.3	Ala (A:84), His (A:122), Asn (A:80), His (A:118), Ala (A:82), Pro (A:138), Leu (A:81), Tyr (A:140)	3
SYK	-8.1	Phe (A:382), Ser (A:379), Lys (A:458), Lys (A:533), Arg (A:498)	3

More negative the binding energy and more the number of hydrogen bonds present in a protein-ligand complex, the interactions become stronger. Therefore, all 11 nominated TNBC targets are determined to have strong interactions with beauvericin, making them

TH-3487_186106116

potential target candidates for further investigations. The binding pocket analysis of each complex has revealed that the interactions involved in the binding of beauvericin with different targets are more or less similar. It mostly involves Pi-Pi stacking with aromatic amino acid residues such as Tyr and Phe, Pi-anion and Pi-cation interactions with negatively charged (Asp, Glu) and positively charged residues (Lys, Arg), respectively. Beauvericin has also formed conventional hydrogen bonds with residues like Tyr, Arg, Lys, Gly, Val, Gln, Ser, Leu, Ala, and Asn to establish strong non-covalent interactions with the target proteins. Apart from these, it has also stabilized the target binding with other non-covalent interactions such as Pi-sigma interactions, carbon hydrogen bonds, Pi-alkyl interaction and Van Der Waals interactions, etc. (**Figure 3.2.4**).

3.2.1.3. Molecular dynamics (MD) simulation studies of beauvericin bound target proteins

Molecular dynamics (MD) simulation is a crucial tool in the validation of target inhibition in drug discovery research. Several studies have utilized MD simulation to validate the inhibitors against respective target proteins. For example it has been employed to validate the potential inhibitors against fibroblast growth factor receptor 1 (FGFR1) (Hamza et al., 2024; Raza et al., 2023). The dynamic behaviour of the target proteins and their interactions with potential inhibitors are further studied with the help of this technique (Naqvi et al., 2018). This study is essential to understand the mechanism of target inhibition, prediction of the effectiveness of potential drug candidates, and stability of the target-inhibitor complexes in a dynamic environment (Liu et al., 2018). Although the interactions between beauvericin and TNBC targets looked more or less stable, their stability in dynamic environments mimicking the microenvironment inside the cells has been studied by molecular dynamics (MD) simulation. Each docked structure has been prepared as per the intracellular microenvironment of the respective target proteins, whether it is a cytosolic or transmembrane protein. Out of 11 shortlisted TNBC targets, only ABCC1 is found to be a transmembrane protein, and others are cytosolic. Therefore, all the target-beauvericin complexes have been prepared accordingly for the simulation study. The simulation results have been analyzed and represented in four different parameters.

TH-3487_186106116

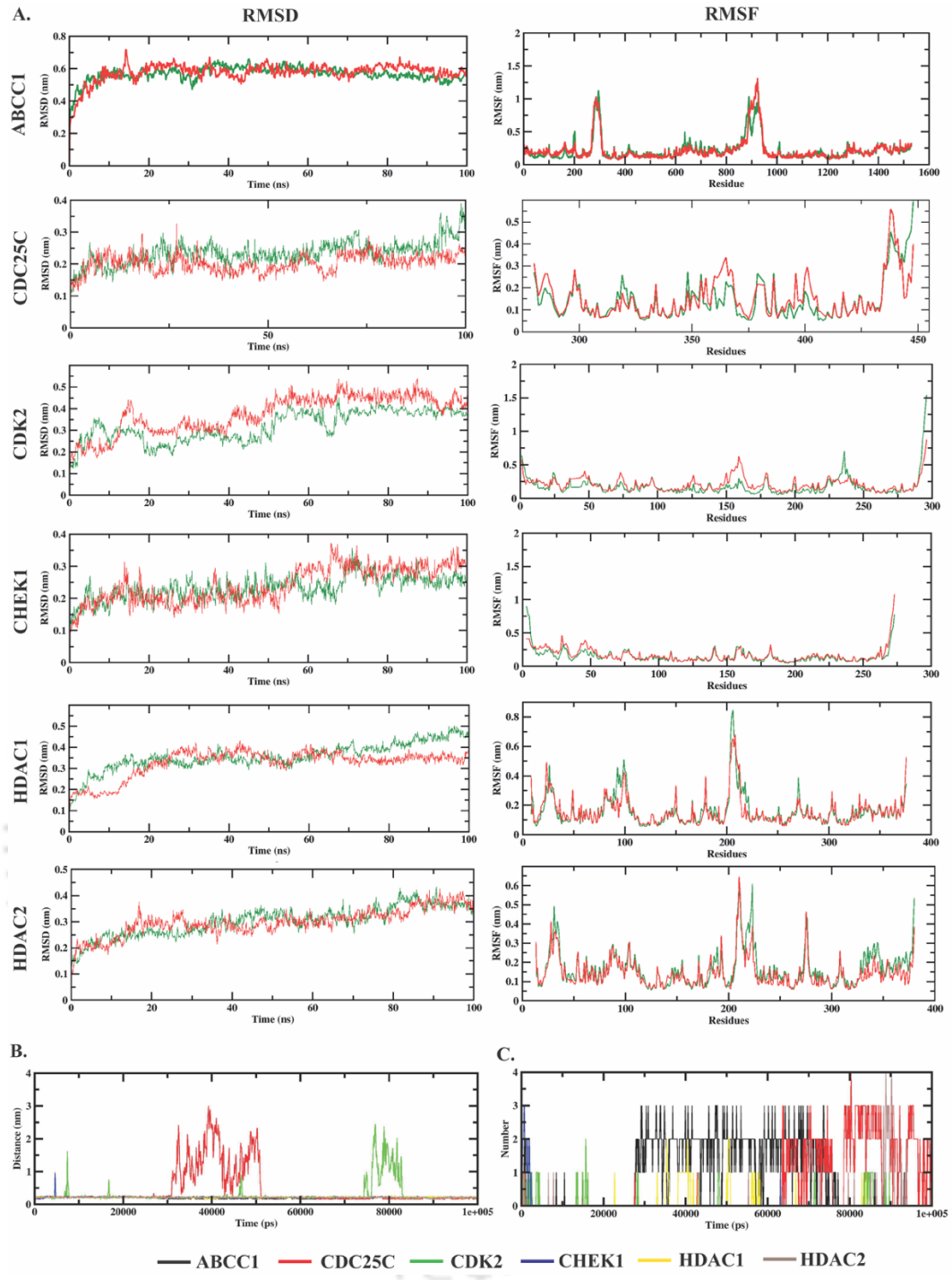

Figure 3.2.5. Molecular dynamics (MD) simulation studies of beauvericin bound targets ABCC1, CDC25C, CDK2, CHEK1, HDAC1 and HDAC2. **(A)** RMSD and RMSF distribution with respective native forms of each target proteins (green – unbound target, red – bound target) and also **(B)** paired distance and **(C)** hydrogen bonds distribution in each beauvericin bound target complex.

TH-3487_186106116

Firstly, the Root Mean Square Deviation (RMSD) that represents the average distance between the atoms of target-inhibitor complex and its unbound form over a period of time. It quantifies the overall structural stability or deviation of the target-inhibitor complex in the course of simulation. RMSD values also provide information about the structural alterations and conformational dynamics of the target-inhibitor complex during simulation. Among the 11 different beauvericin bound target complexes, most of them have shown no significant changes in RMSD as compared to their unbound forms except the complexes with CDK2 and MMP1 (**Figure 3.2.5A** and **3.2.6A**). These two complexes have shown slight changes in the RMSD values throughout the simulation period. Therefore, the results have indicated that except for beauvericin bound CDK2 and MMP1 complexes, others have been stable throughout the simulation process as far as RMSD analysis is concerned.

The second parameter is Root Mean Square Fluctuation (RMSF). It is a measurement of the average fluctuation or deviation of the positions of atoms within the amino acid residues of a protein-inhibitor complex compared to its unbound form over the course of simulation. It delivers useful information about the dynamic behavior of individual amino acid residues present in the protein-inhibitor complex. Residues with higher RMSF values are more flexible and exhibit more significant fluctuation in their positions, while residues with lower RMSF values are more rigid and exhibit less fluctuation. RMSF analysis also helps researchers to identify regions of the protein that are structurally stable or flexible, which can be important for understanding protein dynamics, ligand binding interactions, and conformational changes during the simulation. RMSF analysis of all the complexes has shown no significant variation in the atomic position of the amino acid contents of each target protein compared to their unbound forms (**Figure 3.2.5A** and **3.2.6A**), confirming the stability of all the complexes as far as RMSF analysis is concerned.

TH-3487_186106116

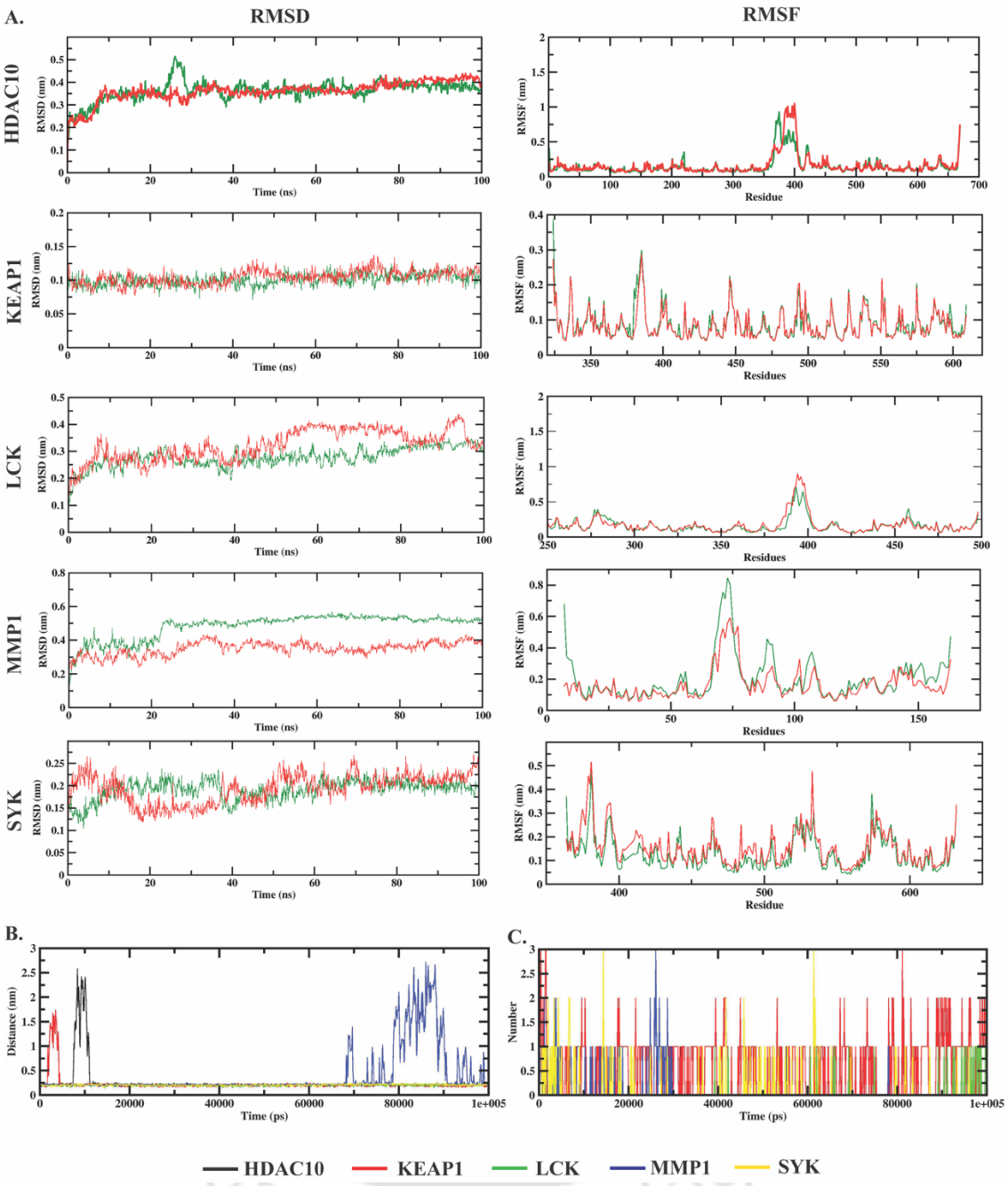

Figure 3.2.6. Molecular dynamics (MD) simulation studies of beauvericin bound targets HDAC10, KEAP1, LCK, MMP1 and SYK. **(A)** RMSD and RMSF distribution with respective native forms of each target proteins (green – unbound target, red – bound target) and also **(B)** paired distance and **(C)** hydrogen bonds distribution of each beauvericin bound target complex.

TH-3487_186106116

The third parameter is hydrogen bonds. Changes in the quantitative values of hydrogen bonds present in a protein-inhibitor complex during simulation positively correlate with its stability, specificity and overall binding affinity of the complex. This analysis has shown variation in the quantitative values of hydrogen bonds formed in each beauvericin-target interactions throughout the simulation. The number of hydrogen bonds has been increased in the beauvericin complexed with ABCC1 and CDC25C, whereas it has been decreased in CHEK1, HDAC10 and MMP1. Apparently, significant changes have not been observed in other target proteins (**Figure 3.2.5C** and **3.2.6C**). This result has indicated that changes in the number of hydrogen bonds throughout the simulation have increased the stability of the beauvericin complexed with ABCC1 and CDC25C and have reduced the stability of complexes with CHEK1, HDAC10 and MMP1, whereas it has not affected the stability of other complexes.

The fourth and crucial parameter to evaluate the stability of all the complexes is the paired distance. It refers to the approximate distance between specific atoms involved in the non-covalent interactions of the target protein and the inhibitor molecule. An increment in the paired distance over time represents the instability of the protein-inhibitor complex, whereas a static paired distance during the simulation period indicates that the complex is stable in the dynamic environment.

This analysis has shown an increment in the atomic distance between the interacting atoms of beauvericin and CDC25C, CDK2, CHEK1, HDAC10, KEAP1 and MMP1 target proteins, making each complex unstable during the simulation. Alternatively, no significant changes have been observed in the paired distance of other target proteins (**Figure 3.2.5B** and **3.2.6B**). Therefore, from the aforementioned analyses, the beauvericin bound structures of CDC25C, CDK2, CHEK1, HDAC10, KEAP1 and MMP1 are found to be unstable. In contrast, the complexes with ABCC1, HDAC1, HDAC2, LCK and SYK are found to be stable in a dynamic environment.

TH-3487_186106116

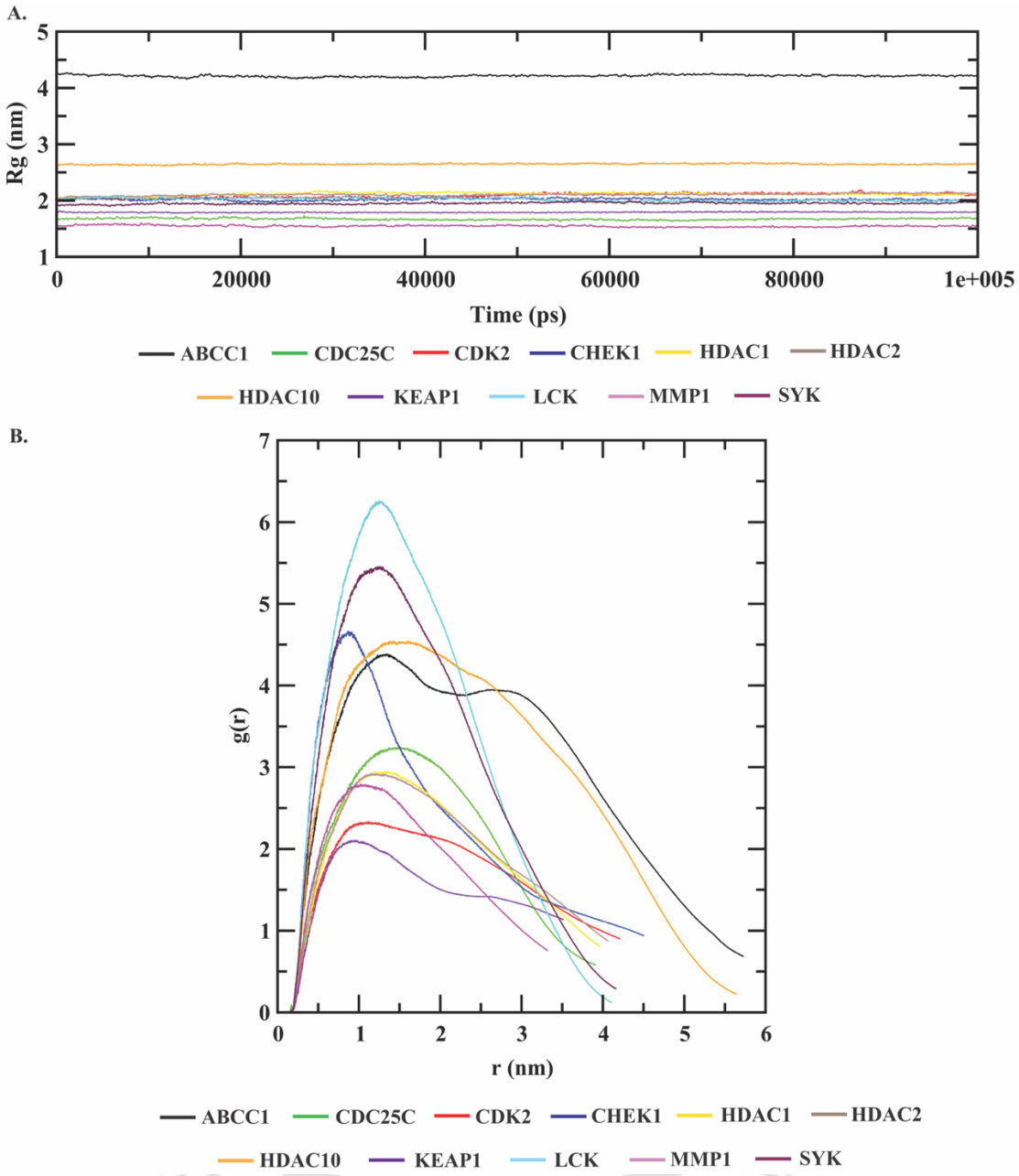

Figure 3.2.7. Molecular dynamics (MD) simulation studies of beauvericin bound targets ABCC1, CDC25C, CDK2, CHEK1, HDAC1, HDAC2, HDAC10, KEAP1, LCK, MMP1 and SYK. **(A)** Distribution of radius of gyration (Rg) and **(B)** Radial distribution function (RDF).

Additionally, two more parameters have also been employed to validate the stability of beauvericin bound target protein complexes. Firstly, the radius of gyration (Rg), that

TH-3487_186106116

quantifies the compactness of a protein-inhibitor complex based on the distribution of its mass around its centre of mass. If the Rg values remain relatively consistent over time throughout the simulation process, the protein-inhibitor complex retains its shape and compactness, conferring stability. Conversely, increment in the Rg values over time indicates loosening of the tightly packed protein-inhibitor complex, whereas reduction in the Rg values over time indicates more compactness of the complex. The Rg analyses of all the 11 complexes have revealed that the Rg values remained constant throughout the simulation process in case of all beauvericin-target complexes, indicating stability of all the complexes (**Figure 3.2.7A**). The last parameter to validate the stability of the complexes is the radial distribution function (RDF). The RDF illustrates the changes in the density of atoms from a reference atom as a function of distance, providing insights into structural details and stability. Stable complexes show a distinct and well-defined peak at specific distances, indicating strong and consistent interactions. Conversely, broad and poorly defined peak indicates more transient interactions, suggesting potential instability. The RDF analyses of all of the beauvericin bound complexes have shown sharp and well-defined peaks except the complexes with CDK2, HDAC10 and KEAP1 with comparatively broader peaks, suggesting more stability in the other complexes. In case of beauvericin-MRP-1 (ABCC1) complex, overlapping of two distinct sharp peaks have been observed, indicating the presence of two distinct, but closely positioned sets of interactions, making the complex more stable (**Figure 3.2.7B**).

Furthermore, the stable beauvericin-target complexes throughout the simulation process (beauvericin bound ABCC1, HDAC1, HDAC2, LCK and SYK) have been compared with their complexes with known inhibitors (Positive control). Sulfinpyrazone, fostamatinib and ellagic acid have been used as known inhibitors of MRP-1 (ABCC1), LCK and SYK, respectively, whereas vorinostat has been used as a positive control inhibitor for both HDAC1 and HDAC2. *In silico* studies showed strong affinity of the known inhibitors for their respective target proteins (**Figure 3.2.8**) by scoring negative binding free energy in molecular docking studies (**Table 3.2.2**).

TH-3487_186106116

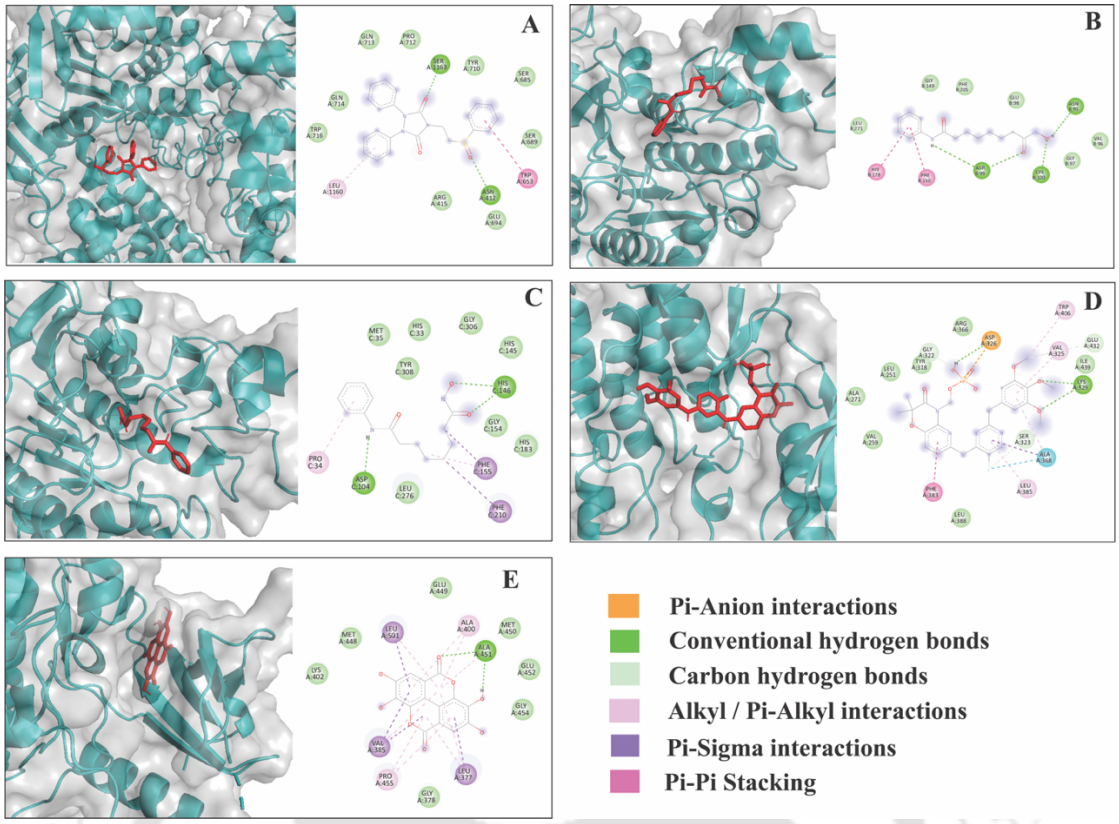

Figure 3.2.8. Molecular docking interactions between the stable TNBC targets of beauvericin and their respective positive control drugs (known inhibitors). **(A)** ABCC1 (MRP-1)-sulfinpyrazone complex, **(B)** HDAC1-vorinostat complex, **(C)** HDAC2-vorinostat complex, **(D)** LCK-fostamatinib complex and **(E)** SYK-Ellagic acid complex.

However, beauvericin has demonstrated a higher affinity than the respective known inhibitors (positive control), as evidenced by more negative binding free energy (Kcal/mol) as compared to the known inhibitors of the respective target proteins (**Table 3.2.2**). This comparison has identified beauvericin as a potent and enduring inhibitor of MRP-1 (ABCC1), HDAC1, HDAC2, LCK and SYK.

TH-3487_186106116

Table 3.2.2. Comparison of average binding free energies between target proteins complexed with beauvericin and respective known inhibitors (Positive control).

Target proteins	Binding free energy (Kcal/mol) with known inhibitors (positive control)	Binding free energy (Kcal/mol) with beauvericin
MRP-1 (ABCC1)	- 6.9	- 9.0
HDAC1	- 5.9	- 7.9
HDAC2	- 6.5	- 7.8
LCK	- 7.8	- 9.1
SYK	- 7.9	- 8.1

Hence, *in silico* analyses have identified ABCC1, HDAC1, HDAC2, LCK and SYK as possible molecular targets of beauvericin. MMPBSA analysis of the stable complexes of beauvericin and the identified targets has also been performed to support the results of MD simulation. This is an efficient and reliable free energy simulation method for protein-inhibitor interactions. The results have revealed the amount of energies involved in several non-covalent interactions to stabilize the interactions between beauvericin and its identified target proteins. Each complex has scored a negative average binding energy (KJ/mol), indicating their stable and favourable interactions and binding affinity. This is supported by several non-covalent energies such as electrostatic energy (KJ/mol), polar solvation energy (KJ/mol), Van Der Waals energy (KJ/mol) and SASA energy (KJ/mol) (**Table 3.2.3**).

TH-3487_186106116

Table 3.2.3. MMPBSA analysis.

Targets	Van Der Waals energy (KJ/mol)	Electrostatic energy (KJ/mol)	Polar solvation energy (KJ/mol)	SASA energy (KJ/mol)	Average binding energy (KJ/mol)
ABCC1	-167.606 ± 25.961	-42.419 ± 28.278	141.292 ± 56.181	-21.436 ± 3.382	-90.169 ± 30.209
HDAC1	-121.892 ± 28.261	-12.191 ± 8.559	105.347 ± 54.763	-15.609 ± 3.581	-44.345 ± 44.706
HDAC2	-116.778 ± 28.033	-6.727 ± 17.893	66.774 ± 35.753	-15.468 ± 2.972	-72.199 ± 22.430
LCK	-174.986 ± 20.971	1.360 ± 13.232	89.343 ± 31.176	-20.767 ± 2.648	-105.051 ± 17.516
SYK	-144.757 ± 39.857	-49.297 ± 42.044	151.411 ± 75.127	-18.238 ± 5.456	-60.881 ± 47.981

The five molecular targets of beauvericin ABCC1, HDAC1, HDAC2, LCK and SYK in TNBC are involved in certain molecular functions that support the progression, drug resistance and sustainability of TNBC cells. The multidrug resistant protein -1 (MRP-1) encoded by ABCC1 serves a major role in ATP hydrolysis mediated efflux of anticancer drugs, resulting in multidrug resistance (Cole, 2014). Hence, inhibition of this protein by beauvericin may increase the therapeutic susceptibility of TNBC cells by reversal of MRP-1 mediated drug resistance. As epigenetic modifications are highly involved in tumor progression and the development of TNBC (Maccallini et al., 2022), inhibition of Histone deacetylase 1 and 2 (HDAC1/2) by beauvericin could be a promising therapeutic strategy in TNBC. Abnormal expression of SYK (spleen tyrosine kinase) and LCK (lymphocyte cell specific protein tyrosine kinase) have been found in TNBC as a regulator of tumour specific immune response (Al Qutami et al., 2023; Muellner et al., 2015). Hence, targeting these proteins may lead to increased survival of TNBC patients.

TH-3487_186106116

Therefore, from *in silico* evidences, it can be hypothesized that beauvericin can be a potential inhibitor of multidrug resistance, epigenetic modulators and cancer specific tyrosine kinases to combat TNBC.

3.2.1.4. Effect of beauvericin on cell viability, intracellular ROS, mitochondrial transmembrane potential and apoptotic death of TNBC cells

Cell viability, oxidative stress, and apoptosis are crucial factors in the therapeutic evaluation of beauvericin in triple-negative breast cancer cells. These factors provide valuable insights into the effectiveness of the metabolite to determine its chemosensitivity or chemoresistance in treating TNBC. Previously reported ionophoric activity of beauvericin could be a major reason behind TNBC cell death (Ojcius et al., 1991). The detrimental effect of beauvericin on TNBC cells has been determined by assessing cell viability. It has shown a concentration dependent inhibition in the viability of MDA-MB-231 and MDA-MB-468 cells exhibiting an IC_{50} (inhibitory concentration of 50% cell population) value of 4.4 µM and 3.9 µM, respectively (**Figure 3.2.9A** and **3.2.9B**). Inhibition of cell viability with a similar dosage are also reported in pancreatic cancer cells PANC-1 (Yahagi et al., 2020). Oxidative stress, the imbalance between ROS production and defensive antioxidative response (Vona et al., 2021), has a major impact on determining the efficacy of a drug candidate in TNBC. Excessive oxidative stress eventually results in oxidative damage to DNA and programmed cell death (Payne et al., 1995), highlighting the importance of assessing this parameter in therapeutic evaluation. Beauvericin has been found to elevate intracellular reactive oxygen species in both TNBC cell lines MDA-MB-231 and MDA-MB-468 cells by approximately 9.0 and 7.9-fold, respectively, as evident by flow cytometric analysis (**Figure 3.2.9C**, **3.2.9D** and **3.2.9E**). As a sequel effect of elevated ROS level, beauvericin might have an impact on mitochondrial health (Guo et al., 2013). Flowcytometric assessment has revealed depolarization of the mitochondrial membrane due to beauvericin treatment in TNBC cells. Approximately 81.4% and 90.6% population of MDA-MB-231 and MDA-MB-468 cells, respectively, have been found to have depolarized mitochondrial membrane when treated with beauvericin at IC_{50} concentration (**Figure 3.2.9F** and **3.2.9G**).

TH-3487_186106116

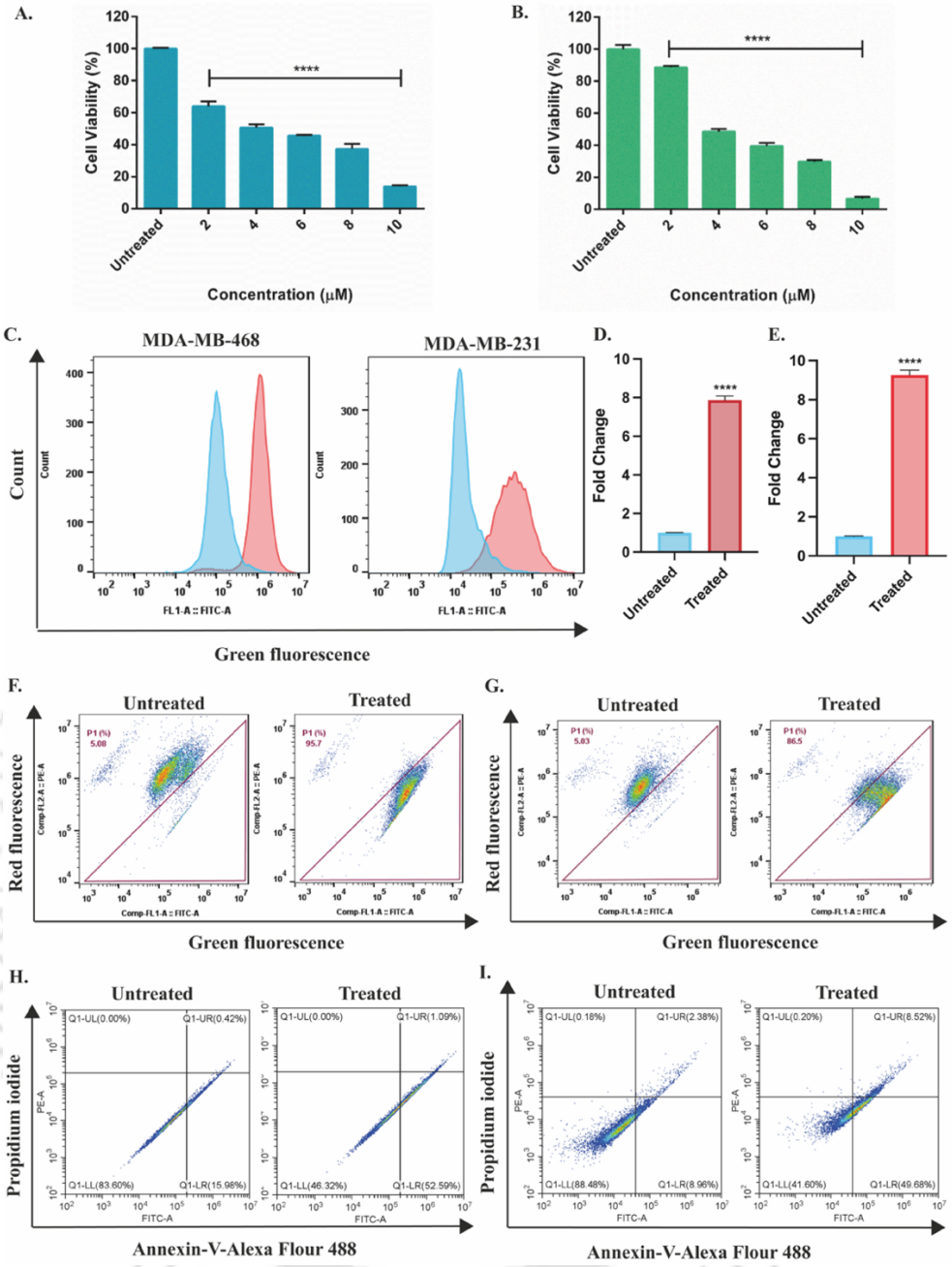

Figure 3.2.9. Effect of beauvericin and its intracellular implications in TNBC cells. Effect of beauvericin on the viability of **A)** MDA-MB-468 and **B)** MDA-MB-231 cells. **C)** Flow cytometric analysis of the intracellular reactive oxygen species (ROS) in MDA-MB-468 and MDA-MB-231 cells. Corresponding fold change in the ROS content of **D)** MDA-MB-468 and **E)** MDA-MB-231 cells. Flow cytometry based quantitative estimation of the mitochondrial membrane depolarization in **F)** MDA-MB-468 and **G)** MDA-MB-231 cells. Flow cytometric estimation of apoptotic population in **H)** MDA-MB-468 and **I)** MDA-MB-231 cells.

TH-3487_186106116

Beauvericin exposure has also reduced the mitochondrial membrane potential in the rat liver cells (Tonshin et al., 2010), Caco-2 colon carcinoma cells (Prosperini et al., 2013), and CHO-K1 Chinese hamster ovary cells (Mallebrera et al., 2016), supporting the findings of this study. Elevation in the intracellular ROS level and subsequent depolarization of the mitochondrial membrane confirmed that beauvericin has induced oxidative stress in TNBC cells. Apoptosis, or programmed cell death, is also a critical aspect of evaluating the therapeutic potential of a drug candidate. Beauvericin has been observed to induce apoptotic death in TNBC cells as a consequence of oxidative stress. The flow cytometric assessment has confirmed induction of apoptosis in approximately 46.8% and 37.2% population of MDA-MB-231 and MDA-MB-468 cells, respectively, when treated with beauvericin at IC_{50} concentration (**Figure 3.2.9H** and **3.2.9I**).

Table 3.2.4. Quantitative estimation of flowcytometric analyses.

Properties	MDA-MB-231	MDA-MB-468
Fold change in ROS	9.0-fold	7.9-fold
Population with depolarized mitochondrial membrane	81.4%	90.6%
Apoptotic cell population	46.8%	37.2%

Similarly, beauvericin has also been found to increase [Ca^{2+}] in CCRF-CEM leukaemia cells, thereby decreasing mitochondrial transmembrane potential by increased cytochrome-c release from mitochondria and subsequently induced apoptosis by increased activity of cytosolic caspase-3 (Jow et al., 2004). Therefore, beauvericin's potential to limit the TNBC cell viability in a concentration dependent manner via oxidative stress mediated induction of apoptotic cell death has been experimentally validated.

TH-3487_186106116

3.2.1.5. Effect of beauvericin in cell cycle progression, clonal expansion and regeneration properties of TNBC cells

Understanding and targeting the cell cycle progression is essential as TNBC cells exhibit uncontrolled proliferation, which contributes to tumour growth and invasion. As a result of its growth inhibitory effect, beauvericin may disrupt the normal distribution of cells in one or more cell cycle phases. This can be due to the activation of various cell cycle checkpoints in response to various stimuli like DNA damage, which ensures the orderly progression of cell cycle events and prevents aberrant mitosis. Activation of various checkpoint proteins usually results in cell cycle arrest that repairs damage and preserves genomic integrity (Damia and Broggini, 2004). Propidium Iodide based flow cytometric analysis of cell cycle progression has shown a significant increment ($p < 0.0001$ as per 2-way ANOVA analysis) of cell population in G1-phase and subsequent reduction in S-phase population due to beauvericin treatment in TNBC cells (**Figure 3.2.10A** and **3.2.10C**). There have been an approximately 20% increment in the G1-phase population and a 15% reduction in the S-phase population in MDA-MB-468 cells, whereas approximately 15% increment in the G1-phase population and a 15% reduction in the S-phase population in MDA-MB-231 cells when treated with beauvericin at IC_{50} concentration (**Figure 3.2.10B** and **3.2.10D**). This analysis has confirmed cell cycle arrest at the G1-phase in both TNBC cell lines as cells were not able to pass on from G1-phase to S-phase due to beauvericin treatment. Furthermore, clonal expansion, where a single cell gives rise to a population of genetically identical cells, is responsible for the progression and spread of TNBC. The regeneration ability of TNBC cells is significant as it determines their ability to resist treatment and potentially lead to relapse (Ding et al., 2020). Beauvericin treatment has caused a significant reduction in the clonal expansion and regeneration ability of TNBC cells, as evidenced by colony formation assay. There have been approximately 2.3 and 2.2-fold reduction in the colony formation abilities of MDA-MB-468 and MDA-MB-231 cells, respectively, when treated at IC_{50} concentration (**Figure 3.2.10E**).

TH-3487_186106116

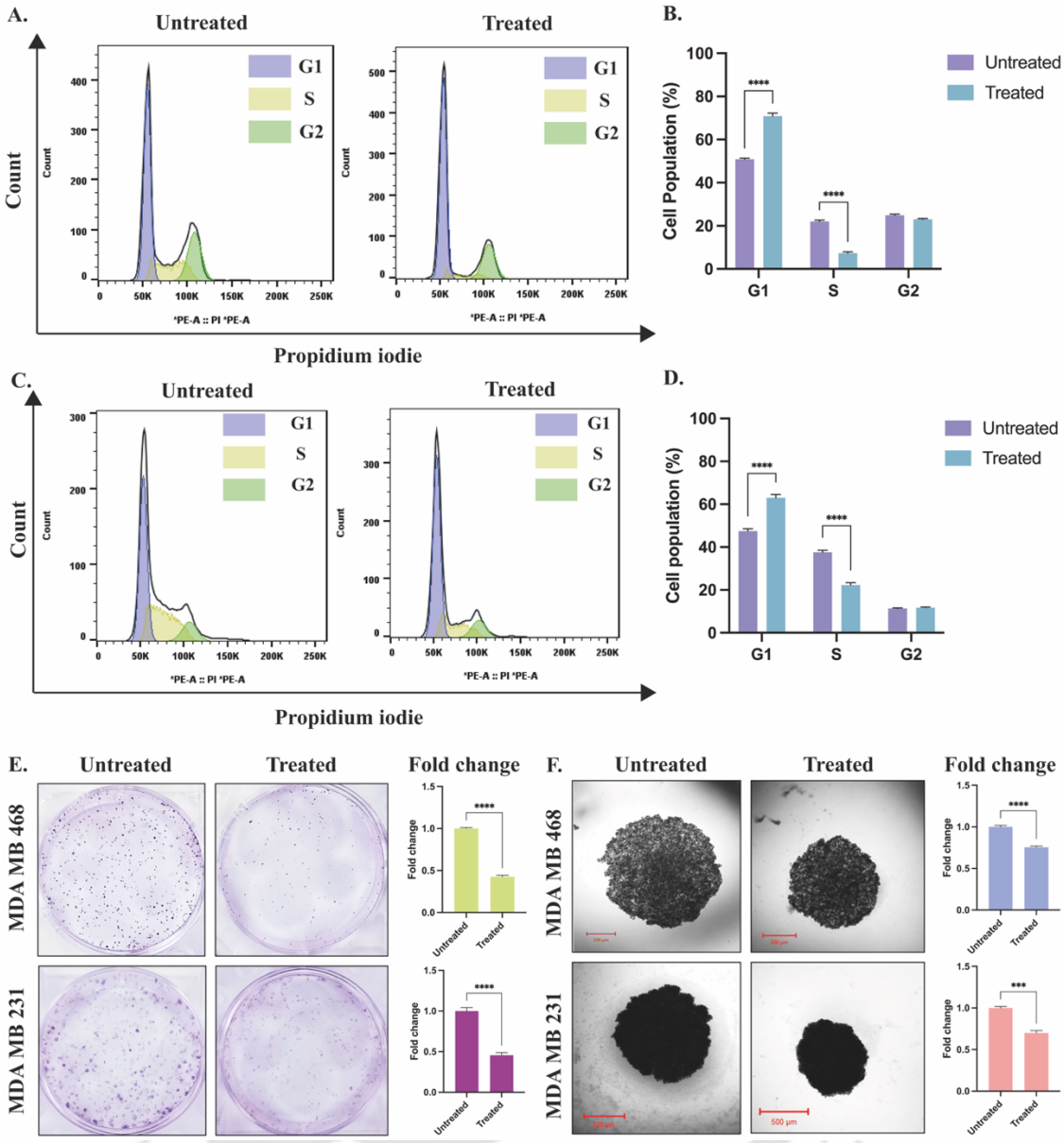

Figure 3.2.10. Effect of beauvericin on cell growth and arrest. Flow cytometric analysis of cell cycle arrest in **A)** MDA-MB-468 and **C)** MDA-MB-231 cells. Corresponding changes in the population distribution of **B)** MDA-MB-468 and **D)** MDA-MB-231 cells in different cell cycle phases. Effect of beauvericin on the **E)** colony formation ability and **F)** spheroid formation ability of MDA-MB-468 and MDA-MB-231 cells and subsequent fold changes.

TH-3487_186106116

Beauvericin has also significantly reduced the spheroid formation ability of TNBC cells, as evidenced by spheroid formation assay. There have been approximately 1.3 and 1.2-fold reduction in the spheroid size (in diameter) of MDA-MB-468 and MDA-MB-231 cells, respectively, when cells were pre-treated with beauvericin at IC_{50} concentration (**Figure 3.2.10F**). These observations has confirmed the ability of beauvericin to significantly reduce the clonal expansion and regeneration capability of TNBC cells.

3.2.1.6. Effect of beauvericin on 3D spheroids of TNBC cells

The significance of spheroid viability in the therapeutic evaluation of beauvericin in TNBC lies in its ability to mimic the complex tumour microenvironment and predict better drug response in clinical settings (Khaitan and Dwarakanath, 2006). Use of spheroids allows to study the effectiveness of beauvericin in a more realistic and representative context, which may ultimately improve clinical outcomes for TNBC patients by enhancing the accuracy and reliability of preclinical drug testing (Mehta et al.,2012). By incorporating the use of spheroids, various factors can be assessed, such as drug penetration, distribution, and efficacy in a three-dimensional environment that closely resembles the tumour *in vivo* (Pinto et al., 2020). Beauvericin has significantly reduced the MDA-MB-468 and MDA-MB-231 spheroids' viability in a concentration dependent fashion, estimating IC_{50} dosage of 10.3 µM and 6.2 µM, respectively (**Figure 3.2.11A** and **3.2.11B**). This observation has confirmed the penetration ability of beauvericin in solid tumours, showing its significant capability to be used for therapeutic purposes in TNBC. Live-dead staining of TNBC spheroids has also visually confirmed the anticancer impact of beauvericin on 3D spheroids. Confocal microscopic images has shown an increment in the red population (Propidium Iodide stained dead cells) as compared to the green population (calcein-AM stained live cells) in 3D spheroids of both MDA-MB468 and MDA-MB-231 cells upon beauvericin treatment (**Figure 3.2.11C** and **3.2.11D**). Hence, the experimental results indicated that beauvericin has significantly reduced the spheroid size (in diameter) (**Figure 3.2.10F**) and also caused death of TNBC cells in 3D spheroids (**Figure 3.2.11**), portraying its therapeutic efficacy in the treatment of TNBC.

TH-3487_186106116

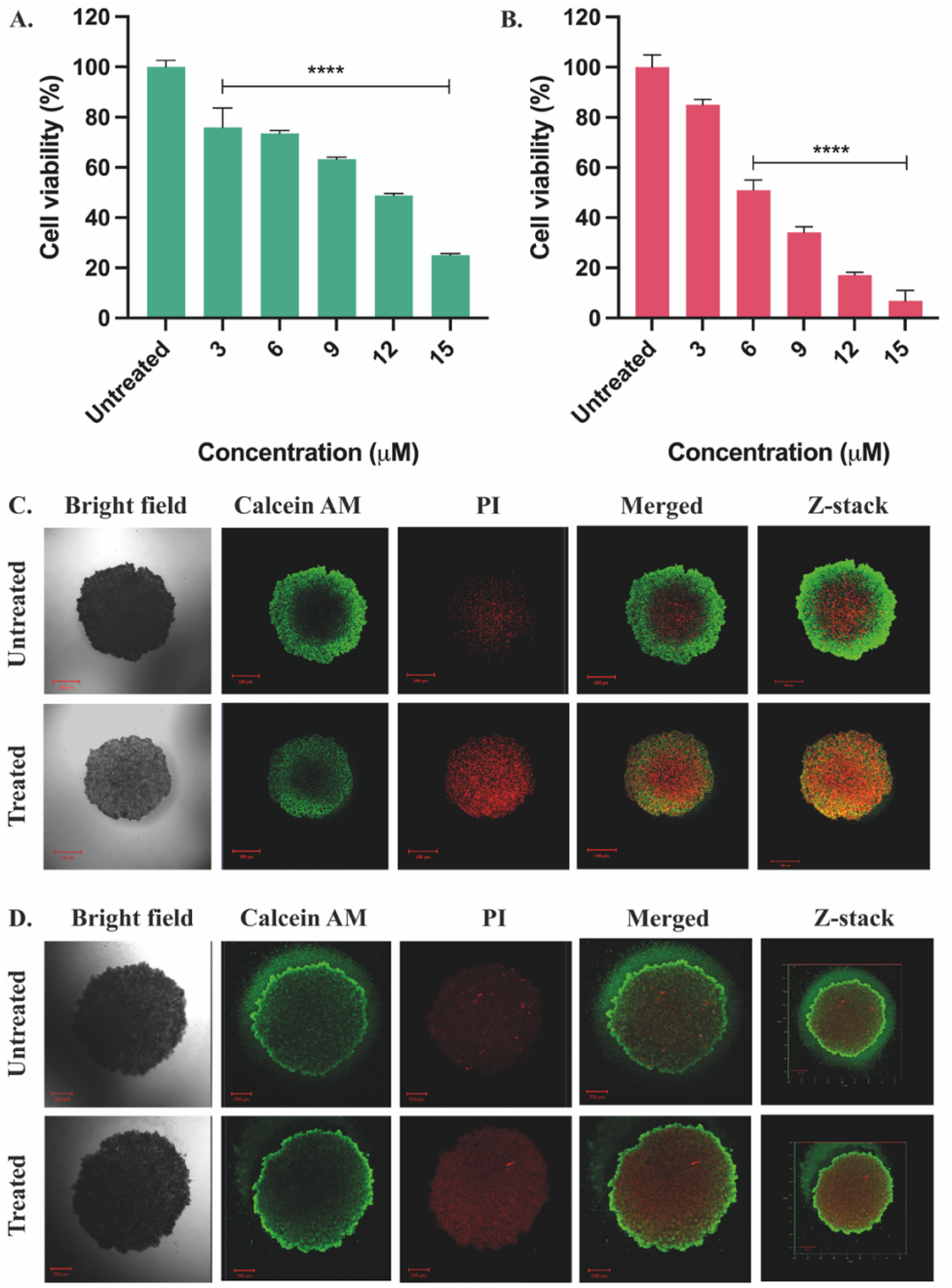

Figure 3.2.11. Effect of beauvericin on 3D spheroids. Changes in the spheroid viability of **A)** MDA-MB-468 and **B)** MDA-MB-231 cells upon beauvericin treatment. Confocal microscopic images of the live and dead cell population in the spheroids of **C)** MDA-MB-468 and **D)** MDA-MB-231 cells upon treatment.

TH-3487_186106116

The findings of this study have broader implications beyond the specific context of TNBC treatment. Beauvericin's ability to target multiple cancer-promoting events, such as multi-drug resistance, epigenetic modulation, and tyrosine kinase signaling, showcases its anticancer potential. The possible inhibition of proteins like MRP-1 (ABCC1), HDAC1, HDAC2, LCK, and SYK suggests that beauvericin could be effective against other cancers that rely on these pathways for growth and survival. Furthermore, induction of oxidative stress-mediated apoptosis and inhibition of cell cycle progression and clonal expansion have indicated its role in preventing tumour formation and progression more efficiently.

Furthermore, detailed experimental validation of *in silico* studies would establish the role of all molecular targets of beauvericin in TNBC. Additionally, the research focus may extend beyond the upregulated targets in TNBC to conduct a comprehensive analysis of all potential molecular targets of beauvericin in other types of cancer. In future, therapeutic efficacy of beauvericin can be further examined on *in vivo* models to understand its therapeutic potential and drug safety.

3.2.2. CONCLUSION

In conclusion, *in silico* studies have successfully identified MRP-1 (ABCC1), HDAC1, HDAC2, LCK and SYK as the possible molecular targets of beauvericin in TNBC, making them potential candidates for further investigation and validation. Successful inhibition of these proteins may lead to sensitization of TNBC cells by potentially reversing MRP-1 mediated multidrug resistance, preventing cancer favoring epigenetic modulations and inhibiting oncogenic tyrosine kinases depended cancer promoting signaling pathways. Additionally, beauvericin has exhibited its anticancer effects *in vitro,* with dose-dependent inhibition of MDA-MB-231 and MDA-MB-468 cell viability. The mechanism of cell death involves the induction of oxidative stress mediated apoptosis, evidenced by elevated intracellular ROS and subsequent depolarization of mitochondrial membrane. Beauvericin has also restricted cell cycle progression at G1 phase and reduced the spheroid formation, clonal expansion and regeneration ability of TNBC cells significantly. Furthermore, it has reduced the viability of TNBC spheroids, indicating substantial therapeutic promise in addressing triple-negative breast cancer.

TH-3487_186106116

TH-3487_186106116

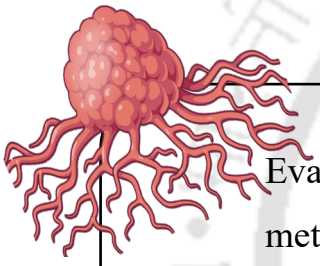

Evaluation of beauvericin's therapeutic effects on the metastatic attributes of triple-negative breast cancer (TNBC) cells.

***ACS Pharmacology & Translational Science*. Vol 7 / Issue 9**

TH-3487_186106116

TH-3487_186106116

GRAPHICAL ABSTRACT

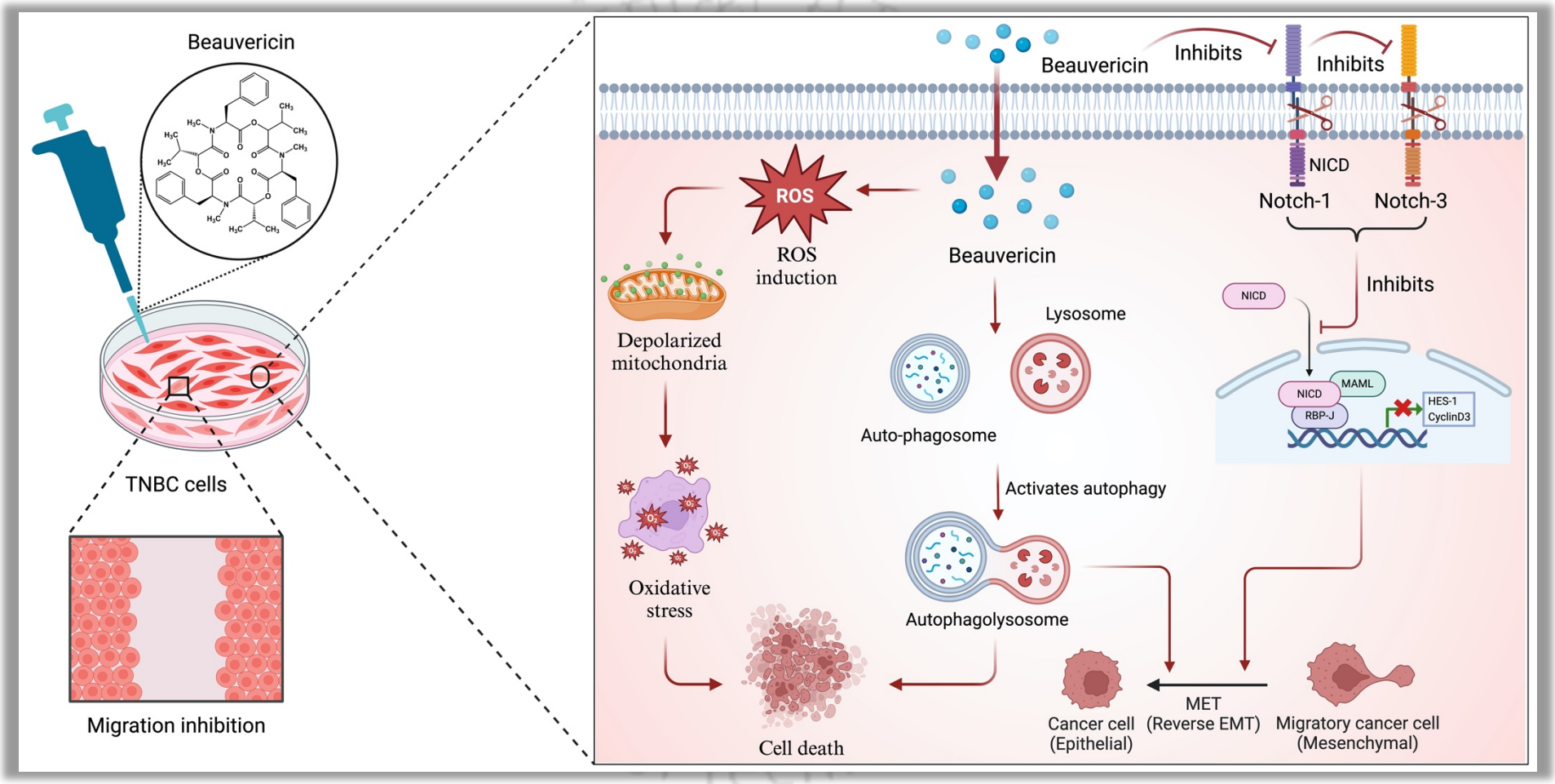

Scheme 3.3: A schematic illustration shows beauvericin's potential to reverse EMT by inhibiting Notch signaling and activating autophagy, which subsequently reduces cellular migration.

TH-3487_186106116

A B S T R A C T

Metastasis stands as a prime contributor to the triple-negative breast cancer (TNBC) associated mortality worldwide, presenting heightened severity and significant challenges due to limited treatment options. Addressing TNBC metastasis necessitates innovative approaches and novel therapeutics to specifically target its propensity of dissemination to distant organs. Targeted therapies capable of reversing epithelial-to-mesenchymal transition (EMT) play a crucial role in suppressing metastasis and enhancing treatment response. Beauvericin, a promising fungal secondary metabolite, exhibits significant potential in diminishing the viability of EMT induced TNBC cells by triggering intracellular oxidative stress, as evidenced by enhanced ROS level and reduced mitochondrial transmembrane potential. In monolayer cultures, it has exhibited an IC_{50} of 2.3 µM in both MDA-MB-468 and MDA-MB-231 cells, while in 3D spheroids, the IC_{50} values are 9.7 µM and 7.1 µM, respectively. Beauvericin has also reduced the migratory capability of MDA-MB-468 and MDA-MB-231 cells by 1.5 and 1.7-fold, respectively. Both qRT-PCR and western blot analysis have shown significant upregulation in the expression of epithelial marker (E-cadherin) and downregulation in the expression of mesenchymal markers (N-cadherin, vimentin, Snail, Slug and β-catenin), following treatment, indicating reversal of EMT. Furthermore, beauvericin has suppressed the Notch signaling pathway by substantially downregulating Notch-1, Notch-3, Hes-1 and cyclinD3 expression and induced autophagy as observed by elevated expression of autophagy markers LC3 and Beclin-1. In conclusion, beauvericin has successfully downregulated TNBC cell survival by inducing oxidative stress and suppressed their migratory potential by reversing EMT through inhibition of Notch signaling and activation of autophagy.

TH-3487_186106116

TH-3487_186106116

3.3.1. RESULTS

3.3.1.1. Impact of beauvericin on the viability of EMT induced TNBC cells

Beauvericin is a bioactive cyclohexadepsipeptide, primally produced by the entomopathogenic fungi *Beauveria bassiana* (Hamill et al., 1969) and various species of *Fusarium* (Logrieco et al., 1998), *Cordyceps* and *Isaria* (Luangsa-ard et al., 2009). In addition to its antimicrobial properties (Meca et al., 2010; Shin et al., 2009; Zhang et al., 2007), beauvericin shows considerable promise in cancer therapy.

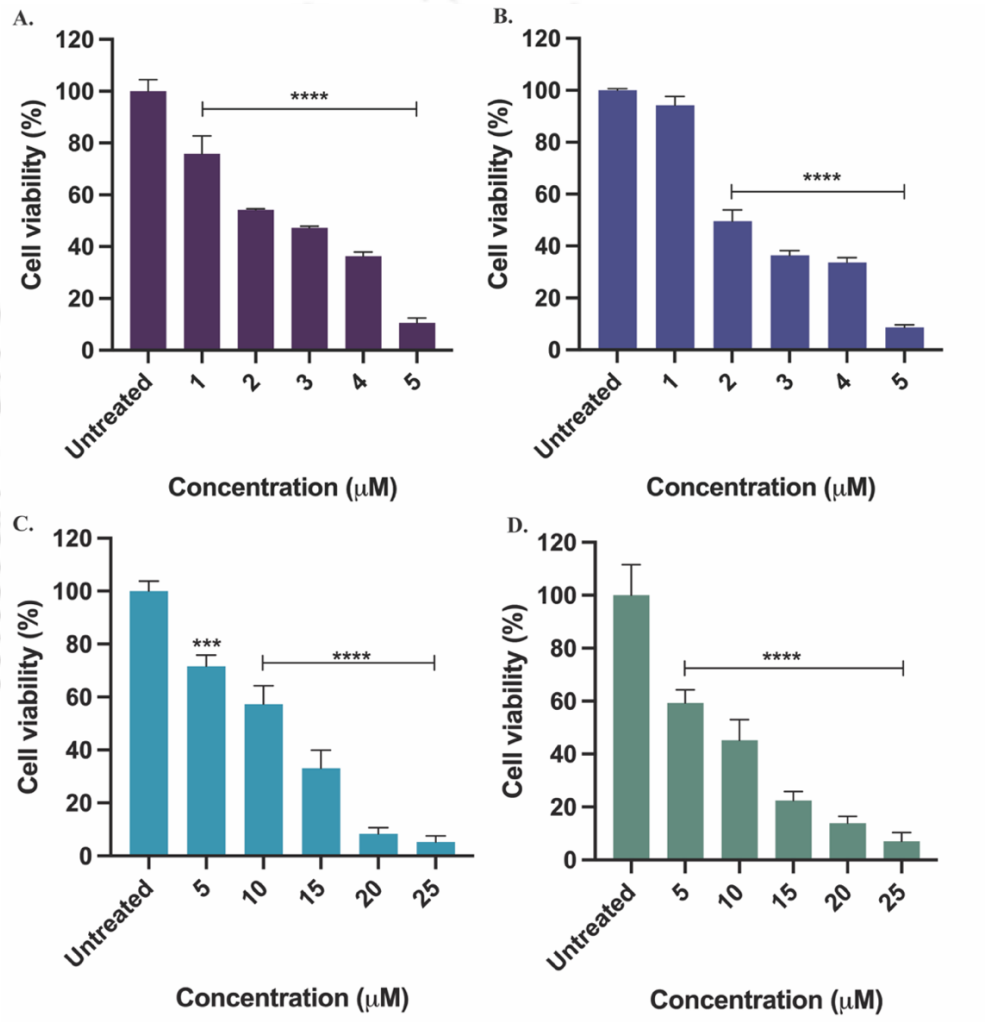

Figure 3.3.1. Cell viability of EMT induced TNBC monolayers and 3D spheroids. Cellular viability of **A)** MDA-MB-468 monolayer and **B)** MDA-MB-231 monolayer upon treatment with increasing beauvericin concentrations. Viability of **C)** MDA-MB-468 spheroids and **D)** MDA-MB-231 spheroids following treatment with increasing dosage of beauvericin.

TH-3487_186106116

In vitro investigations have substantiated its anticancer efficacy against a range of cancer types including lung (Lu et al., 2016), cervical (Kim et al., 2023), leukemia (Jow et al., 2004), pancreatic (Yahagi et al., 2020) and colon (Prosperini et al., 2013) cancers. However, the molecular mechanisms and signaling cascades to impede the events associated with cancer metastasis, such as migration, invasion, angiogenesis and epithelial to mesenchymal transition (EMT) are yet to be explored. In order to investigate its therapeutic impact on invasive triple-negative breast cancer cells, initially, EMT induced MDA-MB-468 and MDA-MB-231 cells have been subjected to treatment with beauvericin. The treatment has revealed a dose dependent reduction in the viability of both cell lines in 2D (monolayers) as well as 3D (spheroids) cell culture models. In the monolayer treatment of both MDA-MB-468 and MDA-MB-231 cells, beauvericin has exhibited an IC_{50} value of 2.3 µM (**Figure 3.3.1A** and **3.3.1B**). However, in case of 3D spheroids of MDA-MB-468 and MDA-MB-231 cells, the IC_{50} values have been estimated as 9.7 µM and 7.1 µM, respectively (**Figure 3.3.1C** and **3.3.1D**). Hence, the findings have indicated that beauvericin possess significant growth inhibitory potential against EMT induced TNBC cells.

3.3.1.2. Induction of oxidative stress in triple-negative breast cancer (TNBC) cells

Oxidative stress refers to an imbalance in the intracellular redox equilibrium, marked by increased levels of reactive oxygen species (ROS) and reduced mitochondrial transmembrane potential (Betteridge, 2000). In order to cope up with the oxidative stress triggered by extracellular stimuli, cells assign the enzymatic antioxidants such as catalases, peroxidases, superoxide dismutase (Halliwell and Gutteridge, 2015) and also the non-enzymatic antioxidants such as glutathione, thioredoxin, ascorbate (Averill-Bates, 2023; Beyer, 1994; Liu, 2023) etc. Beauvericin is known to reduce the antioxidative glutathione (GSH) level and also hinders the activity of glutathione reductase, eventually triggering intracellular oxidative stress (Mallebrera et al., 2014). Oxidative stress plays a crucial role in determining the therapeutic effectiveness of a drug candidate, as the majority of chemotherapeutic agents exert their cytotoxic effects by inducing oxidative stress mediated intracellular damages (Cauli, 2021; Conklin, 2004; Zhang et al., 2018, 2022).

TH-3487_186106116

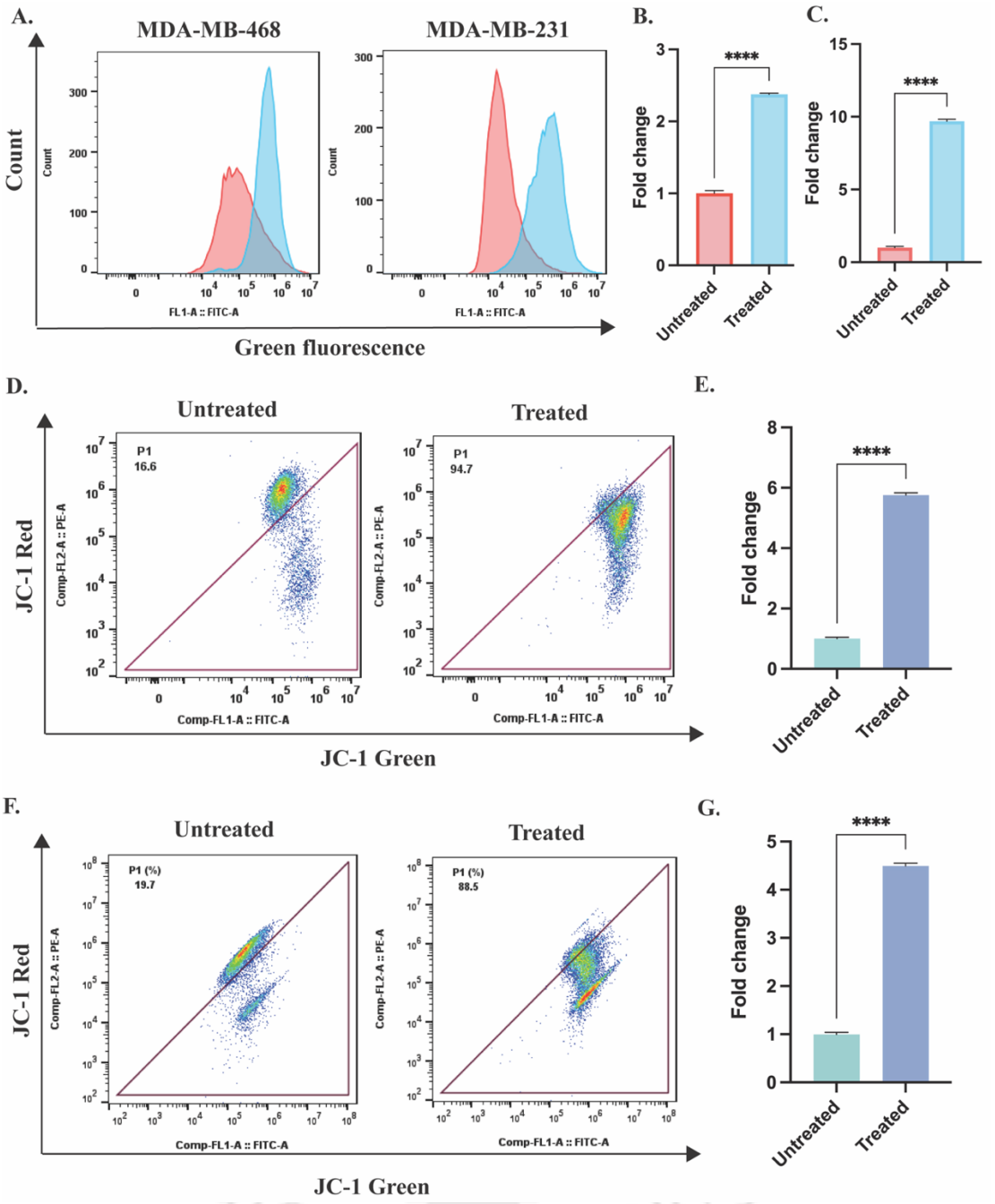

Figure 3.3.2. Flowcytometry based detection and assessment of cellular oxidative stress. A) Flowcytometric analysis of alterations in intracellular reactive oxygen species (ROS) levels in EMT induced TNBC cells upon beauvericin treatment, along with corresponding quantitative depiction of fold changes in **B)** MDA-MB-468 and **C)** MDA-MB-231 cells. Flow cytometric detection of mitochondrial transmembrane potential in EMT induced **D)** MDA-MB-468 and **F)** MDA-MB-231 cells with quantitative estimation of depolarized population in **E)** MDA-MB-468 and **G)** MDA-MB-231 cells.

TH-3487_186106116

Beauvericin has been observed to elevate the intracellular reactive oxygen species (ROS) level by approximately 2.3 and 9.7-fold in EMT induced MDA-MB-468 and MDA-MB-231 cells, respectively, when treated at IC_{50} concentration (**Figure 3.3.2A, 3.3.2B** and **3.3.1C**). It has also reduced the mitochondrial transmembrane potential of the EMT induced TNBC cells as evidenced by flowcytometric analysis (**Figure 3.3.2D** and **3.3.2F**). The quantitative analysis has resulted in approximately 5.7 and 4.5-fold increment in the population of MDA-MB-468 and MDA-MB-231 cells, with depolarized mitochondrial membrane, respectively (**Figure 3.3.2E** and **3.3.2G**), highlighting the hallmark of oxidative stress and associated mitochondrial damage in triple-negative breast cancer. Tumor cells usually have elevated intracellular ROS levels compared to non-cancerous cells, leading to heightened proliferation, enhanced survival with abnormal metabolism, mitochondrial dysfunction and other fates (Kumari et al., 2018). However, triggering higher than usual ROS level in tumor cells often leads to oxidative stress induced cellular death by initiating anti-tumorigenic signaling (Arfin et al., 2021). Hence, beauvericin induced oxidative stress leading to the death of TNBC cells.

3.3.1.3. Migration inhibitory effect of beauvericin on triple-negative breast cancer (TNBC) cells

The enhanced migration observed in TNBC holds significant clinical relevance as it contributes to the aggressive nature and metastatic potential of the disease (Koedoot et al., 2019). Mesenchymal-like TNBC tends to have higher rate of migration compared to other subtypes (Yin et al., 2020). This increased migratory capability allows TNBC cells to invade surrounding tissues, enter the blood stream or lymphatic system and establish a secondary tumor in distant organs, leading to metastasis (O'Reilly et al., 2021). Metastasis is a major driver of poor prognosis in TNBC patients, making the understanding and inhibition of enhanced migration crucial for the development of effective therapeutic strategies. Experimental findings have indicated a significant decline in the migratory capability of MDA-MB-468 and MDA-MB-231 cells as a consequence of beauvericin treatment (**Figure 3.3.3A** and **3.3.3D**).

TH-3487_186106116

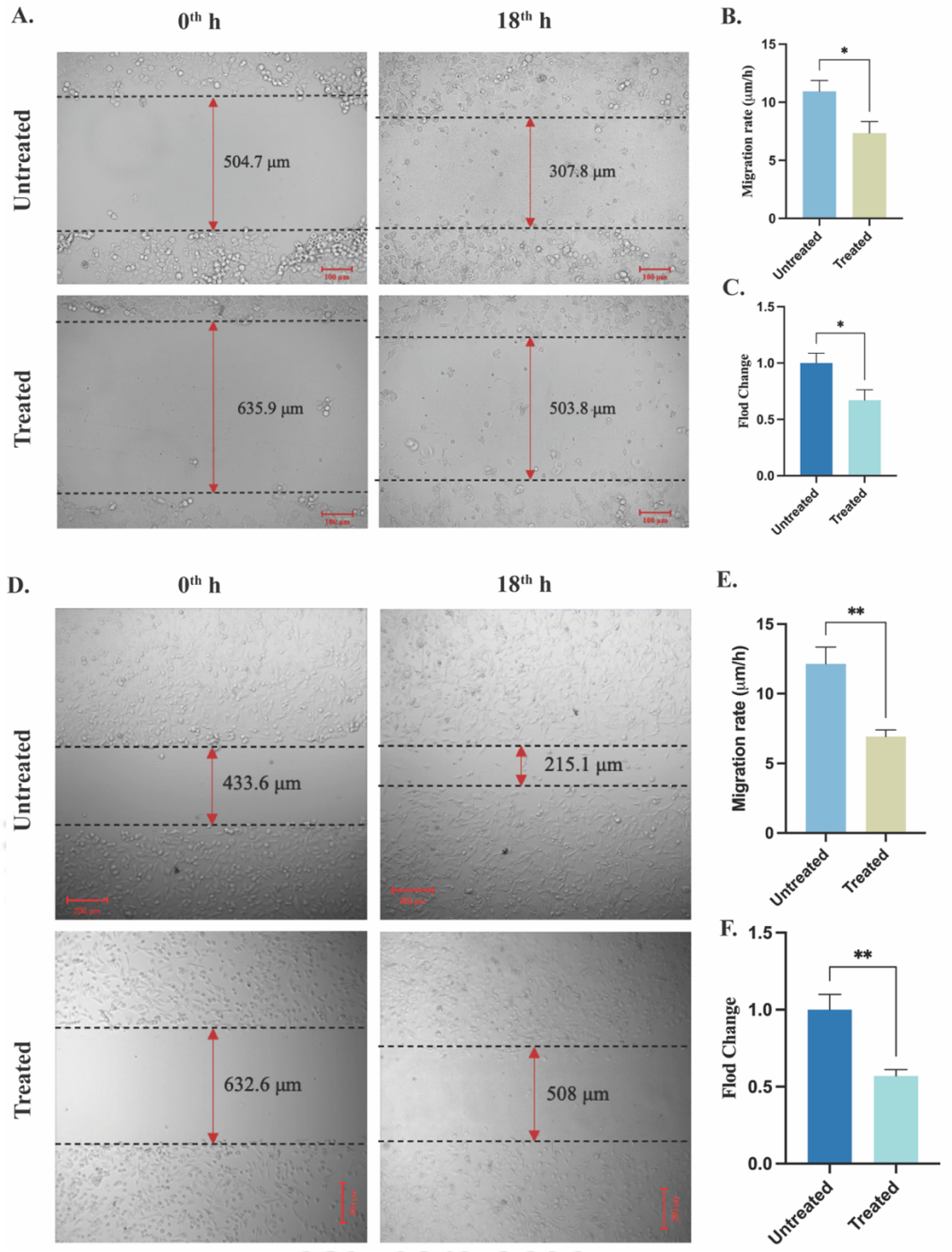

Figure 3.3.3. Assessment of the migration capability of TNBC cells. A) Migration analysis of MDA-MB-468 cells with corresponding quantitative depiction of **B)** migration rate and **C)** fold changes in migration ability upon beauvericin treatment. **D)** Migration analysis of MDA-MB-231 cells with corresponding quantitative estimation of **E)** migration rate and **F)** fold changes in in migration ability upon beauvericin treatment.

TH-3487_186106116

Table 3.3.1. Changes in the migration rate of TNBC cells upon beauvericin treatment.

Cell lines	Samples	Initial distance (µm)	Final distance (µm)	Migrated distance (µm)	Migration rate (µm/h)
MDA-MB-468	Untreated	504.7	307.8	196.9	10.9
	Treated	635.9	503.8	132.1	7.3
MDA-MB-231	Untreated	433.6	215.1	218.5	12.1
	Treated	632.6	508.0	124.6	6.9

The wound closure assay (WCA) has demonstrated reduction in the migration rate of both TNBC cell lines when exposed to beauvericin treatment at respective IC_{50} concentrations (**Table 3.3.1**) (**Figure 3.3.3B** and **3.3.3E**). The quantitative analysis has further revealed approximately 1.5 and 1.7-fold reduction in the migratory ability of MDA-MB-468 and MDA-MB-231 cells, respectively, following beauvericin treatment (**Figure 3.3.3C** and **3.3.3F**).

3.3.1.4. Beauvericin reverses epithelial to mesenchymal transition (EMT) in triple-negative breast cancer (TNBC) cells

Epithelial to mesenchymal transition (EMT) is a multifaceted process where epithelial cells undergo a transformation, adopting the traits typical of mesenchymal cells with increased motility and invasiveness. In this process, epithelial cells experience a significant reduction in the expression of epithelial markers such as E-cadherin, α-catenin and γ-catenin, while the expression of mesenchymal markers like fibronectin, N-cadherin, vimentin, β-catenin, Snail and Slug increases remarkably (Kalluri and Weinberg, 2010). Beauvericin has exhibited a significant upregulation in the expression of epithelial marker E-cadherin, while concurrently downregulating the expression of mesenchymal markers N-cadherin, vimentin, β-catenin, Snail and Slug in EMT induced TNBC cells.

TH-3487_186106116

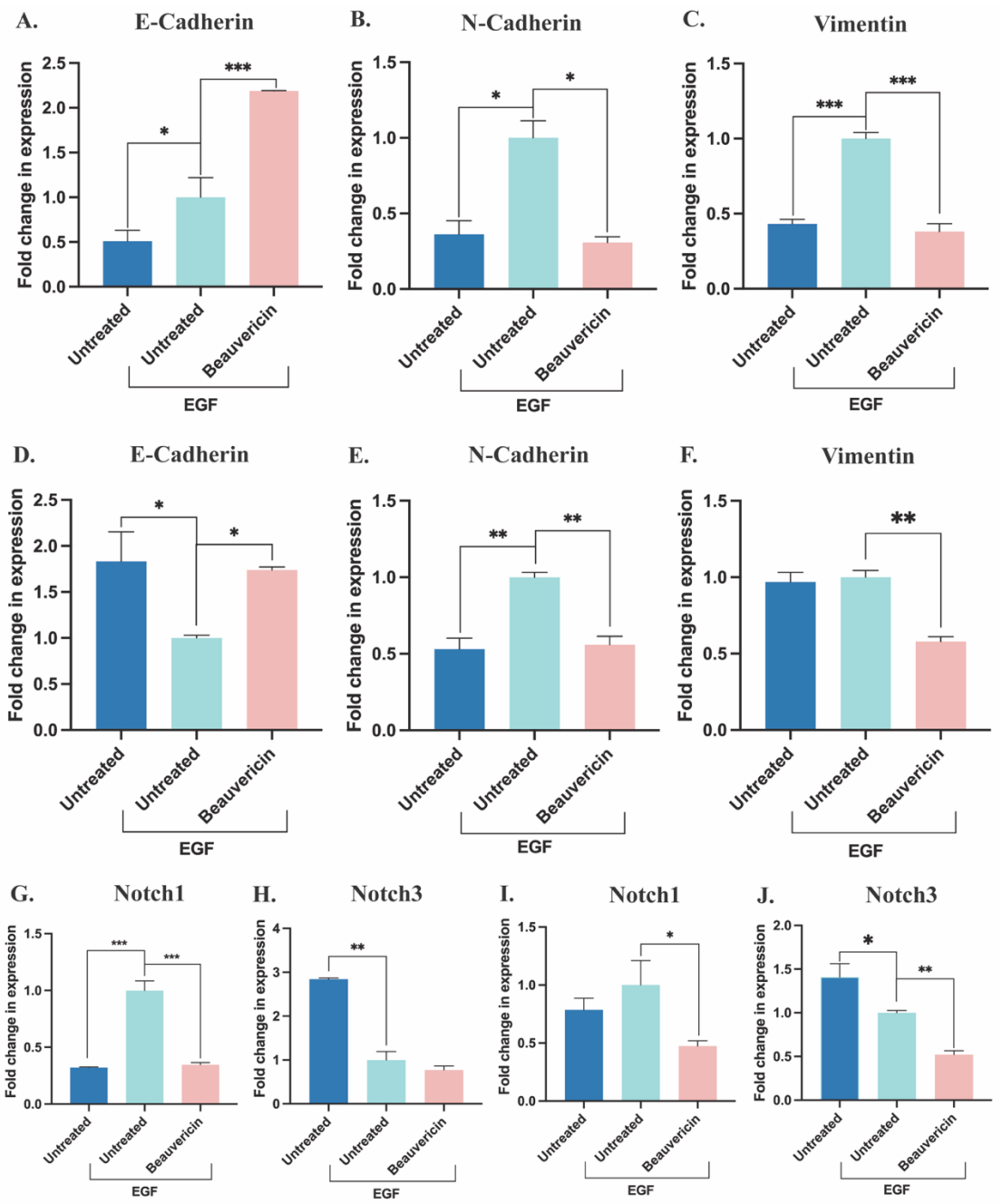

Figure 3.3.4. Expression analysis of EMT markers and Notch receptors by qRT-PCR. Expression profile of **A)** E-cadherin, **B)** N-cadherin and **C)** Vimentin in MDA-MB-468 cells and **D)** E-cadherin, **E)** N-cadherin and **F)** Vimentin in MDA-MB-231 cells. Expression profile of **G)** Notch1 and **H)** Notch3 receptors in MDA-MB-468 cells and **I)** Notch1 and **J)** Notch3 receptors in MDA-MB-231 cells.

TH-3487_186106116

Quantitative-real time PCR (qRT-PCR) has revealed approximately 2.2 and 1.7-fold upregulation in the expression of E-cadherin in EMT induced MDA-MB-468 and MDA-MB-231 cells (**Table 3.3.2**), respectively, following beauvericin treatment at respective IC_{50} concentrations (**Figure 3.3.4A** and **3.3.4D**). Treatment with same dosage has also resulted in a significant downregulation in the expression of mesenchymal markers N-cadherin and Vimentin by approximately 2.2 and 2.6-fold, respectively, in MDA-MB-468 cells (**Figure 3.3.4B** and **3.3.4C**) (**Table 3.3.2**). In MDA-MB-231 cells, the downregulation of N-cadherin and Vimentin is approximately 1.7-fold each (**Figure 3.3.4E** and **3.3.4F**) (**Table 3.3.2**). Immunoblotting experiments have also revealed similar results supporting the findings of qRT-PCR analysis.

Table 3.3.2. Changes in expression of EMT markers and Notch receptor proteins in terms of fold change determined by qRT-PCR.

Cell line	Gene names	Fold change in expression
MDA-MB-468	E-cadherin	2.2 ↑
	N-cadherin	2.2 ↓
	Vimentin	2.6 ↓
	Notch-1	2.9 ↓
	Notch-3	1.3 ↓
MDA-MB-231	E-cadherin	1.7 ↑
	N-cadherin	1.7 ↓
	Vimentin	1.7 ↓
	Notch-1	2.1 ↓
	Notch-3	1.9 ↓

Note: ↑ denotes upregulation in expression; ↓ denotes downregulation in expression.

TH-3487_186106116

The western blot analysis has shown significant reduction in the expression of mesenchymal markers N-cadherin, Vimentin, Slug, Snail and β-catenin (**Figure 3.3.5A**) by approximately 5.2, 2.1, 1.7, 2.6 and 1.4-fold, respectively in MDA-MB-468 cells (**Figure 3.3.5C, 3.3.5D, 3.3.5E, 3.3.5F** and **3.3.5G**), while showing significant upregulation in the expression of epithelial marker E-cadherin (**Figure 3.3.5A**) by approximately 1.4-fold (**Figure 3.3.5B**) (**Table 3.3.3**). In case of MDA-MB-231 cells, the expression of Snail, slug and β-catenin have been downregulated (**Figure 3.3.5L** and **3.3.5M**) by approximately 3.7, 1.7 and 2.7-fold, respectively (**Figure 3.3.5I, 3.3.5J** and **3.3.5K**) (**Table 3.3.3**).

3.3.1.5. Impairment of Notch signaling in triple-negative breast cancer (TNBC) cells

EMT associated signaling pathways are pivotal in triple-negative breast cancer (TNBC) due to their significant contribution in tumor progression, metastasis and therapeutic resistance. Numerous oncogenic pathways, including TGF-β, Hedgehog, Wnt/β-catenin, TNF-α/NFκB, receptor tyrosine kinases (RTKs) and Notch signaling pathways, have been demonstrated to trigger the process of EMT, as all these pathways converge on EMT regulating transcription factors such as Snail, Slug, Twist and Zeb1/2 (Buyuk et al., 2022). Notch signaling primarily regulates the process of EMT in breast cancer cells, along with various other essential processes for metastasis, encompassing survival in low oxygen environment (hypoxia), angiogenesis, infiltration into nearby tissues, survival in the bloodstream, resistance to chemotherapy and establishment of secondary tumour sites (Zhang et al., 2019). Hence, targeting Notch signaling in TNBC offers a therapeutic avenue to combat metastasis and improve patient survival. Beauvericin has been observed to regulate notch signaling by suppressing the expression of Notch receptors (Notch1 and Notch3) in both TNBC cell lines. qRT-PCR analysis has revealed a decrease in Notch1 expression by approximately 2.9-fold and Notch3 expression by approximately 1.3-fold in MDA-MB-468 cells (**Figure 3.3.4G** and **3.3.4H**). Similarly, in MDA-MB-231 cells, Notch1 expression has been downregulated by approximately 2.1-fold and Notch3 expression has been reduced by approximately 1.9-fold (**Figure 3.3.4I** and **3.3.4J**) (**Table 3.3.2**).

TH-3487_186106116

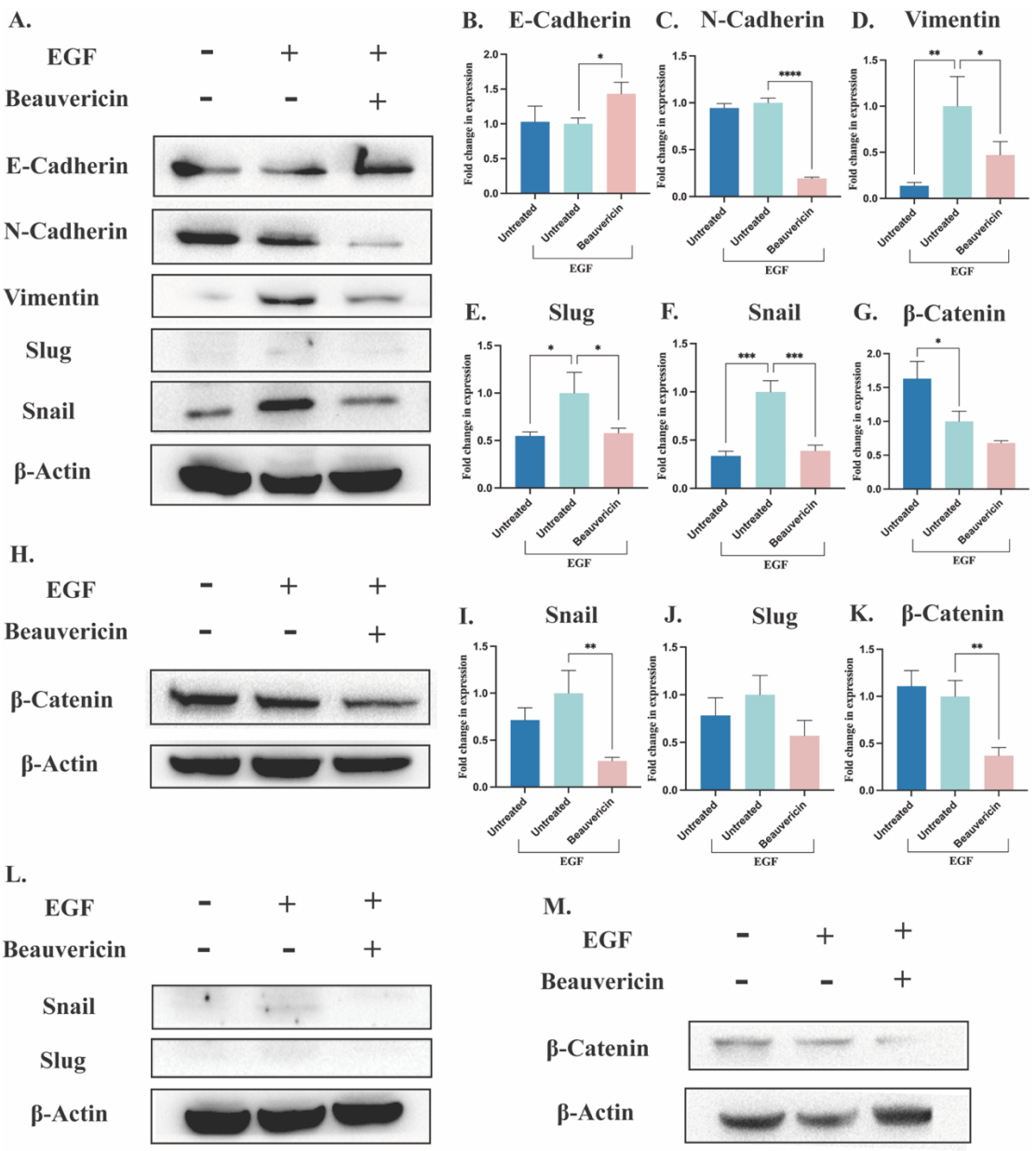

Figure 3.3.5. Protein expression analysis of EMT markers in TNBC cells. Immunoblots depicting alterations in **A)** E-Cadherin, N-Cadherin, Vimentin, Slug, Snail and **H)** β-catenin expression levels in MDA-MB-468 cells, following beauvericin treatment, while corresponding quantitative assessment of expression in terms of fold changes are illustrated in panels **B)**, **C)**, **D)**, **E)**, **F)** and **G)** respectively. Likewise, **L)** and **M)** depicting the immunoblots of Snail, Slug and β-catenin in MDA-MB-231 cells with **I)**, **J)** and **K)** illustrating their quantitative expression level in terms of fold change.

TH-3487_186106116

Furthermore, the expression analysis of Notch downstream proteins have been conducted to evaluate the consequences of suppressing the expression of Notch receptors. Western blot analysis has revealed downregulation in the expression of Notch downstream proteins Hes1 (**Figure 3.3.6A**) by approximately 2.1-fold (**Figure 3.3.6F**) and CyclinD3 (**Figure 3.3.6A**) by approximately 1.7-fold (**Figure 3.3.6G**), in MDA-MB-468 cells (**Table 3.3.3**). Similarly, in MDA-MB-231 cells, there has been a reduction in Hes1 expression (**Figure 3.3.6D**) by approximately 3.2-fold (**Figure 3.3.6J**) and CyclinD3 expression (**Figure 3.3.6D**) by approximately 2.2-fold (**Figure 3.3.6K**) (**Table 3.3.3**). Reduction in the expression of Notch receptor proteins (Notch1 and Notch3) and Notch downstream proteins (Hes1 and CyclinD3) due to beauvericin treatment have indicated its potential to inhibit Notch signaling pathway, eventually reversing EMT mediated metastatic events in TNBC cells.

3.3.1.6. Induction of autophagy in triple-negative breast cancer (TNBC) cells

The degradation of intracellular components, such as proteins and organelles, is facilitated by autophagy, a metabolic process that is widely preserved across organisms (Mizushima et al., 2008). It performs a vital function by repurposing metabolic energy to uphold cellular homeostasis when confronted with diverse stressors (Mizushima, 2007). The progression of cancer metastasis, along with EMT, is directly influenced by EMT related oncogenic signal proteins like Slug, Zeb1/2 and Notch1 etc. These proteins are also functionally linked with autophagy (Zada et al., 2021). Evidences indicate that autophagy plays an important role to suppress EMT and the activation of autophagy might govern reversal of the EMT status in various types of cancer cells (Catalano et al., 2015; Lv et al., 2012; Qin et al., 2015; Zhao et al., 2016). Hence, the scientific findings suggest that activation of autophagy potentially play a direct or indirect role in the inhibition of EMT and associated metastatic consequences. Immunoblotting experiments have unveiled the activation of autophagy in EMT induced TNBC cells following treatment with beauvericin at IC_{50} concentrations.

TH-3487_186106116

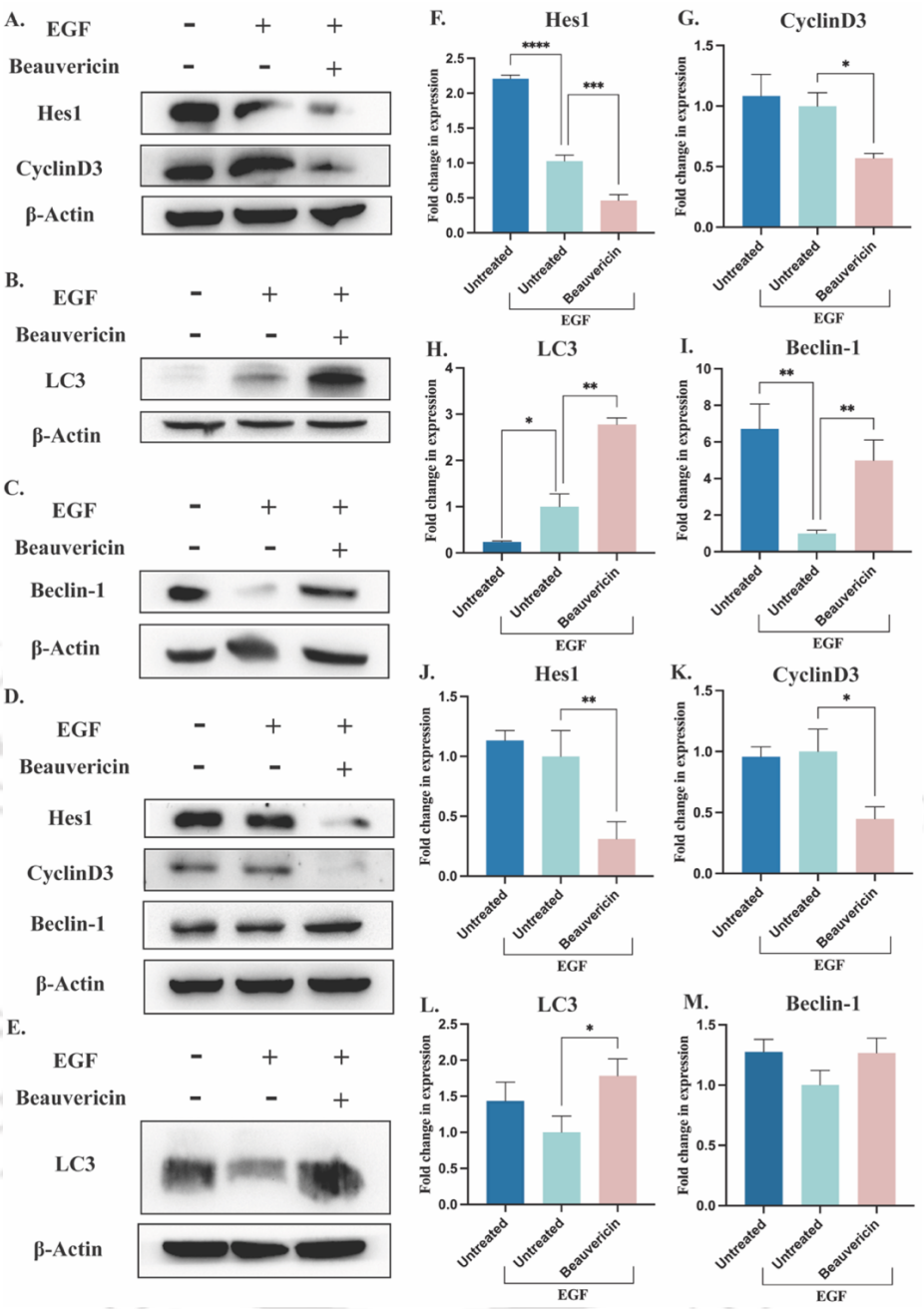

Figure 3.3.6. Expression analysis of Notch signaling and autophagy related proteins in EMT induced TNBC cells. Immunoblots depicting alterations in **A)** Hes-1and CyclinD3 and **B)** LC3 and **C)** Beclin-1 expression levels in MDA-MB-468 cells, due to beauvericin treatment, while corresponding quantitative assessment of expression in terms of fold changes are illustrated in panels **F)**, **G)**, **H)**, and **I)** respectively. Likewise, **D)** and **E)** depicting the immunoblots of Hes-1, CyclinD3, Beclin-1 and LC3 in MDA-MB-231 cells with **J)**, **K)**, **L)** and **M)** illustrating their quantitative expression level in terms of fold change.

TH-3487_186106116

Table 3.3.3. Changes in expression of EMT markers, Notch downstream proteins and autophagy markers in terms of fold change determined by immunoblotting.

Cell line	Protein names	Fold change in expression
MDA-MB-468	E-cadherin	1.4 ↑
	N-cadherin	5.2 ↓
	Vimentin	2.1 ↓
	Slug	1.7 ↓
	Snail	2.6 ↓
	β-catenin	1.4 ↓
	Hes-1	2.1 ↓
	CyclinD3	1.7 ↓
	LC3	2.7 ↑
	Beclin-1	4.9 ↑
MDA-MB-231	Snail	3.7 ↓
	Slug	1.7 ↓
	β-catenin	2.7 ↓
	Hes-1	3.2 ↓
	CyclinD3	2.2 ↓
	LC3	1.7 ↑
	Beclin-1	1.2 ↑

Note: ↑ denotes upregulation in expression; ↓ denotes downregulation in expression.

TH-3487_186106116

The experimental analysis has revealed substantial upregulation of the autophagy indicators LC3 and Beclin-1 by (**Figure 3.3.6B** and **3.3.6C**) approximately 2.7 and 4.9-fold (**Figure 3.3.6H** and **3.3.6I**), respectively, in MDA-MB-468 cells (**Table 3.3.3**). Likewise, in case of MDA-MB-231 cells, the expression levels of LC3 and Beclin-1 (**Figure 3.3.6E** and **3.3.6D**) have shown approximately 1.7 and 1.2-fold upregulation (**Figure 3.3.6L** and **3.3.6M**), respectively (**Table 3.3.3**). These observations suggest that beauvericin follows an autophagy-dependent pathway leading to cellular death in EMT induced TNBC cells, which can be further correlated with beauvericin induced inhibition of Notch signaling and subsequent reversal of EMT.

3.3.2. DISCUSSION

In this research, a comprehensive investigation has been conducted on the varied functions of beauvericin, especially in targeting the metastatic aspect of tripe-negative breast cancer (TNBC). Beauvericin has been implicated as a regulator of survival across various cancer types (Jow et al., 2004; LIN et al., 2005; Prosperini et al., 2013; Wätjen et al., 2014). Its ionophoric nature primarily accounts for its cytotoxic effects in cancer cells (Theuerkauf and Kepler, 2022). Functioning as an ionophore, it facilitates the accumulation of intracellular Ca^{2+} by mobilizing extracellular calcium ions, thereby triggering cellular death due to ionic imbalance (Chen et al., 2006). Furthermore, beauvericin induces apoptotic cell death in leukaemia cells by activating Caspase-3 and promoting increased cytochrome-c release from mitochondria (Jow et al., 2004). Beyond its cytotoxic effects, beauvericin also demonstrates efficacy in inhibiting cellular migration in breast cancer and prostate cancer cells. Additionally, it exhibits antiangiogenic activity in Human Umbilical Vein Endothelial Cells – 2 (HUVEC-2) (Zhan et al., 2007). In continuation with the existing therapeutic insights, this study has further explored the impact of beauvericin in regulating epithelial to mesenchymal transition (EMT) in triple-negative breast cancer cells along with its role in the regulation of EMT associated Notch signaling pathway and autophagic events. Beauvericin demonstrated a dose dependent inhibition in the viability of EMT induced TNBC cells in 2D as well as 3D cell culture models. This observation suggests the potential ability of beauvericin in regulating metastatic breast cancer population *in vitro*. Consistent with this, Beauvericin has also been found to trigger mitochondria derived oxidative stress in

TH-3487_186106116

metastatic TNBC cells. Oxidative stress often contributes in the regulation of cellular viability by triggering apoptotic cell death as observed in the previous researches (Patra et al., 2024). Hence, beauvericin can be considered as a regulator of metastatic TNBC population through oxidative stress mediated cellular death. Additionally, Notch-1 intracellular domain (NICD), a segment of Notch-1, is acknowledged for its ability to prevent oxidative stress mediated cell death by inhibiting the Apoptosis signal regulating kinase – 1 (ASK-1) signaling pathway (Mo et al., 2013). Hence, the downregulation of Notch-1 expression by beauvericin could be accountable for the oxidative stress induced death of TNBC cells.

The metastatic attributes of TNBC cells, including enhanced migration, invasiveness, and angiogenesis, originate from the process of epithelial to mesenchymal transition (EMT). EMT induces mesenchymal properties in TNBC cells, leading to enhanced migratory potential and an elevated risk of secondary tumour development (Mittal, 2018). Therefore, reversing EMT with the aid of beauvericin may halt the dissemination of primary TNBC cells to distant organs. The aforementioned findings in this study have clearly demonstrated beauvericin's capability to effectively reverse EMT in TNBC cells, reinstating their epithelial traits. In addition to promoting metastasis, EMT has also been associated with development of chemotherapeutic resistance in TNBC (Sommers et al., 1992). EMT induced TNBC cells often exhibit stem cell like properties which are inherently resistant to conventional treatments. This plasticity allows TNBC cells to adapt changing microenvironment and evade therapeutic interventions, leading to treatment failure and disease recurrence (Shibue and Weinberg, 2017). Hence, beauvericin induced reversal of EMT in TNBC cells may offer a promising approach to combat EMT induced tumor progression, metastasis and chemotherapeutic resistance of TNBC. Furthermore, the elevated migratory and invasive traits in metastatic TNBC cells are crucial factors influencing the survival of TNBC patients (Piedra-Delgado et al., 2024). Hence, the capability of beauvericin to impede cellular migration is poised to have a critical impact on regulating TNBC-associated mortalities.

In the realm of numerous metastasis associated signaling pathways, Notch holds significant importance in governing the process of EMT (Edwards and Brennan, 2021).

TH-3487_186106116

Hence, directing interventions towards Notch signaling can offer benefits in mitigating the metastatic implications reliant on EMT. In this study, beauvericin has been observed to downregulate Notch-1 and Notch-3 expression along with the Notch downstream proteins Hes-1 and Cyclin D3, in TNBC cells. Numerous studies have established a connection between Notch-1 signaling and TNBC (Speiser et al., 2012). TNBC with overexpressed Notch-1 exhibit significant upregulation of its target genes, including NOTCH3, HES1, MYC, HES4 etc. These elevated expressions contribute to the oncogenic phenotype of TNBC (Wang et al., 2015). Hence, beauvericin mediated inhibition of Notch-1 resulted in reduced expression of Notch-3 and Hes-1, subsequently suppressing the oncogenic characteristics of TNBC. Studies have indicated that heightened expression of miR-3178, a Notch-1 targeting miRNA, results in reduced Notch-1 activity, which eventually suppresses Snail expression and subsequent EMT (Kong et al., 2018). Similarly, targeting Notch-1 by beauvericin has also resulted in reversal of EMT in TNBC cells through regulation of Snail expression. In the TNBC subtype of breast cancer, elevated levels of Hes-1 have been documented, demonstrating a correlation with heightened EMT, increased invasiveness and progression to advanced TNM stage with poor prognosis (Li et al., 2018). Consequently, differential expression of HES-1 in TNBC has been negatively correlated with the survival of TNBC patients (Mamoor, n.d.). Therefore, beauvericin mediated downregulation of HES-1 has effectively regulated the EMT status in TNBC cells, offering enhanced prognostic significance with improved patient survival. Similarly, CylinD3 is involved in cell cycle regulation at G1/S phase through its interaction with cyclin-dependent kinase 4 (CyclinD3/CDK4). Elevated expression of cyclinD3 and subsequent activation of CDK4 contributes to the cell cycle progression and Notch dependent pathogenesis of cancer cells (Joshi et al., 2009). Therefore, downregulation in cyclinD3 expression due to beauvericin treatment aligns with the observation of Cell cycle arrest at G1 phase in TNBC cells, as well as the indirect regulation of EMT through inhibition of Notch signaling. Conversely, inhibition of cyclin D3 decreases the level of antioxidants, NADPH and glutathione, resulting in elevated level of ROS within the cell, which in turn induces apoptotic cell death (Wang et al., 2017). Therefore, supporting the observation of oxidative stress mediated induction of apoptosis by beauvericin in TNBC cells.

TH-3487_186106116

In addition to its role in reversing EMT by Notch inhibition, beauvericin has also been observed to trigger autophagy in TNBC cells. Studies have revealed that autophagy activation is responsible for degradation of Notch intracellular domain (NICD), a crucial element of Notch-1 signaling, which serves as a key regulator of EMT and subsequent metastasis (Zada et al., 2022). This study has additionally demonstrated that LC3, a positive regulator of autophagy, impedes the nuclear translocation of NICD by forming LC3-NICD-SNAI1-SQSTM1 complex, which leads to a reduction in the transcriptional activity of Notch-1's target genes, consequently suppressing cancer cell migration and invasion (Zada et al., 2022). Therefore, the increase in LC3 expression induced by beauvericin in TNBC cells indicates probable degradation of NICD and subsequent attenuation of EMT leading to reduced cell migration. Another study has demonstrated that autophagy induced by AZD8055 and rapamycin reduces the self-renewal ability and tumorigenicity of glioma-initiating cell (GIC) by inhibiting the Notch1 (Tao et al., 2018). Autophagy is also observed to inhibit stem cell differentiation by degrading Notch1 in relevant mouse model (Wu et al., 2016), projecting its therapeutic potential in restricting the differentiation of cancer-stem-cells (CSCs). These observations highlight the therapeutic effectiveness of autophagy activation and Notch1 inhibition in the realms of cancer treatment, supporting the same therapeutic window offered by beauvericin in TNBC cells. Moreover, increased Beclin-1 expression has been positively correlated with E-cadherin expression (Qin et al., 2015), whereas its negative expression is associated with shorter overall survival (Geng et al., 2012), which has validated the findings on beauvericin mediated upregulation of Beclin-1 and subsequent elevation in E-cadherin expression. Hence, activation of autophagy subsequent to beauvericin treatment has ultimately led to the reversal of EMT through inhibition of Notch signaling in TNBC cells.

TH-3487_186106116

3.3.3. CONCLUSION

In conclusion, beauvericin demonstrates considerable efficacy in diminishing the viability of EMT-induced triple-negative breast cancer (TNBC) cells in both monolayers and spheroids. Flow cytometric analysis reveals that this anti-proliferative effect stems from oxidative stress induction, characterized by elevated intracellular reactive oxygen species (ROS) levels and increased mitochondrial transmembrane potential. Furthermore, beauvericin curtails the migration ability of triple-negative breast cancer (TNBC) cells by reversing the epithelial-to-mesenchymal transition (EMT). Comprehensively, treatment with beauvericin leads to elevated expression of epithelial marker E-cadherin, while showing significant reduction in the expression of mesenchymal markers such as N-cadherin, vimentin, Snail, and Slug, confirming the reversal of EMT in TNBC cells. Additionally, beauvericin exerts its EMT regulatory effect by targeting the Notch signaling pathway. Specifically, it inhibits the Notch-1 receptor, thereby impeding the function of Notch-3 and Notch downstream proteins Hes-1 and Cyclin D3, hence, disrupting the Notch pathway-mediated signal transduction and consequent downregulation of EMT. Furthermore, beauvericin induced EMT reversal through Notch inhibition is also correlated with activation of autophagy. Beauvericin induces autophagy-mediated regulation of cellular viability of triple-negative breast cancer (TNBC) cells, marked by significant elevation in the expression of autophagy-inducing proteins LC3 and Beclin-1. This autophagy activation, in turn, inhibits Notch1 signaling by directly interacting with NICD, consequently reversing EMT. Hence, Beauvericin exhibits potential therapeutic promise against metastatic TNBC cells by targeting Notch signaling pathway and activating autophagy, resulting in the reversal of EMT. This shows the potential of beauvericin to reduce metastasis and improve treatment efficacy in TNBC.

TH-3487_186106116

Chapter 4

Conclusion and Future Prospects

TH-3487_186106116

TH-3487_186106116

4.1. Conclusion

The culmination of this thesis emphasizes the significant therapeutic potential of both protein-based and non-protein-based entomopathogenic mycotoxins, specifically the ribotoxin **Anisoplin** from *Metarhizium anisopliae* and secondary metabolite **Beauvericin** from *Beauveria bassiana*, in addressing the formidable challenges of breast cancer treatment, with a particular focus on chemotherapeutic resistance and metastatic events. This comprehensive study provides valuable insights into the mechanisms of action of these mycotoxins and their efficacy in combating different breast cancer subtypes, laying the groundwork for future clinical applications.

The salient conclusions of the research findings of this thesis have been outlined below under specific sub-topics -

Heterologous production, purification and characterization of anisoplin from *Metarhizium anisopliae* and its therapeutic effects on MCF-7 breast cancer cells.

- Emerging chemotherapeutic resistance remains a primary obstacle in breast cancer therapy, necessitating the exploration of novel therapeutic agents. Anisoplin, a ribotoxin derived from entomopathogenic fungi, exhibits promising anticancer properties. The study detailed in this section successfully produced recombinant anisoplin in an Escherichia coli BL21(DE3) expression system, followed by purification and *in silico*, biophysical and functional characterizations.

- The recombinant anisoplin demonstrated a significant reduction in the viability of MCF-7 breast cancer cells in a dose-dependent manner, with an IC_{50} value of 4 μM. This cytotoxic effect was accompanied by a 3.5-fold increase in intracellular reactive oxygen species (ROS), and subsequent depolarization of the mitochondrial membrane, indicating the induction of oxidative stress.

- Detailed analysis revealed that anisoplin induces apoptosis as a consequence of the oxidative stress. Flow cytometric analyses confirmed this apoptosis induction, highlighting the potential of anisoplin as a therapeutic agent.

TH-3487_186106116

- Additionally, anisoplin-treated MCF-7 cells exhibited a significant loss of self-renewal capability, inhibiting clonal expansion and regeneration, which are crucial for cancer recurrence.

- Immunoblotting experiments provided deeper insights into the molecular mechanisms underlying anisoplin's therapeutic effects. The activation of the JNK-dependent MAP kinase signaling pathway, evidenced by the upregulation of phospho-SAPK/JNK expression, indicates initiation of ribotoxic stress response. This activation was further correlated with the NFκB expression profile, leading to cell death.

- These findings highlight anisoplin's ability to induce apoptosis through a well-defined molecular pathway, reinforcing its therapeutic potential in breast cancer treatment.

Evaluation of intracellular therapeutic targets and *in vitro* therapeutic effects of beauvericin on triple-negative breast cancer (TNBC) cells

- Triple negative breast cancer (TNBC) represents a significant global health concern due to its aggressive nature, high mortality rate, and limited treatment options. The urgency for targeted therapies in TNBC is paramount, given its resistance to conventional chemotherapies. Beauvericin, a bioactive fungal secondary metabolite, has demonstrated substantial anticancer potential. This study explored the molecular targets of beauvericin and its therapeutic insights in TNBC cells.

- *In silico* studies using molecular docking and molecular dynamics (MD) simulations identified possible molecular targets for beauvericin, namely MRP-1 (ABCC1), HDAC-1, HDAC-2, LCK, and SYK. These targets are implicated in drug resistance, epigenetic modulation, and oncogenic signaling. The average

TH-3487_186106116

binding energies of beauvericin to these targets ranged from -44.3 to -105 KJ/mol, implying its multifaceted roles in inhibiting these cancer promoting events.

- Beauvericin significantly reduced the viability of MDA-MB-231 and MDA-MB-468 TNBC cells, with IC_{50} concentrations of 4.4 and 3.9 μM, respectively. Concurrently, beauvericin elevated intracellular ROS levels by 9.0 and 7.9 folds in these cell lines, indicating oxidative stress induction. The reduction of mitochondrial transmembrane potential in TNBC cells further confirmed the induction of oxidative stress leading to apoptotic cell death, as observed through flow cytometric analyses.

- Beyond inducing apoptosis, beauvericin also impaired the colony formation and spheroid abilities of TNBC cells, indicating its potential inhibit the cancer recurrence caused by TNBC subtype through restricting clonal expansion and regeneration ability of TNBC cells.

- Ultimately, beauvericin reduced the viability of TNBC spheroids, achieving IC_{50} concentrations of 10.3 and 6.2 μM in MDA-MB-468 and MDA-MB-231 cells, respectively. Visual evidence of TNBC cell death due to beauvericin treatment has further validated its potential as a therapeutic agent for TNBC.

Evaluation of beauvericin's therapeutic effects on the metastatic attributes of triple-negative breast cancer (TNBC) cells

- Metastasis is a primary contributor to TNBC-associated mortality worldwide, presenting heightened severity and significant challenges due to limited treatment options. Addressing TNBC metastasis necessitates innovative approaches and novel therapeutics capable of specifically targeting its propensity for dissemination to distant organs. The ability to reverse epithelial-to-mesenchymal transition (EMT), a critical process in metastasis, is essential in suppressing TNBC spread and enhancing treatment response.

TH-3487_186106116

- Beauvericin has shown significant potential in diminishing the viability of EMT-induced TNBC cells by triggering intracellular oxidative stress. The compound exhibited an IC_{50} of 2.3 μM in monolayer cultures of both MDA-MB-468 and MDA-MB-231 cells. In 3D spheroids, the IC_{50} values were 9.7 μM and 7.1 μM, respectively, demonstrating its efficacy in more complex tumor models.

- Additionally, beauvericin reduced the migratory capability of MDA-MB-468 and MDA-MB-231 cells by 1.5-fold and 1.7-fold, respectively, indicating its potential to inhibit metastasis.

- Molecular analyses through qRT-PCR and western blotting revealed that beauvericin treatment led to a significant upregulation of the epithelial marker E-cadherin and downregulation of mesenchymal markers such as N-cadherin, vimentin, Snail, Slug, and β-catenin. This reversal of EMT highlights beauvericin's potential in targeting metastatic processes. Furthermore, beauvericin suppressed the Notch signaling pathway by downregulating Notch-1, Notch-3, Hes-1, and cyclin D3 expression, which are crucial for TNBC progression, EMT and metastasis.

- The induction of autophagy, observed through elevated expression of autophagy markers LC3 and Beclin-1, adds another dimension to beauvericin's therapeutic profile. Autophagy plays a dual role in cancer, either promoting cell survival or contributing to cell death, depending on the context. In this study, the induction of autophagy by beauvericin suggests a potential mechanism for enhancing cancer cell death, further supporting Notch signaling inhibition mediated reversal of EMT.

TH-3487_186106116

4.2. Implications and Future Directions

The findings from these studies offer a promising outlook for the future of breast cancer therapy, particularly in overcoming chemotherapeutic resistance and addressing metastasis. The use of fungal ribotoxins like anisoplin and secondary metabolites like beauvericin provides a novel and effective alternative to conventional therapies. These compounds' ability to target multiple pathways and induce apoptosis, oxidative stress, and autophagy highlights their multifaceted therapeutic potential.

Future research should focus on the targeted delivery of anisoplin and beauvericin in order to overcome the issues associated with non-specific cytotoxicity. Furthermore, *in vivo* studies and clinical trials are also required to validate the efficacy and safety of these agents in human patients. Additionally, exploring combination therapies that integrate anisoplin and beauvericin with existing treatment regimens could enhance their therapeutic outcomes. The potential for these agents to be incorporated into personalized medicine approaches also warrants investigation, given the diverse molecular targets they affect.

In conclusion, the innovative application of fungal-derived natural products in breast cancer therapy represents a significant advancement in the quest for more effective and targeted cancer treatments. The promising results from anisoplin and beauvericin studies provide a strong foundation for *in vivo* studies and possible clinical applications. By addressing the challenges of chemotherapeutic resistance and metastasis, these therapeutic candidates offer new hope for improved outcomes in breast cancer patients, particularly those with limited treatment options. The ongoing exploration and development of these therapeutic agents hold the potential to transform the therapeutic landscape for breast cancer, offering renewed optimism and improved survival rates for breast cancer patients worldwide.

TH-3487_186106116

TH-3487_186106116

P U B L C A T I O N S

From Thesis Work:

1. **Patra, A.**, Kandasamy, T., Ghosh, S.S., Saini, G.K., 2023. In vitro anticancer effects of recombinant anisoplin through activation of SAPK/JNK and downregulation of NFκB. Toxicology in Vitro 94, 105737. DOI: 10.1016/j.tiv.2023.105737

2. **Patra, A.**, Ghosh, S.S. and Saini, G.K., 2024. Exploring potential molecular targets and therapeutic efficacy of beauvericin in triple-negative breast cancer cells. *Computational Biology and Chemistry*, *112*, p.108154. DOI: 10.1016/j.compbiolchem.2024.108154

3. **Patra, A.**, Arora, A., Ghosh, S.S. and Kaur Saini, G., 2024. Beauvericin Reverses Epithelial-to-Mesenchymal Transition in Triple-Negative Breast Cancer Cells through Regulation of Notch Signaling and Autophagy. *ACS Pharmacology & Translational Science*. DOI: 10.1021/acsptsci.4c00370

From Collaborative Work:

1. Nambiar, S.S., Mohanty, A., **Patra, A.** and Saini, G.K., 2022. Deciphering therapeutic efficacy of mycosynthesized silver nanoparticles using entomopathogenic fungi Metarhizium anisopliae against MCF-7 breast cancer cells in vitro. *bioRxiv*, pp.2022-08. DOI: 10.1101/2022.08.25.505221

2. Adil, L. R.; Bidkar, A. P.; **Patra, A.**; Ghosh, S. S.; Iyer, P. K. Suppression of aggregation caused quenching in pyrene by introducing push-pull dipolar rotor groups and used as a multiresponsive probe and photodynamic therapy (***communicated***).

3. Adil, L. R.**; Patra, A.**; Bidkar, A. P.; Ghosh S. S.; Iyer, P. K. Aggregation induced emission active luminogens for wash free imaging and antimicrobial application against pathogenic bacteria and fungus (***communicated***).

TH-3487_186106116

TH-3487_186106116

C O N F E R E N C E S

1. **Participated** in the workshop entitled **Diagnostic Approaches in Virology**; From 4th – 6th March, 2020; Organized by Department of Biosciences and Bioengineering, Indian Institute of Technology (IIT) Guwahati.

2. Participated in **poster presentation** entitled "**Insights into anticancer potential of recombinant fungal ribotoxin against breast cancer cells in vitro**" in **Research & Industrial Conclave Integration' 2023**; From 14th – 16th May, 2023; Organized by Indian Institute of Technology (IIT) Guwahati.

3. Participated in **poster presentation** entitled "**Synthesis and characterization of entomopathogenic loaded PLGA-CuNC nanocomposite for breast cancer therapy**" in **8th International Conference on Advanced Nanomaterials and Nanotechnology – ICANN 2023**; From 29th November – 1st December, 2023; Organized by Centre for Nanotechnology, Indian Institute of Technology (IIT) Guwahati.

4. Participated in **poster presentation** entitled "**In vitro anticancer effects of recombinant anisoplin through activation of SAPK/JNK and downregulation of NFκB**" in **8th World Cancer Congress - 2024**; From 18th – 20th March, 2024; Organized by Arjyopa Healthcare, Cancer Healer Centre and Central Council for Yoga and Naturopathy at Jawaharlal Nehru University (JNU), New Delhi.

TH-3487_186106116

TH-3487_186106116

A P P E N D I X

Buffers / Reagents	Composition
50X TAE buffer (1L)	242 g tris base in double-distilled H_2O. 57.1 mL glacial acetic acid. 100 mL 0.5 M EDTA solution (pH 8.0) Adjust volume to 1L
2X RNA loading buffer	95 % formamide 0.025 % SDS 0.025 % bromophenol blue 0.025 % xylene cyanol FF 0.025 % ethidium bromide 0.5 mM EDTA.
6X DNA loading buffer (5mL)	1.5mL Glycerol 0.0125g bromophenol blue 0.0125g xylene cyanol FF
Resuspension buffer for plasmid isolation (1L)	50mM Tris-Hcl, pH 8.0, 10mM EDTA 100ug/mL RNase-A (Storage condition - 4°C after adding RNase A)
Lysis buffer for plasmid isolation (1L)	200mM NaOH, 1% SDS Storage condition - RT

TH-3487_186106116

Neutralization buffer for plasmid isolation (1L)	3.0M potassium acetate, pH 5.5 Storage condition - 4˚C or RT
10X Tris-Glycine Buffer (1L)	30.0 g of Tris base 144.0 g of glycine 10.0 g of SDS Store the running buffer at room temperature and dilute to 1X before use.
4X protein loading buffer for SDS-PAGE	0.2 M Tris-HCL 0.4 M Dithiothreitol (DTT) 277 mM SDS 6 mM bromophenol blue 4.3 M glycerol
10X Phosphate buffered saline (1L)	1.37 M NaCl 27 mM KCl 100 mM Na_2HPO_4 18 mM KH_2PO_4
Tris buffered saline (TBS)	1500 mM of Sodium chloride 200 mM of Tris base Adjust pH to 7.6 with Hcl
TBST	TBS + 0.1% Tween 20

TH-3487_186106116

References

TH-3487_186106116

TH-3487_186106116

Ahmad, B., Rizwan, M., Rauf, A., Raza, M., Bashir, S., Molnar, J., Csonka, A., Szabo, D., Mubarak, M.S., Noor, M., Siddiqui, B.S., 2017. Isolation of Chlorogenic Acid from Soil Borne Fungi Screlotium rolfsii, their Reversal of Multidrug Resistance and Anti-proliferative in Mouse Lymphoma Cells. Med Chem (Los Angeles) 13. https://doi.org/10.2174/1573406413666170612110443

Al Qutami, F., Al Halabi, W., Hachim, M.Y., 2023. Identification of Breast Cancer LCK Proto-Oncogene as a Master Regulator of TNBC Neutrophil Enrichment and Polarization. Int J Mol Sci 24, 13269. https://doi.org/10.3390/ijms241713269

Albonico, M., Schutz, L.F., Caloni, F., Cortinovis, C., Spicer, L.J., 2017. In vitro effects of the Fusarium mycotoxins fumonisin B1 and beauvericin on bovine granulosa cell proliferation and steroid production. Toxicon 128, 38–45. https://doi.org/10.1016/j.toxicon.2017.01.019

Altschul, S.F., Gish, W., Miller, W., Myers, E.W., Lipman, D.J., 1990. Basic local alignment search tool. J Mol Biol 215, 403–410. https://doi.org/10.1016/S0022-2836(05)80360-2

Amaravadi, R.K., Kimmelman, A.C., Debnath, J., 2019. Targeting Autophagy in Cancer: Recent Advances and Future Directions. Cancer Discov 9, 1167–1181. https://doi.org/10.1158/2159-8290.CD-19-0292

An, C., Li, X., Li, C., Gao, S., Shang, Z., Wang, B., 2013. Triazoles and Other N-Containing Metabolites from the Marine-Derived Endophytic Fungus *Penicillium chrysogenum* EN-118. Helv Chim Acta 96, 682–687. https://doi.org/10.1002/hlca.201200433

Anders, C., Carey, L.A., Carey, L., 2008. Understanding and Treating Triple-Negative Breast Cancer, Oncology.

Antimycobacterial and Antiplasmodial Cyclodepsipeptides from the Insect Pathogenic Fungus Paecilomyces tenuipes BCC 1614, n.d.

Arfin, S., Jha, N.K., Jha, S.K., Kesari, K.K., Ruokolainen, J., Roychoudhury, S., Rathi, B., Kumar, D., 2021. Oxidative Stress in Cancer Cell Metabolism. Antioxidants 10, 642. https://doi.org/10.3390/antiox10050642

TH-3487_186106116

Asleh, K., Riaz, N., Nielsen, T.O., 2022. Heterogeneity of triple negative breast cancer: Current advances in subtyping and treatment implications. Journal of Experimental & Clinical Cancer Research 41, 265. https://doi.org/10.1186/s13046-022-02476-1

Atanasov, A.G., Zotchev, S.B., Dirsch, V.M., Supuran, C.T., 2021. Natural products in drug discovery: advances and opportunities. Nat Rev Drug Discov 20, 200–216. https://doi.org/10.1038/s41573-020-00114-z

Averill-Bates, D.A., 2023. The antioxidant glutathione. pp. 109–141. https://doi.org/10.1016/bs.vh.2022.09.002

Bae, Y.K., Choi, J.E., Kang, S.H., Lee, S.J., 2015. Epithelial-Mesenchymal Transition Phenotype Is Associated with Clinicopathological Factors That Indicate Aggressive Biological Behavior and Poor Clinical Outcomes in Invasive Breast Cancer. J Breast Cancer 18, 256. https://doi.org/10.4048/jbc.2015.18.3.256

Bai, J.-W., Wei, M., Li, J.-W., Zhang, G.-J., 2020. Notch Signaling Pathway and Endocrine Resistance in Breast Cancer. Front Pharmacol 11. https://doi.org/10.3389/fphar.2020.00924

Baird, L., Yamamoto, M., 2021. NRF2-Dependent Bioactivation of Mitomycin C as a Novel Strategy To Target KEAP1-NRF2 Pathway Activation in Human Cancer. Mol Cell Biol 41. https://doi.org/10.1128/MCB.00473-20

Becker, N., Benhar, I., 2012. Antibody-Based Immunotoxins for the Treatment of Cancer. Antibodies 1, 39–69. https://doi.org/10.3390/antib1010039

Bérdy, J., 2005. Bioactive Microbial Metabolites. J Antibiot (Tokyo) 58, 1–26. https://doi.org/10.1038/ja.2005.1

Betteridge, D.J., 2000. What is oxidative stress? Metabolism 49, 3–8. https://doi.org/10.1016/S0026-0495(00)80077-3

Beyer, R.E., 1994. The role of ascorbate in antioxidant protection of biomembranes: Interaction with vitamin E and coenzyme Q. J Bioenerg Biomembr 26, 349–358. https://doi.org/10.1007/BF00762775

TH-3487_186106116

Bilir, B., Kucuk, O., Moreno, C.S., 2013. Wnt signaling blockage inhibits cell proliferation and migration, and induces apoptosis in triple-negative breast cancer cells. J Transl Med 11, 280. https://doi.org/10.1186/1479-5876-11-280

Biswas, P.K., Park, S.R., An, J., Lim, K.M., Dayem, A.A., Song, K., Choi, H.Y., Choi, Y., Park, K.S., Shin, H.J., Kim, A., Gil, M., Saha, S.K., Cho, S.-G., 2023. The Orphan GPR50 Receptor Regulates the Aggressiveness of Breast Cancer Stem-like Cells via Targeting the NF-kB Signaling Pathway. Int J Mol Sci 24, 2804. https://doi.org/10.3390/ijms24032804

Bolós, V., Mira, E., Martínez-Poveda, B., Luxán, G., Cañamero, M., Martínez-A, C., Mañes, S., de la Pompa, J.L., 2013. Notch activation stimulates migration of breast cancer cells and promotes tumor growth. Breast Cancer Research 15, R54. https://doi.org/10.1186/bcr3447

Brabletz, S., Bajdak, K., Meidhof, S., Burk, U., Niedermann, G., Firat, E., Wellner, U., Dimmler, A., Faller, G., Schubert, J., Brabletz, T., 2011. The ZEB1/miR-200 feedback loop controls Notch signalling in cancer cells. EMBO J 30, 770–782. https://doi.org/10.1038/emboj.2010.349

Brandhorst, T.T., Kenealy, W.R., 1992. Production and localization of restrictocin in Aspergillus restrictus. J Gen Microbiol 138, 1429–1435. https://doi.org/10.1099/00221287-138-7-1429

Bray, F., Laversanne, M., Sung, H., Ferlay, J., Siegel, R.L., Soerjomataram, I., Jemal, A., 2024. Global cancer statistics 2022: GLOBOCAN estimates of incidence and mortality worldwide for 36 cancers in 185 countries. CA Cancer J Clin 74, 229–263. https://doi.org/10.3322/caac.21834

Brown, S.S., Spudich, J.A., 1981. Mechanism of action of cytochalasin: evidence that it binds to actin filament ends. J Cell Biol 88, 487–491. https://doi.org/10.1083/jcb.88.3.487

Buyuk, B., Jin, S., Ye, K., 2022. Epithelial-to-Mesenchymal Transition Signaling Pathways Responsible for Breast Cancer Metastasis. Cell Mol Bioeng 15, 1–13. https://doi.org/10.1007/s12195-021-00694-9

TH-3487_186106116

Cadoná, F.C., Dantas, R.F., de Mello, G.H., Silva-Jr, F.P., 2022. Natural products targeting into cancer hallmarks: An update on caffeine, theobromine, and (+)-catechin. Crit Rev Food Sci Nutr 62, 7222–7241. https://doi.org/10.1080/10408398.2021.1913091

Cardoso, F., Kyriakides, S., Ohno, S., Penault-Llorca, F., Poortmans, P., Rubio, I.T., Zackrisson, S., Senkus, E., 2019. Early breast cancer: ESMO Clinical Practice Guidelines for diagnosis, treatment and follow-up. Annals of Oncology 30, 1194–1220. https://doi.org/10.1093/annonc/mdz173

Carreras-Sangrà, N., Tomé-Amat, J., García-Ortega, L., Batt, C.A., Oñaderra, M., Martínez-Del-Pozo, Á., Gavilanes, J.G., Lacadena, J., 2012. Production and characterization of a colon cancer-specific immunotoxin based on the fungal ribotoxin α-sarcin. Protein Engineering, Design and Selection 25, 425–435. https://doi.org/10.1093/protein/gzs032

Castlebury, L.A., Sutherland, J.B., Tanner, L.A., Henderson, A.L., Cerniglia, C.E., n.d. Use of a bioassay to evaluate the toxicity of beauvericin to bacteria.

Castro, N.P., Fedorova-Abrams, N.D., Merchant, A.S., Rangel, M.C., Nagaoka, T., Karasawa, H., Klauzinska, M., Hewitt, S.M., Biswas, K., Sharan, S.K., Salomon, D.S., 2015. *Cripto-1* as a novel therapeutic target for triple negative breast cancer. Oncotarget 6, 11910–11929. https://doi.org/10.18632/oncotarget.4182

Catalano, M., D'Alessandro, G., Lepore, F., Corazzari, M., Caldarola, S., Valacca, C., Faienza, F., Esposito, V., Limatola, C., Cecconi, F., Di Bartolomeo, S., 2015. Autophagy induction impairs migration and invasion by reversing EMT in glioblastoma cells. Mol Oncol 9, 1612–1625. https://doi.org/10.1016/j.molonc.2015.04.016

Cauli, O., 2021. Oxidative Stress and Cognitive Alterations Induced by Cancer Chemotherapy Drugs: A Scoping Review. Antioxidants 10, 1116. https://doi.org/10.3390/antiox10071116

Chandrashekar, D.S., Karthikeyan, S.K., Korla, P.K., Patel, H., Shovon, A.R., Athar, M., Netto, G.J., Qin, Z.S., Kumar, S., Manne, U., Creighton, C.J., Varambally, S., 2022. UALCAN: An update to the integrated cancer data analysis platform. Neoplasia 25, 18–27. https://doi.org/10.1016/j.neo.2022.01.001

TH-3487_186106116

Chang-Qing, Y., Jie, L., Shi-Qi, Z., Kun, Z., Zi-Qian, G., Ran, X., Hui-Meng, L., Ren-Bin, Z., Gang, Z., Da-Chuan, Y., Chen-Yan, Z., 2020. Recent treatment progress of triple negative breast cancer. Prog Biophys Mol Biol 151, 40–53. https://doi.org/10.1016/j.pbiomolbio.2019.11.007

Chao, C.-H., Chang, C.-C., Wu, M.-J., Ko, H.-W., Wang, D., Hung, M.-C., Yang, J.-Y., Chang, C.-J., 2014. MicroRNA-205 signaling regulates mammary stem cell fate and tumorigenesis. Journal of Clinical Investigation 124, 3093–3106. https://doi.org/10.1172/JCI73351

Chen, B.-F., Tsai, M.-C., Jow, G.-M., 2006. Induction of calcium influx from extracellular fluid by beauvericin in human leukemia cells. Biochem Biophys Res Commun 340, 134–139. https://doi.org/10.1016/j.bbrc.2005.11.166

Chen, Y.-R., Wang, S.-C., Huang, S.-P., Su, C.-C., Liu, P.-L., Cheng, W.-C., Chuu, C.-P., Chen, J.-K., Bao, B.-Y., Lee, C.H., Ke, C.-C., Wu, H.-E., Chang, H.-H., Yeh, H.-C., Li, C.-Y., 2022. Protodioscin inhibits bladder cancer cell migration and growth, and promotes apoptosis through activating JNK and p38 signaling pathways. Biomedicine & Pharmacotherapy 156, 113929. https://doi.org/10.1016/j.biopha.2022.113929

Choy, L., Hagenbeek, T.J., Solon, M., French, D., Finkle, D., Shelton, A., Venook, R., Brauer, M.J., Siebel, C.W., 2017. Constitutive NOTCH3 Signaling Promotes the Growth of Basal Breast Cancers. Cancer Res 77, 1439–1452. https://doi.org/10.1158/0008-5472.CAN-16-1022

Cimmino, A., Mathieu, V., Masi, M., Baroncelli, R., Boari, A., Pescitelli, G., Ferderin, M., Lisy, R., Evidente, M., Tuzi, A., Zonno, M.C., Kornienko, A., Kiss, R., Evidente, A., 2016. Higginsianins A and B, Two Diterpenoid α-Pyrones Produced by *Colletotrichum higginsianum* , with *in Vitro* Cytostatic Activity. J Nat Prod 79, 116–125. https://doi.org/10.1021/acs.jnatprod.5b00779

Cipora, E., Konieczny, M., Karwat, I., Roczniak, W., Babuśka-Roczniak, M., 2018. Surgical method of treatment and level of satisfaction with life among women diagnosed with breast cancer, according to time elapsed since performance of surgery. Annals of

TH-3487_186106116

Agricultural and Environmental Medicine 25, 453–459. https://doi.org/10.26444/aaem/91586

Cleator, S., Heller, W., Coombes, R.C., 2007. Triple-negative breast cancer: therapeutic options. Lancet Oncol 8, 235–244. https://doi.org/10.1016/S1470-2045(07)70074-8

Cohen, B., Shimizu, M., Izrailit, J., Ng, N.F.L., Buchman, Y., Pan, J.G., Dering, J., Reedijk, M., 2010. Cyclin D1 is a direct target of JAG1-mediated Notch signaling in breast cancer. Breast Cancer Res Treat 123, 113–124. https://doi.org/10.1007/s10549-009-0621-9

Cole, S.P.C., 2014. Multidrug resistance protein 1 (mrp1, abcc1), a "multitasking" atp-binding cassette (abc,) transporter. Journal of Biological Chemistry. https://doi.org/10.1074/jbc.R114.609248

Coles, C.E., Griffin, C.L., Kirby, A.M., Titley, J., Agrawal, R.K., Alhasso, A., Bhattacharya, I.S., Brunt, A.M., Ciurlionis, L., Chan, C., Donovan, E.M., Emson, M.A., Harnett, A.N., Haviland, J.S., Hopwood, P., Jefford, M.L., Kaggwa, R., Sawyer, E.J., Syndikus, I., Tsang, Y.M., Wheatley, D.A., Wilcox, M., Yarnold, J.R., Bliss, J.M., Al Sarakbi, W., Barber, S., Barnett, G., Bliss, P., Dewar, J., Eaton, D., Ebbs, S., Ellis, I., Evans, P., Harris, E., James, H., Kirwan, C., Kirk, J., Mayles, H., McIntyre, A., Mills, J., Poynter, A., Provenzano, E., Rawlings, C., Sculpher, M., Sumo, G., Sydenham, M., Tutt, A., Twyman, N., Venables, K., Winship, A., Winstanley, J., Wishart, G., Thompson, A., 2017. Partial-breast radiotherapy after breast conservation surgery for patients with early breast cancer (UK IMPORT LOW trial): 5-year results from a multicentre, randomised, controlled, phase 3, non-inferiority trial. The Lancet 390, 1048–1060. https://doi.org/10.1016/S0140-6736(17)31145-5

Conklin, K.A., 2004. Chemotherapy-Associated Oxidative Stress: Impact on Chemotherapeutic Effectiveness. Integr Cancer Ther 3, 294–300. https://doi.org/10.1177/1534735404270335

COOPER, H.L., BRAVERMAN, R., 1977. The mechanism by which actinomycin D inhibits protein synthesis in animal cells. Nature 269, 527–529. https://doi.org/10.1038/269527a0

TH-3487_186106116

Crowley, L.C., Marfell, B.J., Scott, A.P., Waterhouse, N.J., 2016. Quantitation of Apoptosis and Necrosis by Annexin V Binding , Propidium Iodide Uptake , and Flow Cytometry 953–958. https://doi.org/10.1101/pdb.prot087288

Damia, G., Broggini, M., 2004. Cell Cycle Checkpoint Proteins and Cellular Response to Treatment by Anticancer Agents. Cell Cycle 3, 45–49. https://doi.org/10.4161/cc.3.1.631

Deng, C.-M., Liu, S.-X., Huang, C.-H., Pang, J.-Y., Lin, Y.-C., 2013. Secondary Metabolites of a Mangrove Endophytic Fungus Aspergillus terreus (No. GX7-3B) from the South China Sea. Mar Drugs 11, 2616–2624. https://doi.org/10.3390/md11072616

Dent, R., Trudeau, M., Pritchard, K.I., Hanna, W.M., Kahn, H.K., Sawka, C.A., Lickley, L.A., Rawlinson, E., Sun, P., Narod, S.A., 2007. Triple-Negative Breast Cancer: Clinical Features and Patterns of Recurrence. Clinical Cancer Research 13, 4429–4434. https://doi.org/10.1158/1078-0432.CCR-06-3045

Dey, P., Kundu, A., Kumar, A., Gupta, M., Lee, B.M., Bhakta, T., Dash, S., Kim, H.S., 2020. Analysis of alkaloids (indole alkaloids, isoquinoline alkaloids, tropane alkaloids), in: Recent Advances in Natural Products Analysis. Elsevier, pp. 505–567. https://doi.org/10.1016/B978-0-12-816455-6.00015-9

di Guana, C., Lib, P., Riggsa, P.D., Inouyeb, H., 1988. Vectors that facilitate the expression and purification of foreign peptides in Escherichia coli by fusion to maltose-binding protein. Gene 67, 21–30. https://doi.org/10.1016/0378-1119(88)90004-2

Diana, A., Carlino, F., Franzese, E., Oikonomidou, O., Criscitiello, C., De Vita, F., Ciardiello, F., Orditura, M., 2020. Early Triple Negative Breast Cancer: Conventional Treatment and Emerging Therapeutic Landscapes. Cancers (Basel) 12, 819. https://doi.org/10.3390/cancers12040819

Ding, L., Cao, J., Lin, W., Chen, H., Xiong, X., Ao, H., Yu, M., Lin, J., Cui, Q., 2020. The Roles of Cyclin-Dependent Kinases in Cell-Cycle Progression and Therapeutic Strategies in Human Breast Cancer. Int J Mol Sci 21, 1960. https://doi.org/10.3390/ijms21061960

TH-3487_186106116

Dornetshuber, R., Heffeter, P., Sulyok, M., Schumacher, R., Chiba, P., Kopp, S., Koellensperger, G., Micksche, M., Lemmens-Gruber, R., Berger, W., 2009. Interactions between ABC-transport proteins and the secondary *Fusarium* metabolites enniatin and beauvericin. Mol Nutr Food Res 53, 904–920. https://doi.org/10.1002/mnfr.200800384

Dornetshuber-Fleiss, R., Heffeter, P., Mohr, T., Hazemi, P., Kryeziu, K., Seger, C., Berger, W., Lemmens-Gruber, R., 2013. Destruxins: Fungal-derived cyclohexadepsipeptides with multifaceted anticancer and antiangiogenic activities. Biochem Pharmacol 86, 361–377. https://doi.org/10.1016/j.bcp.2013.05.022

Dorr, R.T., 1992. Bleomycin pharmacology: mechanism of action and resistance, and clinical pharmacokinetics. Semin Oncol 19, 3–8.

Du, L., Yau, C., Brown-Swigart, L., Gould, R., Krings, G., Hirst, G.L., Bedrosian, I., Layman, R.M., Carter, J.M., Klein, M., Venters, S., Shad, S., van der Noordaa, M., Chien, A.J., Haddad, T., Isaacs, C., Pusztai, L., Albain, K., Nanda, R., Tripathy, D., Liu, M.C., Boughey, J., Schwab, R., Hylton, N., DeMichele, A., Perlmutter, J., Yee, D., Berry, D., van't Veer, L., Valero, V., Esserman, L.J., Symmans, W.F., 2021. Predicted sensitivity to endocrine therapy for stage II-III hormone receptor-positive and HER2-negative (HR+/HER2−) breast cancer before chemo-endocrine therapy. Annals of Oncology 32, 642–651. https://doi.org/10.1016/j.annonc.2021.02.011

Dumas, C., Robert, P., Pais, M., Vey, A., Quiot, J.-M., 1994. Insecticidal and cytotoxic effects of natural and hemisynthetic destruxins. Comp Biochem Physiol C Pharmacol Toxicol Endocrinol 108, 195–203. https://doi.org/10.1016/1367-8280(94)90031-0

Dzoyem, J.P., Melong, R., Tsamo, A.T., Maffo, T., Kapche, D.G.W.F., Ngadjui, B.T., McGaw, L.J., Eloff, J.N., 2017. Cytotoxicity, antioxidant and antibacterial activity of four compounds produced by an endophytic fungus Epicoccum nigrum associated with entada abyssinica. Revista Brasileira de Farmacognosia 27, 251–253. https://doi.org/10.1016/j.bjp.2016.08.011

Early Breast Cancer Trialists' Collaborative Group (EBCTCG), 2011. Relevance of breast cancer hormone receptors and other factors to the efficacy of adjuvant tamoxifen:

TH-3487_186106116

patient-level meta-analysis of randomised trials. The Lancet 378, 771–784. https://doi.org/10.1016/S0140-6736(11)60993-8

EBCTCG (Early Breast Cancer Trialists' Collaborative Group), 2014. Effect of radiotherapy after mastectomy and axillary surgery on 10-year recurrence and 20-year breast cancer mortality: meta-analysis of individual patient data for 8135 women in 22 randomised trials. The Lancet 383, 2127–2135. https://doi.org/10.1016/S0140-6736(14)60488-8

Eberhardt, J., Santos-Martins, D., Tillack, A.F., Forli, S., 2021. AutoDock Vina 1.2.0: New Docking Methods, Expanded Force Field, and Python Bindings. J Chem Inf Model 61, 3891–3898. https://doi.org/10.1021/acs.jcim.1c00203

Edwards, A., Brennan, K., 2021. Notch Signalling in Breast Development and Cancer. Front Cell Dev Biol 9. https://doi.org/10.3389/fcell.2021.692173

Elsebai, M., Ghabbour, H., Mehiri, M., 2016. Unusual Nitrogenous Phenalenone Derivatives from the Marine-Derived Fungus Coniothyrium cereale. Molecules 21, 178. https://doi.org/10.3390/molecules21020178

Endo, Y., Wool, I.G., 1982. The site of action of alpha-sarcin on eukaryotic ribosomes. The sequence at the alpha-sarcin cleavage site in 28 S ribosomal ribonucleic acid. Journal of Biological Chemistry 257, 9054–9060. https://doi.org/10.1016/S0021-9258(18)34241-8

Eruslanov, E., Kusmartsev, S., 2010. Identification of ROS Using Oxidized DCFDA and Flow-Cytometry. pp. 57–72. https://doi.org/10.1007/978-1-60761-411-1_4

Fedele, M., Cerchia, L., Chiappetta, G., 2017. The Epithelial-to-Mesenchymal Transition in Breast Cancer: Focus on Basal-Like Carcinomas. Cancers (Basel) 9, 134. https://doi.org/10.3390/cancers9100134

Feeley, L.P., Mulligan, A.M., Pinnaduwage, D., Bull, S.B., Andrulis, I.L., 2014. Distinguishing luminal breast cancer subtypes by Ki67, progesterone receptor or TP53 status provides prognostic information. Modern Pathology 27, 554–561. https://doi.org/10.1038/modpathol.2013.153

TH-3487_186106116

Ficheux, A.S., Sibiril, Y., Parent-Massin, D., 2012. Co-exposure of Fusarium mycotoxins: In vitro myelotoxicity assessment on human hematopoietic progenitors. Toxicon 60, 1171–1179. https://doi.org/10.1016/j.toxicon.2012.08.001

Figueroa-Magalhães, M.C., Jelovac, D., Connolly, R.M., Wolff, A.C., 2014. Treatment of HER2-positive breast cancer. The Breast 23, 128–136. https://doi.org/10.1016/j.breast.2013.11.011

Flanagan, M.D., Lin, S., 1980. Cytochalasins block actin filament elongation by binding to high affinity sites associated with F-actin. Journal of Biological Chemistry 255, 835–838. https://doi.org/10.1016/S0021-9258(19)86105-7

Franken, N.A.P., Rodermond, H.M., Stap, J., Haveman, J., Bree, C. Van, 2006. Clonogenic assay of cells in vitro 1, 2315–2319. https://doi.org/10.1038/nprot.2006.339

Frederick GROVE, J., Pople, M., 1980. THE INSECTICIDAL ACTIVITY OF BEAUVERIC1N AND THE ENNIATIN COMPLEX, Mycopathologia.

Gallo, K., Goede, A., Preissner, R., Gohlke, B.-O., 2022. SuperPred 3.0: drug classification and target prediction—a machine learning approach. Nucleic Acids Res 50, W726–W731. https://doi.org/10.1093/nar/gkac297

Găman, A.M., Egbuna, C., Găman, M.-A., 2020. Natural bioactive lead compounds effective against haematological malignancies, in: Phytochemicals as Lead Compounds for New Drug Discovery. Elsevier, pp. 95–115. https://doi.org/10.1016/B978-0-12-817890-4.00006-8

García-Ortega, L., Álvarez-García, E., Gavilanes, J.G., Martínez-del-Pozo, Á., Joseph, S., 2010. Cleavage of the sarcin-ricin loop of 23S rRNA differentially affects EF-G and EF-Tu binding. Nucleic Acids Res 38, 4108–4119. https://doi.org/10.1093/nar/gkq151

Gasteiger, E., Hoogland, C., Gattiker, A., Duvaud, S., Wilkins, M.R., Appel, R.D., Bairoch, A., 2005. The Proteomics Protocols Handbook. The Proteomics Protocols Handbook 571–608. https://doi.org/10.1385/1592598900

Geng, Q.-R., Xu, D.-Z., He, L.-J., Lu, J.-B., Zhou, Z.-W., Zhan, Y.-Q., Lu, Y., 2012. Beclin-1 Expression Is a Significant Predictor of Survival in Patients with Lymph Node-

TH-3487_186106116

Positive Gastric Cancer. PLoS One 7, e45968. https://doi.org/10.1371/journal.pone.0045968

George, B., Kantarjian, H., Jabbour, E., Jain, N., 2016. Role of Inotuzumab Ozogamicin in the Treatment of Relapsed/Refractory Acute Lymphoblastic Leukemia. Immunotherapy 8, 135–143. https://doi.org/10.2217/imt.15.108

Gfeller, D., Grosdidier, A., Wirth, M., Daina, A., Michielin, O., Zoete, V., 2014. SwissTargetPrediction: a web server for target prediction of bioactive small molecules. Nucleic Acids Res 42, W32–W38. https://doi.org/10.1093/nar/gku293

Ghosh, S., Das, S.K., Sinha, K., Ghosh, B., Sen, K., Ghosh, N., Sil, P.C., 2024. The Emerging Role of Natural Products in Cancer Treatment. Arch Toxicol 98, 2353–2391. https://doi.org/10.1007/s00204-024-03786-3

Gianni, L., Pienkowski, T., Im, Y.-H., Roman, L., Tseng, L.-M., Liu, M.-C., Lluch, A., Staroslawska, E., de la Haba-Rodriguez, J., Im, S.-A., Pedrini, J.L., Poirier, B., Morandi, P., Semiglazov, V., Srimuninnimit, V., Bianchi, G., Szado, T., Ratnayake, J., Ross, G., Valagussa, P., 2012. Efficacy and safety of neoadjuvant pertuzumab and trastuzumab in women with locally advanced, inflammatory, or early HER2-positive breast cancer (NeoSphere): a randomised multicentre, open-label, phase 2 trial. Lancet Oncol 13, 25–32. https://doi.org/10.1016/S1470-2045(11)70336-9

Gilson, M.K., Liu, T., Baitaluk, M., Nicola, G., Hwang, L., Chong, J., 2016. BindingDB in 2015: A public database for medicinal chemistry, computational chemistry and systems pharmacology. Nucleic Acids Res 44, D1045–D1053. https://doi.org/10.1093/nar/gkv1072

Giuli, M. V., Giuliani, E., Screpanti, I., Bellavia, D., Checquolo, S., 2019. Notch Signaling Activation as a Hallmark for Triple-Negative Breast Cancer Subtype. J Oncol 2019, 1–15. https://doi.org/10.1155/2019/8707053

Goddette, D.W., Frieden, C., 1986. Actin polymerization. The mechanism of action of cytochalasin D. Journal of Biological Chemistry 261, 15974–15980. https://doi.org/10.1016/S0021-9258(18)66662-1

TH-3487_186106116

Goyal, A., Batra, J.K., 2000. Inclusion of a furin-sensitive spacer enhances the cytotoxicity of ribotoxin restrictocin containing recombinant single-chain immunotoxins. Biochemical Journal 345, 247–254. https://doi.org/10.1042/0264-6021:3450247

Gozlan, O., Sprinzak, D., 2023. Notch signaling in development and homeostasis. Development 150. https://doi.org/10.1242/dev.201138

Greenburg, G., Hay, E.D., 1982. Epithelia suspended in collagen gels can lose polarity and express characteristics of migrating mesenchymal cells. J Cell Biol 95, 333–339. https://doi.org/10.1083/jcb.95.1.333

Griffiths, C.L., Olin, J.L., 2012. Triple Negative Breast Cancer: A Brief Review of its Characteristics and Treatment Options. J Pharm Pract 25, 319–323. https://doi.org/10.1177/0897190012442062

Gugnoni, M., Sancisi, V., Gandolfi, G., Manzotti, G., Ragazzi, M., Giordano, D., Tamagnini, I., Tigano, M., Frasoldati, A., Piana, S., Ciarrocchi, A., 2017. Cadherin-6 promotes EMT and cancer metastasis by restraining autophagy. Oncogene 36, 667–677. https://doi.org/10.1038/onc.2016.237

Guo, C., Sun, L., Chen, X., Zhang, D., 2013. Oxidative stress, mitochondrial damage and neurodegenerative diseases. Neural Regen Res 8, 2003–14. https://doi.org/10.3969/j.issn.1673-5374.2013.21.009

Guo, L., Kong, D., Liu, J., Zhan, L., Luo, L., Zheng, W., Zheng, Q., Chen, C., Sun, S., 2023. Breast cancer heterogeneity and its implication in personalized precision therapy. Exp Hematol Oncol 12, 3. https://doi.org/10.1186/s40164-022-00363-1

Habib, I., Chohan, Tahir Ali, Chohan, Talha Ali, Batool, F., Khurshid, U., Khursheed, A., Raza, A., Ansari, M., Hussain, A., Anwar, S., Awadh Ali, N.A., Saleem, H., 2024. Integrated computational approaches for designing potent pyrimidine-based CDK9 inhibitors: 3D-QSAR, docking, and molecular dynamics simulations. Comput Biol Chem 108, 108003. https://doi.org/10.1016/j.compbiolchem.2023.108003

Hall, T., Biosciences, I., Carlsbad, C., 2011. BioEdit: An important software for molecular biology. GERF Bulletin of Biosciences 2, 60–61.

TH-3487_186106116

Halliwell, B., Gutteridge, J.M.C., 2015. Free Radicals in Biology and Medicine. Oxford University Press. https://doi.org/10.1093/acprof:oso/9780198717478.001.0001

Hamill, R.L., Higgens, C.E., Boaz, H.E., Gorman, M., 1969. The structure op beauvericin, a new depsipeptide antibiotic toxic to. Tetrahedron Lett 10, 4255–4258. https://doi.org/10.1016/S0040-4039(01)88668-8

Hamza, S., Abid, A., Khanum, A., Chohan, Talha Ali, Saleem, H., Maqbool Khan, K., Khurshid, U., Butt, J., Anwar, S., Alafnan, A., Ansari, S.A., Qayyum, A., Raza, A., Chohan, Tahir Ali, 2024. 3D-QSAR, docking and molecular dynamics simulations of novel Pyrazolo-pyridazinone derivatives as covalent inhibitors of FGFR1: a scientific approach for possible anticancer agents. J Biomol Struct Dyn 42, 2242–2256. https://doi.org/10.1080/07391102.2023.2212306

HANADA, M., SUGAWARA, K., KANETA, K., TODA, S., NISHIYAMA, Y., TOMITA, K., YAMAMOTO, H., KONISHI, M., OKI, T., 1992. Epoxomicin, a new antitumor agent of microbial origin. J Antibiot (Tokyo) 45, 1746–1752. https://doi.org/10.7164/antibiotics.45.1746

Hasan, S., Ahmad, A., Purwar, A., Khan, N., Kundan, R., Gupta, G., 2013. Production of extracellular enzymes in the entomopathogenic fungus Verticillium lecanii. Bioinformation 9, 238–242. https://doi.org/10.6026/97320630009238

Hausner, T.-P., Atmadja, J., Nierhaus, K.H., 1987. Evidence that the G2661 region of 23S rRNA is located at the ribosomal binding sites of both elongation factors. Biochimie 69, 911–923. https://doi.org/10.1016/0300-9084(87)90225-2

Haviland, J.S., Owen, J.R., Dewar, J.A., Agrawal, R.K., Barrett, J., Barrett-Lee, P.J., Dobbs, H.J., Hopwood, P., Lawton, P.A., Magee, B.J., Mills, J., Simmons, S., Sydenham, M.A., Venables, K., Bliss, J.M., Yarnold, J.R., 2013. The UK Standardisation of Breast Radiotherapy (START) trials of radiotherapy hypofractionation for treatment of early breast cancer: 10-year follow-up results of two randomised controlled trials. Lancet Oncol 14, 1086–1094. https://doi.org/10.1016/S1470-2045(13)70386-3

Hay, E.D., 1995. An Overview of Epithelio-Mesenchymal Transformation. Cells Tissues Organs 154, 8–20. https://doi.org/10.1159/000147748

TH-3487_186106116

Heo, L., Park, H., Seok, C., 2013. GalaxyRefine: Protein structure refinement driven by side-chain repacking. Nucleic Acids Res 41, 384–388. https://doi.org/10.1093/nar/gkt458

Hill, L., Browne, G., Tulchinsky, E., 2013. ZEB/miR-200 feedback loop: At the crossroads of signal transduction in cancer. Int J Cancer 132, 745–754. https://doi.org/10.1002/ijc.27708

Hollstein, U., 1974. Actinomycin. Chemistry and mechanism of action. Chem Rev 74, 625–652. https://doi.org/10.1021/cr60292a002

Horak, I., Engelbrecht, G., Rensburg, P.J.J., Claassens, S., 2019. Microbial metabolomics: essential definitions and the importance of cultivation conditions for utilizing *Bacillus* species as bionematicides. J Appl Microbiol 127, 326–343. https://doi.org/10.1111/jam.14218

Huang, C.H., Chen, Y.T., Lin, J.H., Wang, H.T., 2018. Acrolein induces ribotoxic stress in human cancer cells regardless of p53 status. Toxicology in Vitro 52, 265–271. https://doi.org/10.1016/j.tiv.2018.06.022

Hwang, S.-Y., Park, S., Kwon, Y., 2019. Recent therapeutic trends and promising targets in triple negative breast cancer. Pharmacol Ther 199, 30–57. https://doi.org/10.1016/j.pharmthera.2019.02.006

Iordanov, M.S., Pribnow, D., Magun, J.L., Dinh, T.H., Pearson, J.A., Chen, S.L., Magun, B.E., 1997. Ribotoxic stress response: activation of the stress-activated protein kinase JNK1 by inhibitors of the peptidyl transferase reaction and by sequence-specific RNA damage to the alpha-sarcin/ricin loop in the 28S rRNA. Mol Cell Biol 17, 3373–3381. https://doi.org/10.1128/mcb.17.6.3373

Ivascu, A., Kubbies, M., 2006. Rapid Generation of Single-Tumor Spheroids for High-Throughput Cell Function and Toxicity Analysis. SLAS Discovery 11, 922–932. https://doi.org/10.1177/1087057106292763

Jang, M.H., Kim, H.J., Kim, E.J., Chung, Y.R., Park, S.Y., 2015. Expression of epithelial-mesenchymal transition–related markers in triple-negative breast cancer: ZEB1 as a

TH-3487_186106116

potential biomarker for poor clinical outcome. Hum Pathol 46, 1267–1274. https://doi.org/10.1016/j.humpath.2015.05.010

Jayaweera, S.P.E., Wanigasinghe Kanakanamge, S.P., Rajalingam, D., Silva, G.N., 2021. Carfilzomib: A Promising Proteasome Inhibitor for the Treatment of Relapsed and Refractory Multiple Myeloma. Front Oncol 11. https://doi.org/10.3389/fonc.2021.740796

Jetzt, A.E., Cheng, J.S., Tumer, N.E., Cohick, W.S., 2009. Ricin A-chain requires c-Jun N-terminal kinase to induce apoptosis in nontransformed epithelial cells. International Journal of Biochemistry and Cell Biology 41, 2503–2510. https://doi.org/10.1016/j.biocel.2009.08.007

Jin, C.Y., Park, C., Hong, S.H., Han, M.H., Jeong, J.W., Xu, H. De, Liu, H.M., Kim, G.Y., Kim, W.J., Yoo, Y.H., Choi, Y.H., 2013. Synergistic induction of TRAIL-mediated apoptosis by anisomycin in human hepatoma cells via the BH3-only protein Bid and c-Jun/AP-1 signaling pathway. Biomedicine and Pharmacotherapy 67, 321–328. https://doi.org/10.1016/j.biopha.2012.11.005

Jo, S., Kim, T., Im, W., 2007. Automated Builder and Database of Protein/Membrane Complexes for Molecular Dynamics Simulations. PLoS One 2, e880. https://doi.org/10.1371/journal.pone.0000880

Jo, S., Kim, T., Iyer, V.G., Im, W., 2008. CHARMM-GUI: A web-based graphical user interface for CHARMM. J Comput Chem 29, 1859–1865. https://doi.org/10.1002/jcc.20945

Johnston, J.B., 2011. Mechanism of Action of Pentostatin and Cladribine in Hairy Cell Leukemia. Leuk Lymphoma 52, 43–45. https://doi.org/10.3109/10428194.2011.570394

Jones, T.D., Hearn, A.R., Holgate, R.G.E., Kozub, D., Fogg, M.H., Carr, F.J., Baker, M.P., Lacadena, J., Gehlsen, K.R., 2016. A deimmunised form of the ribotoxin, α-sarcin, lacking CD4+ T cell epitopes and its use as an immunotoxin warhead. Protein Eng Des Sel 29, 531–540. https://doi.org/10.1093/protein/gzw045

TH-3487_186106116

Joshi, I., Minter, L.M., Telfer, J., Demarest, R.M., Capobianco, A.J., Aster, J.C., Sicinski, P., Fauq, A., Golde, T.E., Osborne, B.A., 2009. Notch signaling mediates G1/S cell-cycle progression in T cells via cyclin D3 and its dependent kinases. Blood 113, 1689–1698. https://doi.org/10.1182/blood-2008-03-147967

Jow, G.-M., Chou, C.-J., Chen, B.-F., Tsai, J.-H., 2004. Beauvericin induces cytotoxic effects in human acute lymphoblastic leukemia cells through cytochrome c release, caspase 3 activation: the causative role of calcium. Cancer Lett 216, 165–173. https://doi.org/10.1016/j.canlet.2004.06.005

Jumper, J., Evans, R., Pritzel, A., Green, T., Figurnov, M., Ronneberger, O., Tunyasuvunakool, K., Bates, R., Žídek, A., Potapenko, A., Bridgland, A., Meyer, C., Kohl, S.A.A., Ballard, A.J., Cowie, A., Romera-Paredes, B., Nikolov, S., Jain, R., Adler, J., Back, T., Petersen, S., Reiman, D., Clancy, E., Zielinski, M., Steinegger, M., Pacholska, M., Berghammer, T., Bodenstein, S., Silver, D., Vinyals, O., Senior, A.W., Kavukcuoglu, K., Kohli, P., Hassabis, D., 2021. Highly accurate protein structure prediction with AlphaFold. Nature 596, 583–589. https://doi.org/10.1038/s41586-021-03819-2

Kalluri, R., Weinberg, R.A., 2010. The basics of epithelial-mesenchymal transition. Journal of Clinical Investigation 120, 1786–1786. https://doi.org/10.1172/JCI39104C1

Kan, L.L.-Y., Chan, B.C.-L., Leung, P.-C., Wong, C.-K., 2023. Natural-Product-Derived Adjunctive Treatments to Conventional Therapy and Their Immunoregulatory Activities in Triple-Negative Breast Cancer. Molecules 28, 5804. https://doi.org/10.3390/molecules28155804

Kanokmedhakul, K., Kanokmedhakul, S., Suwannatrai, R., Soytong, K., Prabpai, S., Kongsaeree, P., 2011. Bioactive meroterpenoids and alkaloids from the fungus Eurotium chevalieri. Tetrahedron 67, 5461–5468. https://doi.org/10.1016/j.tet.2011.05.066

Keibel, A., Singh, V., Sharma, M., 2009. Inflammation, Microenvironment, and the Immune System in Cancer Progression. Curr Pharm Des 15, 1949–1955. https://doi.org/10.2174/138161209788453167

TH-3487_186106116

Kelley, L. a, Mezulis, S., Yates, C.M., Wass, M.N., Sternberg, M.J.E., 2015. Europe PMC Funders Group The Phyre2 web portal for protein modelling , prediction and analysis. Nat Protoc 10, 845–858. https://doi.org/10.1038/nprot.2015.053.The

Khaitan, D., Dwarakanath, B.S., 2006. Multicellular spheroids as an *in vitro* model in experimental oncology: applications in translational medicine. Expert Opin Drug Discov 1, 663–675. https://doi.org/10.1517/17460441.1.7.663

Khan, R.Z., Badros, A., 2012. Role of carfilzomib in the treatment of multiple myeloma. Expert Rev Hematol 5, 361–372. https://doi.org/10.1586/ehm.12.26

Kim, H.G., Sung, N.Y., Kim, J.H., Cho, J.Y., 2023. In vitro anti-cancer effects of beauvericin through inhibition of actin polymerization and Src phosphorylation. Phytomedicine 109, 154573. https://doi.org/10.1016/j.phymed.2022.154573

Kim, S.-H., Sehrawat, A., Singh, S. V., 2012. Notch2 activation by benzyl isothiocyanate impedes its inhibitory effect on breast cancer cell migration. Breast Cancer Res Treat 134, 1067–1079. https://doi.org/10.1007/s10549-012-2043-3

Koba, M., Konopa, J., 2005. [Actinomycin D and its mechanisms of action]. Postepy Hig Med Dosw (Online) 59, 290–8.

Koedoot, E., Fokkelman, M., Rogkoti, V.-M., Smid, M., van de Sandt, I., de Bont, H., Pont, C., Klip, J.E., Wink, S., Timmermans, M.A., Wiemer, E.A.C., Stoilov, P., Foekens, J.A., Le Dévédec, S.E., Martens, J.W.M., van de Water, B., 2019. Uncovering the signaling landscape controlling breast cancer cell migration identifies novel metastasis driver genes. Nat Commun 10, 2983. https://doi.org/10.1038/s41467-019-11020-3

Kollman, P.A., Massova, I., Reyes, C., Kuhn, B., Huo, S., Chong, L., Lee, M., Lee, T., Duan, Y., Wang, W., Donini, O., Cieplak, P., Srinivasan, J., Case, D.A., Cheatham, T.E., 2000. Calculating Structures and Free Energies of Complex Molecules: Combining Molecular Mechanics and Continuum Models. Acc Chem Res 33, 889–897. https://doi.org/10.1021/ar000033j

Kong, P., Chen, L., Yu, M., Tao, J., Liu, J., Wang, Y., Pan, H., Zhou, W., Wang, S., 2018. miR-3178 inhibits cell proliferation and metastasis by targeting Notch1 in triple-

TH-3487_186106116

negative breast cancer. Cell Death Dis 9, 1059. https://doi.org/10.1038/s41419-018-1091-y

Kontomanolis, E., Panteliadou, M., Giatromanolaki, A., Pouliliou, S., Efremidou, E., Limberis, V., Galazios, G., Sivridis, E., Koukourakis, M.I., 2014. Delta-like ligand 4 (DLL4) in the plasma and neoplastic tissues from breast cancer patients: correlation with metastasis. Medical Oncology 31, 945. https://doi.org/10.1007/s12032-014-0945-0

Kreitman, R.J., 2001. Toxin-labeled monoclonal antibodies. Curr Pharm Biotechnol 2, 313–25. https://doi.org/10.2174/1389201013378635

Kuleshov, M. V., Jones, M.R., Rouillard, A.D., Fernandez, N.F., Duan, Q., Wang, Z., Koplev, S., Jenkins, S.L., Jagodnik, K.M., Lachmann, A., McDermott, M.G., Monteiro, C.D., Gundersen, G.W., Ma'ayan, A., 2016. Enrichr: a comprehensive gene set enrichment analysis web server 2016 update. Nucleic Acids Res 44, W90–W97. https://doi.org/10.1093/nar/gkw377

Kumari, R., Kumar, R., Lynn, A., 2014. *g_mmpbsa* —A GROMACS Tool for High-Throughput MM-PBSA Calculations. J Chem Inf Model 54, 1951–1962. https://doi.org/10.1021/ci500020m

Kumari, S., Badana, A.K., G, M.M., G, S., Malla, R., 2018. Reactive Oxygen Species: A Key Constituent in Cancer Survival. Biomark Insights 13, 117727191875539. https://doi.org/10.1177/1177271918755391

Kyriakis, J.M., Avruch, J., 2001. Mammalian mitogen-activated protein kinase signal transduction pathways activated by stress and inflammation. Physiol Rev 81, 807–869. https://doi.org/10.1152/physrev.2001.81.2.807

Lacadena, J., Álvarez-García, E., Carreras-Sangrà, N., Herrero-Galán, E., Alegre-Cebollada, J., García-Ortega, L., Oñaderra, M., Gavilanes, J.G., Martínez del Pozo, Á., 2007. Fungal ribotoxins: molecular dissection of a family of natural killers. FEMS Microbiol Rev 31, 212–237. https://doi.org/10.1111/j.1574-6976.2006.00063.x

TH-3487_186106116

Lacadena, J., Martínez del Pozo, A., Lacadena, V., Martínez-Ruiz, A., Mancheño, J.M., Oñaderra, M., Gavilanes, J.G., 1998. The cytotoxin α-sarcin behaves as a cyclizing ribonuclease. FEBS Lett 424, 46–48. https://doi.org/10.1016/S0014-5793(98)00137-9

Lai, X., Li, G., Lin, B., Yang, H., 2017. Interference of Notch 1 inhibits the proliferation and invasion of breast cancer cells: Involvement of the β-catenin signaling pathway. Mol Med Rep. https://doi.org/10.3892/mmr.2017.8161

Lamanna, N., Kalaycio, M., Maslak, P., Jurcic, J.G., Heaney, M., Brentjens, R., Zelenetz, A.D., Horgan, D., Gencarelli, A., Panageas, K.S., Scheinberg, D.A., Weiss, M.A., 2006. Pentostatin, Cyclophosphamide, and Rituximab Is an Active, Well-Tolerated Regimen for Patients With Previously Treated Chronic Lymphocytic Leukemia. Journal of Clinical Oncology 24, 1575–1581. https://doi.org/10.1200/JCO.2005.04.3836

Laskowski, R.A., MacArthur, M.W., Moss, D.S., Thornton, J.M., 1993. PROCHECK: a program to check the stereochemical quality of protein structures. J Appl Crystallogr 26, 283–291. https://doi.org/10.1107/s0021889892009944

Lawson, D.A., Bhakta, N.R., Kessenbrock, K., Prummel, K.D., Yu, Y., Takai, K., Zhou, A., Eyob, H., Balakrishnan, S., Wang, C.-Y., Yaswen, P., Goga, A., Werb, Z., 2015. Single-cell analysis reveals a stem-cell program in human metastatic breast cancer cells. Nature 526, 131–135. https://doi.org/10.1038/nature15260

Lázaro-Gorines, R., Ruiz-de-la-Herrán, J., Navarro, R., Sanz, L., Álvarez-Vallina, L., Martínez-del-Pozo, A., Gavilanes, J.G., Lacadena, J., 2019. A novel Carcinoembryonic Antigen (CEA)-Targeted Trimeric Immunotoxin shows significantly enhanced Antitumor Activity in Human Colorectal Cancer Xenografts. Sci Rep 9, 1–13. https://doi.org/10.1038/s41598-019-48285-z

Lee, C.W., Simin, K., Liu, Q., Plescia, J., Guha, M., Khan, A., Hsieh, C.-C., Altieri, D.C., 2008. A functional Notch–survivin gene signature in basal breast cancer. Breast Cancer Research 10, R97. https://doi.org/10.1186/bcr2200

Lee, H.-S., Song, H.-H., Jeong, J.-H., Shin, C.-G., Choi, S.-U., Lee, C., 2008. Cytotoxicities of enniatins H, I, and MK1688 from Fusarium oxysporum KFCC 11363P. Toxicon 51, 1178–1185. https://doi.org/10.1016/j.toxicon.2008.02.002

TH-3487_186106116

Lee, J., Cheng, X., Swails, J.M., Yeom, M.S., Eastman, P.K., Lemkul, J.A., Wei, S., Buckner, J., Jeong, J.C., Qi, Y., Jo, S., Pande, V.S., Case, D.A., Brooks, C.L., MacKerell, A.D., Klauda, J.B., Im, W., 2016. CHARMM-GUI Input Generator for NAMD, GROMACS, AMBER, OpenMM, and CHARMM/OpenMM Simulations Using the CHARMM36 Additive Force Field. J Chem Theory Comput 12, 405–413. https://doi.org/10.1021/acs.jctc.5b00935

Lehmann, B.D., Bauer, J.A., Chen, X., Sanders, M.E., Chakravarthy, A.B., Shyr, Y., Pietenpol, J.A., 2011. Identification of human triple-negative breast cancer subtypes and preclinical models for selection of targeted therapies. Journal of Clinical Investigation 121, 2750–2767. https://doi.org/10.1172/JCI45014

Lemkul, J., 2019. From Proteins to Perturbed Hamiltonians: A Suite of Tutorials for the GROMACS-2018 Molecular Simulation Package [Article v1.0]. Living J Comput Mol Sci 1, 1–53. https://doi.org/10.33011/livecoms.1.1.5068

Leong, K.G., Niessen, K., Kulic, I., Raouf, A., Eaves, C., Pollet, I., Karsan, A., 2007. Jagged1-mediated Notch activation induces epithelial-to-mesenchymal transition through Slug-induced repression of E-cadherin. J Exp Med 204, 2935–2948. https://doi.org/10.1084/jem.20071082

Leontovich, A.A., Jalalirad, M., Salisbury, J.L., Mills, L., Haddox, C., Schroeder, M., Tuma, A., Guicciardi, M.E., Zammataro, L., Gambino, M.W., Amato, A., Di Leonardo, A., McCubrey, J., Lange, C.A., Liu, M., Haddad, T., Goetz, M., Boughey, J., Sarkaria, J., Wang, L., Ingle, J.N., Galanis, E., D'Assoro, A.B., 2018. NOTCH3 expression is linked to breast cancer seeding and distant metastasis. Breast Cancer Research 20, 105. https://doi.org/10.1186/s13058-018-1020-0

Li, X., Cao, Y., Li, M., Jin, F., 2018. Upregulation of HES1 Promotes Cell Proliferation and Invasion in Breast Cancer as a Prognosis Marker and Therapy Target via the AKT Pathway and EMT Process. J Cancer 9, 757–766. https://doi.org/10.7150/jca.22319

Li, X., He, S., Ma, B., 2020. Autophagy and autophagy-related proteins in cancer. Mol Cancer 19, 12. https://doi.org/10.1186/s12943-020-1138-4

TH-3487_186106116

Li, Y.-L., Yi, J.-L., Cai, J., Zhou, X.-M., Chen, L., Zhuo, X., Lai, X.-Y., 2022. Two new bioactive secondary metabolites from the endophytic fungus *Talaromyces assiutensis* JTY2. Nat Prod Res 36, 3695–3700. https://doi.org/10.1080/14786419.2021.1881961

LIN, H., LEE, Y., CHEN, B., TSAI, M., LU, J., CHOU, C., JOW, G., 2005. Involvement of Bcl-2 family, cytochrome and caspase 3 in induction of apoptosis by beauvericin in human non-small cell lung cancer cells. Cancer Lett 230, 248–259. https://doi.org/10.1016/j.canlet.2004.12.044

Litwin, A., Nowak, M., Różalska, S., 2020. Entomopathogenic fungi: unconventional applications. Rev Environ Sci Biotechnol 19, 23–42. https://doi.org/10.1007/s11157-020-09525-1

Liu, W.Z., Boucias, D.G., McCoy, C.W., 1995. Extraction and Characterization of the Insecticidal Toxin Hirsutellin A Produced by Hirsutella thompsonii var. thompsonii. Exp Mycol. https://doi.org/10.1006/emyc.1995.1032

Liu, X., Shi, D., Zhou, S., Liu, Hongli, Liu, Huanxiang, Yao, X., 2018. Molecular dynamics simulations and novel drug discovery. Expert Opin Drug Discov 13, 23–37. https://doi.org/10.1080/17460441.2018.1403419

Liu, Z., 2023. Antioxidant activity of the thioredoxin system. Biophys Rep 9, 22–28. https://doi.org/10.52601/bpr.2023.230002

Loeb, L.A., Loeb, K.R., Anderson, J.P., 2003. Multiple mutations and cancer. Proceedings of the National Academy of Sciences 100, 776–781. https://doi.org/10.1073/pnas.0334858100

Logrieco, A., Moretti, A., Castella, G., Kostecki, M., Golinski, P., Ritieni, A., Chelkowski, J., 1998. Beauvericin Production by *Fusarium* Species. Appl Environ Microbiol 64, 3084–3088. https://doi.org/10.1128/AEM.64.8.3084-3088.1998

Lu, B., Natarajan, E., Balaji Raghavendran, H.R., Markandan, U.D., 2023. Molecular Classification, Treatment, and Genetic Biomarkers in Triple-Negative Breast Cancer: A Review. Technol Cancer Res Treat 22, 153303382211452. https://doi.org/10.1177/15330338221145246

TH-3487_186106116

Lu, C.-L., Lin, H.-I., Chen, B.-F., Jow, G.-M., 2016. Beauvericin-induced cell apoptosis through the mitogen-activated protein kinase pathway in human nonsmall cell lung cancer A549 cells. J Toxicol Sci 41, 429–437. https://doi.org/10.2131/jts.41.429

Lu, S., Wang, J., Chitsaz, F., Derbyshire, M.K., Geer, R.C., Gonzales, N.R., Gwadz, M., Hurwitz, D.I., Marchler, G.H., Song, J.S., Thanki, N., Yamashita, R.A., Yang, M., Zhang, D., Zheng, C., Lanczycki, C.J., Marchler-Bauer, A., 2020. CDD/SPARCLE: The conserved domain database in 2020. Nucleic Acids Res 48, D265–D268. https://doi.org/10.1093/nar/gkz991

Lu, W., Kang, Y., 2019. Epithelial-Mesenchymal Plasticity in Cancer Progression and Metastasis. Dev Cell 49, 361–374. https://doi.org/10.1016/j.devcel.2019.04.010

Luangsa-ard, J.J., Berkaew, P., Ridkaew, R., Hywel-Jones, N.L., Isaka, M., 2009. A beauvericin hot spot in the genus Isaria. Mycol Res 113, 1389–1395. https://doi.org/10.1016/j.mycres.2009.08.017

Lv, Q., Wang, W., Xue, J., Hua, F., Mu, R., Lin, H., Yan, J., Lv, X., Chen, X., Hu, Z.-W., 2012. DEDD Interacts with PI3KC3 to Activate Autophagy and Attenuate Epithelial–Mesenchymal Transition in Human Breast Cancer. Cancer Res 72, 3238–3250. https://doi.org/10.1158/0008-5472.CAN-11-3832

M., V.R., T., M.S., C., K.A., V., R., 2010. The Mechanism for Activation of GTP Hydrolysis on the Ribosome 330, 835–839.

Maccallini, C., Ammazzalorso, A., De Filippis, B., Fantacuzzi, M., Giampietro, L., Amoroso, R., 2022. HDAC Inhibitors for the Therapy of Triple Negative Breast Cancer. Pharmaceuticals. https://doi.org/10.3390/ph15060667

MacLean-Fletcher, S., 1980. Mechanism of action of cytochalasin B on actin. Cell 20, 329–341. https://doi.org/10.1016/0092-8674(80)90619-4

Maina, C. V, Riggs, P.D., Iii, A.G.G., Slatko, B.E., Moran, L.S., John, A., Mereynolds, L.A., Guan, C., 1988. An Escherichia coli vector to express and purify foreign proteins by fusion to and separation from maltose-binding protein 74, 365–373.

TH-3487_186106116

Mallebrera, B., Font, G., Ruiz, M.J., 2014. Disturbance of antioxidant capacity produced by beauvericin in CHO-K1 cells. Toxicol Lett 226, 337–342. https://doi.org/10.1016/j.toxlet.2014.02.023

Mallebrera, B., Juan-Garcia, A., Font, G., Ruiz, M.-J., 2016. Mechanisms of beauvericin toxicity and antioxidant cellular defense. Toxicol Lett 246, 28–34. https://doi.org/10.1016/j.toxlet.2016.01.013

Mamoor, S., n.d. HES1 expression associates with survival in triple negative breast cancer.

Mano, M.S., Awada, A., 2004. Primary chemotherapy for breast cancer: the evidence and the future. Annals of Oncology 15, 1161–1171. https://doi.org/10.1093/annonc/mdh302

Marcucci, F., Stassi, G., De Maria, R., 2016. Epithelial–mesenchymal transition: a new target in anticancer drug discovery. Nat Rev Drug Discov 15, 311–325. https://doi.org/10.1038/nrd.2015.13

Martin, T.A., Goyal, A., Watkins, G., Jiang, W.G., 2005. Expression of the Transcription Factors Snail, Slug, and Twist and Their Clinical Significance in Human Breast Cancer. Ann Surg Oncol 12, 488–496. https://doi.org/10.1245/ASO.2005.04.010

Masi, M., Andolfi, A., Mathieu, V., Boari, A., Cimmino, A., Moreno Y Banuls, L., Vurro, M., Kornienko, A., Kiss, R., Evidente, A., 2013. Fischerindoline, a pyrroloindole sesquiterpenoid isolated from Neosartorya pseudofischeri, with in vitro growth inhibitory activity in human cancer cell lines. Tetrahedron 69, 7466–7470. https://doi.org/10.1016/j.tet.2013.06.031

Mathieu, V., Superchi, S., Masi, M., Scafato, P., Kornienko, A., Evidente, A., 2022. In Vitro Effects of Fungal Phytotoxins on Cancer Cell Viability: First Insight into Structure Activity Relationship of a Potent Metabolite of Cochliobolus australiensis Radicinin. Toxins (Basel) 14, 517. https://doi.org/10.3390/toxins14080517

Matsuyama, S., Reed, J.C., 2000. Mitochondria-dependent apoptosis and cellular pH regulation. Cell Death Differ 7, 1155–1165. https://doi.org/10.1038/sj.cdd.4400779

Mayrovitz, H.N. (Ed.), 2022. Breast Cancer. Exon Publications. https://doi.org/10.36255/exon-publications-breast-cancer

TH-3487_186106116

Meca, G., Sospedra, I., Soriano, J.M., Ritieni, A., Moretti, A., Mañes, J., 2010. Antibacterial effect of the bioactive compound beauvericin produced by Fusarium proliferatum on solid medium of wheat. Toxicon 56, 349–354. https://doi.org/10.1016/j.toxicon.2010.03.022

Medina, M.A., Oza, G., Sharma, A., Arriaga, L.G., Hernández Hernández, J.M., Rotello, V.M., Ramirez, J.T., 2020. Triple-Negative Breast Cancer: A Review of Conventional and Advanced Therapeutic Strategies. Int J Environ Res Public Health 17, 2078. https://doi.org/10.3390/ijerph17062078

Mehta, G., Hsiao, A.Y., Ingram, M., Luker, G.D., Takayama, S., 2012. Opportunities and challenges for use of tumor spheroids as models to test drug delivery and efficacy. Journal of Controlled Release 164, 192–204. https://doi.org/10.1016/j.jconrel.2012.04.045

Micsonai, A., Wien, F., Bulyáki, É., Kun, J., Moussong, É., Lee, Y.H., Goto, Y., Réfrégiers, M., Kardos, J., 2018. BeStSel: A web server for accurate protein secondary structure prediction and fold recognition from the circular dichroism spectra. Nucleic Acids Res 46, W315–W322. https://doi.org/10.1093/nar/gky497

Miele, L., Golde, T., Osborne, B., 2006. Notch Signaling in Cancer. Curr Mol Med 6, 905–918. https://doi.org/10.2174/156652406779010830

Miller, S.P., Bodley, J.W., 1988. The ribosomes of Aspergillus giganteus are sensitive to the cytotoxic action of α-sarcin. FEBS Lett 229, 388–390. https://doi.org/10.1016/0014-5793(88)81162-1

Mittal, V., 2018. Epithelial Mesenchymal Transition in Tumor Metastasis. Annual Review of Pathology: Mechanisms of Disease 13, 395–412. https://doi.org/10.1146/annurev-pathol-020117-043854

Mizushima, N., 2007. Autophagy: process and function. Genes Dev 21, 2861–2873. https://doi.org/10.1101/gad.1599207

TH-3487_186106116

Mizushima, N., Levine, B., Cuervo, A.M., Klionsky, D.J., 2008. Autophagy fights disease through cellular self-digestion. Nature 451, 1069–1075. https://doi.org/10.1038/nature06639

Mo, J.-S., Yoon, J.-H., Ann, E.-J., Ahn, J.-S., Baek, H.-J., Lee, H.-J., Kim, S.-H., Kim, Y.-D., Kim, M.-Y., Park, H.-S., 2013. Notch1 modulates oxidative stress induced cell death through suppression of apoptosis signal-regulating kinase 1. Proceedings of the National Academy of Sciences 110, 6865–6870. https://doi.org/10.1073/pnas.1209078110

Mohamed, M.S., Veeranarayanan, S., Poulose, A.C., Nagaoka, Y., Minegishi, H., Yoshida, Y., Maekawa, T., Kumar, D.S., 2014. Biochimica et Biophysica Acta Type 1 ribotoxin-curcin conjugated biogenic gold nanoparticles for a multimodal therapeutic approach towards brain cancer. BBA - General Subjects 1840, 1657–1669. https://doi.org/10.1016/j.bbagen.2013.12.020

Mohan, C.D., Rangappa, S., Nayak, S.C., Jadimurthy, R., Wang, L., Sethi, G., Garg, M., Rangappa, K.S., 2022. Bacteria as a treasure house of secondary metabolites with anticancer potential. Semin Cancer Biol 86, 998–1013. https://doi.org/10.1016/j.semcancer.2021.05.006

Moo, T.-A., Sanford, R., Dang, C., Morrow, M., 2018. Overview of Breast Cancer Therapy. PET Clin 13, 339–354. https://doi.org/10.1016/j.cpet.2018.02.006

Muellner, M.K., Mair, B., Ibrahim, Y., Kerzendorfer, C., Lechtermann, H., Trefzer, C., Klepsch, F., Müller, A.C., Leitner, E., Macho-Maschler, S., Superti-Furga, G., Bennett, K.L., Baselga, J., Rix, U., Kubicek, S., Colinge, J., Serra, V., Nijman, S.M., 2015. Targeting a cell state common to triple-negative breast cancers. Mol Syst Biol 11. https://doi.org/10.15252/msb.20145664

Mukhtar, M., Saleem, M., Nazir, M., Riaz, N., Shafiq, N., Saleem, H., Tauseef, S., Khan, S., Ehsan Mazhar, M., Bakhsh Tareen, R., Mahmood, M.H. ur R., Tousif, M.I., Ojha, S.C., 2023. Identification of pyrrolizidine alkaloids and flavonoid glycosides through HR-LCMS/MS analysis, biological screening, DFT and molecular docking studies on Heliotropium dasycarpum Ledeb. Arabian Journal of Chemistry 16, 104655. https://doi.org/10.1016/j.arabjc.2023.104655

TH-3487_186106116

Nanda, R., Chow, L.Q.M., Dees, E.C., Berger, R., Gupta, S., Geva, R., Pusztai, L., Pathiraja, K., Aktan, G., Cheng, J.D., Karantza, V., Buisseret, L., 2016. Pembrolizumab in Patients With Advanced Triple-Negative Breast Cancer: Phase Ib KEYNOTE-012 Study. Journal of Clinical Oncology 34, 2460–2467. https://doi.org/10.1200/JCO.2015.64.8931

Naqvi, A.A.T., Mohammad, T., Hasan, G.M., Hassan, Md.I., 2018. Advancements in Docking and Molecular Dynamics Simulations Towards Ligand-receptor Interactions and Structure-function Relationships. Curr Top Med Chem 18, 1755–1768. https://doi.org/10.2174/1568026618666181025114157

Nematicidal Activity of Beauvericin Produced by the Fungus Fusarium bulbicola, n.d.

New Beauvericins, Potentiators of Antifungal Miconazole Activity, Produced by Beauveria sp. FKI-1366, n.d.

Newman, D.J., Cragg, G.M., 2020. Natural Products as Sources of New Drugs over the Nearly Four Decades from 01/1981 to 09/2019. J Nat Prod 83, 770–803. https://doi.org/10.1021/acs.jnatprod.9b01285

Newman, D.J., Cragg, G.M., 2016. Natural Products as Sources of New Drugs from 1981 to 2014. J Nat Prod 79, 629–661. https://doi.org/10.1021/acs.jnatprod.5b01055

Nilanonta, C., Isaka, M., Kittakoop, P., Trakulnaleamsai, S., Tanticharoen, M., Thebtaranonth, Y., 2002. Precursor-directed biosynthesis of beauvericin analogs by the insect pathogenic fungus Paecilomyces tenuipes BCC 1614. Tetrahedron 58, 3355–3360. https://doi.org/10.1016/S0040-4020(02)00294-6

Ojcius, D.M., Zychlinsky, A., Zheng, L.M., Young, J.D.-E., 1991. Ionophore-induced apoptosis: Role of DNA fragmentation and calcium fluxes. Exp Cell Res 197, 43–49. https://doi.org/10.1016/0014-4827(91)90477-C

Olmo, N., Turnay, J., De Buitrago, G.G., De Silanes, I.L., Gavilanes, J.G., Lizarbe, M.A., 2001. Cytotoxic mechanism of the ribotoxin α-sarcin: Induction of cell death via apoptosis. Eur J Biochem 268, 2113–2123. https://doi.org/10.1046/j.1432-1327.2001.02086.x

TH-3487_186106116

Olombrada, M., Medina, P., Budia, F., Gavilanes, J.G., Martínez-Del-Pozo, Á., García-Ortega, L., 2017. Characterization of a new toxin from the entomopathogenic fungus Metarhizium anisopliae: The ribotoxin anisoplin. Biol Chem 398, 135–142. https://doi.org/10.1515/hsz-2016-0119

Olson, B.H., Goerner, G.L., 1965. Alpha Sarcin, a New Antitumor Agent. Appl Microbiol 13, 314–321. https://doi.org/10.1128/am.13.3.314-321.1965

O'Reilly, D., Sendi, M. Al, Kelly, C.M., 2021. Overview of recent advances in metastatic triple negative breast cancer. World J Clin Oncol 12, 164–182. https://doi.org/10.5306/wjco.v12.i3.164

Pal, S., St. Leger, R.J., Wu, L.P., 2007. Fungal Peptide Destruxin A Plays a Specific Role in Suppressing the Innate Immune Response in Drosophila melanogaster. Journal of Biological Chemistry 282, 8969–8977. https://doi.org/10.1074/jbc.M605927200

Pampanella, L., Petrocelli, G., Abruzzo, P.M., Zucchini, C., Canaider, S., Ventura, C., Facchin, F., 2024. Cytochalasins as Modulators of Stem Cell Differentiation. Cells 13, 400. https://doi.org/10.3390/cells13050400

Pastor-Anglada, M., PÃ©rez-Torras, S., 2015. Nucleoside transporter proteins as biomarkers of drug responsiveness and drug targets. Front Pharmacol 6. https://doi.org/10.3389/fphar.2015.00013

Patra, A., Kandasamy, T., Ghosh, S.S., Saini, G.K., 2024. In vitro anticancer effects of recombinant anisoplin through activation of SAPK/JNK and downregulation of NFκB. Toxicology in Vitro 94, 105737. https://doi.org/10.1016/j.tiv.2023.105737

Patridge, E., Gareiss, P., Kinch, M.S., Hoyer, D., 2016. An analysis of FDA-approved drugs: natural products and their derivatives. Drug Discov Today 21, 204–207. https://doi.org/10.1016/j.drudis.2015.01.009

Payne, C.M., Bernstein, C., Bernstein, H., 1995. Apoptosis Overview Emphasizing the Role of Oxidative Stress, DNA Damage and Signal- Transduction Pathways. Leuk Lymphoma 19, 43–93. https://doi.org/10.3109/10428199509059662

TH-3487_186106116

Pedras, M.S.C., Biesenthal, C.J., Zaharia, I.L., 2000. Comparison of the phytotoxic activity of the phytotoxin destruxin B and four natural analogs. Plant Science 156, 185–192. https://doi.org/10.1016/S0168-9452(00)00253-3

Pedras, M.S.C., Irina Zaharia, L., Ward, D.E., 2002. The destruxins: synthesis, biosynthesis, biotransformation, and biological activity. Phytochemistry 59, 579–596. https://doi.org/10.1016/S0031-9422(02)00016-X

Perelman, A., Wachtel, C., Cohen, M., Haupt, S., Shapiro, H., Tzur, A., 2012. JC-1: Alternative excitation wavelengths facilitate mitochondrial membrane potential cytometry. Cell Death Dis 3, 1–7. https://doi.org/10.1038/cddis.2012.171

Perou, C.M., Sørlie, T., Eisen, M.B., van de Rijn, M., Jeffrey, S.S., Rees, C.A., Pollack, J.R., Ross, D.T., Johnsen, H., Akslen, L.A., Fluge, Ø., Pergamenschikov, A., Williams, C., Zhu, S.X., Lønning, P.E., Børresen-Dale, A.-L., Brown, P.O., Botstein, D., 2000. Molecular portraits of human breast tumours. Nature 406, 747–752. https://doi.org/10.1038/35021093

Piedra-Delgado, L., Chambergo-Michilot, D., Morante, Z., Fairen, C., Jerves-Coello, F., Luque-Benavides, R., Casas, F., Bustamante, E., Razuri-Bustamante, C., Torres-Roman, J.S., Fuentes, H., Gomez, H., Narvaez-Rojas, A., De la Cruz-Ku, G., Araujo, J., 2024. Survival according to the site of metastasis in triple-negative breast cancer patients: The Peruvian experience. PLoS One 19, e0293833. https://doi.org/10.1371/journal.pone.0293833

Pinto, B., Henriques, A.C., Silva, P.M.A., Bousbaa, H., 2020. Three-Dimensional Spheroids as In Vitro Preclinical Models for Cancer Research. Pharmaceutics 12, 1186. https://doi.org/10.3390/pharmaceutics12121186

Priya, S., Satheeshkumar, P.K., 2020. Natural products from plants, in: Functional and Preservative Properties of Phytochemicals. Elsevier, pp. 145–163. https://doi.org/10.1016/B978-0-12-818593-3.00005-1

Priyanka Vegesana, B., 2023. Bleomycin induced flagellate dermatitis: A clinical image Clinical Image Journal of Clinical Images and Medical Case Reports. Open Access 4. https://doi.org/10.52768/2766-7820/2746

TH-3487_186106116

Prosperini, A., Juan-García, A., Font, G., Ruiz, M.J., 2013. Beauvericin-induced cytotoxicity via ROS production and mitochondrial damage in Caco-2 cells. Toxicol Lett 222, 204–211. https://doi.org/10.1016/j.toxlet.2013.07.005

Pujadas, G., Vaque, M., Ardevol, A., Blade, C., Salvado, M., Blay, M., Fernandez-Larrea, J., Arola, L., 2008. Protein-ligand Docking: A Review of Recent Advances and Future Perspectives. Curr Pharm Anal 4, 1–19. https://doi.org/10.2174/157341208783497597

Qin, W., Li, C., Zheng, W., Guo, Q., Zhang, Y., Kang, M., Zhang, B., Yang, B., Li, B., Yang, H., Wu, Y., 2015. Inhibition of autophagy promotes metastasis and glycolysis by inducing ROS in gastric cancer cells. Oncotarget 6, 39839–39854. https://doi.org/10.18632/oncotarget.5674

Rathore, D., Nayak, S.K., Batra, J.K., 1997. Overproduction of fungal ribotoxin α-sarcin in Escherichia coli: Generation of an active immunotoxin. Gene 190, 31–35. https://doi.org/10.1016/S0378-1119(96)00696-8

Raza, A., Chohan, Tahir Ali, Sarfraz, M., Chohan, Talha Ali, Imran Sajid, M., Tiwari, R.K., Ansari, S.A., Alkahtani, H.M., Yasmeen Ansari, S., Khurshid, U., Saleem, H., 2023. Molecular modeling of pyrrolo-pyrimidine based analogs as potential FGFR1 inhibitors: a scientific approach for therapeutic drugs. J Biomol Struct Dyn 41, 14358–14371. https://doi.org/10.1080/07391102.2023.2187638

Redza-Dutordoir, M., Averill-Bates, D.A., 2016. Activation of apoptosis signalling pathways by reactive oxygen species. Biochim Biophys Acta Mol Cell Res. https://doi.org/10.1016/j.bbamcr.2016.09.012

Reiter, Y., Pastan, I., 1998. Recombinant Fv immunotoxins and Fv fragments as novel agents for cancer therapy and diagnosis. Trends Biotechnol 16, 513–20. https://doi.org/10.1016/s0167-7799(98)01226-8

Roy, A., Kucukural, A., Zhang, Y., 2010. I-TASSER: A unified platform for automated protein structure and function prediction. Nat Protoc 5, 725–738. https://doi.org/10.1038/nprot.2010.5

TH-3487_186106116

Ruiz, M.J., Franzova, P., Juan-García, A., Font, G., 2011. Toxicological interactions between the mycotoxins beauvericin, deoxynivalenol and T-2 toxin in CHO-K1 cells in vitro. Toxicon 58, 315–326. https://doi.org/10.1016/j.toxicon.2011.07.015

Ruiz, M.-J., Macáková, P., Juan-García, A., Font, G., 2011. Cytotoxic effects of mycotoxin combinations in mammalian kidney cells. Food and Chemical Toxicology 49, 2718–2724. https://doi.org/10.1016/j.fct.2011.07.021

Salari, N., Faraji, Farahnaz, Jafarpour, S., Faraji, Fatemeh, Rasoulpoor, S., Dokaneheifard, S., Mohammadi, M., 2022. Anti-cancer Activity of Chrysin in Cancer Therapy: a Systematic Review. Indian J Surg Oncol 13, 681–690. https://doi.org/10.1007/s13193-022-01550-6

Sanz, J.L., Amils, R., 1984. Sensitivity of thermoacidophilic archaebacteria to α-sarcin. FEBS Lett 171, 63–66. https://doi.org/10.1016/0014-5793(84)80460-3

Sauter, K.A.D., Magun, E.A., Iordanov, M.S., Magun, B.E., 2010. ZAK is required for doxorubicin, a novel ribotoxic stressor, to induce SAPK activation and apoptosis in HaCaT cells. Cancer Biol Ther 10, 258–266. https://doi.org/10.4161/cbt.10.3.12367

Schindler, D.G., Davies, J.E., 1977. Specific cleavage of ribosomal RNA caused by alpha sarcin. Nucleic Acids Res 4, 1097–1110. https://doi.org/10.1093/nar/4.4.1097

Sen, P., Kandasamy, T., Ghosh, S.S., 2023. Multi-targeting TACE/ADAM17 and gamma-secretase of notch signalling pathway in TNBC via drug repurposing approach using Lomitapide. Cell Signal 102, 110529. https://doi.org/10.1016/j.cellsig.2022.110529

Senkus, E., Łacko, A., 2017. Over-treatment in metastatic breast cancer. The Breast 31, 309–317. https://doi.org/10.1016/j.breast.2016.06.024

Shao, S., Zhao, Xiaoai, Zhang, X., Luo, M., Zuo, X., Huang, S., Wang, Y., Gu, S., Zhao, Xinhan, 2015. Notch1 signaling regulates the epithelial–mesenchymal transition and invasion of breast cancer in a Slug-dependent manner. Mol Cancer 14, 28. https://doi.org/10.1186/s12943-015-0295-3

Shekhar-Guturja, T., Tebung, W.A., Mount, H., Liu, N., Köhler, J.R., Whiteway, M., Cowen, L.E., 2016. Beauvericin potentiates azole activity via inhibition of multidrug efflux,

TH-3487_186106116

blocks Candida albicans morphogenesis, and is effluxed via Yor1 and circuitry controlled by Zcf29. Antimicrob Agents Chemother 60, 7468–7480. https://doi.org/10.1128/AAC.01959-16

Shelke Roscoe, J. A. , Morrow, G. R. , Colman, L. K. , Banerjee, T. K. , & Kirshner, J. J., A.R., 2008. Optimization of the CHARMM additive force field for DNA: Improved treatment of the BI/BII conformational equilibrium. Bone 23, 1–7. https://doi.org/10.1021/ct200723y.Optimization

Shibue, T., Weinberg, R.A., 2017. EMT, CSCs, and drug resistance: the mechanistic link and clinical implications. Nat Rev Clin Oncol 14, 611–629. https://doi.org/10.1038/nrclinonc.2017.44

Shifrin, V.I., Anderson, P., 1999. Trichothecene Mycotoxins Trigger a Ribotoxic Stress Response That Activates c-Jun N-terminal Kinase and p38 Mitogen-activated Protein Kinase and Induces Apoptosis * 274, 13985–13992.

Shin, C.G., An, D.G., Song, H.H., Lee, C., 2009. Beauvericin and enniatins H, i and MK1688 are new potent inhibitors of human immunodeficiency virus type-1 integrase. Journal of Antibiotics 62, 687–690. https://doi.org/10.1038/ja.2009.102

Shor, B., Gerber, H.-P., Sapra, P., 2015. Preclinical and clinical development of inotuzumab-ozogamicin in hematological malignancies. Mol Immunol 67, 107–116. https://doi.org/10.1016/j.molimm.2014.09.014

Siegel, R.L., Miller, K.D., Fuchs, H.E., Jemal, A., 2021. Cancer Statistics, 2021. CA Cancer J Clin 71, 7–33. https://doi.org/10.3322/caac.21654

Sinawe, H., Casadesus, D., 2024. Mitomycin.

Sivaganesh, V., Promi, N., Maher, S., Peethambaran, B., 2021. Emerging Immunotherapies against Novel Molecular Targets in Breast Cancer. Int J Mol Sci 22, 2433. https://doi.org/10.3390/ijms22052433

Sivandzade, F., Bhalerao, A., Cucullo, L., 2019. Analysis of the Mitochondrial Membrane Potential Using the Cationic JC-1 Dye as a Sensitive Fluorescent Probe. Bio Protoc 9, 1–13. https://doi.org/10.21769/bioprotoc.3128

TH-3487_186106116

Snodgrass, R.G., Collier, A.C., Coon, A.E., Pritsos, C.A., 2010. Mitomycin C Inhibits Ribosomal RNA. Journal of Biological Chemistry 285, 19068–19075. https://doi.org/10.1074/jbc.M109.040477

Sommers, C.L., Heckford, S.E., Skerker, J.M., Worland, P., Torri, J.A., Thompson, E.W., Byers, S.W., Gelmann, E.P., 1992. Loss of epithelial markers and acquisition of vimentin expression in adriamycin- and vinblastine-resistant human breast cancer cell lines. Cancer Res 52, 5190–7.

Sondergaard, T.E., Fredborg, M., Oppenhagen Christensen, A.M., Damsgaard, S.K., Kramer, N.F., Giese, H., Sørensen, J.L., 2016. Fast Screening of Antibacterial Compounds from Fusaria. Toxins (Basel) 8. https://doi.org/10.3390/toxins8120355

Song, K.-A., Niederst, M.J., Lochmann, T.L., Hata, A.N., Kitai, H., Ham, J., Floros, K. V., Hicks, M.A., Hu, H., Mulvey, H.E., Drier, Y., Heisey, D.A.R., Hughes, M.T., Patel, N.U., Lockerman, E.L., Garcia, A., Gillepsie, S., Archibald, H.L., Gomez-Caraballo, M., Nulton, T.J., Windle, B.E., Piotrowska, Z., Sahingur, S.E., Taylor, S.M., Dozmorov, M., Sequist, L. V., Bernstein, B., Ebi, H., Engelman, J.A., Faber, A.C., 2018. Epithelial-to-Mesenchymal Transition Antagonizes Response to Targeted Therapies in Lung Cancer by Suppressing BIM. Clinical Cancer Research 24, 197–208. https://doi.org/10.1158/1078-0432.CCR-17-1577

Sousa, J.M.C., Matos, L.A., Alcântara, D.F.A., Ribeiro, H.F., Santos, L.S., Oliveira, M.N., Brito-Junior, L.C., Khayat, A.S., Guimarães, A.C., Cunha, L.A., Burbano, R.R., Bahia, M.O., 2013. Cellular responses induced in vitro by pestheic acid, a fungal metabolite, in a gastric adenocarcinoma cell line (PG100). Genetics and Molecular Research 12, 4106–4115. https://doi.org/10.4238/2013.October.1.1

Speiser, J., Foreman, K., Drinka, E., Godellas, C., Perez, C., Salhadar, A., Erşahin, Ç., Rajan, P., 2012. Notch-1 and Notch-4 Biomarker Expression in Triple-Negative Breast Cancer. Int J Surg Pathol 20, 137–143. https://doi.org/10.1177/1066896911427035

Spudich, J.A., Lin, S., 1972. Cytochalasin B, Its Interaction with Actin and Actomyosin from Muscle. Proceedings of the National Academy of Sciences 69, 442–446. https://doi.org/10.1073/pnas.69.2.442

TH-3487_186106116

Strnad, V., Ott, O.J., Hildebrandt, G., Kauer-Dorner, D., Knauerhase, H., Major, T., Lyczek, J., Guinot, J.L., Dunst, J., Miguelez, C.G., Slampa, P., Allgäuer, M., Lössl, K., Polat, B., Kovács, G., Fischedick, A.-R., Wendt, T.G., Fietkau, R., Hindemith, M., Resch, A., Kulik, A., Arribas, L., Niehoff, P., Guedea, F., Schlamann, A., Pötter, R., Gall, C., Malzer, M., Uter, W., Polgár, C., 2016. 5-year results of accelerated partial breast irradiation using sole interstitial multicatheter brachytherapy versus whole-breast irradiation with boost after breast-conserving surgery for low-risk invasive and in-situ carcinoma of the female breast: a randomised, phase 3, non-inferiority trial. The Lancet 387, 229–238. https://doi.org/10.1016/S0140-6736(15)00471-7

Šudomová, M., Berchová-Bímová, K., Marzocco, S., Liskova, A., Kubatka, P., Hassan, S., 2021. Berberine in Human Oncogenic Herpesvirus Infections and Their Linked Cancers. Viruses 13, 1014. https://doi.org/10.3390/v13061014

Sun, Z., Andersson, R., n.d. NF-B ACTIVATION AND INHIBITION: A REVIEW.

Suzuki-Karasaki, M., Ochiai, T., Suzuki-Karasaki, Y., 2014. Crosstalk between mitochondrial ROS and depolarization in the potentiation of TRAIL-induced apoptosis in human tumor cells. Int J Oncol 44, 616–628. https://doi.org/10.3892/ijo.2013.2215

Tamura, K., Stecher, G., Kumar, S., 2021. MEGA11: Molecular Evolutionary Genetics Analysis Version 11. Mol Biol Evol 38, 3022–3027. https://doi.org/10.1093/molbev/msab120

Tang, F., Tang, G., Xiang, J., Dai, Q., Rosner, M.R., Lin, A., 2002. The Absence of NF-κB-Mediated Inhibition of c-Jun N-Terminal Kinase Activation Contributes to Tumor Necrosis Factor Alpha-Induced Apoptosis. Mol Cell Biol 22, 8571–8579. https://doi.org/10.1128/mcb.22.24.8571-8579.2002

Tao, Z., Li, T., Ma, H., Yang, Y., Zhang, C., Hai, L., Liu, P., Yuan, F., Li, J., Yi, L., Tong, L., Wang, Y., Xie, Y., Ming, H., Yu, S., Yang, X., 2018. Autophagy suppresses self-renewal ability and tumorigenicity of glioma-initiating cells and promotes Notch1 degradation. Cell Death Dis 9, 1063. https://doi.org/10.1038/s41419-018-0957-3

Telli, M.L., Ford, J.M., 2010. Novel Treatment Approaches for Triple-Negative Breast Cancer. Clin Breast Cancer 10, E16–E22. https://doi.org/10.3816/CBC.2010.s.003

TH-3487_186106116

Teponno, R., Noumeur, S., Helaly, S., Hüttel, S., Harzallah, D., Stadler, M., 2017. Furanones and Anthranilic Acid Derivatives from the Endophytic Fungus Dendrothyrium variisporum. Molecules 22, 1674. https://doi.org/10.3390/molecules22101674

Theuerkauf, M., Kepler, J., 2022. Ionophoric Activity of Cyclic Depsipeptides from Beauveria bassiana Diplom-Ingenieurin in the Master's Program Biophysik.

Thorn, C.F., Oshiro, C., Marsh, S., Hernandez-Boussard, T., McLeod, H., Klein, T.E., Altman, R.B., 2011. Doxorubicin pathways. Pharmacogenet Genomics 21, 440–446. https://doi.org/10.1097/FPC.0b013e32833ffb56

Tokmakov, A.A., Kurotani, A., Sato, K.I., 2021. Protein pI and Intracellular Localization. Front Mol Biosci 8, 1–6. https://doi.org/10.3389/fmolb.2021.775736

Tolaney, S.M., Barry, W.T., Guo, H., Dillon, D., Dang, C.T., Yardley, D.A., Moy, B., Marcom, P.K., Albain, K.S., Rugo, H.S., Ellis, M.J., Shapira, I., Wolff, A.C., Carey, L.A., Overmoyer, B., Partridge, A.H., Hudis, C.A., Krop, I.E., Burstein, H.J., Winer, E.P., 2017. Seven-year (yr) follow-up of adjuvant paclitaxel (T) and trastuzumab (H) (APT trial) for node-negative, HER2-positive breast cancer (BC). Journal of Clinical Oncology 35, 511–511. https://doi.org/10.1200/JCO.2017.35.15_suppl.511

Tomasz, M., 1995. Mitomycin C: small, fast and deadly (but very selective). Chem Biol 2, 575–579. https://doi.org/10.1016/1074-5521(95)90120-5

Tomé-Amat, J., Herrero-Galán, E., Oñaderra, M., Martínez-Del-Pozo, Á., Gavilanes, J.G., Lacadena, J., 2015a. Preparation of an engineered safer immunotoxin against colon carcinoma based on the ribotoxin hirsutellin A. FEBS Journal 282, 2131–2141. https://doi.org/10.1111/febs.13262

Tomé-Amat, J., Olombrada, M., Ruiz-de-la-Herrán, J., Pérez-Gómez, E., Andradas, C., Sánchez, C., Martínez, L., Martínez-del-Pozo, Á., Gavilanes, J.G., Lacadena, J., 2015b. Efficient in vivo antitumor effect of an immunotoxin based on ribotoxin α-sarcin in nude mice bearing human colorectal cancer xenografts. Springerplus 4. https://doi.org/10.1186/s40064-015-0943-5

TH-3487_186106116

Tong, Y., Liu, M., Zhang, Y., Liu, X., Huang, R., Song, F., Dai, H., Ren, B., Sun, N., Pei, G., Bian, J., Jia, X.M., Huang, G., Zhou, X., Li, S., Zhang, B., Fukuda, T., Tomoda, H., Ōmura, S., Cannon, R.D., Calderone, R., Zhang, L., 2016. Beauvericin counteracted multi-drug resistant Candida albicans by blocking ABC transporters. Synth Syst Biotechnol 1, 158–168. https://doi.org/10.1016/j.synbio.2016.10.001

Tonshin, A.A., Teplova, V. V., Andersson, M.A., Salkinoja-Salonen, M.S., 2010. The Fusarium mycotoxins enniatins and beauvericin cause mitochondrial dysfunction by affecting the mitochondrial volume regulation, oxidative phosphorylation and ion homeostasis. Toxicology 276, 49–57. https://doi.org/10.1016/j.tox.2010.07.001

Trendowski, M., 2015. Using cytochalasins to improve current chemotherapeutic approaches. Anticancer Agents Med Chem 15, 327–35. https://doi.org/10.2174/1871520614666141016164335

Turnay, J., Olmo, N., Jiménez, alfredo, Lizarbe, M.A., Gavilanes, J.G., 1993. Kinetic study of the cytotoxic effect of α-sarcin, a ribosome inactivating protein from Aspergillus giganteus, on tumour cell lines: protein biosynthesis inhibition and cell binding. Mol Cell Biochem 122, 39–47. https://doi.org/10.1007/BF00925735

Urbaniak, M., Waśkiewicz, A., Stępień, Ł., 2020. Fusarium Cyclodepsipeptide Mycotoxins: Chemistry, Biosynthesis, and Occurrence. Toxins (Basel) 12, 765. https://doi.org/10.3390/toxins12120765

Uttarkar, A., Kishore, A.P., Srinivas, S.M., Rangappa, S., Kusanur, R., Niranjan, V., 2023. Coumarin derivative as a potent drug candidate against triple negative breast cancer targeting the frizzled receptor of wingless-related integration site signaling pathway. J Biomol Struct Dyn 41, 1561–1573. https://doi.org/10.1080/07391102.2021.2022536

van der Zanden, S.Y., Qiao, X., Neefjes, J., 2021. New insights into the activities and toxicities of the old anticancer drug doxorubicin. FEBS J 288, 6095–6111. https://doi.org/10.1111/febs.15583

Verweij, J., Pinedo, H.M., 1990. Mitomycin C: mechanism of action, usefulness and limitations. Anticancer Drugs 1, 5–13.

TH-3487_186106116

Viegas, A., Herrero-Galán, E., Oñaderra, M., MacEdo, A.L., Bruix, M., 2009. Solution structure of hirsutellin A - New insights into the active site and interacting interfaces of ribotoxins. FEBS Journal 276, 2381–2390. https://doi.org/10.1111/j.1742-4658.2009.06970.x

Vind, A.C., Genzor, A.V., Bekker-Jensen, S., 2020. Ribosomal stress-surveillance: Three pathways is a magic number. Nucleic Acids Res 48, 10648–10661. https://doi.org/10.1093/nar/gkaa757

Vona, R., Pallotta, L., Cappelletti, M., Severi, C., Matarrese, P., 2021. The Impact of Oxidative Stress in Human Pathology: Focus on Gastrointestinal Disorders. Antioxidants 10, 201. https://doi.org/10.3390/antiox10020201

Walzl, A., Unger, C., Kramer, N., Unterleuthner, D., Scherzer, M., Hengstschläger, M., Schwanzer-Pfeiffer, D., Dolznig, H., 2014. The Resazurin Reduction Assay Can Distinguish Cytotoxic from Cytostatic Compounds in Spheroid Screening Assays. SLAS Discovery 19, 1047–1059. https://doi.org/10.1177/1087057114532352

Wang, C.-F., Yang, X.-Q., Shi, W.-Z., Long, X., Su, S., Cen, R.-H., Yang, Y.-B., Ding, Z.-T., 2022. The production of broad-spectrum antibiotics from phytopathogen Epicoccum sorghinum by culturing in host edible mushroom Thelephora ganbajun extract. Phytochemistry 200, 113221. https://doi.org/10.1016/j.phytochem.2022.113221

Wang, D.-Y., Jiang, Z., Ben-David, Y., Woodgett, J.R., Zacksenhaus, E., 2019. Molecular stratification within triple-negative breast cancer subtypes. Sci Rep 9, 19107. https://doi.org/10.1038/s41598-019-55710-w

Wang, H., Nicolay, B.N., Chick, J.M., Gao, X., Geng, Y., Ren, H., Gao, H., Yang, G., Williams, J.A., Suski, J.M., Keibler, M.A., Sicinska, E., Gerdemann, U., Haining, W.N., Roberts, T.M., Polyak, K., Gygi, S.P., Dyson, N.J., Sicinski, P., 2017. The metabolic function of cyclin D3–CDK6 kinase in cancer cell survival. Nature 546, 426–430. https://doi.org/10.1038/nature22797

Wang, K., Zhang, Q., Li, D., Ching, K., Zhang, C., Zheng, X., Ozeck, M., Shi, S., Li, X., Wang, H., Rejto, P., Christensen, J., Olson, P., 2015. PEST Domain Mutations in Notch Receptors Comprise an Oncogenic Driver Segment in Triple-Negative Breast Cancer

TH-3487_186106116

Sensitive to a γ-Secretase Inhibitor. Clinical Cancer Research 21, 1487–1496. https://doi.org/10.1158/1078-0432.CCR-14-1348

Waterhouse, A., Bertoni, M., Bienert, S., Studer, G., Tauriello, G., Gumienny, R., Heer, F.T., De Beer, T.A.P., Rempfer, C., Bordoli, L., Lepore, R., Schwede, T., 2018. SWISS-MODEL: Homology modelling of protein structures and complexes. Nucleic Acids Res 46, W296–W303. https://doi.org/10.1093/nar/gky427

Wätjen, W., Debbab, A., Hohlfeld, A., Chovolou, Y., Proksch, P., 2014. The mycotoxin beauvericin induces apoptotic cell death in H4IIE hepatoma cells accompanied by an inhibition of NF-κB-activity and modulation of MAP-kinases. Toxicol Lett 231, 9–16. https://doi.org/10.1016/j.toxlet.2014.08.021

Weinberg, R.A., 1996. How Cancer Arises 275, 62–70. https://doi.org/10.2307/24993349

Weston, C.R., Davis, R.J., 2007. The JNK signal transduction pathway. Curr Opin Cell Biol 19, 142–149. https://doi.org/10.1016/j.ceb.2007.02.001

Wiederstein, M., Sippl, M.J., 2007. ProSA-web: Interactive web service for the recognition of errors in three-dimensional structures of proteins. Nucleic Acids Res 35, 407–410. https://doi.org/10.1093/nar/gkm290

Wishart, D.S., Feunang, Y.D., Guo, A.C., Lo, E.J., Marcu, A., Grant, J.R., Sajed, T., Johnson, D., Li, C., Sayeeda, Z., Assempour, N., Iynkkaran, I., Liu, Y., Maciejewski, A., Gale, N., Wilson, A., Chin, L., Cummings, R., Le, D., Pon, A., Knox, C., Wilson, M., 2018. DrugBank 5.0: a major update to the DrugBank database for 2018. Nucleic Acids Res 46, D1074–D1082. https://doi.org/10.1093/nar/gkx1037

Wu, C.-C., Chen, T.-H., Liu, B.-L., Wu, L.-C., Chen, Y.-C., Tzeng, Y.-M., Hsu, S.-L., 2013. Destruxin B Isolated from Entomopathogenic Fungus *Metarhizium anisopliae* Induces Apoptosis via a Bcl-2 Family-Dependent Mitochondrial Pathway in Human Nonsmall Cell Lung Cancer Cells. Evidence-Based Complementary and Alternative Medicine 2013, 1–11. https://doi.org/10.1155/2013/548929

Wu, E.L., Cheng, X., Jo, S., Rui, H., Song, K.C., Dávila-Contreras, E.M., Qi, Y., Lee, J., Monje-Galvan, V., Venable, R.M., Klauda, J.B., Im, W., 2014. CHARMM-GUI

TH-3487_186106116

Membrane Builder toward realistic biological membrane simulations. J Comput Chem 35, 1997–2004. https://doi.org/10.1002/jcc.23702

Wu, H., Wang, S., Weng, D., Xing, H., Song, X., Zhu, T., Xia, X., Weng, Y., Xu, G., Meng, L., Zhou, J., Ma, D., 2008. Reversal of the malignant phenotype of ovarian cancer A2780 cells through transfection with wild-type PTEN gene. Cancer Lett 271, 205–214. https://doi.org/10.1016/j.canlet.2008.06.018

Wu, Q., Patocka, J., Kuca, K., 2019a. Beauvericin, A Fusarium Mycotoxin: Anticancer Activity, Mechanisms, and Human Exposure Risk Assessment. Mini-Reviews in Medicinal Chemistry 19, 206–214. https://doi.org/10.2174/1389557518666180928161808

Wu, Q., Wu, W., Fu, B., Shi, L., Wang, X., Kuca, K., 2019b. JNK signaling in cancer cell survival. Med Res Rev 39, 2082–2104. https://doi.org/10.1002/med.21574

Wu, X., Fleming, A., Ricketts, T., Pavel, M., Virgin, H., Menzies, F.M., Rubinsztein, D.C., 2016. Autophagy regulates Notch degradation and modulates stem cell development and neurogenesis. Nat Commun 7, 10533. https://doi.org/10.1038/ncomms10533

Wu, X.-F., Xu, R., Ouyang, Z.-J., Qian, C., Shen, Y., Wu, X.-D., Gu, Y.-H., Xu, Q., Sun, Y., 2013. Beauvericin Ameliorates Experimental Colitis by Inhibiting Activated T Cells via Downregulation of the PI3K/Akt Signaling Pathway. PLoS One 8, e83013. https://doi.org/10.1371/journal.pone.0083013

Xia, S., Li, Y., Rosen, E.M., Laterra, J., 2007. Ribotoxic Stress Sensitizes Glioblastoma Cells to Death Receptor – Induced Apoptosis : Requirements for c-Jun NH 2 -Terminal Kinase and Bim 5, 783–793. https://doi.org/10.1158/1541-7786.MCR-06-0433

Xiao, Y., He, L., Dong, Y., Huang, Y., Ma, L., Li, W., 2023. Highly Expressed LINC00958 Modulates the Growth and Epithelial-Mesenchymal Transition of Bladder Cancer Cells Through *SAPK/JNK* Signaling Pathway. Cancer Biother Radiopharm 38, 405–414. https://doi.org/10.1089/cbr.2022.0005

TH-3487_186106116

Xu, L., Wang, Jihua, Zhao, J., Li, P., Shan, T., Wang, Jingguo, Li, X., Zhou, L., n.d. Beauvericin from the Endophytic Fungus, Fusarium redolens, Isolated from Dioscorea zingiberensis and Its Antibacterial Activity.

Xue, S., He, L., Zhang, X., Zhou, J., Li, F., Wang, X., 2017. Expression of Jagged1/Notch3 Signaling Pathway and their Relationship with the Tumor Angiogenesis in TNBC. Arch Med Res 48, 169–179. https://doi.org/10.1016/j.arcmed.2017.03.014

Yahagi, H., Yahagi, T., Furukawa, M., Matsuzaki, K., 2020. Antiproliferative and Antimigration Activities of Beauvericin Isolated from Isaria sp. on Pancreatic Cancer Cells. Molecules 25, 4586. https://doi.org/10.3390/molecules25194586

Yahara, I., Harada, F., Sekita, S., Yoshihira, K., Natori, S., 1982. Correlation between effects of 24 different cytochalasins on cellular structures and cellular events and those on actin in vitro. J Cell Biol 92, 69–78. https://doi.org/10.1083/jcb.92.1.69

Yang, H., Villani, R.M., Wang, H., Simpson, M.J., Roberts, M.S., Tang, M., Liang, X., 2018. The role of cellular reactive oxygen species in cancer chemotherapy. Journal of Experimental and Clinical Cancer Research 37, 1–10. https://doi.org/10.1186/s13046-018-0909-x

Yin, L., Duan, J.-J., Bian, X.-W., Yu, S., 2020. Triple-negative breast cancer molecular subtyping and treatment progress. Breast Cancer Research 22, 61. https://doi.org/10.1186/s13058-020-01296-5

Yoo, S., Kim, M.Y., Cho, J.Y., 2017. Beauvericin, a cyclic peptide, inhibits inflammatory responses in macrophages by inhibiting the NF-κB pathway. Korean Journal of Physiology and Pharmacology 21, 449–456. https://doi.org/10.4196/kjpp.2017.21.4.449

Yuan, Y., Huang, W., Chen, K., Ling, E., 2020. Beauveria bassiana ribotoxin inhibits insect immunity responses to facilitate infection via host translational blockage. Dev Comp Immunol 106, 103605. https://doi.org/10.1016/j.dci.2019.103605

Zada, S., Hwang, J.S., Ahmed, M., Lai, T.H., Pham, T.M., Elashkar, O., Kim, D.R., 2021. Cross talk between autophagy and oncogenic signaling pathways and implications for

TH-3487_186106116

cancer therapy. Biochimica et Biophysica Acta (BBA) - Reviews on Cancer 1876, 188565. https://doi.org/10.1016/j.bbcan.2021.188565

Zada, S., Hwang, J.S., Lai, T.H., Pham, T.M., Ahmed, M., Elashkar, O., Kim, W., Kim, D.R., 2022. Autophagy-mediated degradation of NOTCH1 intracellular domain controls the epithelial to mesenchymal transition and cancer metastasis. Cell Biosci 12, 17. https://doi.org/10.1186/s13578-022-00752-3

Zagami, P., Carey, L.A., 2022. Triple negative breast cancer: Pitfalls and progress. NPJ Breast Cancer. https://doi.org/10.1038/s41523-022-00468-0

Zhan, J., Burns, A.M., Liu, M.X., Faeth, S.H., Gunatilaka, A.A.L., 2007. Search for Cell Motility and Angiogenesis Inhibitors with Potential Anticancer Activity: Beauvericin and Other Constituents of Two Endophytic Strains of *Fusarium oxysporum*. J Nat Prod 70, 227–232. https://doi.org/10.1021/np060394t

Zhang, H., Ruan, C., Bai, X., Zhang, M., Zhu, S., Jiang, Y., 2016. Isolation and identification of the antimicrobial agent beauvericin from the endophytic Fusarium oxysporum 5-19 with NMR and ESI-MS/MS. Biomed Res Int 2016. https://doi.org/10.1155/2016/1084670

Zhang, J., Lei, W., Chen, X., Wang, S., Qian, W., 2018. Oxidative stress response induced by chemotherapy in leukemia treatment (Review). Mol Clin Oncol. https://doi.org/10.3892/mco.2018.1549

Zhang, J., Shao, X., Sun, H., Liu, K., Ding, Z., Chen, J., Fang, L., Su, W., Hong, Y., Li, Huashun, Li, Hongchang, 2016. NUMB negatively regulates the epithelial-mesenchymal transition of triple-negative breast cancer by antagonizing Notch signaling.

Zhang, L., Yan, K., Zhang, Y., Huang, R., Bian, J., Zheng, C., Sun, H., Chen, Z., Sun, N., An, R., Min, F., Zhao, W., Zhuo, Y., You, J., Song, Y., Yu, Z., Liu, Z., Yang, K., Gao, H., Dai, H., Zhang, X., Wang, J., Fu, C., Pei, G., Liu, J., Zhang, S., Goodfellow, M., Jiang, Y., Kuai, J., Zhou, G., Chen, X., 2007. High-throughput synergy screening identifies microbial metabolites as combination agents for the treatment of fungal infections.

TH-3487_186106116

Zhang, S., Chung, W.-C., Wu, G., Egan, S.E., Miele, L., Xu, K., 2015. Manic Fringe Promotes a Claudin-Low Breast Cancer Phenotype through Notch-Mediated PIK3CG Induction. Cancer Res 75, 1936–1943. https://doi.org/10.1158/0008-5472.CAN-14-3303

Zhang, Y., Ding, C., Zhu, W., Li, X., Chen, T., Liu, Q., Zhou, S., Zhang, T.-C., Ma, W., 2022. Chemotherapeutic drugs induce oxidative stress associated with DNA repair and metabolism modulation. Life Sci 289, 120242. https://doi.org/10.1016/j.lfs.2021.120242

Zhang, Y., Xie, Z., Guo, X., Xiao, X., Xiong, L., 2019. Notch and breast cancer metastasis: Current knowledge, new sights and targeted therapy (Review). Oncol Lett. https://doi.org/10.3892/ol.2019.10653

Zhao, L., Zhang, B., 2017. Doxorubicin induces cardiotoxicity through upregulation of death receptors mediated apoptosis in cardiomyocytes. Sci Rep 7, 44735. https://doi.org/10.1038/srep44735

Zhao, Z., Zhao, J., Xue, J., Zhao, X., Liu, P., 2016. Autophagy inhibition promotes epithelial-mesenchymal transition through ROS/HO-1 pathway in ovarian cancer cells, Am J Cancer Res.

Zhong, Y., Shen, S., Zhou, Y., Mao, F., Lin, Y., Guan, J., Xu, Y., Zhang, S., Liu, X., Sun, Q., 2016. NOTCHI is a poor prognostic factor for breast cancer and is associated with breast cancer stem cells. Onco Targets Ther 9, 6865–6871. https://doi.org/10.2147/OTT.S109606

Zhou, B., Lin, W., Long, Y., Yang, Y., Zhang, H., Wu, K., Chu, Q., 2022. Notch signaling pathway: architecture, disease, and therapeutics. Signal Transduct Target Ther 7, 95. https://doi.org/10.1038/s41392-022-00934-y

Zhou, S.-F., Li, J.-P., Yang, Y.-X., Liu, Q.-L., Zhou, Z.-W., Pan, S., He, Z., Zhang, X., Yang, T., Pan, S.-Y., Duan, W., He, S.-M., Chen, X.-W., Qiu, J., 2015. The pan-inhibitor of Aurora kinases danusertib induces apoptosis and autophagy and suppresses epithelial-to-mesenchymal transition in human breast cancer cells. Drug Des Devel Ther 1027. https://doi.org/10.2147/DDDT.S74412

TH-3487_186106116

Zi, D., Zhou, Z.-W., Yang, Y.-J., Huang, L., Zhou, Z.-L., He, S.-M., He, Z.-X., Zhou, S.-F., 2015. Danusertib Induces Apoptosis, Cell Cycle Arrest, and Autophagy but Inhibits Epithelial to Mesenchymal Transition Involving PI3K/Akt/mTOR Signaling Pathway in Human Ovarian Cancer Cells. Int J Mol Sci 16, 27228–27251. https://doi.org/10.3390/ijms161126018

Zouaoui, N., Mallebrera, B., Berrada, H., Abid-Essefi, S., Bacha, H., Ruiz, M.-J., 2016. Cytotoxic effects induced by patulin, sterigmatocystin and beauvericin on CHO–K1 cells. Food and Chemical Toxicology 89, 92–103. https://doi.org/10.1016/j.fct.2016.01.010

Zumsteg, Z.S., Morrow, M., Arnold, B., Zheng, J., Zhang, Z., Robson, M., Traina, T., McCormick, B., Powell, S., Ho, A.Y., 2013. Breast-Conserving Therapy Achieves Locoregional Outcomes Comparable to Mastectomy in Women with T1-2N0 Triple-Negative Breast Cancer. Ann Surg Oncol 20, 3469–3476. https://doi.org/10.1245/s10434-013-3011-9

TH-3487_186106116